

# **Stoichiometry of the Photocatalytic Fuel Production by the Reformation of Aqueous Acetic Acid**

Von der Naturwissenschaftlichen Fakultät der  
Gottfried Wilhelm Leibniz Universität Hannover

zur Erlangung des Grades

**Doktorin der Naturwissenschaften (Dr. rer. nat.)**

genehmigte Dissertation

von

Saher Hamid, M.S. (Pakistan)

geboren am 18.01.1989 in Lahore (Pakistan)

2018



Referent: Prof . Dr. rer. nat. Detlef W. Bahnemann

Korreferent: Prof. Dr. rer. nat. Nadja-Carola Bigall

Tag der Promotion: 21.06.2018



*Dedicated to*  
*My Parents*



*The ultimate measure of a man is not where he stands in moments of comfort and convenience, but where he stands at time of challenges and controversy.*

*Martin Luther King, Jr.*





### Acknowledgements

First of all, I would like to express my deepest gratitude to my supervisor, **Prof. Dr. Detlef Bahnemann**, for giving me the opportunity to work under his kind supervision. His excellent academic guidance, inspiring and enthusiastic reviews, motivational support and discussions are much esteemed.

I would also like to thank **Prof. Dr. Thomas Scheper** for agreeing to be a referee of my thesis. My sincere thanks also go to **Prof. Dr. Nadja-Carola Bigall** for showing her consent to act as a co-referee of my thesis.

For the financial support during my research work, I would like to thank **Bundesministerium für Bildung und Forschung (BMBF) (Project ‘Duasol’ Nr. 03SF0482C)**.

I would also like to extend my sincere and special appreciation to **Dr. Ralf Dillert** for his valuable input in terms of thoughtful scientific discussions as well as his great help throughout my Ph. D. His efforts and way of teaching is greatly appreciated.

In addition, I would also convey my intimate gratitude to **Dr. Jenny Schneider** and **Dr. Irina Ivanova** for their academic guidance as well as friendly support during my stay in Germany.

For their continuous support to carry out analytical characterizations including XRD, NMR and TEM measurements, I would also like to thank **Prof. Dr. Armin Feldhoff** at the Institut für Physikalische Chemie und Elektrochemie, Leibniz Universität Hannover, **Dr. Jörg Fohrer**, Institut für Organische Chemie, Leibniz Universität Hannover and Laboratorium für Nano- und Quantenengineering, Leibniz Universität Hannover, respectively.

My sincere appreciation also goes to **Mrs. Kerstin Hellmuth** (Leibnizhaus / administrator) for her emotional and friendly support during my stay in Germany.

In any organization, the qualitative and comfortable environment at the work place plays a very constructive role in one's performance towards his/her duties. For this, I would like to thank all members in the research group of Prof. Bahnemann (AK Bahnemann) for their help, cooperation and maintaining a very friendly environment. Ph. D. itself isn't an easy title to earn. However, presence of some loving and caring friends in life makes its realization comparatively easier. I also consider myself lucky enough to have some good friends including **Narmina Balayeva**, and **Dr. Didem Muharrem Seleci**, who stood with me in all hard times and, therefore, feel extremely grateful to all of them.

## **Acknowledgements**

Last but by no means the least, I'm extremely indebted to my beloved family which has truly been the driving force behind all this hard work and success! I wouldn't hesitate to acknowledge all their names starting from **Samina Hamid** (my beloved mother), **Hamid Ali Mukhtar** (an affectionate father), **Dr. Muhammad Fahad Ehsan** (my loving husband, without whose continuous support and encouragement this wouldn't have been possible), **Muhammad Zayan Fahad** (the love of my life, my son), **Sadaf Yasir** (my friend cum elder sister), **Ahsan Hamid** (a caring younger brother) and my in-laws. Without their prayers, support, and motivation, I would have never been able to achieve this Ph. D. degree.

### Kurzzusammenfassung

In den letzten Jahren haben photokatalytische Reaktionssysteme viel Aufmerksamkeit erregt, um sowohl Energie- als auch Umweltprobleme zu beheben. Eine dieser photokatalytischen Reaktionen umfasst die Umwandlung von wässrigen organischen Schadstoffen, die aus Industrieabfällen resultieren, in nutzbare Kraftstoffe (d.h.  $H_2$  und Kohlenwasserstoffe) mittels Solarlicht. Mangelndes Verständnis für den Reaktionsmechanismus beschränkt jedoch die praktische Realisierung dieser Systeme. Daher ist die Grundlagenforschung auf diesem Gebiet sehr wichtig, um die photokatalytische Effizienz dieser Systeme zu verbessern.

Diese Arbeit befasst sich mit der gleichzeitigen molekularen Wasserstoffproduktion und dem Abbau organischer Schadstoffe. Essigsäure ( $CH_3COOH$ ) wurde als organischer Modell-Schadstoff und mit Co-Katalysator geladenes  $TiO_2$  als Photokatalysator verwendet. Die Parameter, die die photokatalytische Umwandlung von wässriger Essigsäure in Kohlendioxid ( $CO_2$ ), molekularen Wasserstoff ( $H_2$ ), Methan ( $CH_4$ ) und Ethan ( $C_2H_6$ ) unter Verwendung von Co-Katalysator-beladenen  $TiO_2$ -Partikeln unter anaeroben Bedingungen beeinflussen, wurden untersucht. Verschiedene Metalle und Metalloxide wie Pt, Rh, Au, Ag,  $IrO_2$  und  $RuO_2$  wurden auf die Oberfläche von  $TiO_2$  als Elektronenakzeptoren aufgebracht, was die Reduktionsreaktion (d.h. die Bildung von  $H_2$ ) erleichterte. Die beobachteten Mengen an  $CO_2$  und  $CH_4$  stiegen in folgender Reihenfolge an:  $Ag/TiO_2 < Au/TiO_2 < Rh/TiO_2 < RuO_2/TiO_2 < IrO_2/TiO_2 < Pt/TiO_2$ . Im Gegensatz dazu war die Reihenfolge, in der die entwickelten Mengen an  $H_2$  zunahmen, relativ unterschiedlich. Es wurde beobachtet, dass die Bildungsraten der Hauptreaktionsprodukte ( $CO_2$ ,  $H_2$ ,  $CH_4$  und  $C_2H_6$ ) und ihre entsprechende Produktverteilung stark sowohl von (1) der Konzentration der Essigsäure als auch von (2) der Beladung des Photokatalysators mit verschiedenen Metallen und Metalloxide beeinflusst worden ist. Es wurde gefunden, dass die Co-Katalysatoren mit höheren Werten der Austrittsarbeit, die  $H_2$ -Entwicklungsreaktion bei niedrigeren Konzentrationen von Essigsäure erleichtern. Unter Verwendung höherer Essigsäurekonzentrationen wurden die Reaktionsprodukte, die aus einem mit Kohlenwasserstoffen angereicherten Gasgemisch bestanden, unter Verwendung des Co-Katalysators mit niedrigeren Werten der Austrittsarbeit (Ag und  $IrO_2$ ) erhalten. Es wurde festgestellt, dass der pH-Wert der verwendeten Suspension eine Schlüsselrolle bei der Wahl der

## Kurzzusammenfassung

Reaktionswege für die photokatalytische Zersetzung von wässriger Essigsäure spielt. Es wurde festgestellt, dass eine Erhöhung des pH-Werts vom Sauren zum Basischen zu völlig unterschiedlichen Verhältnissen zwischen den entwickelten Mengen an  $\text{H}_2$  und Kohlenwasserstoffen führt. Zum Beispiel ist bei einem pH-Wert von 2 das Verhältnis  $\frac{n(\text{H}_2)}{n(\text{CH}_4)} = 0.6$  und bei einem pH-Wert von 9 das Verhältnis  $\frac{n(\text{H}_2)}{n(\text{CH}_4)} = 58$ . Stöchiometrische Berechnungen für die entwickelten Mengen der Hauptreaktionsprodukte zeigen eindeutig die Bildung anderer organischer Zwischenprodukte während der photoinduzierten Umwandlung von wässriger Essigsäure an. In Abhängigkeit vom pH-Wert der Suspension wurde beobachtet, dass der photokatalytische Abbau von Essigsäure unterschiedlichen Reaktionsmechanismen folgt. Um die Ergebnisse der lichtinduzierten Umwandlung von wässriger Essigsäure zu interpretieren, wurden Experimente mit markierten Isotopen durchgeführt. Diese Experimente sollen Aufschluss über den Ursprung von entwickeltem  $\text{H}_2$  und  $\text{CH}_4$  durch Analyse der Protonenaustauschreaktion zwischen Essigsäure und Wassermolekül geben. Ein detaillierter Mechanismus für die photokatalytische Zersetzung von wässriger Essigsäure wurde anhand der Resultate erstellt.

**Stichwörter:** Photokatalyse, Essigsäure, Cokatalysator-beladenes  $\text{TiO}_2$ , Oberflächenladung, H/D-Austauschreaktion, Solarbrennstoff.

## Abstract

In recent years, photocatalytic reaction systems gained much attention to address both energy and environmental issues. One of these photocatalytic reactions involve the conversion of aqueous organic pollutants resulting from industrial waste into value added fuels (*i.e.*, H<sub>2</sub>, and hydrocarbons) by means of solar-light. However, less understanding about reaction mechanism limits the practical realization of such vital process. Therefore, fundamental research in this field is very important to improve the photocatalytic efficiency of these systems.

This work is an assessment for the simultaneous molecular hydrogen production and organic pollutant degradation. Acetic acid (CH<sub>3</sub>COOH) has been used as a model organic pollutant and co-catalyst loaded TiO<sub>2</sub> as the photocatalyst. The parameters influencing the photocatalytic conversion of aqueous acetic acid into carbon dioxide (CO<sub>2</sub>), molecular hydrogen (H<sub>2</sub>), methane (CH<sub>4</sub>) and ethane (C<sub>2</sub>H<sub>6</sub>) employing co-catalysts loaded TiO<sub>2</sub> particles under anaerobic conditions have been investigated. Various metals and metal oxides such as Pt, Rh, Au, Ag, IrO<sub>2</sub>, and RuO<sub>2</sub> were loaded onto the surface of TiO<sub>2</sub> acting as efficient electron traps while facilitating the reduction reaction (*i.e.*, formation of H<sub>2</sub>). The evolved amounts of CO<sub>2</sub> and CH<sub>4</sub> were observed to increase in the following sequence: Ag/TiO<sub>2</sub> < Au/TiO<sub>2</sub> < Rh/TiO<sub>2</sub> < RuO<sub>2</sub>/TiO<sub>2</sub> < IrO<sub>2</sub>/TiO<sub>2</sub> < Pt/TiO<sub>2</sub>. On the contrary, the order in which evolved amounts of H<sub>2</sub> increased was relatively different. The formation rates of the main reaction products (CO<sub>2</sub>, H<sub>2</sub>, CH<sub>4</sub>, and C<sub>2</sub>H<sub>6</sub>) and their corresponding product distribution were observed to be strongly affected by both (1) the concentration of acetic acid, and (2) the loading of photocatalyst with various metals and metal oxides. The co-catalysts having higher values of work function were found to facilitate the H<sub>2</sub> evolution reaction at lower concentrations of acetic acid. Employing higher acetic acid concentrations, the reaction products consisting of a gas mixture enriched with hydrocarbons were obtained by using the co-catalyst with lower values of the work function (Ag and IrO<sub>2</sub>). The pH value of the employed suspension was found to play a key role in defining the reaction pathways for the photocatalytic decomposition of aqueous acetic acid. An increase in pH value from more acidic to more basic media was observed to result in entirely different ratios between evolved amounts of H<sub>2</sub> and hydrocarbons. For example, at pH 2 the ratio:  $\frac{n(\text{H}_2)}{n(\text{CH}_4)} = 0.6$ , which becomes:  $\frac{n(\text{H}_2)}{n(\text{CH}_4)} = 58$  at pH 9. Stoichiometric calculations for the evolved amounts of the main

## **Abstract**

reaction products clearly indicate the formation of other organic probe molecules during the photo-induced transformation of aqueous acetic acid. Depending on the pH value of the suspension, the photocatalytic degradation of acetic acid was observed to follow different reaction mechanisms. For the first time, isotopic labelling experiments were performed in order to interpret the results obtained from the light-induced conversion of aqueous acetic acid. These experiments were carried out mainly to see the origin of evolved H<sub>2</sub> and CH<sub>4</sub> by analysing the proton exchange reaction between acetic acid and water molecules. A detailed mechanism for the photocatalytic decomposition of aqueous acetic acid has been elucidated.

**Keywords:** photocatalysis, acetic acid, co-catalyst loaded TiO<sub>2</sub>, surface charge, H/D exchange reaction, solar fuel.

## Table of Contents

<b>1. Introduction</b> .....	<b>1</b>
1.1 Historical background.....	1
1.2 Literature survey.....	4
1.2.1 Molecular hydrogen and methane as energy fuels.....	4
1.2.1.1 H <sub>2</sub> production.....	4
1.2.1.2 CH <sub>4</sub> production.....	5
1.2.2 The principle of semiconductor photocatalysis.....	6
1.2.3 Semiconductor surface modifications.....	7
1.2.3.1 TiO <sub>2</sub> based photocatalysts.....	7
1.2.3.2 Noble metal co-catalysts.....	8
1.2.3.3 Metal-oxide co-catalysts.....	11
1.2.4 Acetic acid as an organic pollutant.....	13
1.2.4.1 Photocatalytic oxidation of aqueous acetic acid in the presence of air/O <sub>2</sub> .....	13
1.2.4.2 Photocatalytic conversion of aqueous acetic acid in the absence of air/O <sub>2</sub> .....	16
1.3 Objectives.....	19
<b>2. Materials and experimental methods</b> .....	<b>23</b>
2.1 Materials.....	23
2.2 Noble metals loaded TiO <sub>2</sub> .....	23
2.3 Metal-oxides loaded TiO <sub>2</sub> .....	24
2.4 Characterization techniques.....	24
2.4.1 X-ray diffraction.....	24
2.4.2 Transmission electron microscopy.....	25
2.4.3 Specific surface area measurements.....	25
2.4.4 Diffuse UV-vis spectroscopy.....	25
2.5 Photocatalytic measurements.....	25
2.6 Photonic efficiency determination.....	27
2.7 Nuclear magnetic resonance spectroscopy.....	28
<b>3. Results</b> .....	<b>29</b>
3.1 Material characterizations.....	29

## Table of Contents

3.1.1	Structural and optical properties .....	29
3.2	Photocatalytic experiments.....	35
3.2.1	Bare P25 TiO <sub>2</sub> as a photocatalyst.....	35
3.2.2	Surface modified TiO <sub>2</sub> as a photocatalyst.....	36
3.2.3	Effect of various acetic acid concentrations.....	40
3.2.4	Effect of different pH values.....	45
3.2.5	Isotopic labelling study .....	50
3.2.5.1	Formation of carbon dioxide .....	50
3.2.5.2	Formation of molecular hydrogen and molecular deuterium .....	52
3.2.5.3	Formation of methanes .....	56
3.2.5.4	Nuclear magnetic resonance study .....	60
<b>4.</b>	<b>Discussion.....</b>	<b>64</b>
4.1	General Remarks .....	64
4.2	Factors influencing the reaction rates and product distribution.....	67
4.2.1	Effect of co-catalyst .....	67
4.2.2	Effect of concentration .....	78
4.2.3	Effect of pH.....	84
4.2.4	Isotopic labelling studies.....	91
4.3	Mechanistic considerations.....	102
4.3.1	Basic processes for the photocatalytic degradation of aqueous acetic acid .....	102
4.3.2	Kolbe vs. Hofer-Moest reaction mechanism .....	109
4.3.3	Proton exchange reaction .....	110
<b>5.</b>	<b>Summary and conclusions.....</b>	<b>113</b>
<b>6.</b>	<b>References.....</b>	<b>120</b>
<b>7.</b>	<b>Appendix.....</b>	<b>132</b>
7.1	Additional information .....	132
7.2	Publications .....	135
7.3	Conferences and presentations .....	137
7.3.1	Oral presentations.....	137
7.3.2	Poster presentations.....	138
<b>8.</b>	<b>Curriculum vitae.....</b>	<b>CXXXIX</b>



## Abbreviations

SC	Semiconductor
XRD	X-ray Diffraction
TEM	Transmission Electron Microscopy
BET	Specific Surface Area (Brunauer-Emmett-Teller)
UV	Ultraviolet
Vis	Visible
QMS	Quadrupole Mass Spectrometer
NMR	Nuclear Magnetic Resonance
EPR	Electron Paramagnetic Resonance
HER	Hydrogen Evolution Reaction
NHE	Normal Hydrogen Electrode
PER	Proton Exchange Reaction
$c_0$	Initial Concentration
$n_0$	Initial Number of Moles

## Symbols

$\Delta G^0$	Gibbs Free Energy
$E_{CB}$	Conduction Band Edge
$E_{VB}$	Valance Band Edge
$E_g$	Band Gap Energy
$e_{CB}^-$	Conduction Band Electrons
$h_{VB}^+$	Valance Band Holes
$\Phi$	Work Function
$\zeta$	Photonic Efficiency
$\lambda$	Wavelength
$h$	Planck's Constant
$c$	Speed of Light

## Abbreviations

$I_0$	Number of Absorbed Photons
$N_A$	Avogadro Constant
$A$	Illuminated Area
$d$	Diameter
$\pi$	Mathematical Constant
$pK_a$	Dissociation Constant
$pH_{zpc}$	Point of Zero Charge
$\bullet OH$	Hydroxyl Radical
$\bullet CH_3$	Methyl Radical

## Units

TW	Terawatt
$\mu mol$	Micromole
h	Hour
mL	Mililiter
a.u.	Arbitrary Units
%	Percentage
wt %	Percentage by Weight
$^{\circ}C$	Grad Celsius
g	Grams
M	Molar Mass
v	Volume
L	Liter
J	Joule
eV	Electron Volt
mW	Milliwatt
cm	Centimeter
nm	Nanometer
$\text{\AA}$	Ångström

x

### 1. Introduction

Energy demands and related environmental problems are the growing concern of the present era. In 2010, the worldwide average energy consumption rate was  $\approx 15 - 17$  TW, which is expected to boost around  $25 - 27$  TW by 2050 [1]. Currently,  $\approx 85\%$  of world's energy requirements is fulfilled by the fossil fuels (Figure 1). However, the 21<sup>st</sup> century started with the realization to explore long term solutions for readily depleting fossil fuels, which dominated in the past. Other than the depletion, their combustion also results in the formation of carbon dioxide ( $\text{CO}_2$ ) being released directly into the environment which is a greenhouse gas and a primary contributor towards global warming [2]. In order to meet the world's energy demands, photocatalytic water splitting into molecular hydrogen ( $\text{H}_2$ ) and molecular oxygen ( $\text{O}_2$ ) as well as the photocatalytic reforming of aqueous organic/inorganic compounds from industrial wastes into value-added fuels (*i.e.*  $\text{H}_2$  and hydrocarbons) has been the focus of attention for scientists since the last four decades.

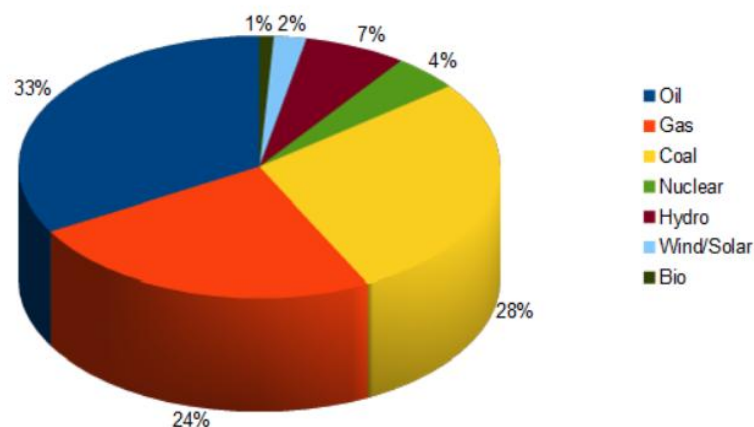


**Figure 1:** Global primary energy consumption by 2016 [3]

#### 1.1 Historical background

For the first time in 1911, the word 'photocatalysis' appeared in some scientific communications, almost 76 years later the term 'catalysis' introduced by Berzelius. Only preliminary experiments

## 1. Introduction

had been done in this field by 1970's [4-7]. However, in early 1970's, the first world's energy crisis came into view due to the economic situation in Arab petroleum exporting countries thus leading to the future scarceness of oil availability. This oil crisis then forced scientists to think about an alternative as well as renewable energy source. During this time (in 1972), two Japanese scientists, Fujishima and Honda [8], performed water ( $\text{H}_2\text{O}$ ) photolysis experiments on an electrochemical set-up employing rutile  $\text{TiO}_2$  as anode and platinum (Pt) as cathode. They used near UV light and obtained a water splitting reaction into  $\text{H}_2$  and  $\text{O}_2$ . The idea behind these experiments was to obtain  $\text{H}_2$  gas from solar light induced water splitting, which then can be used as a renewable energy fuel. In particular,  $\text{H}_2$  is a main energy-dense fuel and acquired from an abundantly available source ( $\text{H}_2\text{O}$ ). When  $\text{H}_2$  is used either in a fuel cell or burnt directly, it only generates  $\text{H}_2\text{O}$  in reversible reaction and does not result in any pollutants or greenhouse gases [9, 10]. The report published by Fujishima and Honda [8] opened new horizons for scientists to develop the possibilities for significant  $\text{H}_2$  production from immensely available sources *i.e.*,  $\text{H}_2\text{O}$  and sunlight. The concept of photocatalysis is actually generated from the natural photosynthesis process, where plants absorb solar energy from sunlight and convert it into the chemical energy (Figure 2).

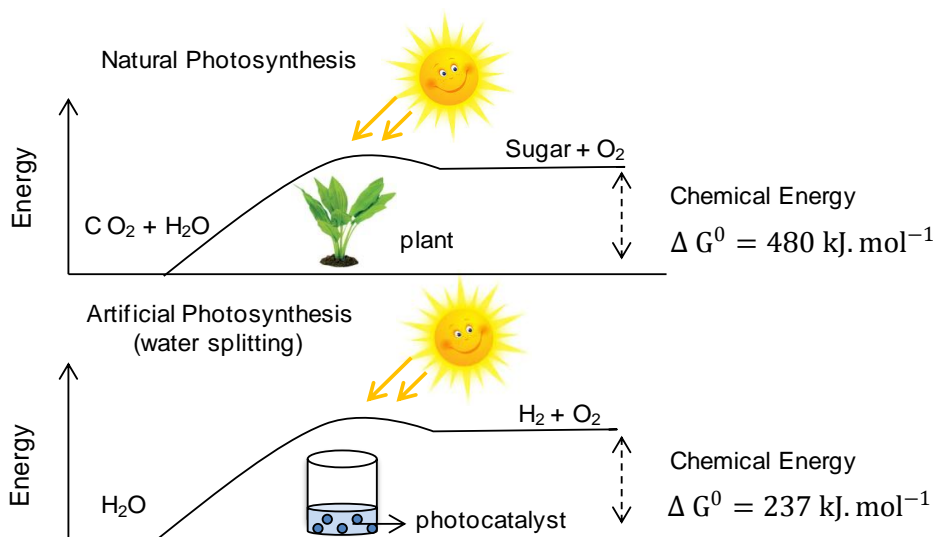


**Figure 2:** Natural photosynthesis vs. artificial photosynthesis.

## 1. Introduction

The chemical energy is stored in the bonds of glucose along with a huge positive change in the Gibbs free energy ( $\Delta G^0 = 480 \text{ kJ} \cdot \text{mol}^{-1}$ ) as shown in Figure 2. Similarly, the decomposition of  $\text{H}_2\text{O}$  molecule into  $\text{H}_2$  and  $\text{O}_2$  employing sunlight and a photocatalyst material mimics the natural photosynthesis reaction thus providing a very attractive method for the conversion of readily available solar energy into the chemical energy (*i.e.*,  $\text{H}_2$ ) [11, 12]. The solar  $\text{H}_2$  produced by this method can efficiently fulfill the world's electricity as well the chemical energy needs, by powering a small mobile phone to submarine [13].

In photocatalytic reactions, usually semiconductor (SC) materials are employed as photocatalysts [14]. According to the pioneering report published by Fujishima and Honda [8], a complete photocatalytic water splitting reaction was achieved only in the presence of a single-crystal titania ( $\text{TiO}_2$ ) anode and Pt cathode while applying an external bias along with UV irradiation. From a practical point of view, the fabrication of appropriate photo anode materials with suitable band gap structures is rather an expensive and complicated process. Therefore, by 1980's, the principle of photocatalytic SC cell was extended to the SC particulate suspension systems in order to obtain the required reactions.

The use of SC particulate system was first initiated by Bard and co-workers [15-17], where they employed Pt loaded  $\text{TiO}_2$  particles representing a short-circuit photoelectrochemical (PEC) cell. These SC particulate systems appeared to be cost effective as well as much simpler to synthesize in comparison to the single crystal SC electrodes. Moreover, the light absorption efficiency of suspensions can be much higher than SC electrodes. Another advantage of using the particulate system is that a variety of materials can be employed as photocatalysts which might not be available as single-crystal electrodes due to their high resistivity[18]. Finally, the photocatalytic particulate SC reaction systems exhibit a vast range of potential applications, when large-scale  $\text{H}_2$  production is considered [19].

On the contrary, in a photocatalytic reaction system, the SC particulates have very low spatial separation among oxidative and reductive sites hence giving rise to an undesired back reaction *i.e.*, formation of  $\text{H}_2\text{O}$  [17]. Thus, the efficiency of a photocatalytic water splitting reaction into  $\text{H}_2$  and  $\text{O}_2$  employing particulate system becomes very low in comparison to a PEC cell system. It has been reported in literature that by using photocatalytic particulate semiconductor systems, the  $\text{H}_2\text{O}$  decomposition reaction into  $\text{H}_2$  and  $\text{O}_2$  can only be obtained at higher temperature or reduced pressure values [20]. Therefore, according to the economical perspective, the

## **1. Introduction**

photocatalytic splitting of H<sub>2</sub>O into H<sub>2</sub> and O<sub>2</sub> seemed to be uncompetitive. Alternatively, many scientific reports are also published in literature demonstrating the mineralization of organic waste water by means of photocatalysis [21, 22]. Technical systems for the photocatalytic waste water treatment were already designed and tested successfully on the pilot plant scale [23-25]. However, at ambient temperature, the photocatalytic conversion of H<sub>2</sub>O into considerable amounts of H<sub>2</sub> employing semiconductor particles can only be obtained in the presence of organic/inorganic compounds *i.e.*, alcohols, carboxylic acids, and sulfides [13, 26-29]. Hence, simultaneous waste water treatment and H<sub>2</sub> evolution *via* photocatalysis has been recommended while employing a SC particulate system [30]. The advantage of this reaction system is that in one reaction, two important aspects of current era can be addressed *i.e.*, (1) formation of H<sub>2</sub>, which can be used as a fuel and (2) degradation of organic compounds present in waste water resulting from the industrial wastes thus solving the environmental problems.

Even though a large number of efforts have been made in the past 40 years after the initiative work of Bard and co-workers, a photocatalytic reaction system producing significant amounts of H<sub>2</sub> has not been achieved for its practical realization. So, it is very important to continue the fundamental research in this field with the aim to develop a reproducible and efficient reaction system in order to meet world's energy requirements, where H<sub>2</sub> can be used as a solar fuel and industrial waste can be converted into useful reaction products.

### **1.2 Literature survey**

#### **1.2.1 Molecular hydrogen and methane as energy fuels**

##### **1.2.1.1 H<sub>2</sub> production**

H<sub>2</sub> is amongst the most common elements present on the earth, while the occurrence of H<sub>2</sub> in its elemental form does not exist in significant amounts. Usually, it appears in H<sub>2</sub>O and biomass. At present, the primary sources for the production of H<sub>2</sub> gas include: organic wastes, hydropower, heavy oil, coal, solar and wind energy etc., [26]. Now a day, for the production of ammonia, H<sub>2</sub> gas is a pre-requisite. Also the use of H<sub>2</sub> in chemical processes *e.g.*, sulfur removal from gasoline, transformation of heavy hydrocarbons into the diesel fuel, etc., cannot be neglected. Therefore,

## 1. Introduction

the demand of H<sub>2</sub> gas is increasing day by day. Other than these traditional uses, the idea to use H<sub>2</sub> gas as an energy fuel is considered as a breakthrough in order to meet the worldwide energy requirements. The advantage of using H<sub>2</sub> gas as a transportation fuel is that the chemical energy stored in the H-H bond can be utilized by reaction with O<sub>2</sub> while forming H<sub>2</sub>O as the final product. Consequently the combustion of H<sub>2</sub> fuel will result in a pollution-free environment. Currently, the steam methane reforming (SMR) process has been used by the industries for the synthesis of H<sub>2</sub> gas [31]. However, SMR is a complicated process which involves many catalytic steps for the H<sub>2</sub> production. According to the present scenario, the conversion of wastewater, resulting mainly from industries, into H<sub>2</sub> and valuable fuels employing sunlight would be an intermediate step in-between the current fossil fuel reforming process and the dream of solar energy utilization for various applications. Thus, simultaneous H<sub>2</sub> production and organic pollutant degradation achieved in one reaction system employing solar light is assumed to provide a clean environment and long-term solutions for global energy needs.

### 1.2.1.2 CH<sub>4</sub> production

Almost 95% of natural gas consists of CH<sub>4</sub>, while it also contains other hydrocarbons such as ethane (C<sub>2</sub>H<sub>6</sub>) and propane (C<sub>3</sub>H<sub>8</sub>) in minor percentages. Generally, CH<sub>4</sub> is regarded as a clean energy fuel because its molecular structure is comprised of one carbon (C) atom attached to the 4 hydrogen (H) atoms. In comparison to the diesel which contains complicated long chain organic molecules and produces hazardous compounds upon its combustion, the burning of CH<sub>4</sub> results in the formation of minor amounts of CO<sub>2</sub> and water only ( $\text{CH}_4 + 2\text{O}_2 \rightarrow \text{CO}_2 + 2\text{H}_2\text{O} + \text{energy}$ ). While using it as a transportation fuel, CH<sub>4</sub> releases almost 29 % less CO<sub>2</sub> in the environment as compared to the diesel and petroleum. However, the current process (fossil fuels incineration) for CH<sub>4</sub> generation is not environment friendly and requires elevated temperature conditions. Also, the burning of fossil fuels, in order to produce CH<sub>4</sub>, directly releases dangerous gases to the environment thus contributing in the air pollution. Hence, the idea to produce CH<sub>4</sub> by photocatalytic conversion of industrial organic waste can simultaneously solve both energy and environmental problems.

## 1. Introduction

### 1.2.2 The principle of semiconductor photocatalysis

In photocatalytic reactions, semiconductor (SC) materials are of great importance with respect to their electronic structure and corresponding electronic properties. For instance, SC materials are comprised of a band structure which includes valence band (VB) and conduction band (CB), while the difference between VB and CB with an appropriate width is regarded as the band-gap energy ( $E_g$ ) of SC. The  $E_g$  of SC materials plays a key role while defining the wavelength sensitivity for its irradiation [32]. According to the electronic properties of a SC, it can be further categorized as a (1) direct band-gap and (2) indirect band-gap semiconductor. For example, cadmium sulfide and zinc sulfide which are direct band-gap SC materials having higher absorption coefficients and exhibit a steep absorption onset. In comparison to this,  $TiO_2$  which is an indirect band-gap SC material shows an absorption tail and flat onset [32].

Upon illumination, a SC material absorbs photons having energy equal or higher than its  $E_g$ . As a result, electrons ( $e^-$ ) and holes ( $h^+$ ) are generated in the CB and VB of SC, respectively. These photo-generated charge carriers (conduction band electrons ( $e_{CB}^-$ ) and valence band electrons ( $h_{VB}^+$ )) can either migrate to the SC surface or they can recombine while releasing energy in the form of heat/photons. The direct photocatalytic water splitting for  $H_2$  production is mainly limited by the fast recombination rate of photo-generated charge carriers, which results in a poor photocatalytic activity [14]. However in a photocatalytic reaction, where organic pollutants are employed as sacrificial reagents and a metal is loaded on the surface of the photocatalyst [33-37] (Figure 3), efficient oxidation and reduction reactions are carried out by the photo-generated charge carriers ( $h_{VB}^+$  and  $e_{CB}^-$ ). For example, adsorbed molecules of  $H_2O$  and employed organic pollutant oxidized by  $h_{VB}^+$  lead to the formation of  $H^+$ ,  $\bullet OH$ ,  $\bullet R$  intermediates and other reaction products. On the other hand, at the same time, a reduction reaction mainly at the surface of metal loaded onto the SC particles is carried out by the  $e_{CB}^-$  leading to the formation of  $H_2$  as a final product.



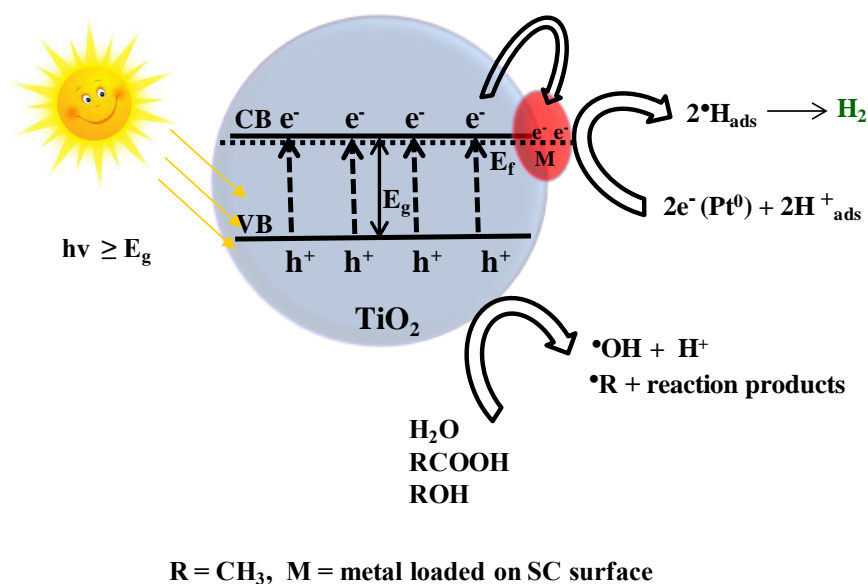


**Figure 3:** Basic principle of photocatalysis employing metal loaded semiconductor (SC) particulate system and aqueous organic pollutant.

### 1.2.3 Semiconductor surface modifications

#### 1.2.3.1 TiO<sub>2</sub> based photocatalysts

A wide variety of semiconductor (SC) materials has been employed as photocatalysts [38]. Among various n-type SC materials, titanium dioxide (TiO<sub>2</sub>) is found to be one of the most active photocatalysts for the hydrogen evolution reaction (HER) till date [14, 39, 40]. On one side, its low cost, high stability and non-toxic nature, and on the other side, its suitable electronic band alignments such as position of conduction band (CB) and valence band (VB) to achieve a simultaneous redox reaction for aqueous organic compound decomposition makes TiO<sub>2</sub> one of the most attractive photocatalysts [40]. A large number of reports have been published in literature demonstrating the efficient photocatalytic activities employing TiO<sub>2</sub> for HER [33, 34, 41-44]. In general, the photocatalytic activity by using bare TiO<sub>2</sub> particles even in the presence of organic electron donors is very low. Therefore, TiO<sub>2</sub> has been used with various surface modifications, so that an efficient amount of H<sub>2</sub> can be produce.

## 1. Introduction

### 1.2.3.2 Nobel metal co-catalysts

The activity of a photocatalytic reaction is primarily reliant on the efficient separation of photo-generated charge carriers (*i.e.*,  $e_{CB}^-$  and  $h_{VB}^+$ ) and their transport. However, the fast recombination of photo-generated charge carriers is one of the biggest limitations in this field and hence very challenging to overcome. In order to solve the complexity of rapid  $e_{CB}^-$  and  $h_{VB}^+$  recombination, metal/SC heterojunction systems have been used extensively. Usually, noble metals are loaded on the surface of SC material where they play a key role while improving the efficiency for hydrogen evolution reaction (HER) [45-49].

When noble metals are deposited on the semiconductor (SC) surface, the migration of photo-generated charge carriers is significantly enhanced instead of their prompt recombination [50, 51]. Typically, in metal/SC heterojunction systems, a Schottky barrier is formed at the metal/SC interface due to which noble metals act as efficient electron traps while facilitating the reduction reaction (*e.g.*, formation of  $H_2$ ) [52]. In addition to this, the noble metals and SC material have different Fermi level positions ( $E_f$ ). Therefore, when they combine with each other, the electrons start migrating from the CB of SC located at more negative values to the CB of metal having comparatively more positive values. As a result, the metal surface gets saturated with electrons while leaving the SC depleted with electrons. Due to the excess negative charges appeared at the metal/SC interface, the SC bands bend in the direction of metal/SC contact. Hence, this formed barrier is called a Schottky barrier which acts as to hinder the unwanted back reaction *e.g.*, reverse transport of electrons to the SC as shown in Figure 4 [40]. During a photocatalytic reaction, when photo-generated  $e_{CB}^-$  are trapped at the surface of so called co-catalyst (noble metals), the photogenerated  $h_{VB}^+$  remain at the surface of host SC photocatalyst thereby facilitating the efficient charge separation [53, 54].

In particular, the concept of Schottky barrier formation is recommended for photoelectrochemical (PEC) cell, where an interfacial contact is developed between metal (*e.g.*, Pt electrode) and n-type SC (*e.g.*,  $TiO_2$  electrode). Conversely, in particulate systems where the surface of SC is loaded with metal nanoparticles, the formation of a Schottky barrier could be highly questionable. For instance, Litter *et al.* [55] reported the formation of different oxidation states for Pt nanoparticles as  $Pt^0$ ,  $Pt^{+2}$  and  $Pt^{+4}$  while employing Pt/ $TiO_2$  particles.

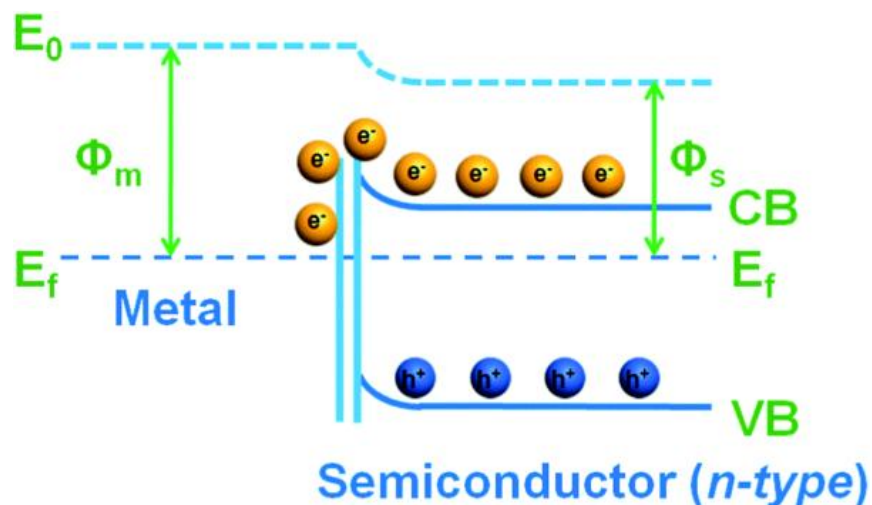


**Figure 4:** Formation of a Schottky barrier at the metal/SC interface in the equilibrium.  $E_f$  = Fermi level of metal,  $E_0$  = vacuum level,  $\Phi_M$  = the work function of metal,  $\Phi_S$  = Schottky barrier height [54].

One of the most important parameter while choosing the suitable co-catalyst is its work function ( $\Phi$ ) value. The  $\Phi$  is defined as the energy needed to transfer an electron from the  $E_f$  to the vacuum. The higher  $\Phi$  means a lower  $E_f$  and bigger energy difference between metal/SC interface thus enhancing photo-generated charge separation [56].

Typically, two methods are commonly used for the deposition of metal nanoparticles on the surface of photocatalyst: (1) Impregnation method, where the specific metal precursor in the form of solution is mixed with the photocatalyst. Afterwards, a thermal treatment is given to this mixture according to the desired co-catalyst requirements [53]. (2) The second method is called as: *in-situ* photodeposition, where the mixture of SC powders and specific metal ions is irradiated in the presence of an appropriate holes scavenger. The metal cations are reduced by the SC electrons thus creating active sites on the SC surface in the form of metal nanoparticles [53]. Eastman *et al.* [57] examined the effect of various metal loadings including platinum (Pt), gold (Au) and silver (Ag) on the surface of  $\text{TiO}_2$ . In their studies, Pt was found to be the most active co-catalyst followed by Au and Ag. The author explained the difference in the catalytic activities with respect to the  $\Phi$  values of the employed metal. For instance, the  $\Phi_{\text{Pt}} = 5.65$  eV,  $\Phi_{\text{Au}} = 5.10$  eV and  $\Phi_{\text{Ag}} = 4.00$  eV. Anpo *et al.* [58] studied the light-induced electron transfer reaction from  $\text{TiO}_2$  to Pt particles *via* electron spin resonance (EPR) spectroscopy. Anpo and co-workers

## 1. Introduction

observed that the presence of Pt islands on the surface of  $\text{TiO}_2$  results in a reduced  $\text{Ti}^{3+}$  species meaning that the significant electron migration occurs from  $\text{TiO}_2$  to the Pt particles. The electrons gathered at Pt particles can then react with the surface adsorbed protons ( $\text{H}^+$ ) thus reducing the  $\text{H}^+$  into hydrogen atoms ( $\text{H}^\bullet$ ). These adsorbed  $\text{H}^\bullet$  subsequently combine with each other while forming  $\text{H}_2$  as a reaction product. They also stated that the  $\text{H}_2\text{O}$  reduction overpotential is reduced in the presence of Pt nanoparticles, so a significant hydrogen evolution reaction (HER) can be obtained. Nevertheless, depending on the electronic structures of various photocatalysts, Pt does not always illustrate the highest photocatalytic activity when compared with other noble metal co-catalysts. Hara *et al.* [59] observed the effect of numerous metal loadings on tantalum oxynitride (TaON) photocatalysts and found only Ru/TaON as an active photocatalyst. Their study showed that the deposition of Pt, Ir and Rh on the surface of TaON results in a poor HER as compared to Ru/TaON. The authors related this observation with the electronic properties developed in between the Ru and TaON, which efficiently promote the electron transfer from TaON to Ru. In another study, Kennedy *et al.* [60] demonstrated the bimetallic/ $\text{TiO}_2$  particulates resulting in a significant HER. They deposited Au-Ag particles on the surface of  $\text{TiO}_2$  and compared the obtained results with those acquired by the deposition of Au and Ag separately on the surface of  $\text{TiO}_2$ . The enhanced amounts from HER were observed by Kennedy and co-workers only in the presence of bimetallic/ $\text{TiO}_2$  particles. They claimed that the presence of two metals on  $\text{TiO}_2$  surface leads the electron transportation from one metal surface to another, hence resulting in the longer life time of photo-generated charge carriers thus significantly increasing the amounts of  $\text{H}_2$  formation.

Recently, Chen *et al.* [61] published a report exhibiting the comparison between the employment of expensive metal (Au) and low cost metallic Nickel (Ni) nanoparticles onto  $\text{TiO}_2$  for HER. They prepared Ni nanoparticles with particle size ranging between of 1- 2 nm, and provided experimental evidences confirming the formation of  $\text{Ni}^0/\text{TiO}_2$  as the leading Ni specie. The authors claimed that the comparative amounts of  $\text{H}_2$  were produced while employing Au/ $\text{TiO}_2$  and Ni/ $\text{TiO}_2$  as photocatalysts. Chen and co-workers also claimed that Ni particles were highly dispersed on the surface of  $\text{TiO}_2$ , and can be efficiently employed as a replacement of expensive noble metal co-catalysts *e. g.*, Pt or Au. This means that, while choosing a suitable co-catalyst, the high  $\Phi$  value of metal co-catalysts is not the only parameter that should be considered. There are other factors that should not be neglected, for instance, the size of metal nanoparticles, the

physical characteristic of interface between the metal and SC, and the contact between metal ions and the photocatalyst surface, etc., [62].

### 1.2.3.3 Metal-oxide co-catalysts

In general, there are two main properties a co-catalyst should have: (1) the ability to extract either photo-generated  $e_{CB}^-$  or  $h_{VB}^+$  from the surface of photocatalyst, and (2) the capability to create active reaction sites while decreasing the activation energy for the gas formation. Even though noble metal co-catalysts act as competent electron traps, a major drawback of their utilization is that they also catalyze the undesired reverse reaction, *e.g.*,  $H_2O$  formation from the dissolved  $H_2$  and  $O_2$  in the suspension system [63]. In addition to this, the higher cost of noble metals limits their practical realization. Therefore, research has now also focused on the use of transition metal oxides *e.g.*,  $Ru_2O$ ,  $IrO_2$ ,  $Cu_xO$ ,  $CuO$  as co-catalysts. However, depending on their oxidation states, metal oxides often facilitate the oxidation reaction such as the degradation of  $H_2O$  or employed organic pollutant molecules [13, 64-67].

Foo and co-workers [68] studied the effect of copper (II) oxide ( $CuO$ ) nanoparticles on the  $TiO_2$  surface for HER. In their work, three types of copper such as  $Cu-CuO-Cu_2O$  were detected during different reaction stages. The authors state that the  $Cu$  is reduced to  $Cu_2O$  during the photocatalytic reaction. They also observed the formation of  $Cu-Cu_2O$  where  $Cu$  served as a core and  $Cu_2O$  depicts the formation of thin shells around  $Cu$  core. Hence, the significant amount of  $H_2$  formation was attributed in their studies to the high surface area of  $Cu-Cu_2O_{thin\ shell}/TiO_2$  particles and the corresponding less surface defects. In another study, Moon *et al.* [69] showed that the size-tunable  $CuO$  nanodots deposited on the  $TiO_2$  surface result in an enhanced amount of  $H_2$  formation. In the presence of a sacrificial reagent, they observed the reduction of  $CuO$  nanoparticles into  $Cu^0$ . The  $Cu$  nanoparticles then fulfil the requirements of an efficient electron trap while acting as a co-catalyst and assisting the reduction reaction *i.e.*, formation of  $H_2$ . They asserted that the  $H_2$  formation rates obtained by the employment of  $Cu$  nanodots/ $TiO_2$  particulate systems could reach to the half of the  $H_2$  formation rate achieved by expensive  $Pt/TiO_2$  system.

In many studies,  $RuO_2$  has also been investigated and assumed to be an appropriate co-catalyst for HER due to its metallic characteristics [70]. Recently, Uddin *et al.* [71] examined the role of  $RuO_2$  loadings for HER on the surface of mesoporous  $TiO_2$  particles. The mechanistic studies

## 1. Introduction

have been carried out in their work *via* EPR spectroscopy. The obtained results from EPR investigations for the bare TiO<sub>2</sub> particles demonstrated fewer amounts of trapped electrons (Ti<sup>3+</sup>) and trapped holes (O<sup>-</sup>). On the other hand, RuO<sub>2</sub>/TiO<sub>2</sub> particles revealed the generation of Ti<sup>3+</sup> and O<sup>-</sup> species in much higher amounts. This means that deposition of RuO<sub>2</sub> onto the surface of TiO<sub>2</sub> gives an efficient photo-generated charge separation thus leading to an enhanced amount of H<sub>2</sub> formation. In comparison to this, the recombination of photo-generated charge carriers was observed to be very high in case of bare TiO<sub>2</sub> and was confirmed by the EPR signal intensity. Moreover, the authors also observed that the amount of co-catalyst loading is a very important parameter and should be chosen appropriately. Uddin and co-workers found 5 wt % RuO<sub>2</sub>/TiO<sub>2</sub> as the optimized photocatalyst while exhibiting H<sub>2</sub> formation rate as 618 μmol h<sup>-1</sup>. Conversely, bare TiO<sub>2</sub> produced only 29 μmol h<sup>-1</sup> in their experiments. They ascribed significant amount of H<sub>2</sub> formation to the favourable band-bending which occurs at the RuO<sub>2</sub>/TiO<sub>2</sub> interface.

Nevertheless, the use of metal oxides as co-catalysts mainly for HER is a tricky process and, therefore, requires an activation treatment. For example, special synthesis parameters are applied to achieve an appropriate oxidation state that should be suitable to attain an efficient HER [72, 73]. Also, there appear limitations while applying this approach for some photocatalyst materials e.g., oxynitrides, which are thermally unstable and cannot stand with all the treatments required to acquire desired oxidation states for transition metal oxides co-catalysts [74]. Hence, it has been suggested by Domen *et al.* [75] that the utilization of dual co-catalysts consisting of a metal core such as Rh, Ir, Pt and a metal oxide shell such as Cr<sub>2</sub>O<sub>3</sub> can solve this difficulty to some extent. Another advantage of employment of these core-shell particles is that they can be deposited on the surface of photocatalysts by a simple *in-situ* photodeposition method.

Moreover, Khan *et al.* [76] illustrated the effect of dual co-catalyst in one of their latest reports where one co-catalyst is considered to lead the reduction reaction and other improves the simultaneous oxidation reaction. In their studies, experiments were performed by using CoO<sub>x</sub>/TiO<sub>2</sub> and Palladium (Pd)/CoO<sub>x</sub>/TiO<sub>2</sub> composites. It has been observed by Khan and co-workers that the presence of CoO<sub>x</sub> on the surface of TiO<sub>2</sub> acts as to scavenge h<sub>VB</sub><sup>+</sup> from TiO<sub>2</sub> instead of their reduction into Co<sup>2+</sup> hence resulting in an enhanced amount of H<sub>2</sub> formation. Further analysis of their data depicts that the deposition of Pd nanoparticles onto the composite CoO<sub>x</sub>/TiO<sub>2</sub> increased the H<sub>2</sub> formation to a great extent. They stated that the transfer of electrons arises from the VB of CoO into the VB of TiO<sub>2</sub> thus improving the oxidation reaction for H<sub>2</sub>O

molecules. At the same time, Pd nanoparticles provide more reduction sites hence improving the formation of  $H_2$ . In this way, the undesired back reaction *i.e.*, formation of  $H_2O$ , can be overcome.

### 1.2.4 Acetic acid as an organic pollutant

Generally, in photocatalytic reforming reactions, alcohols, formaldehydes and carboxylic acids are employed as organic pollutants acting as sacrificial reagents [13]. Acetic acid ( $CH_3COOH$ ) is one of the common organic compounds resulting from industrial waste. At higher temperatures ( $> 39\text{ }^\circ\text{C}$ ) values, the concentrated form of acetic acid converts into explosive vapours [77], so its degradation is very important. At present, the decomposition of acetic acid is widely carried out by the acidolysis process. A major drawback of the acidolysis method is the requirement of elevated temperatures and special experimental conditions [78]. However, the conversion of acetic acid by means of photocatalysis into useful fuels is an environment friendly procedure that doesn't necessitate expensive experimental techniques and high temperature conditions. The photocatalytic decomposition of aqueous acetic acid has been reported under both: (1) aerobic (in the presence of air/ $O_2$ ) [79-81], and (2) anaerobic (in the absence of air/ $O_2$ ) [37, 82, 83] conditions. However, depending on different reaction conditions, the reaction products and their distribution were observed to vary greatly.

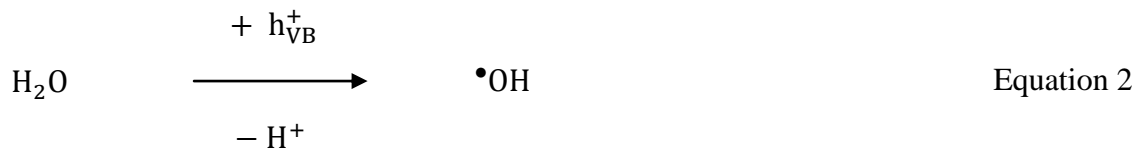
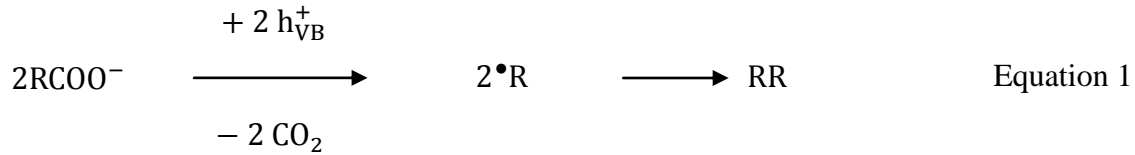
Usually, the photocatalytic degradation of aqueous acetic acid results in the formation of alcohols and organic acids *e.g.*,  $CH_3OH$ ,  $HCHO$ ,  $HCOOH$ ,  $HOCH_2COOH$ , and  $OHCCOOH$  etc., as final reaction products in an air/ $O_2$  atmosphere [79]. On the other hand, the photocatalytic conversion of aqueous acetic acid in the absence of air/ $O_2$  yields  $H_2$  and hydrocarbons (*i.e.*,  $CH_4$  and  $C_2H_6$ ) in significant amounts which can be used as renewable solar fuels [83].

#### 1.2.4.1 Photocatalytic oxidation of aqueous acetic acid in the presence of air/ $O_2$

For a typical reaction system containing SC photocatalyst, the photocatalytic oxidation of carboxylic acids follows a photo-Kolbe reaction mechanism [84]. An electrochemical reaction in which the decomposition of aqueous carboxylic acid ( $RCOOH$ ,  $R = CH_3$ ) results in the formation of  $CO_2$  as the primary reaction product and  $\bullet R$  as the primary reaction intermediate is called a

## 1. Introduction

Kolbe reaction as shown in Equation 1 [85, 86]. Here, the initial step of the Kolbe mechanism includes a reaction between the semiconductor (SC) surface adsorbed carboxylic acid molecule and the photo-generated SC  $h_{VB}^+$  (Equation 1). At the same time, the adsorbed  $H_2O$  molecules on the surface of SC material react with  $h_{VB}^+$  and result in the formation of  $\bullet OH$  and  $H^+$  (Equation 2).



During the light-induced oxidation of acetic acid/acetate under aerobic conditions, the Kolbe reaction intermediate ( $\bullet CH_3$ ) further reacts with the  $O_2$  adsorbed on the surface of SC thus forming  $\bullet O_2CH_3$  (Equation 3).



Moreover, a non-Kolbe reaction between acetic acid/acetate molecule and  $\bullet OH$  occur simultaneously giving  $\bullet CH_2COO^-$  as a reaction intermediate (Equation 4). Subsequently, the formed  $\bullet CH_2COO^-$  reacts with the SC adsorbed  $O_2$  molecules yielding  $\bullet O_2CH_2COO^-$  (Equation 5).



Wolff and co-workers [80] studied the photocatalytic decomposition of aqueous acetate solutions in the presence of  $O_2$  while employing  $TiO_2$  as a photocatalyst. Due to the presence of air/ $O_2$  acting as an electron scavenger, the presence of a co-catalyst at the  $TiO_2$  surface was not



## 1. Introduction

necessary in their experiments. Wolff *et al.* investigated the effect of varying pH values from acidic to alkaline region and observed that the reaction mechanism follows two different pathways: (1) at pH values < 6, the reaction proceeds through direct oxidation of acetic acid molecule by TiO<sub>2</sub> valence band hole (h<sub>VB</sub><sup>+</sup>) yielding Kolbe intermediate (Equation 1). While, (2) at pH values > 6, an indirect reaction path exists for the photocatalytic decomposition of acetate, where the acetate molecule reacts with a hydroxyl radical (<sup>•</sup>OH) (Equation 4).

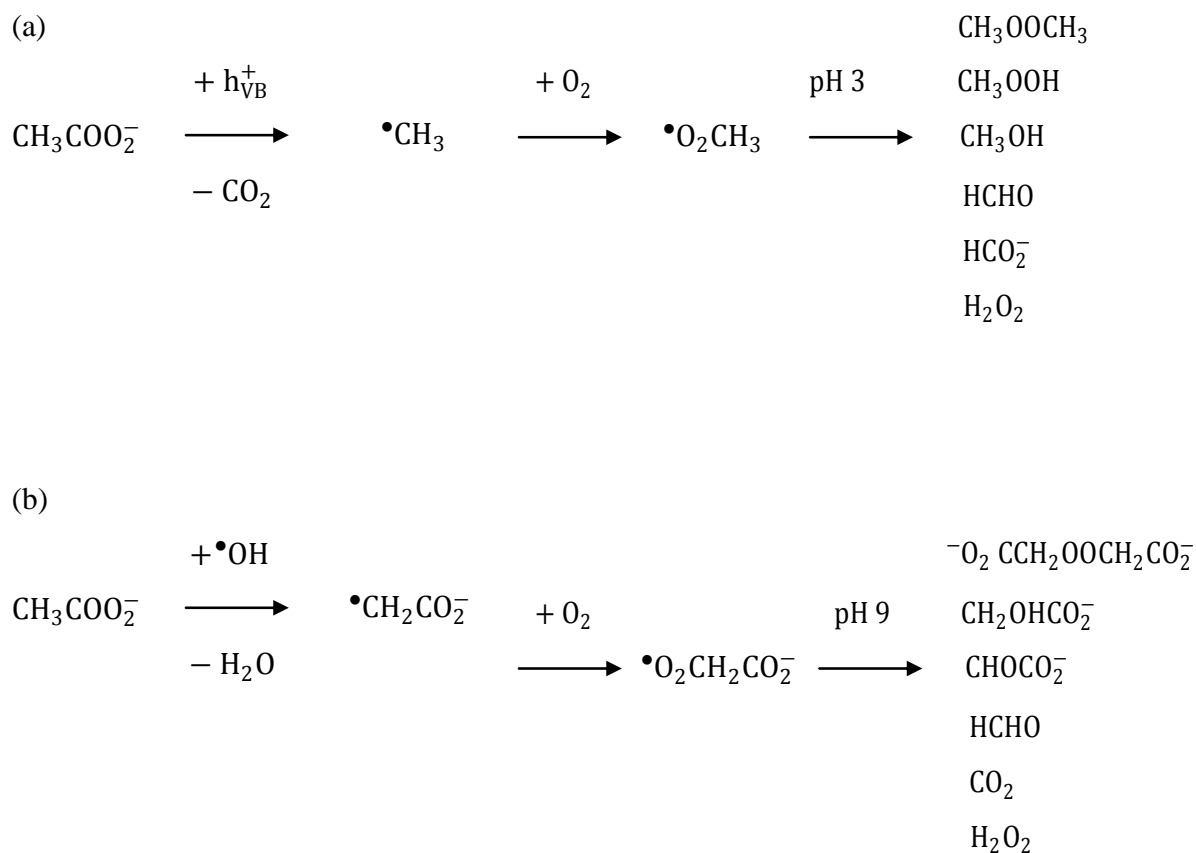


**Figure 5:** proposed reaction mechanism for the photocatalytic decomposition of aqueous acetate at (a) pH 3, (b) pH 9 [81].

Belhadj *et al.* [81] examined the photocatalytic oxidation of aqueous acetate in the presence of air/O<sub>2</sub> via ATR-FTIR and EPR spectroscopy. Their FTIR analysis showed that the change in pH values from more acidic to more basic region results in the adsorption of acetate molecule on the

## 1. Introduction

surface of TiO<sub>2</sub> with different orientations. For instance, at acidic pH values the adsorption of acetate molecule onto the surface of TiO<sub>2</sub> occurred in the form of bidentate structure while basic pH favours the adsorption of acetate in the form of monodentate structure. This means that the major and minor reaction products at different pH values would be different. Through EPR investigations, they also confirmed that the photocatalytic oxidation of aqueous acetate by h<sub>VB</sub><sup>+</sup> is a dominant reaction pathway for pH < 7 while the reaction proceeds by the oxidation of acetate molecule with •OH at pH ≥ 7. These observations were related to the intensity of EPR signals at different pH values. A reaction scheme leading to different reaction products at different pH regions has been reported by Belhadj and co-workers (Figure 5) [81].

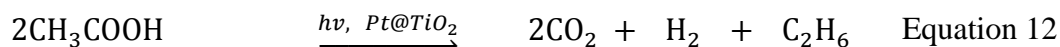
### 1.2.4.2 Photocatalytic conversion of aqueous acetic acid in the absence of air/O<sub>2</sub>

About 40 years ago, numerous reports were published by Bard and co-workers [36, 87, 88] where they discussed the photo-induced transformation of aqueous acetic acid into H<sub>2</sub>, CH<sub>4</sub>, C<sub>2</sub>H<sub>6</sub> and CO<sub>2</sub> as the primary reaction products under anaerobic conditions. They investigated both Pt/TiO<sub>2</sub> particles as well as Pt/TiO<sub>2</sub> electrode systems. As a general conclusion, the authors stated that the photocatalytic degradation of aqueous acetic acid in the absence of air/O<sub>2</sub> proceeds by a photo-Kolbe reaction mechanism (Equation 1). Subsequently, the formation of alkanes is expected by the reaction of primary intermediates as given in Equations 6 – 10 [89].



During the light-induced decarboxylation reaction of aqueous acetic acid, the occurrence of •CH<sub>3</sub> as a primary reaction intermediate has been confirmed by Kraeutler *et al.* [84] via EPR spectroscopy. Hence, the overall reaction mechanism for the photocatalytic degradation of aqueous acetic acid (CH<sub>3</sub>COOH) in acidic pH media was expressed as follow (Equation 11 – 12) [36, 84, 87]:

## 1. Introduction



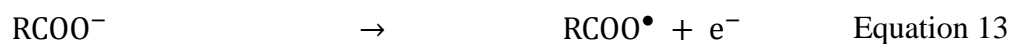
However, no proof for the stoichiometric reaction (Equation 11 - 12) by the complete degradation of employed acetic acid concentration can be found in literature. Yoneyama *et al.* [90] investigated the parameters affecting the distribution of reaction products during photocatalytic decomposition of aqueous acetic acid employing Pt/TiO<sub>2</sub> particles both in the absence and in the presence of Pd<sup>2+</sup> acting as an oxidizing agent. They observed the formation of H<sub>2</sub> and C<sub>2</sub>H<sub>6</sub> as minor reaction products while CH<sub>4</sub> and CO<sub>2</sub> as main reaction products in the absence of Pd<sup>2+</sup>. In their study, CH<sub>4</sub> was found to be the major reaction product with higher yields, even in the presence of Pd<sup>2+</sup>, where H<sub>2</sub> production was completely suppressed. They claimed that the deposition of Pd<sup>2+</sup>, a H<sub>2</sub> generation catalyst, acts as an electron scavenger in the solution during photo-deposition process and therefore suppresses the hydrogen evolution reaction. Yoneyama and co-workers also examined the reaction kinetics by varying the light intensity. They found a linear relationship between the formed amount of •CH<sub>3</sub> resulting from decarboxylation of acetic acid and the light intensity of the employed lamp. Moreover, the effect of different acetic acid concentrations (1 – 8.2 M) has also been studied by Yoneyama and co-workers [90]. They observed that the increase in the concentration of acetic acid from 1 – 5 M also results in an enhanced formation rates for all reaction products, while further increase in the concentration was found to result in lowering the formation rates for all reaction products.

Recently, Mozia *et al.* [35, 91-94] published a series of papers conferring the photocatalytic degradation of aqueous acetic acid under anaerobic conditions while utilizing TiO<sub>2</sub> with various surface modifications (such as Fe, Fe<sub>3</sub>O<sub>4</sub>, Fe<sub>2</sub>O<sub>3</sub> and CuO). In all of their studies, H<sub>2</sub>, CO<sub>2</sub>, and CH<sub>4</sub> were observed as main reaction products while C<sub>2</sub>H<sub>6</sub> and C<sub>3</sub>H<sub>8</sub> were detected as the minor reaction products. However, the formation rates of these reaction products were observed to vary with respect to the TiO<sub>2</sub> surface modifications. For instance [35], Fe-modified TiO<sub>2</sub> exhibits a significant amount for HER and CH<sub>4</sub> only when 20 wt % Fe/TiO<sub>2</sub> powders were calcined at 500 °C. They also stated that an increase in the acetic acid concentration from 0.01 to 1 M results in the enhanced amounts of all reaction products, whereas, the formation rates of all reaction products start to decrease at higher concentration values. Mozia and co-workers [91] also

## 1. Introduction

investigated the effect of CuO nanoparticles over TiO<sub>2</sub> (rutile) photocatalyst. They did not observe significant HER in these experiments, while considerable amounts of CO<sub>2</sub> and CH<sub>4</sub> were obtained when CuO/TiO<sub>2</sub> (rutile) was employed as a photocatalyst. In another study, Heciak *et al.* [95] utilized CuO/TiO<sub>2</sub> composites mainly for the photocatalytic transformation of aqueous acetic acid into H<sub>2</sub>. The presence of metallic Cu nanoparticles was confirmed by XRD measurement. Higher formation rates for all reaction products were observed only when both CuO and Cu<sub>2</sub>O were present on the TiO<sub>2</sub> surface.

Sakata *et al.* revealed that the change in pH values from acidic to basic media leads to the different reaction mechanisms during photocatalytic decomposition of aqueous carboxylic acids. They examined aqueous acetic, propionic and butyric acids employing Pt/TiO<sub>2</sub> (anatase, rutile) particles. By doing both liquid phase and gas phase analysis for all employed carboxylic acids, they observed that the photo-decomposition of carboxylic acid proceeds by a photo-Kolbe reaction only at pH < 7. On the other hand, in alkaline pH media (pH > 7) the photo-Kolbe reaction occurs only as a minor reaction. There exists another mechanism known as Hofer-Moest reaction for the light-induced decomposition of carboxylic acids. According to which, the carboxylate anions discharged anodically (Equation 13) while forming  $\bullet\text{R}$  and CO<sub>2</sub>. However, in the subsequent reactions, alcohols, olefins and aldehydes are formed as reaction products [96, 97]. The Hofer-Moest reaction is expressed in Equations 13 – 16.



Following the Hofer-Moest reaction, at pH values > 7, the overall reaction for complete degradation of aqueous acetic acid can be explain as follow (Equation 17):



For deep insight about the reaction mechanism of photocatalytic aqueous acetic acid degradation, only two reports are present in literature discussing the isotopic labelling experiments. The

## 1. Introduction

experiments were performed to see the origin of H<sub>2</sub>, and CH<sub>4</sub> formation during photocatalytic decomposition of aqueous acetic acid. Bard and co-workers [84] examined the influence of mono-deuterated aqueous acetic acid in a photocatalytic reaction by using Pt/TiO<sub>2</sub> as a photocatalyst. In their study, for HER, the reaction system Pt/TiO<sub>2</sub>-CH<sub>3</sub>COOD-H<sub>2</sub>O was found to exhibit the formation of D<sub>2</sub>: HD: H<sub>2</sub> as reaction products with a ratio of 2: 1.1: 0.6, respectively. Moreover, the analysis for methane depicts the formation of CH<sub>3</sub>D ≈ 45 % and CH<sub>4</sub> ≈ 55 % as reaction products. It has been argued by authors that there does not occur any proton exchange reaction at the methyl group (CH<sub>3</sub>) of acetic acid while the H<sub>2</sub> was formed by H<sup>+</sup> coming either from H<sub>2</sub>O or carboxylic group (COOH) of acetic acid. Sakata *et al.* [37] also carried out isotopic labelling experiment with a reaction system containing Pt/TiO<sub>2</sub>-CH<sub>3</sub>COOH-D<sub>2</sub>O. The photocatalytic experiments were performed in the presence and in the absence of AgNO<sub>3</sub> as an electron scavenger. Sakata and co-workers performed these experiments mainly to see the reaction pathways for CH<sub>4</sub> formation. Their data analysis revealed that without the employment of AgNO<sub>3</sub>, the main reaction product was CH<sub>3</sub>D while the presence of AgNO<sub>3</sub> gives rise to the formation of CH<sub>4</sub> as a major reaction product.

Huck *et al.* [98] investigated the light-induced proton exchange reaction in carboxylic acids *via* photolysis. Their studies demonstrated that the carboxylic acids formed methyl substituted aromatic ketones upon illumination. Hence, the methyl group becomes activated and, in the presence of D<sub>2</sub>O as a solvent, a fast proton exchange reaction is very likely to occur at the methyl group of carboxylic acid. Recently, Mirich *et al.* [99] inspected the gas-phase heterogeneous catalytic reaction to scrutinize the proton exchange reactions for decomposition of carboxylic acids. The authors found that in the presence of a suitable catalyst (Pd/Al in their study), a proton exchange reaction at the methyl group of carboxylic acid occurs at elevated temperature values.

### 1.3 Objectives

Recently, the synthesis of large variety of new photocatalytic materials has been the focus of research in order to obtain competent HER. However, mechanistic aspects of photocatalytic reaction system while utilizing the standard SC materials (i.e., TiO<sub>2</sub>) are still unclear. Moreover, photocatalytic test reactions are usually performed in the laboratories *via* a classical gas chromatograph (GC) system attached to a batch photoreactor. The long term experiments over a

## 1. Introduction

large scale of time cannot be carried out in batch system due to the overpressure in the photoreactor. Also, a GC does not allow doing any isotopic labelling studies while permitting only limited detection of gases (*i.e.*, H<sub>2</sub>, CO<sub>2</sub>, and O<sub>2</sub>). Therefore, in this work, we have used a photoreactor attached to the quadrupole mass spectrometer (QMS) which allows continuous detection of all gaseous products evolved during the photocatalytic reaction.

The scientific objective of this thesis is not the development of new photocatalytic materials but the elucidation of the mechanistic aspects during the photocatalytic aqueous organic pollutant degradation into value-added fuels (*i.e.*, H<sub>2</sub>, hydrocarbons) employing Pt/TiO<sub>2</sub> as a photocatalyst. The Pt/TiO<sub>2</sub> particles employed in this work have been synthesized *via* an impregnation method and were provided by H.C. Starck Company (Goslar, Germany) within the frame work of a joint BMBF project ('Duasol'). Here, acetic acid, which is hazardous and highly corrosive in its concentrated form, and exists in the industrial wastes, has been chosen as a model organic compound. Generally, the mineralization of acetic acid requires expensive experimental techniques. Comparatively, the conversion of aqueous acetic acid into useful fuels (*i.e.*, H<sub>2</sub>, and hydrocarbons) by means of photocatalysis is an environment friendly method and does not require special conditions.

Starting from the preliminary work of Krauetler and Bard [36, 87], many reports have been published in literature while discussing the reaction mechanism for the photocatalytic decomposition of aqueous acetic acid [35, 37, 90, 100, 101]. Many published papers reported the formation of CO<sub>2</sub>, H<sub>2</sub>, CH<sub>4</sub>, and C<sub>2</sub>H<sub>6</sub> as main reaction products during the photo-induced transformation of aqueous acetic acid by using Pt/TiO<sub>2</sub> powders and electrodes. However, details with respect to following important parameters are still unclear and missing in the literature:

- (1) Effect of TiO<sub>2</sub> surface modification by various co-catalysts.
- (2) Effect of different acetic acid concentrations.
- (3) pH values (ranges from acidic to basic).
- (4) Isotopic labelling experiments.

Hence, the central aim of this thesis is to address above mentioned points in order to clarify the reaction mechanism for photocatalytic degradation of aqueous acetic acid in more detailed way.

The questions that need to be answered include:

## 1. Introduction

Do different co-catalysts loadings onto the surface of photocatalyst affect the product distribution?

Whether various initial concentrations of the reactant affect product distribution?

Do pH values changing from acidic to alkaline media affect the primary reaction intermediates and respective reaction products? Does pH variation over a range of values lead to different reaction mechanisms?

How isotopic labelling experiments will help to understand the reaction mechanism? How experimental results can be interpreted mechanistically?

Regarding the possibility of a technical application, how photocatalytic fuel production from effluents containing acetic acid can be improved?

The effect of various co-catalysts loaded TiO<sub>2</sub> including noble metals (Pt, Rh, Au and Ag) and metal oxides (IrO<sub>2</sub>, and RuO<sub>2</sub>) on the reaction intermediates and reaction products resulting from the photocatalytic transformation of aqueous acetic acid has been examined. These experiments are considered to help in identifying the most appropriate co-catalyst for the production of valuable energy fuels.

It has been reported by Yoneyama *et al.* [90] that the increase in initial concentration of acetic acid up to 5 M results in an enhanced amounts of all reaction products including CO<sub>2</sub>, H<sub>2</sub>, and hydrocarbons. On the contrary, Zheng *et al.* [100] demonstrated that an increase in the initial concentration of aqueous acetic acid between 0.04 – 0.11 M results in the formation of higher amounts of H<sub>2</sub> but they observed a gradual decrease in the formed amounts of H<sub>2</sub> when concentration was further increased to 0.26 M. Considering these opposing reports, the initial concentration of acetic acid is varied in the range of 0.05 – 5 M, and the effect of various concentrations on the reaction rates and product distribution has been inspected in detail.

It has been published in literature [37] that the photocatalytic decomposition of aqueous acetic acid results in the formation of CO<sub>2</sub>, H<sub>2</sub>, and hydrocarbons (*i.e.*, CH<sub>4</sub> and C<sub>2</sub>H<sub>6</sub>) over Pt/TiO<sub>2</sub>. However, an increase in the initial pH of the employed suspension from strong acidic to strong basic regime results in a significantly increased amount of H<sub>2</sub> formation and drastically decreased amounts of hydrocarbons. In another study, [100] the photocatalytic degradation of aqueous acetic acid with Pt/TiO<sub>2</sub> depicts a significant decrease in H<sub>2</sub> as well as hydrocarbons formation

## 1. Introduction

rate when initial pH of the suspension was shifted from acidic to basic media. Due to these contradictory reports, the effect of initial pH values on the reaction rates and product distribution has been re-investigated in the present work.

Conflicting reviews exist in literature while discussing the photocatalytic hydrogen evolution reaction (HER) with simultaneous degradation of an organic probe molecule. According to a group of scientists,  $H_2$  is produced by a  $H_2O$  splitting reaction even in the presence of an organic electron donor [102, 103], whereas, other group of scientists regarded this as a photocatalytic reforming phenomenon [13, 26-28]. In order to solve the controversies about  $H_2$  evolution reaction, isotopic labelling experiments are very important. In addition, the model organic pollutant such as acetic acid results in the formation of  $H_2$  as well as  $CH_4$  as the major reaction products. In such systems, it becomes even more complicated to gather details about the origin of formed reaction products. Only few reports are published in literature demonstrating the origin of  $H_2$  evolution by means of isotopic labelling experiments during photocatalytic decomposition of aqueous acetic acid. In these papers, authors only discussed the proton exchange reaction (PER) at carboxylic group (COOH) of acetic acid while PER at the methyl group ( $CH_3$ ) of acetic acid has not been discussed. Also, inadequate information is available about the effects of different isotopes on the reaction rates and product distribution resulting from photocatalytic decomposition of aqueous acetic acid. In this study, the analysis for HER employing different isotopes of acetic acid as well as solvents has been done. For the first time, the PER at both carboxylic, and methyl group of acetic acid has been investigated *via* spectroscopic techniques such as quadrupole mass spectrometer (QMS) and nuclear magnetic resonance (NMR). The effect of different isotopes on the reaction rates, reaction intermediates and reaction products has also been investigated for the first time.



## 2. Materials and experimental methods

### 2.1 Materials

In order to modify the surface of TiO<sub>2</sub> with various metals and metal oxides, all required chemicals were bought from Sigma Aldrich and used as received. For the preparation of all aqueous solutions and suspensions, deionized water was used from a SARTORIUS ARIUM 611 device with a resistivity of 18.2 MΩ·cm. Pure Acetic acid (purity ≥ 100 %) and different isotopes of acetic acid such as CD<sub>3</sub>COOD (purity, 99.9 atom % D) and CH<sub>3</sub>COOD (purity, 99 atom % D) were purchased from Sigma Aldrich with highest purity. Deuterium oxide (D<sub>2</sub>O) (purity, 99.9 atom % D) was also bought from Sigma Aldrich. The pH as well as pD adjustments were done by using perchloric acid (HClO<sub>4</sub>) which was also purchased from Sigma Aldrich.

### 2.2 Noble metals loaded TiO<sub>2</sub>

Commercial TiO<sub>2</sub> (P25) powders were obtained from Evonik Aeroxide, Germany. 1 wt % Pt-deposited-TiO<sub>2</sub> (P25) powders were synthesized and supplied by H.C starck company, Goslar, Germany. The Pt/TiO<sub>2</sub> powders were prepared in H. C. Starck Company by a conventional impregnation method employing commercial TiO<sub>2</sub> (P25) powders and chloroplatinic acid (H<sub>2</sub>PtCl<sub>6</sub> · 6H<sub>2</sub>O) as a Pt precursor. In brief, a conical flask was filled by 20 g of TiO<sub>2</sub> powder, 100 mL deionized water and 4.45 mL H<sub>2</sub>PtCl<sub>6</sub> (≥ 8.9 %) solution. The conical flask then sealed with a rubber septum stopper and given an ultrasonic bath for about 6 hours. In the next step, obtained solution was washed, dried and grinded properly. The Pt/TiO<sub>2</sub> powders were used for our experiments without any further purification. Other than Pt/TiO<sub>2</sub>, the effect of rhodium (Rh), gold (Au) and silver (Ag) depositions on the surface of TiO<sub>2</sub> acting as a co-catalyst has also been investigated in this work. For this purpose, a typical *in-situ* photodeposition method has been used as described in the literature [104]. In order to obtain 1 wt % metal-loaded-TiO<sub>2</sub>, aqueous solutions of (NH<sub>4</sub>)<sub>3</sub>RhCl<sub>6</sub> with Rh ≥ 99.99 %, HAuCl<sub>4</sub> · 3H<sub>2</sub>O with Au ≥ 49.00 %, and AgNO<sub>3</sub> with Ag ≥ 99.99 % were used. For instance, a stock solution of 0.01 M was prepared from (NH<sub>4</sub>)<sub>3</sub>RhCl<sub>6</sub> metal precursor. Afterwards, 254 μL from 0.01M (NH<sub>4</sub>)<sub>3</sub>RhCl<sub>6</sub> was added into the photoreactor containing 25 mg TiO<sub>2</sub> (P25) powder, 50 mL water and 0.5 M acetic acid.

## 2. Materials and experimental methods

Subsequently, the suspension was purged with Argon (Ar) for 20 minutes along with continuous stirring in order to remove the dissolved O<sub>2</sub> from the suspension. In the next step, the photoreactor was air sealed followed by a continuous 1 hour Ar flow in the head space of the photoreactor. As a last step, the lamp was switched on thus the 1 wt % Rh loadings on the TiO<sub>2</sub> surface were expected to occur during the photocatalytic reaction. The same method was used for the deposition of other noble metal co-catalysts. For example, 128 μL from a stock solution of H<sub>2</sub>AuCl<sub>4</sub>·3H<sub>2</sub>O prepared with 0.01 M gives 1 wt % Au/TiO<sub>2</sub> particles and 234 μL from AgNO<sub>3</sub> prepared with 0.01 M results in the formation of 1 wt % Ag/TiO<sub>2</sub> powders.

### 2.3 Metal-oxides loaded TiO<sub>2</sub>

An impregnation method has been used for the synthesis of metal oxide-loaded TiO<sub>2</sub> particles. The procedure was chosen according to the published literature [105]. A stock solution of 0.01 M from (NH<sub>3</sub>)<sub>6</sub>RuCl<sub>3</sub> with Ru ≥ 99.98 % was prepared to get ruthenium oxide (RuO<sub>2</sub>) loaded TiO<sub>2</sub> powders. In order to obtain 1 wt % RuO<sub>2</sub>/TiO<sub>2</sub>, 9.99 mL of 0.01 M (NH<sub>3</sub>)<sub>6</sub>RuCl<sub>3</sub> was introduced into a porcelain crucible containing 1g TiO<sub>2</sub> (P25) powder. This suspension was evaporated by giving a thermal treatment (water bath). Afterwards, the dried powder was calcined in a furnace under air/O<sub>2</sub> environment at various temperature values (*e.g.*, 350, 400, and 450 °C). The calcined powders were then grinded in the mortar and pestle to get homogeneous particles. The same method was repeated to get iridium oxide (IrO<sub>2</sub>) loaded TiO<sub>2</sub> where 5.255 mL from a 0.01 M Na<sub>2</sub>IrCl<sub>6</sub>·H<sub>2</sub>O with Ir ≥ 99.99 % assumed to give 1 wt % IrO<sub>2</sub>/TiO<sub>2</sub> particles.

### 2.4 Characterization techniques

#### 2.4.1 X-ray diffraction

For the phase analysis of TiO<sub>2</sub> powders X-ray diffraction (XRD) patterns were recorded by using Bruker D8 Advance instrument. The XRD patterns for all samples were obtained at room temperature employing Cu K $\alpha$  radiations over a range of 2 $\theta$  from 5° – 110° in Bragg-Brentano geometry. For the interpretation of the obtained results Rietveld method was used in the TOPAS 4.2 (Bruker-AXS) software.

## 2. Materials and experimental methods

### 2.4.2 Transmission electron microscopy

The analysis for particle size and their distribution were done by Transmission electron microscopy (TEM). The instrument TEM Tecnai G2 F20 TMP (FEI) with field emission gun at 200 kV acceleration voltages was used.

### 2.4.3 Specific surface area measurements

The single point specific surface area of pure and surface modified TiO<sub>2</sub> powders were calculated by Brunauer-Emmett-Teller (BET) model [106]. For this purpose, FlowSorb II 2300 device from Micromeritics, USA with a gas mixture of nitrogen (N<sub>2</sub>) (30 %) and helium (He) (70 %) in order to determine the adsorption was used. Prior to the BET measurements, a heat treatment of up to 130 °C was given to the samples for about an hour so that all the impurities will be removed.

### 2.4.4 Diffuse UV-vis spectroscopy

The diffuse reflectance spectra of pure, metals and metal oxides loaded TiO<sub>2</sub> were obtained *via* Varian Cary 100 Scan UV-vis spectrophotometer. The spectral ranges were adjusted as 200 – 800 nm employing an Ulbricht sphere. As a reference material barium sulfate was used, that provides a measurement with 100 % reflectance. The conversion of reflectance signals into F(R) for all materials was done according to the Kubelka-Munk theory [107].

### 2.5 Photocatalytic measurements

A 100 cm<sup>3</sup> double jacket quartz photoreactor with two necks (one for gas in and other for gas out) was used to carry out all the photocatalytic experiments. For the analysis of gaseous products during the photocatalytic reaction, the photoreactor was combined with Hidden HPR-20 quadrupole mass spectrometer (QMS). A continuous Ar flow was used during the measurements, while the adjustment of Ar flow was handled by a mass flow controller. A schematic illustration of photocatalytic set-up is given in Figure 6. This experimental set-up facilitates the monitoring of product formation rates during the entire course of photocatalytic reaction. For a reaction, 25

## 2. Materials and experimental methods

mg photocatalyst was added into the 0.5 M aqueous solution of acetic acid with a total photoreactor volume of 50 mL. This photoreactor was then put on a continuous stirring and the suspension was purged with Ar for 20 – 30 minutes so that the dissolved O<sub>2</sub> will be removed. Afterwards, the reactor was air tight with the help of rubber septum and attached to the QMS by metal flanges. The Ar flow with a rate of 50 cm<sup>3</sup> min<sup>-1</sup> was continued for 10 – 20 minutes again in the headspace of the photoreactor to ensure the removal of O<sub>2</sub> from the system. In the next step, the Ar flow switch to 10 cm<sup>3</sup> min<sup>-1</sup> and held constant during the complete photocatalytic reaction. Prior to the illumination, the photoreactor was kept under dark for at-least one hour to obtain a stabilization of all gaseous compounds with respect to their assigned signals. Once the stabilization of all signals was achieved, the lamp was switched on for 15 hours in most of the experiments. An Osram XBO 1000 Watt Xenon (Xe) arc lamp enclosed in a Müller LAX 1000 lamp housing was used as a light source in all of the experiments. After 15 h, once the lamp was switched off a decrease in the formation rate for all reaction system was obvious and possible to see on the experimental set-up. However, the signals were continued to be calculated by QMS until all the formed products reached to the baseline.

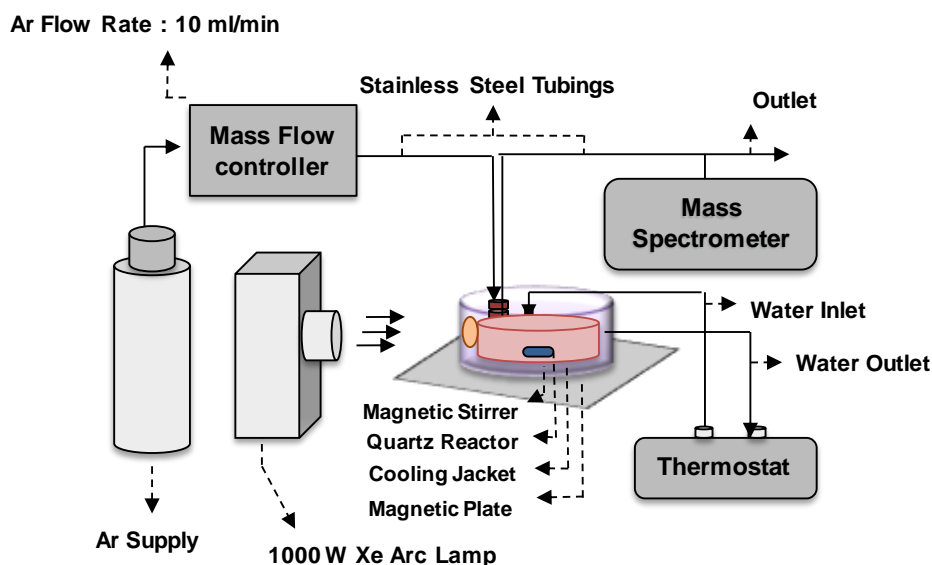


**Figure 6:** Schematic illustration of Photocatalytic-Set up.

## 2. Materials and experimental methods

During all photocatalytic reactions, the temperature of the photoreactor was kept constant by attaching it to a thermostat from Julabo Company. The QMS was calibrated with diluted gasses (1 – 2 % in Ar) obtained from Linda Company. The QMS calibration was done to do quantitative analysis of all reaction products formed during the photocatalytic reaction.

### 2.6 Photonic efficiency determination

In order to determine the photocatalytic activity, the photonic efficiency ( $\zeta$ ) for all reaction products was calculated as described in the literature [108]. The photonic efficiency is generally defined as:

$$\zeta [\%] = \frac{\text{production rate}}{\text{photon flux}} \times 100 \quad \text{Equation 18}$$

Here, production rate represents the formation rate of the gaseous products exiting the photoreactor, and photon flux corresponds to the incident number of photons per unit area per time.

The photon flux can be defined as follow:

$$\text{Photon flux} = I_0 \times A \quad \text{Equation 19}$$

The area of the window of photoreactor is represented by  $A$  whereas  $I_0$  illustrates the absorbed number of photons and explain as follow:

$$I_0 = \frac{I \cdot \lambda}{N_a \cdot h \cdot c} \quad \text{Equation 20}$$

Here,  $I$  is the total number of photons coming to the window of photoreactor by,  $\lambda$  illustrates the wavelength according to the TiO<sub>2</sub> band gap energy,  $N_a = 6.023 \times 10^{23} \text{ mol}^{-1}$  is Avogadro constant,  $h = 6.63 \times 10^{-34} \text{ Js}$  is the Planck's constant and  $c = 3 \times 10^8 \text{ ms}^{-1}$  corresponds to the speed of light.

## 2. Materials and experimental methods

For the calculations of photonic efficiency in the present work,  $\lambda = 365 \text{ nm}$  and  $I = 30 \text{ mW cm}^{-2}$  was used. The area is given by the diameter ( $D = 3.5 \text{ cm}$ ) of the window of photoreactor and was calculated to be  $A = (\pi/4) \times D^2 = 9.6162 \text{ cm}^2$

### 2.7 Nuclear magnetic resonance spectroscopy

For mechanistic investigations, Bruker 400 MHz Ascend with Avance-III console and broadband Prodigy Probe proton nuclear magnetic resonance (NMR) spectroscopy was used. For the NMR sample preparation, first a photocatalytic experiment was performed. After 15 h of illumination, the suspension was taken from the photoreactor and was shifted to the Ar purged NMR quartz tube through an Ar purged syringe. The NMR tube was then immediately put in the NMR sample holder to analyse the sample. All the samples for NMR analysis were prepared in the same way.

## **3. Results**

### **3.1 Material characterizations**

#### **3.1.1 Structural and optical properties**

The photocatalyst materials including commercial TiO<sub>2</sub> P25 as well as synthesized noble metals and metal-oxides loaded TiO<sub>2</sub> particles were characterized by analytical techniques in order to get the information about their morphological and optical characteristics. Figure 7 exhibits the XRD patterns for pure as well as synthesized metals and metal oxides loaded TiO<sub>2</sub> particles. In addition to this, an XRD pattern for 1 wt % RuO<sub>2</sub>/TiO<sub>2</sub> powders calcined at different temperature values (350 – 450 °C) can also be seen in Figure 8. Data presented both in Figure 7 and 8 demonstrated that the loading of 1 wt % metal or metal oxide on the surface of TiO<sub>2</sub> particles is beyond the detection limit of the XRD instrument and cannot be seen in the obtained results. For instance, in all of the synthesized materials, TiO<sub>2</sub> anatase (A) (JCPDS # 01-075-2545) and rutile (R) (JCPDS # 01-073-1782) peaks are obvious and comparable with those obtained from pure P25 TiO<sub>2</sub>. However, no other peak corresponding to any metal or metal oxide compound can be seen. Also, 1 wt % metal or metal oxide loadings on the surface of TiO<sub>2</sub> does not exhibit any shift in its crystal structure. Additionally, the thermal treatment up to 450 °C does not seem (Figure 8) to affect the crystal structure of P25 TiO<sub>2</sub> particles. These results can be ascribed to the fact that the deposited metals and metal oxides cocatalysts stayed on the surface of TiO<sub>2</sub> particles and do not enter in its crystal lattice.

The Particle size of the synthesized powders was determined by means of TEM and is given in the Figures 9 and 10. Here, the dark spherical structures depict the corresponding metal or metal oxide nanoparticles (NP) while the bright spheres exhibit TiO<sub>2</sub> particles (Figure 9). The distribution of metal or metal oxide NP (Figure 9) seems to be quite uniform in most of the synthesized materials. However, in case of RuO<sub>2</sub>/TiO<sub>2</sub>, agglomerates are more obvious. The particle size of both metal as well as metal oxide and TiO<sub>2</sub> was observed to be in the range of 15 – 25 nm.

### 3. Results

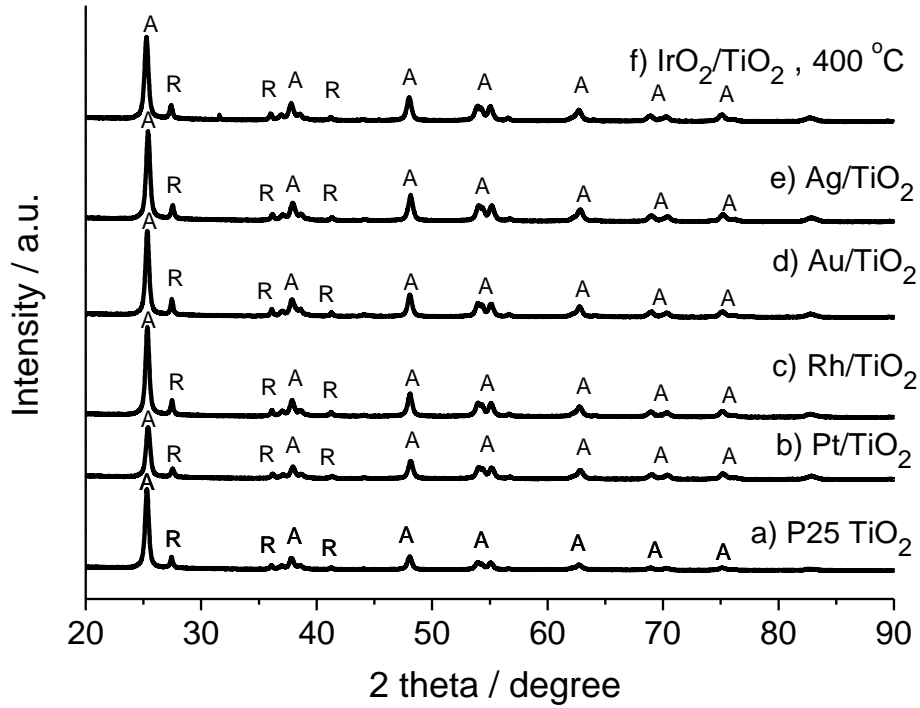


**Figure 7:** XRD patterns for the (a) Bare P25 TiO<sub>2</sub> powders, (b – e) metal loaded TiO<sub>2</sub> powders and (f) metal-oxide loaded TiO<sub>2</sub> particles calcined at 400 °C.

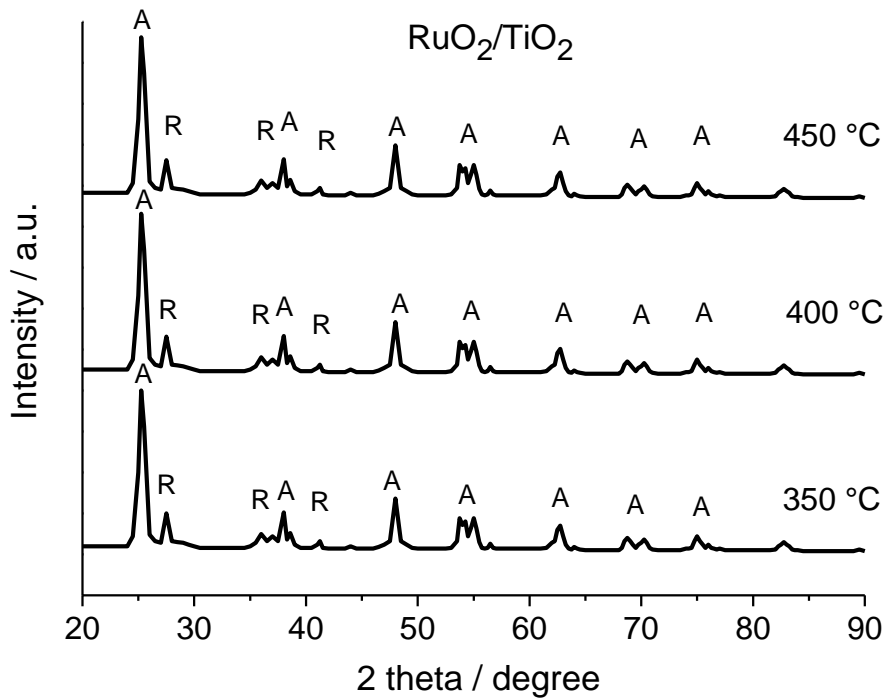


**Figure 8:** XRD patterns for the RuO<sub>2</sub>/TiO<sub>2</sub> powders calcined at 350, 400 and 450 °C.



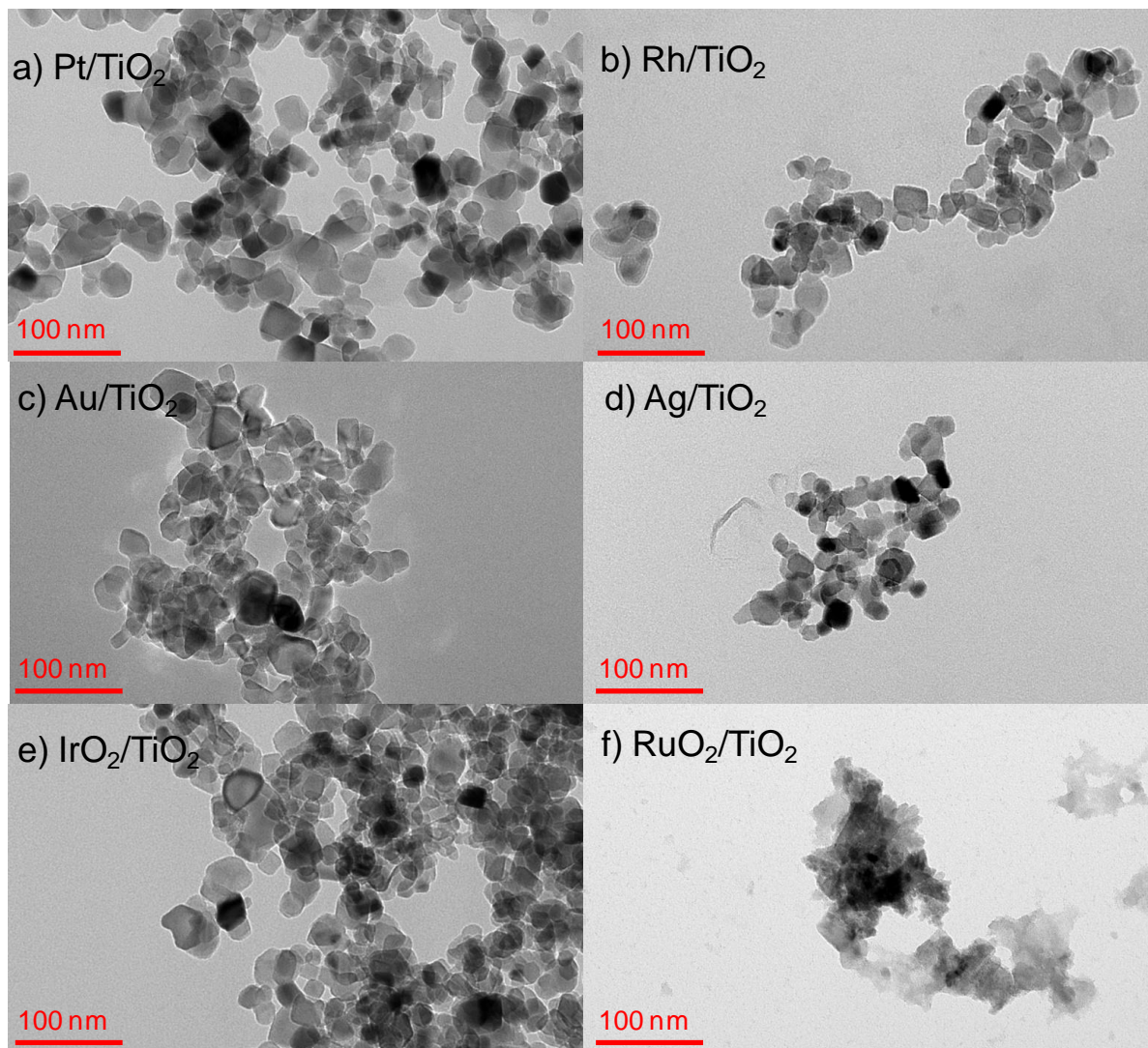


**Figure 9:** TEM micrographs for (a – d) metal loaded TiO<sub>2</sub> and (e – f) metal oxide (calcined at 400 °C) loaded TiO<sub>2</sub> particles.

In the high resolution TEM micrographs (Figure 10), the crystal lattice is quite obvious for all synthesized materials. Also, a metal or metal oxide-TiO<sub>2</sub> interface can be seen very clearly. Once again, the RuO<sub>2</sub>/TiO<sub>2</sub> powders represent big agglomerates and do not give any appropriate information about particle size and distribution.

### 3. Results

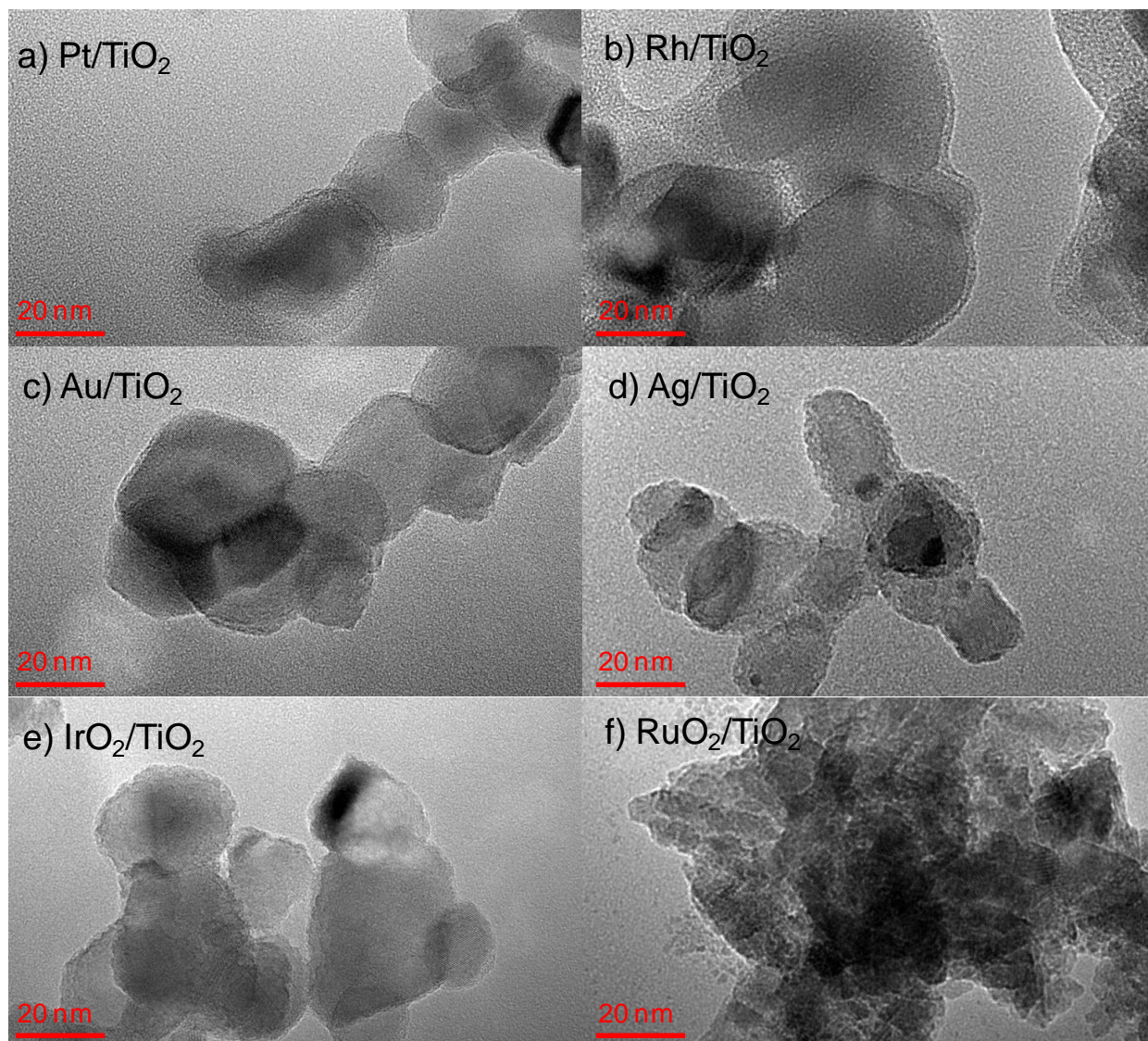


**Figure10:** High resolution TEM micrographs for (a – d) metal loaded TiO<sub>2</sub> and (e – f) metal oxide (calcined at 400 °C) loaded TiO<sub>2</sub> particles.

The single point BET surface areas of all prepared noble metals and metal oxides loaded TiO<sub>2</sub> particles were calculated by N<sub>2</sub> adsorption measurements and are presented in Table 1 and Table 2. It can be seen in Table 1 that the loading of various metals on the surface of TiO<sub>2</sub> gives negligible changes in BET surface area as compared to the pure TiO<sub>2</sub> particles. It is also obvious in Table 2 that the calcination of metal oxide modified TiO<sub>2</sub> powders at different temperature values results in almost same values for the BET surface areas. This means, once again, that the

thermal treatment up to 450 °C on the TiO<sub>2</sub> powders does not affect their physical and chemical properties. Hence, these results match well with the obtained XRD data for all the samples.

**Table 1:** BET surface areas for pure and metal loaded TiO<sub>2</sub>.

Photocatalyst	Synthesis Method	BET Surface Area / m <sup>2</sup> g <sup>-1</sup>
P25 TiO <sub>2</sub>	commercial powder	51
Pt/TiO <sub>2</sub>	impregnation method	51
Rh/TiO <sub>2</sub>	photodeposition method	50
Au/TiO <sub>2</sub>	photodeposition method	50
Ag/TiO <sub>2</sub>	photodeposition method	48

**Table 2:** BET surface areas for pure and metal loaded TiO<sub>2</sub>.

Photocatalyst	Synthesis Method	BET Surface Area / m <sup>2</sup> g <sup>-1</sup>
IrO <sub>2</sub> /TiO <sub>2</sub>	impregnation method, 350 °C	50
IrO <sub>2</sub> /TiO <sub>2</sub>	impregnation method, 400 °C	51
IrO <sub>2</sub> /TiO <sub>2</sub>	impregnation method, 450 °C	48
RuO <sub>2</sub> /TiO <sub>2</sub>	impregnation method, 350 °C	50
RuO <sub>2</sub> /TiO <sub>2</sub>	impregnation method, 400 °C	49
RuO <sub>2</sub> /TiO <sub>2</sub>	impregnation method, 450 °C	49

The optical properties of the employed materials were observed by using diffuse reflectance UV-vis spectroscopy. In a photocatalytic reaction, one of the most crucial steps is the choice of a photocatalyst material with suitable absorption properties. Figure 11, 12 and 13 demonstrate the absorption spectra of pure, metals loaded TiO<sub>2</sub> as well as metal oxides loaded TiO<sub>2</sub> at varying temperatures (*i.e.*, 350, 400, and 450 °C), respectively. The conversion of diffuse reflectance signals into absorption was done according to the Kubelka-Munk theory. It can be seen in Figure 11 that the employment of various noble metals on the surface of TiO<sub>2</sub> does not result in the shift

### 3. Results

of their absorption spectra ( $F(R)$ ) as compared to the absorption spectrum of bare  $\text{TiO}_2$ . It is also obvious from Figure 12 and 13 that the thermal treatment of up to  $450\text{ }^\circ\text{C}$  does not cause any changes in the absorption spectra of metal oxide loaded  $\text{TiO}_2$  powders. The obtained results also show that the synthesis methods used in this study for the loading of noble metals as well metal oxides does not support extension of  $\text{TiO}_2$  absorption in the visible range.

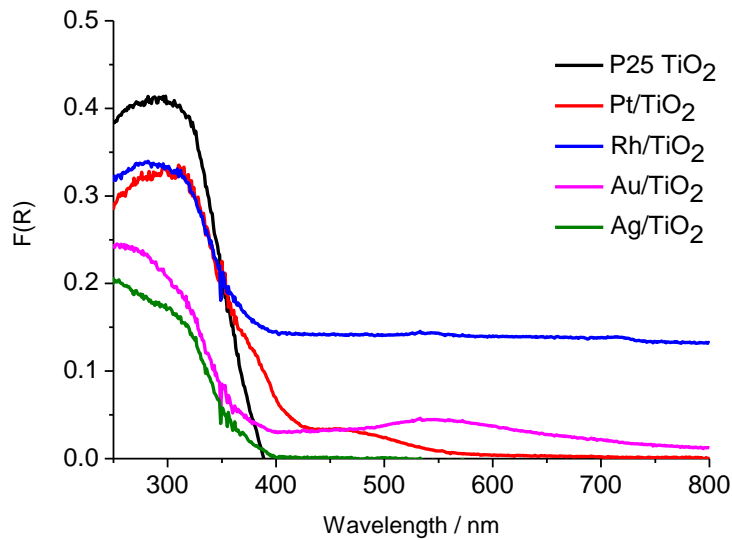


**Figure 11:** Diffuse reflectance spectra of pure and noble metals loaded  $\text{TiO}_2$  particles.

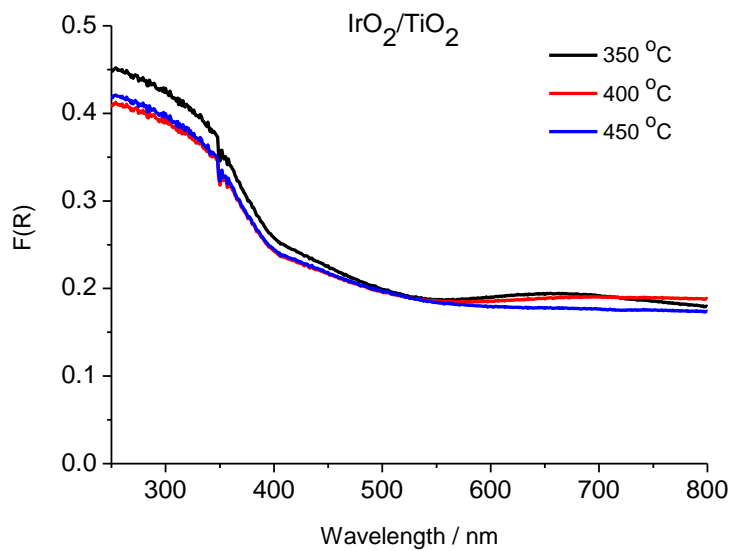


**Figure 12:** Diffuse reflectance spectra of  $\text{IrO}_2/\text{TiO}_2$  particles.

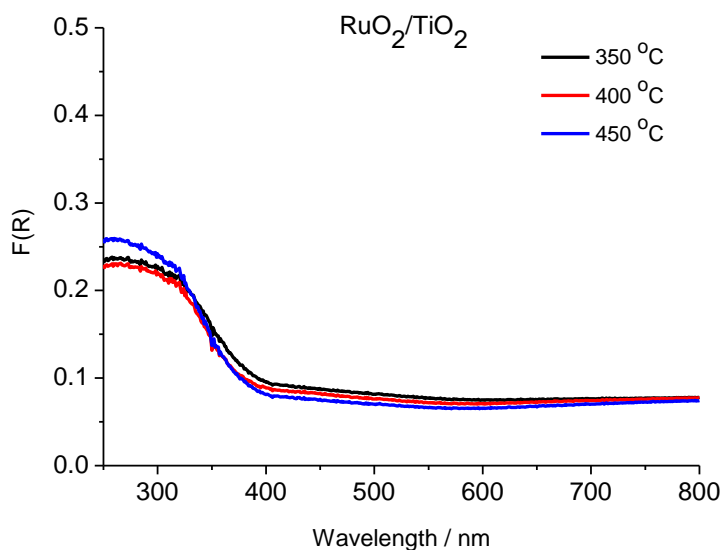


**Figure 13:** Diffuse reflectance spectra of  $\text{RuO}_2/\text{TiO}_2$  particles.

### 3.2 Photocatalytic experiments

#### 3.2.1 Bare P25 $\text{TiO}_2$ as a photocatalyst

Blank experiments for the anaerobic photocatalytic degradation of aqueous acetic acid into useful solar fuels have been done (1) in the presence of  $\text{TiO}_2$  as a photocatalyst suspended in  $\text{H}_2\text{O}$ , without employing any sacrificial reagent while illuminating with UV (A) light, (2) in the presence of a co-catalyst and aqueous solution of acetic acid but without any semiconducting material and illuminating with UV (A) light, and (3) bare  $\text{TiO}_2$  suspended in aqueous acetic acid illuminating with UV (A) light. No formation of molecular hydrogen or hydrocarbons was observed from controlled experiments with reaction system 1 and 2. However, reaction system 3, where bare  $\text{TiO}_2$  was used as a photocatalyst and aqueous acetic acid as an electron donor or sacrificial reagent, exhibits poor photocatalytic activity as presented in Figure 14. It can be seen (Figure 14) that the photo-induced transformation of aqueous acetic acid into  $\text{CO}_2$ ,  $\text{CH}_4$ ,  $\text{H}_2$  and  $\text{C}_2\text{H}_6$  occurred with very low formation rates (Figure 14a) and corresponding less formed amounts (Figure 14b), which are close to the detection limits of the quadrupole mass spectrometer (QMS).

### 3. Results

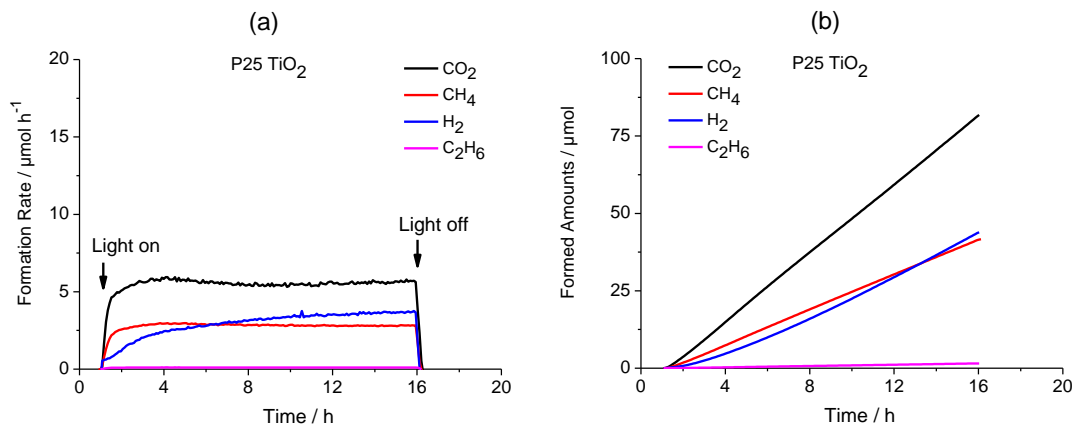


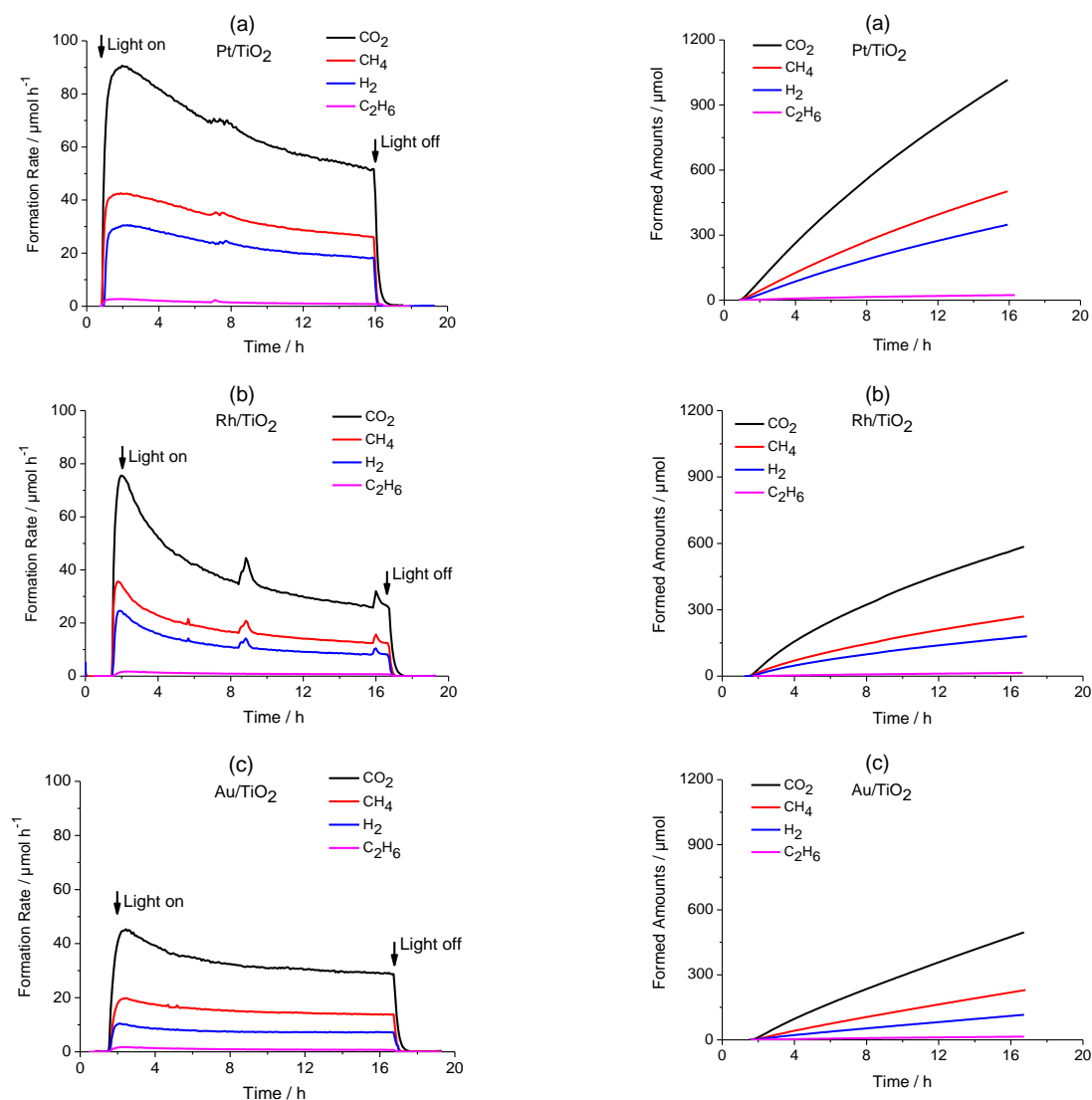
**Figure 14:** Formation rates (a) and amounts (b) of the main reaction products *i.e.*, CO<sub>2</sub>, H<sub>2</sub>, CH<sub>4</sub> and C<sub>2</sub>H<sub>6</sub>, photocatalytically formed from aqueous suspensions containing P25 TiO<sub>2</sub> as the photocatalyst. *Experimental conditions:* photocatalyst concentration = 0.5 g L<sup>-1</sup>, initial acetic acid concentration = 0.5 M, pH 2, suspension volume = 50 mL, irradiation time = 15 h, irradiation intensity  $I_{250-1450} = 30 \text{ mW cm}^{-2}$ .

#### 3.2.2 Surface modified TiO<sub>2</sub> as a photocatalyst

In order to improve the photocatalytic activity, the surface of TiO<sub>2</sub> powders was loaded with various metals (Pt, Rh, Au, and Ag) and metal oxides (IrO<sub>2</sub> and RuO<sub>2</sub>). Photocatalytic runs performed with metal or metal oxide loaded TiO<sub>2</sub> particles suspended in 0.5 M aqueous acetic acid solutions are given in Figure 15 and 16. For metal oxides (IrO<sub>2</sub> and RuO<sub>2</sub>) loaded TiO<sub>2</sub> particles, the calcination treatment of 400 °C was found to result in higher photocatalytic activities (data not shown) than 350 °C and 450 °C. Therefore, IrO<sub>2</sub>/TiO<sub>2</sub> and RuO<sub>2</sub>/TiO<sub>2</sub> calcined at 400 °C were used for further analysis in this work. The main reaction products resulting from the photocatalytic decomposition of acetic acid are CO<sub>2</sub>, CH<sub>4</sub>, and H<sub>2</sub> while various alkanes C<sub>x</sub>H<sub>2x+2</sub>, where  $x \leq 3$  are also formed as minor reaction products. Details regarding the minor reaction products can be found in the published report [83]. Figure 15 represents the plots obtained from quadrupole mass spectrometer (QMS) for the formation rates of the main reaction products versus irradiation time. Before starting the photocatalytic reaction, the photoreactor was kept under dark for at least 1 h with continuous magnetic stirring and Ar flow rate of 10  $\text{cm}^3 \cdot \text{min}^{-1}$  so that a stabilization of the corresponding gaseous signals can be achieved in the

### 3. Results

QMS. Immediately after the lamp was switched on, formation of all gaseous compounds (Figure 15) was determined by QMS. Usually, the formation rates of all gaseous products require 30 – 40 minutes (depending on the reaction conditions) to achieve their maximum observed value. Once the maximum observed rate was achieved by the evolved reaction products, a decreasing trend in most of the experimental runs has been observed. However, after a few hours of irradiation, the reaction rates seemed to become constant indicating the surface changes in the photocatalyst in the presence of light. This means that the total time of irradiation is a key factor to determine the efficiency of a photocatalytic reaction. The amounts of the formed gases have been calculated by doing the integration of formation rates as given in Figure 16.



### 3. Results

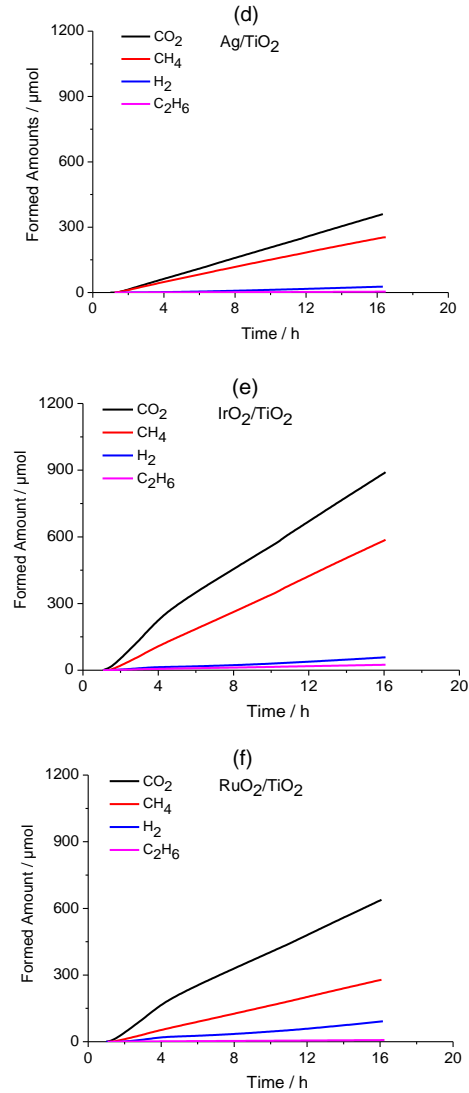
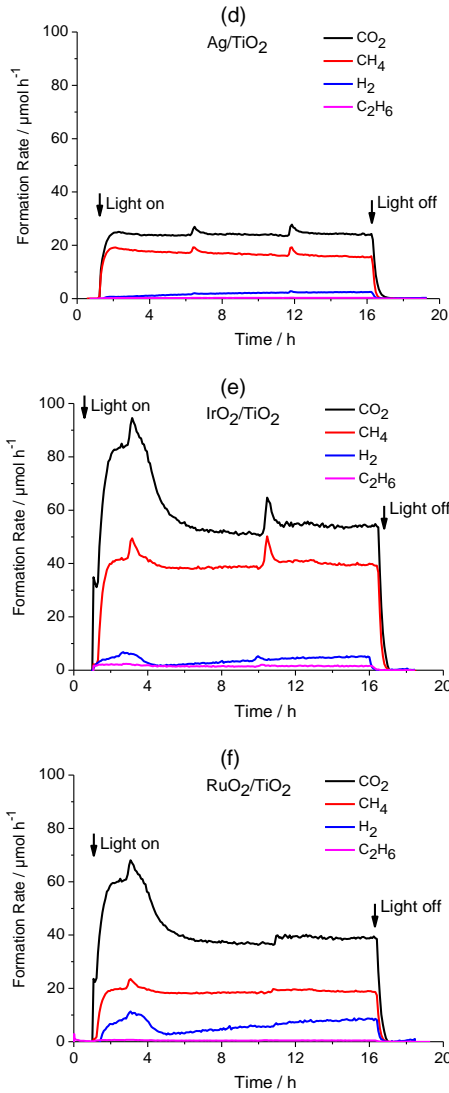


**Figure 15:** Photocatalytic formation rates of the main reaction products *i.e.*,  $\text{CO}_2$ ,  $\text{H}_2$ ,  $\text{CH}_4$  and  $\text{C}_2\text{H}_6$ , from aqueous acetic acid employing  $\text{TiO}_2$ -based photocatalysts. *Experimental conditions:* photocatalyst concentration =  $0.5 \text{ g L}^{-1}$ , co-catalyst loading = 1 wt %, acetic acid concentration = 0.5 M, pH 2, suspension volume = 50 mL, irradiation time = 15 h, irradiation intensity  $I_{250\text{-}I_{450}} = 30 \text{ mW cm}^{-2}$ .

**Figure 16:** Photocatalytically formed amounts of the main reaction products *i.e.*,  $\text{CO}_2$ ,  $\text{H}_2$ ,  $\text{CH}_4$  and  $\text{C}_2\text{H}_6$ , from aqueous acetic acid employing  $\text{TiO}_2$ -based photocatalysts. *Experimental conditions:* photocatalyst concentration =  $0.5 \text{ g L}^{-1}$ , co-catalyst loading = 1 wt %, acetic acid concentration = 0.5 M, pH 2, suspension volume = 50 mL, irradiation time = 15 h, irradiation intensity  $I_{250\text{-}I_{450}} = 30 \text{ mW cm}^{-2}$ .



The data analysis of the obtained results shows that the loading of various co-catalysts on TiO<sub>2</sub> surface does not affect the reaction products but affects the formation rates  $r_i = dn_i/dt$  to a great extent (Figure 15). As a result, the formed amounts  $n_i = \int_t r_i dt$  changed significantly (Figure 16). In all experimental runs, CO<sub>2</sub> was observed as the major reaction product within the range of 1027 (Pt/TiO<sub>2</sub>) – 357 (Ag/TiO<sub>2</sub>)  $\mu\text{mol}$  while keeping all experimental conditions (such as initial acetic acid concentration, pH, photocatalyst amount etc.,) same (Figure 17). The order in which formed amounts of CO<sub>2</sub> decrease employing different co-catalysts was acquired as: Pt/TiO<sub>2</sub> > IrO<sub>2</sub>/TiO<sub>2</sub> > RuO<sub>2</sub>/TiO<sub>2</sub> > Rh/TiO<sub>2</sub> > Au/TiO<sub>2</sub> > Ag/TiO<sub>2</sub> (Figure 17), demonstrating the use of metal oxides as an appropriate co-catalyst.

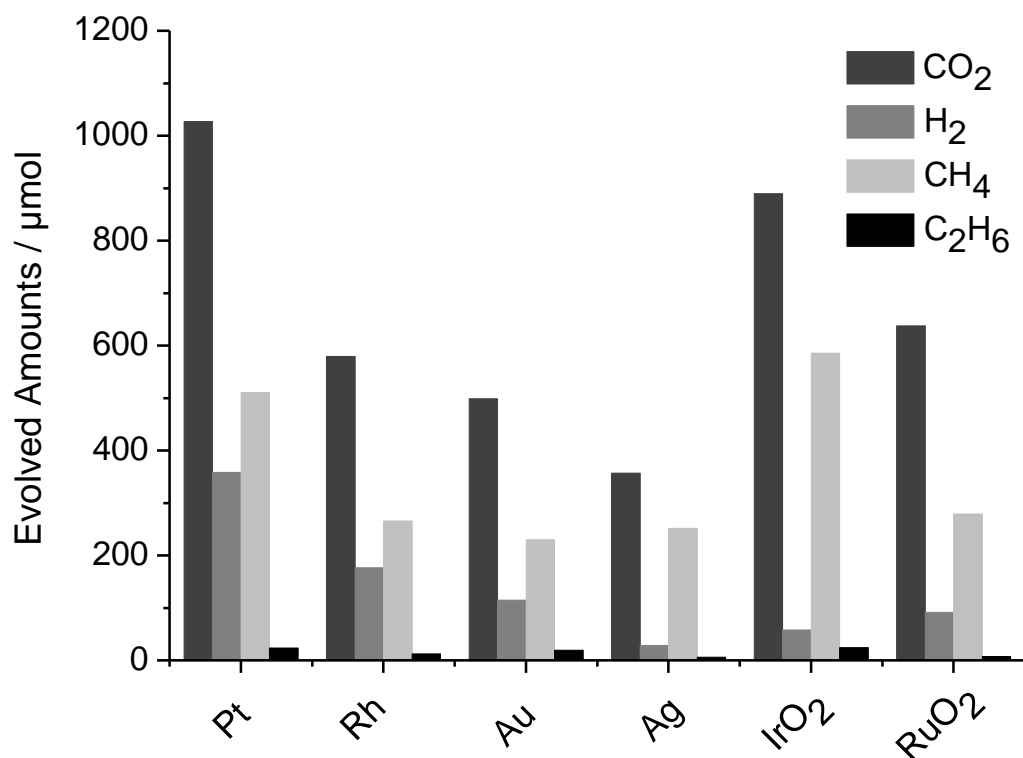


**Figure 17:** Amounts of the main reaction products, *i.e.*, CO<sub>2</sub>, H<sub>2</sub>, CH<sub>4</sub>, and C<sub>2</sub>H<sub>6</sub>, photocatalytically formed from aqueous acetic acid after an irradiation time of 15 h in the presence of noble metal and metal oxide loaded TiO<sub>2</sub> as the photocatalysts. *Experimental conditions:* as in Figure 15 – 16.

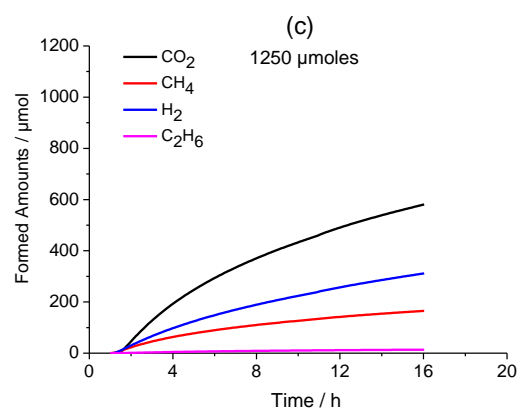
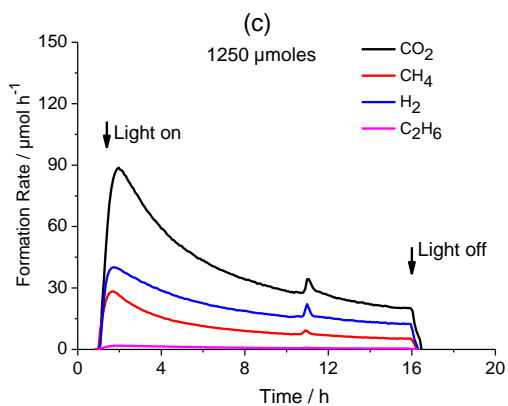
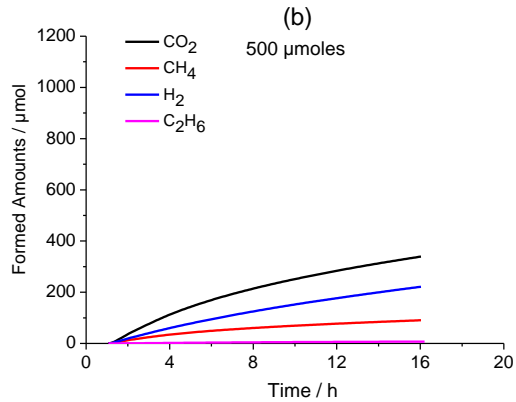
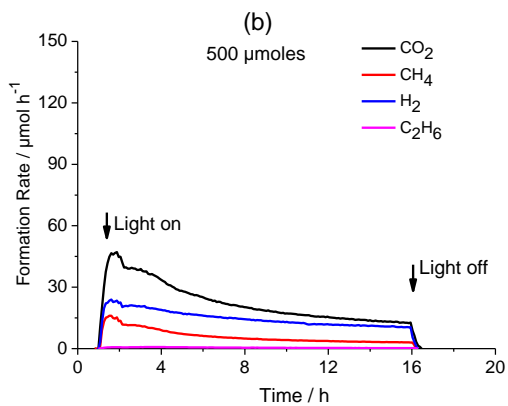
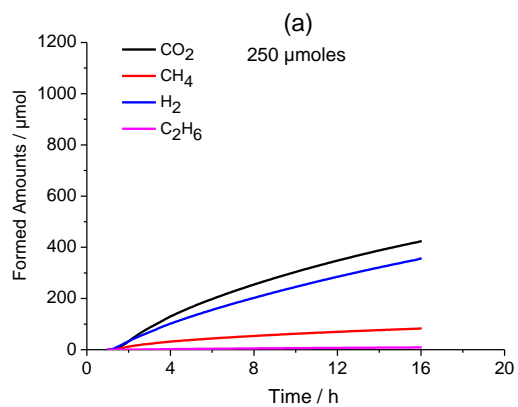
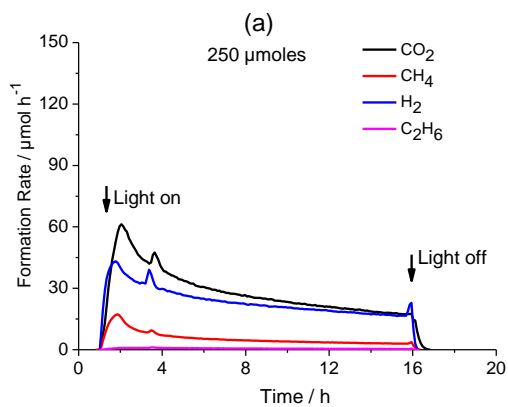
### 3. Results

The second main reaction product, resulting from the photocatalytic decomposition of aqueous acetic acid which is very useful for the energy applications was CH<sub>4</sub>. The amounts of CH<sub>4</sub> formation during 15 h of illumination was found to vary from 586 (IrO<sub>2</sub>/TiO<sub>2</sub>) – 230 (Au/TiO<sub>2</sub>) μmol. As the third major reaction product, H<sub>2</sub> was observed to be varying in the range of 375 (Pt/TiO<sub>2</sub>) – 29 (Ag/TiO<sub>2</sub>) μmol. The formed amounts as well as formation rates for H<sub>2</sub> were observed to decrease in the following order: Pt/TiO<sub>2</sub> > Rh/TiO<sub>2</sub> > Au/TiO<sub>2</sub> > IrO<sub>2</sub>/TiO<sub>2</sub> > RuO<sub>2</sub>/TiO<sub>2</sub> > Ag/TiO<sub>2</sub> (Figure 17) meaning that the metal oxides are poor co-catalysts for the reduction reaction of H<sup>+</sup> generated during the photocatalytic reaction. However, in general, it can be seen (Figure 17) that the significant amounts for simultaneous oxidation and reduction products were obtained for Pt loaded TiO<sub>2</sub> particles. For example, at the same time, 495 μmoles of CH<sub>4</sub> and 375 μmoles for H<sub>2</sub> were obtained for Pt/TiO<sub>2</sub> only. Therefore, Pt/TiO<sub>2</sub> powder was employed as the optimal photocatalyst in this study for further investigations.

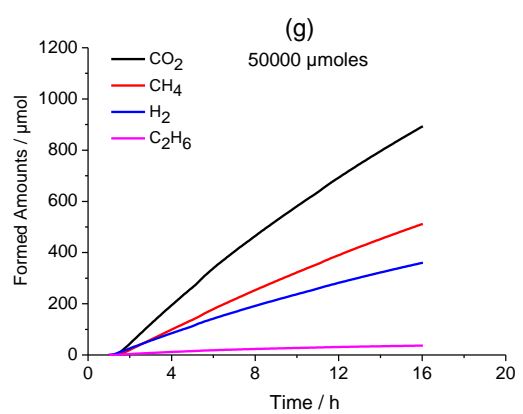
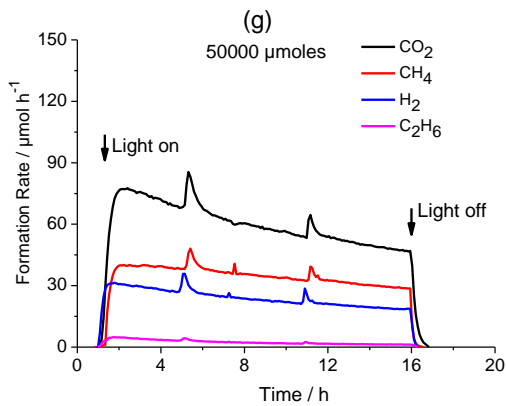
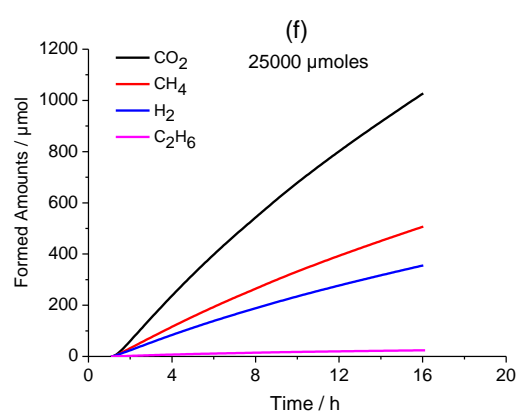
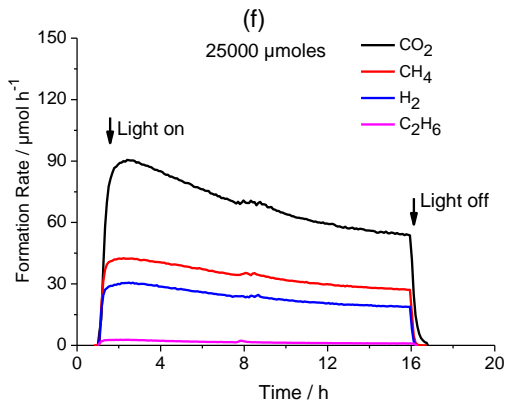
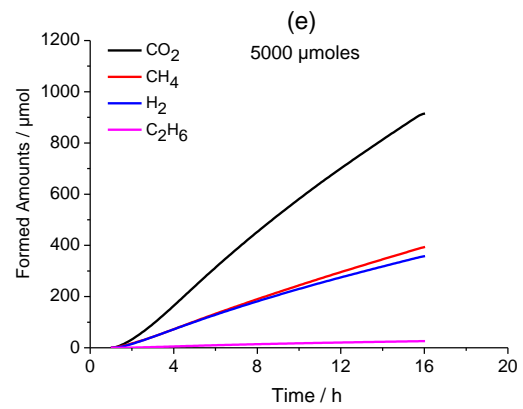
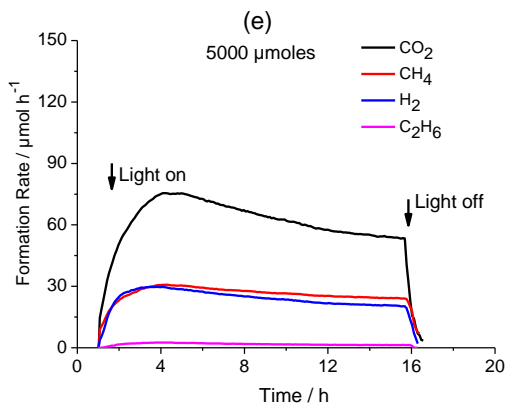
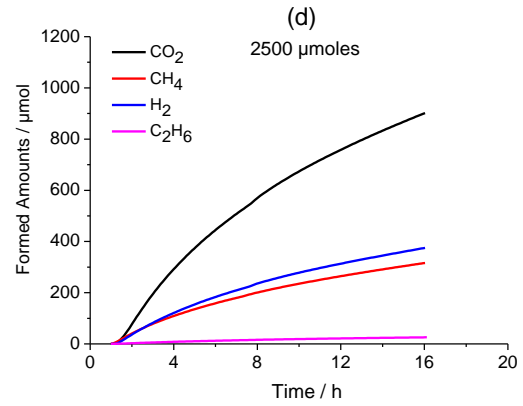
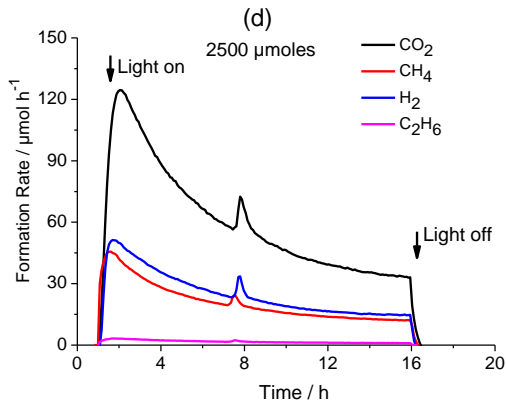
#### 3.2.3 Effect of various acetic acid concentrations

It is well known that the varying concentration of reactants affects the reaction rates. The effect of initial acetic acid concentrations ( $c_0$ ) ranging between  $0.005 \text{ M} \leq c_0 \leq 5 \text{ M}$  corresponding to  $250 \text{ μmol} \leq n_0 \leq 250000 \text{ μmol}$  ( $n_0$  = initial number of acetic acid moles) over Pt/TiO<sub>2</sub> particles have been examined while keeping other reaction conditions constant (*i.e.*, photocatalyst amount 25 mg, reactor volume 50 mL, pH 2). Results depicting the effect of various acetic acid concentrations on the formation of reaction products and their distribution are given in Figure 18 and 19. Here, Figure 18 demonstrates the formation rates of the main reaction products while relating formed amounts are presented in Figure 19.

### 3. Results



### 3. Results



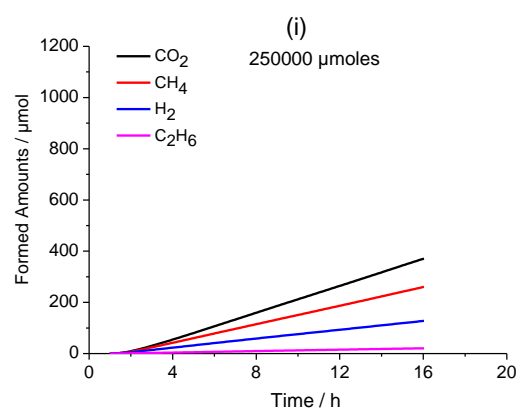
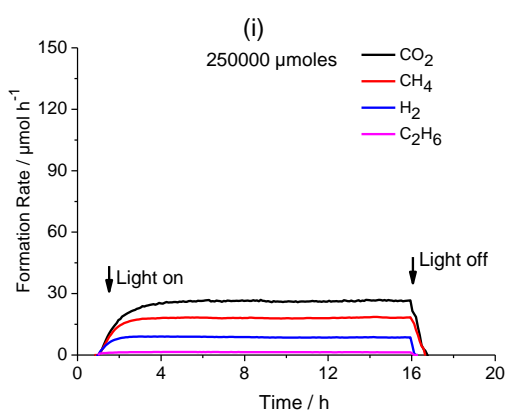
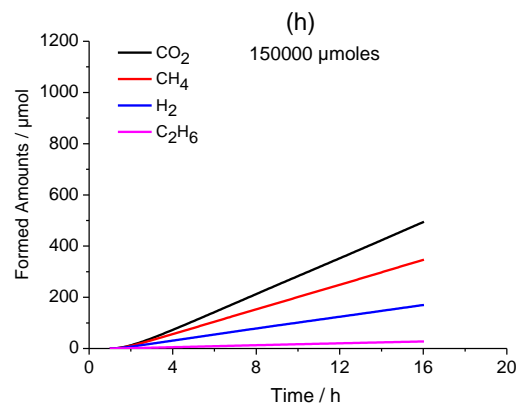
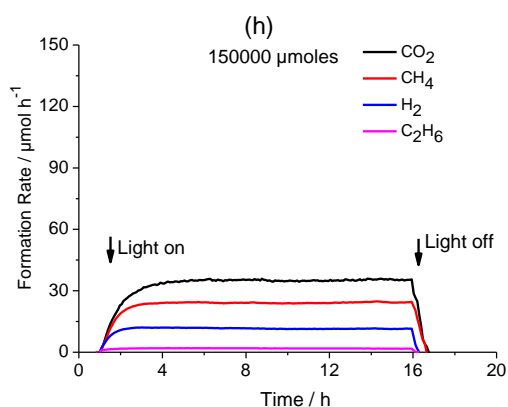


**Figure 18:** Photocatalytic formation rates of the main reaction products *i.e.*, CO<sub>2</sub>, H<sub>2</sub>, CH<sub>4</sub> and C<sub>2</sub>H<sub>6</sub>, formed from aqueous suspensions containing 1 wt % Pt/TiO<sub>2</sub> as the photocatalyst and varying initial amounts of acetic acid. *Experimental conditions:* photocatalyst concentration = 0.5 g L<sup>-1</sup>, 0.005 M ≤ initial acetic acid concentration ≤ 5 M, pH 2, suspension volume = 50 mL, irradiation time = 15 h, irradiation intensity I<sub>250-450</sub> = 30 mW cm<sup>-2</sup>.

**Figure 19:** Photocatalytically formed amounts of the main reaction products *i.e.*, CO<sub>2</sub>, H<sub>2</sub>, CH<sub>4</sub> and C<sub>2</sub>H<sub>6</sub>, formed from aqueous suspensions containing 1 wt % Pt/TiO<sub>2</sub> as the photocatalyst and varying initial amounts of acetic acid. *Experimental conditions:* photocatalyst concentration = 0.5 g L<sup>-1</sup>, 0.005 M ≤ initial acetic acid concentration ≤ 5 M, pH 2, suspension volume = 50 mL, irradiation time = 15 h, irradiation intensity I<sub>250-450</sub> = 30 mW cm<sup>-2</sup>.

### 3. Results

It can be seen in Figure 20 that the change in the concentration ( $c_0$ ) of acetic acid from lower (0.005 M) – higher (5 M) value results in the formation of  $\text{CO}_2$ ,  $\text{CH}_4$  and  $\text{H}_2$  as the main reaction products while  $\text{C}_2\text{H}_6$  as a minor product. These results match well with those obtained by changing the  $\text{TiO}_2$  surface with various metal and metal oxide co-catalysts. However, again, the different  $c_0$  seemed to affect the formation rates and subsequent amounts of the formed reaction products to a great extent. For example,  $0.005 \text{ M} \leq c_0 \leq 0.05 \text{ M}$  analogous to  $250 \mu\text{mol} \leq n_0 \leq 2500 \mu\text{mol}$  exhibits an efficient increase in the formed amounts of all reaction products (Figure 20).

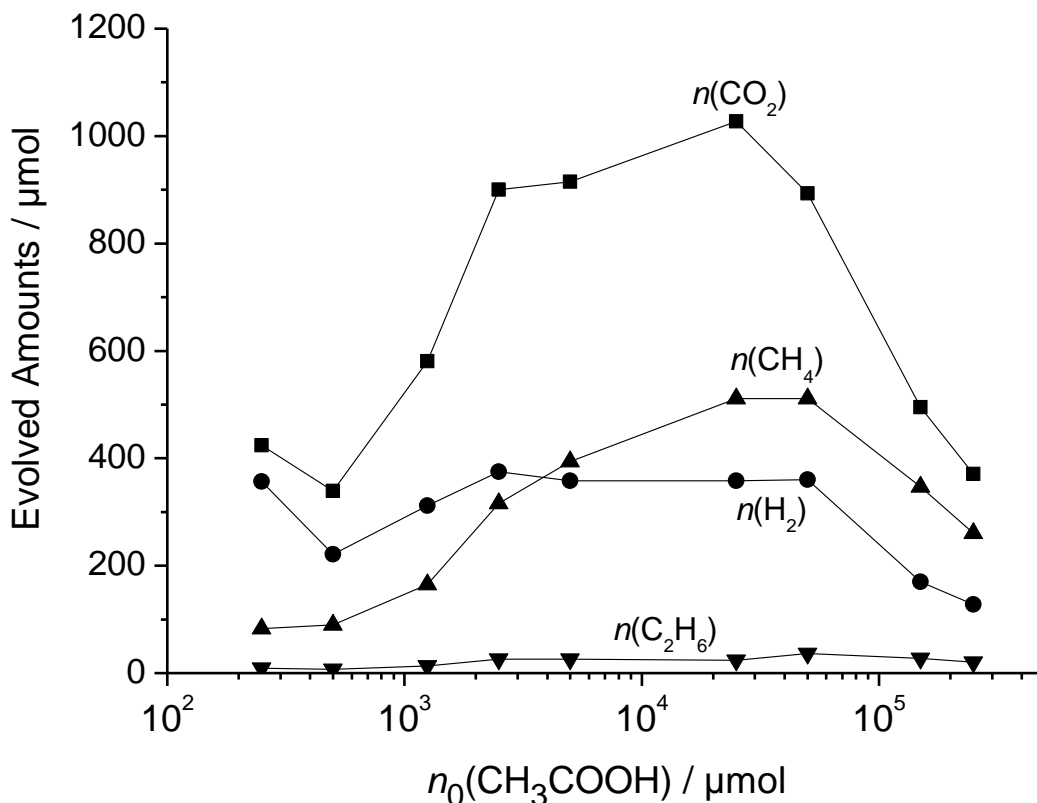


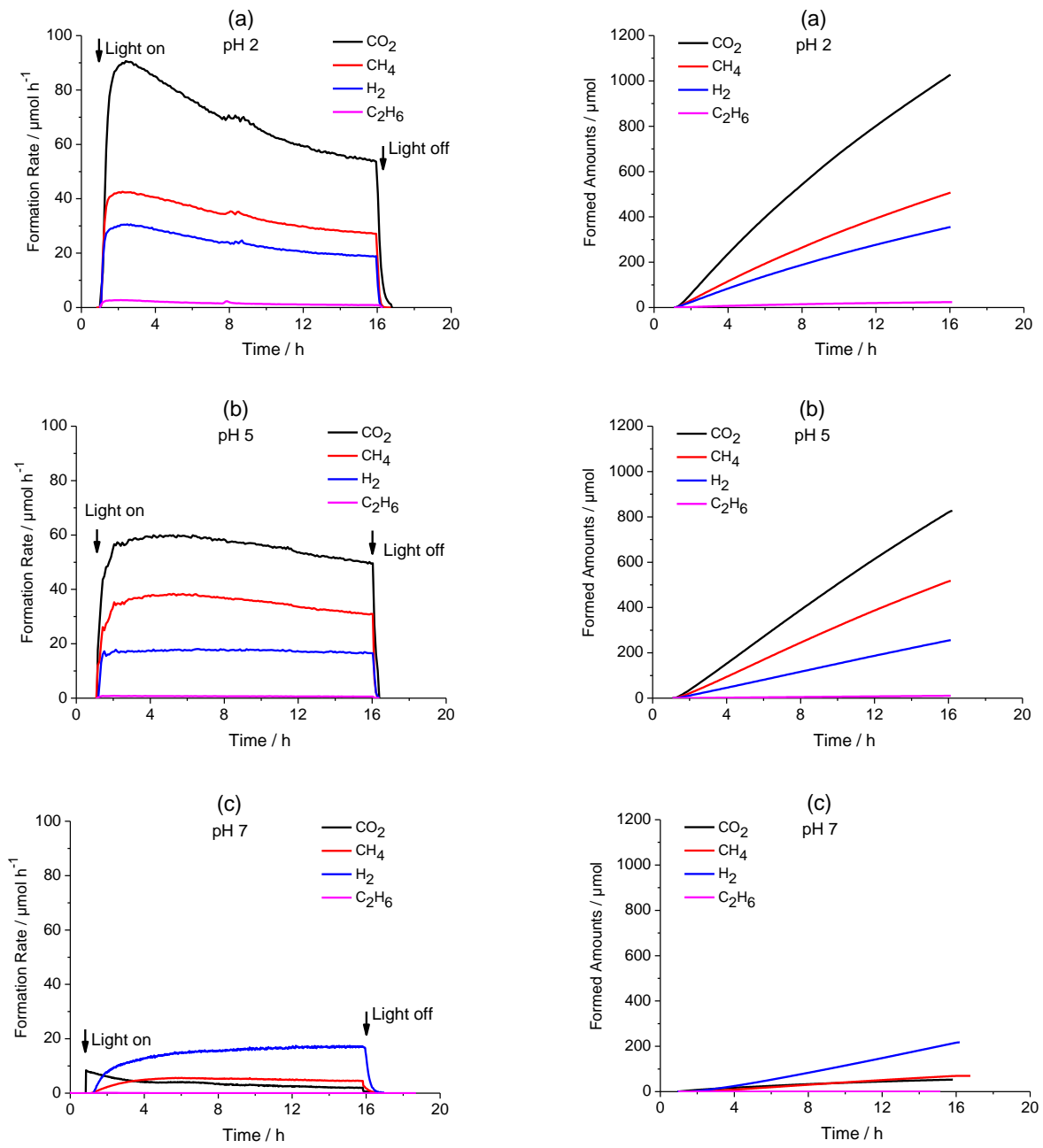
**Figure 20:** Amounts of the main reaction products *i.e.*,  $\text{CO}_2$ ,  $\text{H}_2$ ,  $\text{CH}_4$ , and  $\text{C}_2\text{H}_6$ , photocatalytically formed from aqueous suspensions containing 1 wt % Pt/ $\text{TiO}_2$  as the photocatalyst and varying amounts of acetic acid after an irradiation time of 15 h. *Experimental conditions:* as in Figure 18 – 19.

The change in the  $c_0$  of acetic acid among 0.05 M – 1 M corresponding to ( $2500 \mu\text{mol} \leq n_0 \leq 5000 \mu\text{mol}$ ,  $n_0$  = initial number of acetic acid moles) gives the reaction products with approximately constant amounts with the experimental error of  $\pm 10\%$ . However, a further increase in the acetic acid  $c_0 > 1$  M ( $5000 \mu\text{mol}$ ) illustrates a decreasing trend in the formation of all reaction products. It should also be noted that over the range of  $0.005 \text{ M} \leq c_0 \leq 0.05 \text{ M}$  ( $250 \mu\text{mol} \leq n_0 \leq 2500 \mu\text{mol}$ ), the principal reaction product is  $\text{H}_2$ . On the other hand,  $0.1 \text{ M} \leq c_0 \leq 5 \text{ M}$  ( $5000 \mu\text{mol} \leq n_0 \leq 250000 \mu\text{mol}$ ) demonstrates  $\text{CH}_4$  as the main reaction product. Hence, a composition enriched in  $\text{H}_2$  with hydrocarbons mixture then changes to a composition poor in  $\text{H}_2$  with increasing the  $c_0$  of acetic acid. It is obvious that both energy fuels (*i.e.*,  $\text{H}_2$ ,  $\text{CH}_4$ ) depict the highest evolved amounts simultaneously when initial concentration of acetic acid was 0.5 M (Figure 20). Therefore, 0.5 M was chosen as the optimized value for acetic acid concentration.

#### 3.2.4 Effect of different pH values

For the mechanistic investigations, pH value is one of the key parameters. After analysing the optimized conditions for the suitable co-catalyst and acetic acid concentration, effect of various pH media on the reaction rates and product distribution from photo-induced degradation of aqueous acetic acid has been studied in the present work. The results obtained by varying the initial pH value of suspension over a range of values such as:  $2 \leq \text{pH} \leq 11$  employing Pt/TiO<sub>2</sub> and 0.5 M acetic acid are shown in Figure 21, 22, 23 and 24. Here,  $\text{CO}_2$ ,  $\text{CH}_4$ , and  $\text{H}_2$  were found to be the main reaction products and  $\text{C}_2\text{H}_6$  as the minor product at  $\text{pH} < 7$ , while an increase in the  $\text{pH}$  ( $\geq 7$ ) results in decreasing amounts of the  $\text{CO}_2$ ,  $\text{CH}_4$  and  $\text{C}_2\text{H}_6$ . Moreover, the  $\text{H}_2$  formation seemed to be constant in between the range of  $5 \leq \text{pH} \leq 9$ , but further increase in the  $\text{pH} > 9$  value results in lowering the  $\text{H}_2$  formation. Figure 21 illustrates the formation rates of the main reaction products and Figure 22 is a representation of the formed amounts for  $2 \leq \text{pH} \leq 11$ .

### 3. Results





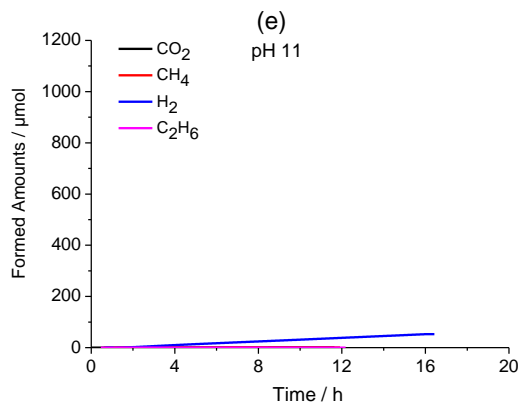
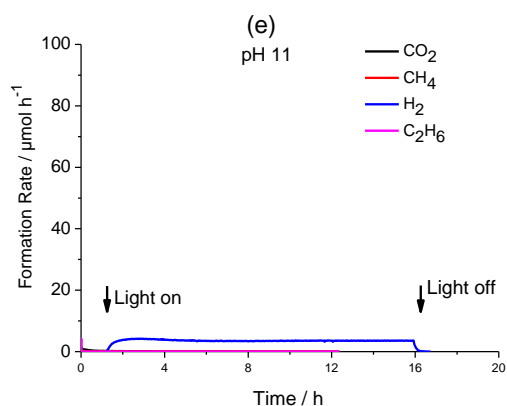
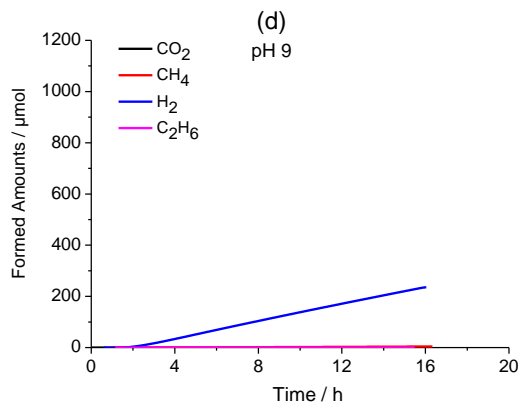
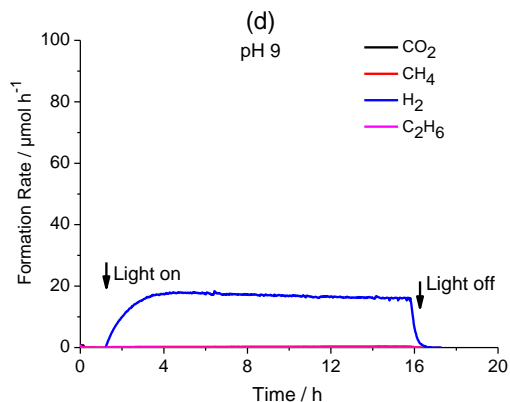


**Figure 21:** Photocatalytic formation rates of the main reaction products, *i.e.*, CO<sub>2</sub>, H<sub>2</sub>, CH<sub>4</sub> and C<sub>2</sub>H<sub>6</sub> from aqueous acetic acid employing 1 wt % Pt/TiO<sub>2</sub>. *Experimental conditions:* photocatalyst concentration = 0.5 g L<sup>-1</sup>, initial acetic acid concentration = 0.5 M, 2 ≤ initial pH ≤ 11 (adjusted by NaOH), suspension volume = 50 mL, irradiation time = 15 h, irradiation intensity I<sub>250-450</sub> = 30 mW cm<sup>-2</sup>.

**Figure 22:** Photocatalytically formed amounts of the main reaction products, *i.e.*, CO<sub>2</sub>, H<sub>2</sub>, CH<sub>4</sub> and C<sub>2</sub>H<sub>6</sub> from aqueous acetic acid employing 1 wt % Pt/TiO<sub>2</sub>. *Experimental conditions:* photocatalyst concentration = 0.5 g L<sup>-1</sup>, initial acetic acid concentration = 0.5 M, 2 ≤ initial pH ≤ 11 (adjusted by NaOH), suspension volume = 50 mL, irradiation time = 15 h, irradiation intensity I<sub>250-450</sub> = 30 mW cm<sup>-2</sup>.

### 3. Results

It is obvious from the Figure 21 that the photocatalytic reaction system containing Pt/TiO<sub>2</sub> as a photocatalyst suspended in 0.5 M acetic acid at pH 2 quantitatively demonstrates the formation of reaction products in their atomic ratios as:  $\left(0.6 < \frac{n(C)}{n(O)} < 0.9, 1.0 < \frac{n(H)}{n(O)} < 2.0, \text{ and } 1.4 < \frac{n(H)}{n(C)} < 2.1\right)$  after 15 h of irradiation. In comparison to this, the expected ratios of the atoms forming CH<sub>3</sub>COOH molecule is:  $\left(\frac{n(C)}{n(O)}=1, \frac{n(H)}{n(O)}=2, \text{ and } \frac{n(H)}{n(C)}=2\right)$  (Equation 10 – 11). The obtained results thus suggest the formation of other by-products than the main reaction products. The qualitative data analysis through QMS confirmed the existence of a large number of by-products such as CO, C<sub>3</sub>H<sub>8</sub>, CH<sub>3</sub>OH, C<sub>2</sub>H<sub>5</sub>OH, HCHO, CH<sub>3</sub>CHO, and HCOOH in the gas phase (Figure 23).

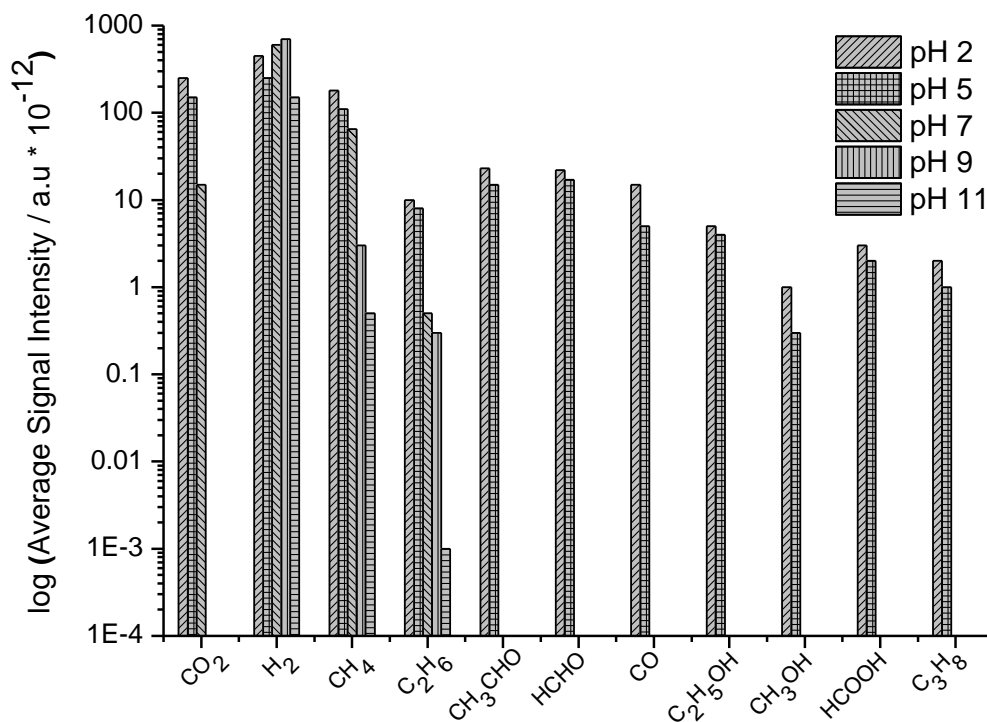


**Figure 23:** Time-averaged signal intensities of all gaseous reaction products formed during the photocatalytic conversion of aqueous acetic acid employing 1 wt % Pt TiO<sub>2</sub>, *Experimental conditions:* photocatalyst concentration = 0.5 g L<sup>-1</sup>, initial acetic acid concentration = 0.5 M, 2 ≤ initial pH ≤ 11 (adjusted by NaOH), suspension volume = 50 mL, irradiation time = 15 h, irradiation intensity I<sub>250-450</sub> = 30 mW cm<sup>-2</sup>.

### 3. Results

It can be seen in Figure 23 that the amounts of formed by-products are insignificant as compared to the main reaction products ( $\text{CO}_2$ ,  $\text{CH}_4$ , and  $\text{H}_2$ ). Therefore, a quantitative analysis of only main reaction products and one minor product ( $\text{C}_2\text{H}_6$ ) has been done. In Figure 24, the amounts of the evolved gaseous product are presented over a range of pH values such as:  $2 \leq \text{pH} \leq 11$ . It should be noted that at  $\text{pH} < 7$ , the ratio between the formed amounts of  $\text{H}_2$  and  $\text{CH}_4$  is:  $\frac{n(\text{H}_2)}{n(\text{CH}_4)} < 1$  meaning that the formation of  $\text{CH}_4$  is preferred. On the contrary, for  $\text{pH} \geq 7$  the ratio between the formed amounts of  $\frac{n(\text{H}_2)}{n(\text{CH}_4)}$  and  $\frac{n(\text{H}_2)}{n(\text{C}_2\text{H}_6)}$  continue to rise with increasing the pH value indicating the suppression of alkanes formation (Figure 24). Thus,  $\text{H}_2$  was observed as the only reaction product in higher amounts. Additionally, at  $\text{pH} \geq 7$ , the  $\text{CO}_2$  is converted into carbonate ( $\text{CO}_3^{2-}$ ) and bicarbonate ( $\text{HCO}_3^-$ ) [109]. So,  $\text{CO}_2$  cannot be detected in the gas phase by QMS but it remains present in the aqueous suspensions.

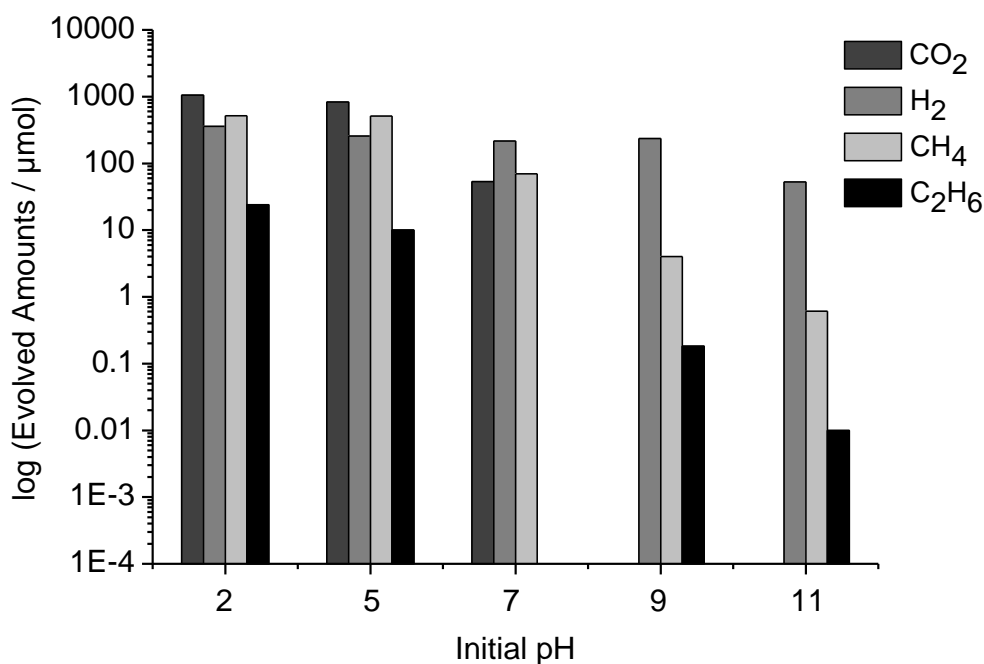


**Figure 24:** Amounts of the main reaction products *i.e.*,  $\text{CO}_2$ ,  $\text{H}_2$ ,  $\text{CH}_4$ , and  $\text{C}_2\text{H}_6$ , photocatalytically formed from aqueous suspensions containing 1 wt %  $\text{Pt/TiO}_2$  as the photocatalyst and varying initial pH values after an irradiation time of 15 h. *Experimental conditions:* as in Figure 21 – 22.

### 3. Results

#### 3.2.5 Isotopic labelling study

Mechanistic investigations for the photocatalytic decomposition of aqueous acetic acid were done by means of isotopic labelling studies. For this purpose, photocatalytic reaction systems containing isotopically different solutions of acetic acid and water were analysed. The details of the reaction systems are as follow:

- (i) Pt/TiO<sub>2</sub>-CH<sub>3</sub>COOH-H<sub>2</sub>O
- (ii) Pt/TiO<sub>2</sub>-CD<sub>3</sub>COOD-H<sub>2</sub>O
- (iii) Pt/TiO<sub>2</sub>-CH<sub>3</sub>COOD-H<sub>2</sub>O
- (iv) Pt/TiO<sub>2</sub>-CD<sub>3</sub>COOD-D<sub>2</sub>O
- (v) Pt/TiO<sub>2</sub>-CH<sub>3</sub>COOH-D<sub>2</sub>O
- (vi) Pt/TiO<sub>2</sub>-CH<sub>3</sub>COOD-D<sub>2</sub>O

For these experiments, only the main reaction products were quantified. In general, carbon dioxide (CO<sub>2</sub>) molecular hydrogen (H<sub>2</sub>), molecular deuterium (D<sub>2</sub>), HD and methane in different isotopic composition (*i.e.*, CH<sub>4</sub>, CH<sub>3</sub>D, CD<sub>3</sub>H, and CD<sub>4</sub>) were detected as the reaction products from all reaction systems (i – vi). The formation rates and the product distribution were observed to vary according to the employed reaction conditions. Here, Pt/TiO<sub>2</sub> was used as a photocatalyst employing 0.5 M acetic acid at pH ≈ pD = 2. The pD adjustments were carried out according to the Gross-Butler-Purlee-theory (pD = pH + 0.44) [110].

##### 3.2.5.1 Formation of carbon dioxide

In all six reaction systems (i – vi), CO<sub>2</sub> was found as the major reaction product evolved in highest amounts as compared to the H<sub>2</sub>, D<sub>2</sub>, HD, CH<sub>4</sub>, CH<sub>3</sub>D, CD<sub>3</sub>H, and CD<sub>4</sub>. Figure 25 and 26 show the CO<sub>2</sub> formation rates and corresponding formed amounts, respectively, for all reaction systems (i – vi). During 15 h of illumination, the decrease in the CO<sub>2</sub> formation rate was found to be much larger in suspensions containing H<sub>2</sub>O as a solvent (Figure 25a) in comparison to the suspensions having D<sub>2</sub>O as a solvent (Figure 25b).

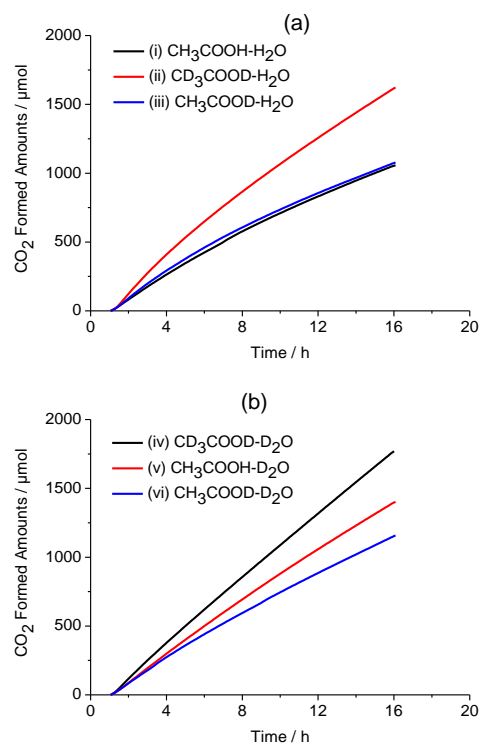
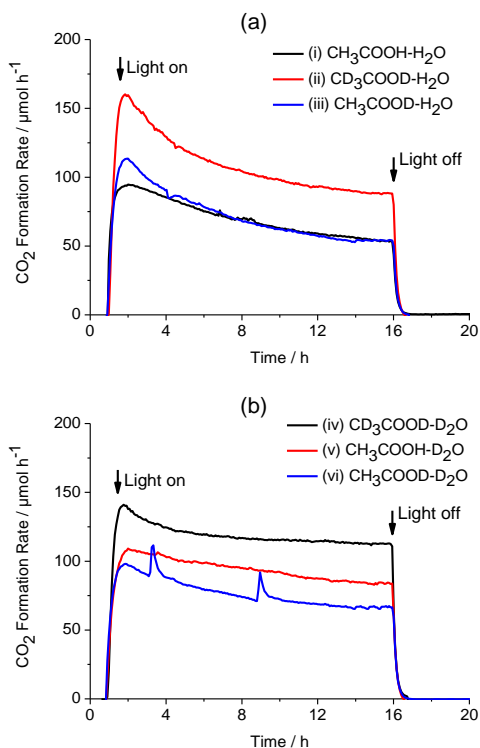


**Figure 25:** Photocatalytic formation rate of CO<sub>2</sub> for (a) reaction systems i, ii, iii and (b) reaction systems iv, v, vi employing 1 wt % Pt TiO<sub>2</sub>, photocatalyst concentration = 0.5 g L<sup>-1</sup>, acetic acid concentration = 0.5 M, pH ≈ pD = 2, reactor volume = 50 m L, irradiation time = 15 h, irradiation intensity: I<sub>250-450</sub> = 30 mW cm<sup>-2</sup>.

**Figure 26:** Photocatalytically formed amount of CO<sub>2</sub> for (a) reaction systems i, ii, iii and (b) reaction systems iv, v, vi employing 1 wt % Pt TiO<sub>2</sub>, photocatalyst concentration = 0.5 g L<sup>-1</sup>, acetic acid concentration = 0.5 M, pH ≈ pD = 2, reactor volume = 50 m L, irradiation time = 15 h, irradiation intensity: I<sub>250-450</sub> = 30 mW cm<sup>-2</sup>.

The solvent (*i.e.*, H<sub>2</sub>O, D<sub>2</sub>O) also seems to affect the photo-decarboxylation rate (Figure 25). For example, the higher evolved amount of CO<sub>2</sub> from reaction system (v) having D<sub>2</sub>O as solvent than (i) containing H<sub>2</sub>O as a solvent determines that the decarboxylation of CH<sub>3</sub>COOH is fast in D<sub>2</sub>O than in H<sub>2</sub>O. Moreover, Figure 27 shows that the reaction systems (ii and iv) containing CD<sub>3</sub>COOD depicts higher amounts of CO<sub>2</sub> formation in comparison to the system (i, iii, iv, and

### 3. Results

v) having  $\text{CH}_3\text{COOH}$  or  $\text{CH}_3\text{COOD}$ . This means that the photo-decarboxylation of  $\text{CD}_3\text{COOD}$  is easier than  $\text{CH}_3\text{COOH}$  and  $\text{CH}_3\text{COOD}$ .

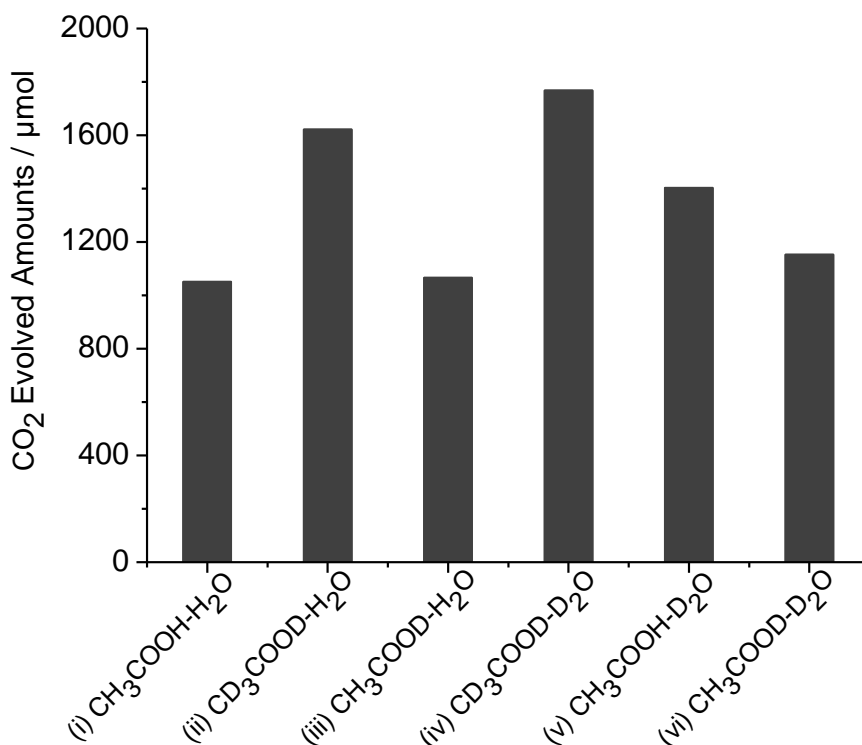


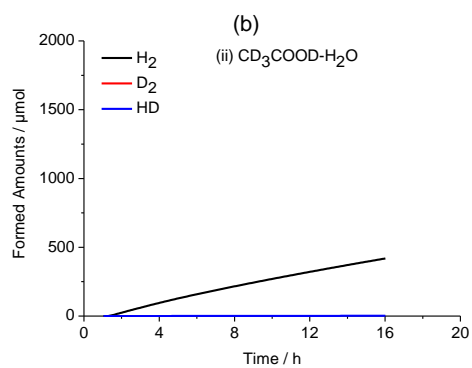
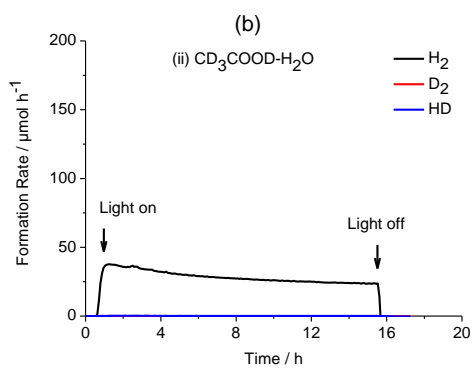
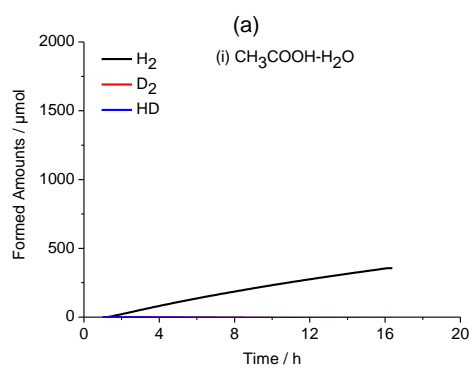
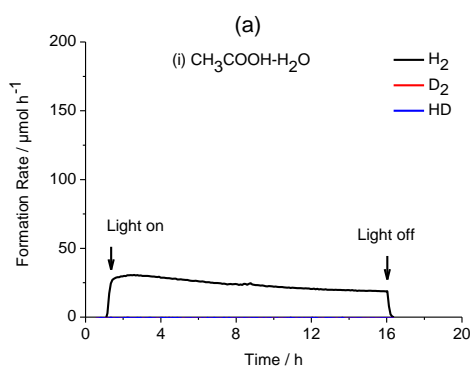
**Figure 27:** Amounts of the  $\text{CO}_2$ , photocatalytically formed from aqueous suspensions containing 1 wt % Pt/TiO<sub>2</sub> as the photocatalyst after an irradiation time of 15 h. *Experimental conditions:* as in Figure 25 – 26.

#### 3.2.5.2 Formation of molecular hydrogen and molecular deuterium

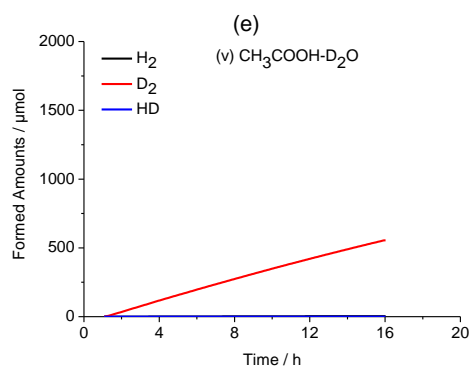
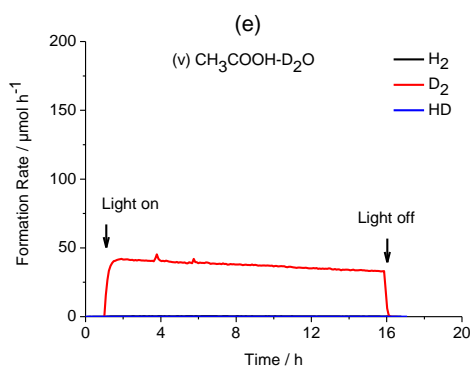
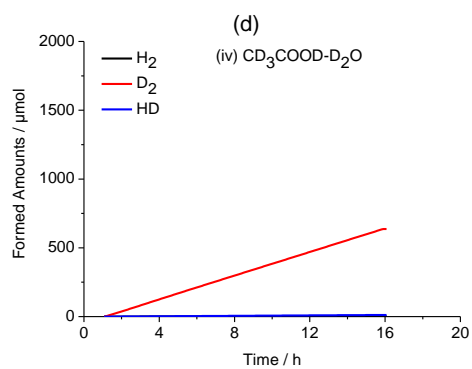
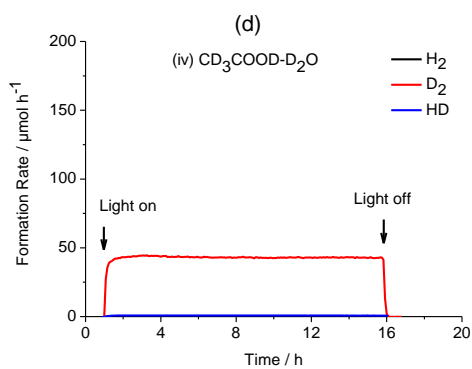
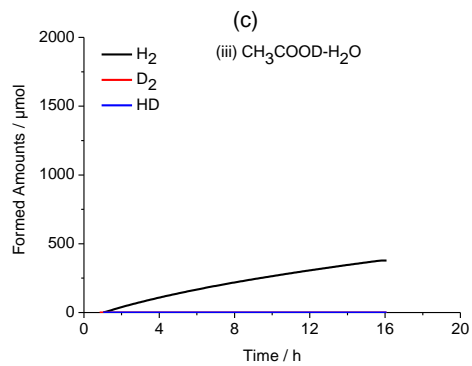
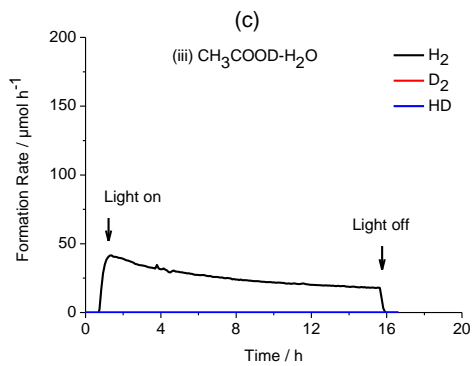
The photocatalytic decomposition of acetic acid employing reaction systems (i – vi) results in the formation of molecular hydrogen ( $\text{H}_2$ ), molecular deuterium ( $\text{D}_2$ ) and HD as presented in Figure 28 and 29. Here, Figure 28 represents the formation rates and Figure 29 illustrates the evolved amounts of  $\text{H}_2$ ,  $\text{D}_2$ , and HD. It can be seen in Figure 30 that the formation of main species (i.e.,  $\text{H}_2$ ,  $\text{D}_2$ , and HD) depends on the solvent being employed. For instance,  $\text{H}_2$  and  $\text{D}_2$  are produced as the major reaction products with significant amounts employing reaction systems (i) containing  $\text{H}_2\text{O}$  and (iv) having  $\text{D}_2\text{O}$  as a solvent, respectively. No traces for HD were detected in system (i)

### 3. Results

but negligible traces of HD were observed in reaction system (iv) as shown in Figure 30. It should also be taken into account that the reaction rates for  $D_2$  formation remain quite stable during the 15 h of illumination in systems (iii, iv, and v) having  $D_2O$  as a solvent. In comparison to this, the reaction rates for  $H_2$  formation in reaction systems (i, ii, and iii) during 15 h of illumination exhibit a decreasing trend (Figure 28a, 28d).



### 3. Results





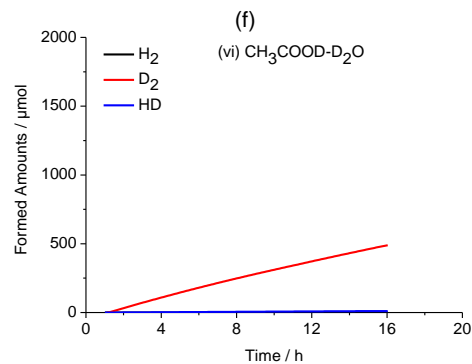
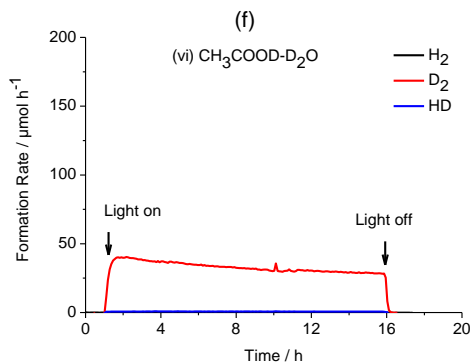


**Figure 28:** Photocatalytic formation rates of the  $H_2$ ,  $D_2$  and HD for: (a) reaction system-i (b) reaction system-ii (c) reaction system-iii (d) reaction system-iv (e) reaction system-v (f) reaction system-vi, employing 1 wt % Pt  $TiO_2$ , photocatalyst concentration =  $0.5 \text{ g L}^{-1}$ , acetic acid concentration =  $0.5 \text{ M}$ ,  $pH \approx pD = 2$ , reactor volume =  $50 \text{ mL}$ , irradiation time =  $15 \text{ h}$ , irradiation intensity :  $I_{250-450} = 30 \text{ mW cm}^{-2}$ .

**Figure 29:** Photocatalytically formed amounts of the  $H_2$ ,  $D_2$  and HD for: (a) reaction system-i (b) reaction system-ii (c) reaction system-iii (d) reaction system-iv (e) reaction system-v (f) reaction system-vi, employing 1 wt % Pt  $TiO_2$ , photocatalyst concentration =  $0.5 \text{ g L}^{-1}$ , acetic acid concentration =  $0.5 \text{ M}$ ,  $pH \approx pD = 2$ , reactor volume =  $50 \text{ mL}$ , irradiation time =  $15 \text{ h}$ , irradiation intensity :  $I_{250-450} = 30 \text{ mW cm}^{-2}$ .

Moreover, the evolved amounts for  $D_2$  ( $642 \text{ } \mu\text{mol}$ ) in system (iv) Pt/ $TiO_2$ - $CD_3COOD-D_2O$  were approximately two times higher than the evolved amounts of  $H_2$  in system (i) Pt/ $TiO_2$ - $CH_3COOH-H_2O$  (Figure 30). These results support the data obtained for  $CO_2$  evolution (chapter 3.2.5.1). The higher amount of  $D_2$  formation (iv, v, and vi) in comparison to  $H_2$  formation illustrates that the decarboxylation of  $CD_3COOD$  is faster than  $CH_3COOH$ .

### 3. Results

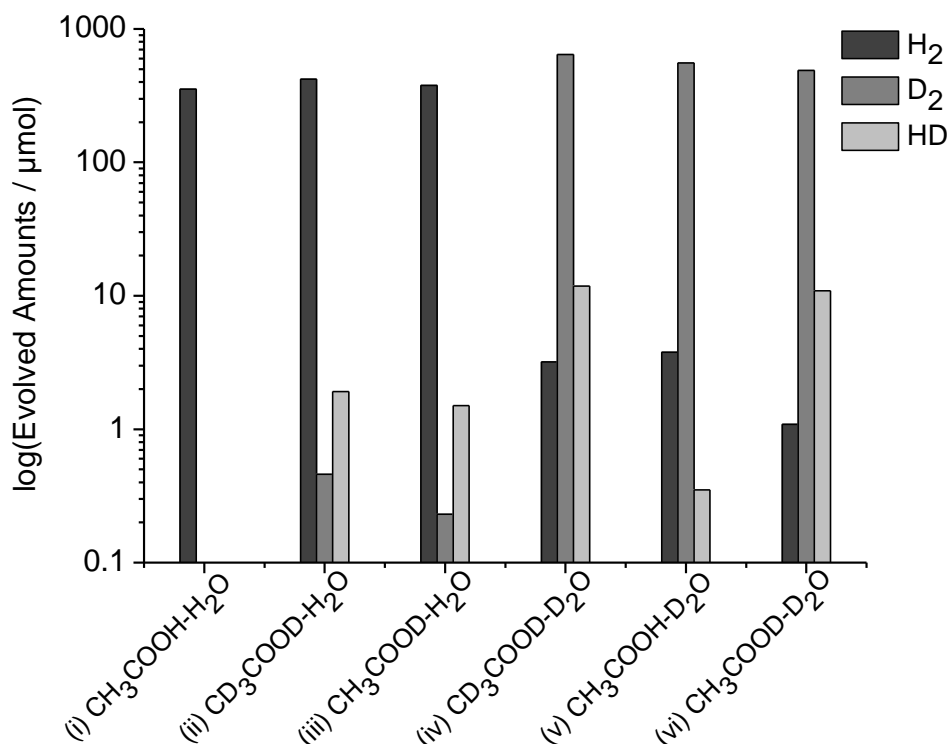
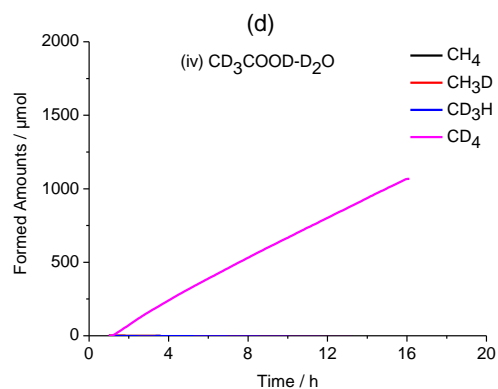
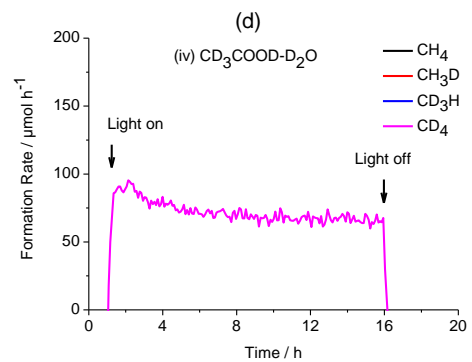
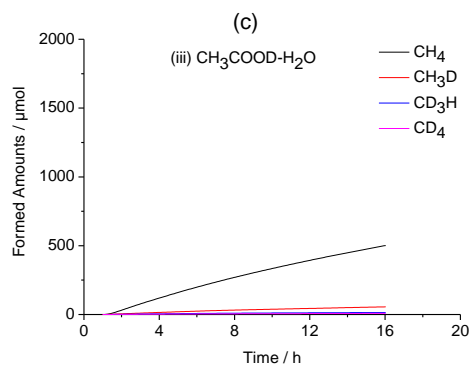
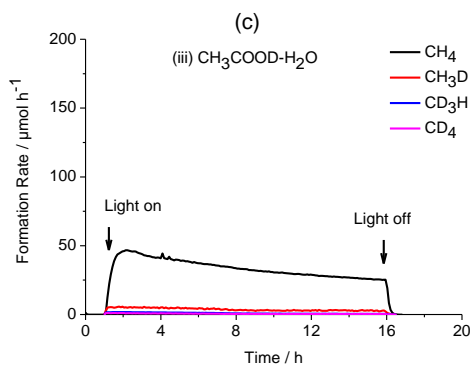
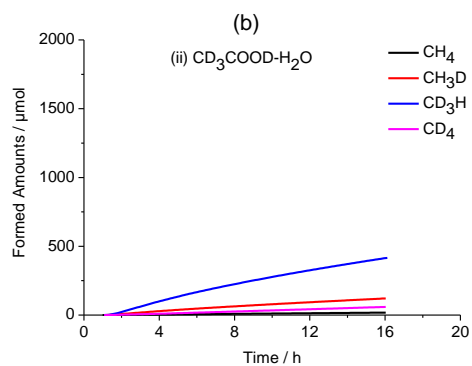
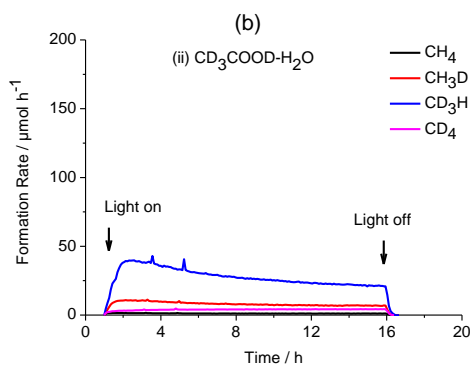
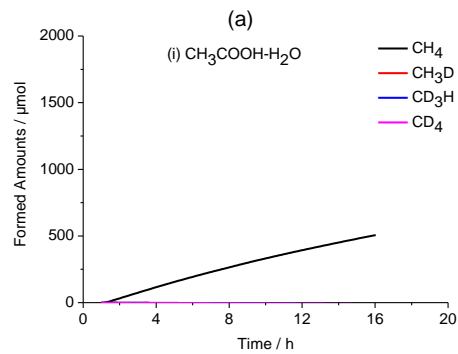
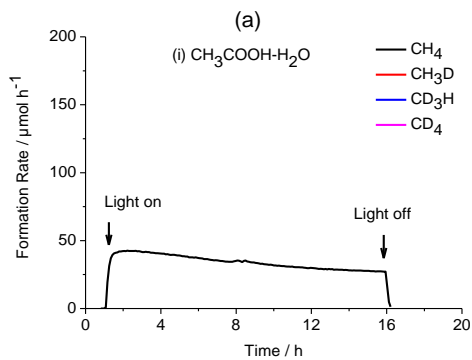


**Figure 30:** Amounts of the H<sub>2</sub>, D<sub>2</sub>, and HD, photocatalytically formed from aqueous suspensions containing 1 wt % Pt/TiO<sub>2</sub> as the photocatalyst after an irradiation time of 15 h. *Experimental conditions:* as in Figure 28 – 29.

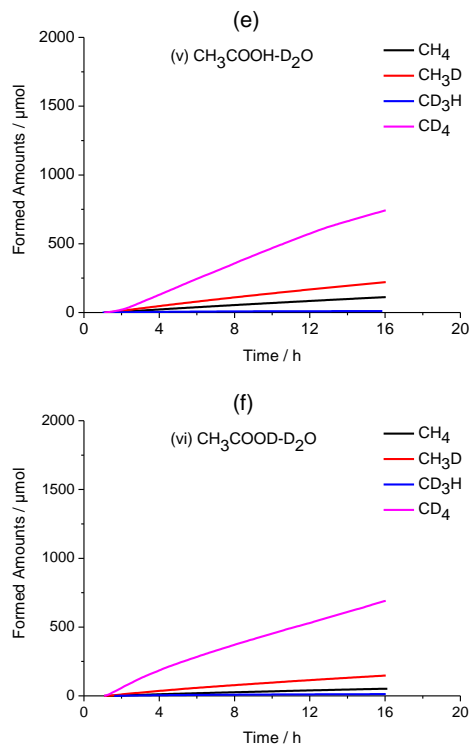
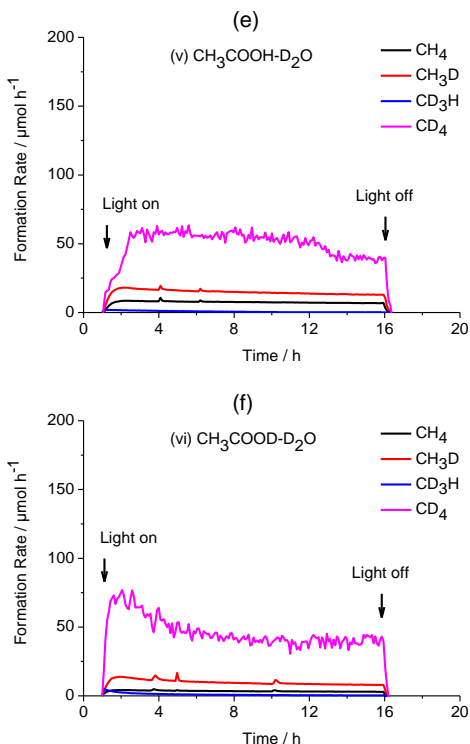
#### 3.2.5.3 Formation of methanes

Figure 31 and 32 represent the formation rates and relative formed amounts, respectively, for the methane formation resulting from the photocatalytic degradation of acetic acid employing reaction systems (i – vi). It can be seen in Figure 31a, 31d, 32a, and 32d that CH<sub>4</sub> (507 μmol) and CD<sub>4</sub> (1066 μmol) were found to be the only reaction products in reaction systems (i) Pt/TiO<sub>2</sub>-CH<sub>3</sub>COOH-H<sub>2</sub>O and (iv) Pt/TiO<sub>2</sub>-CD<sub>3</sub>COOD-D<sub>2</sub>O, respectively. However, further analyses for the reaction systems (ii, iii, v, and vi) consisting of H/D mixtures illustrate the formation of four types of methane being different in isotopic composition such as: CH<sub>4</sub>, CH<sub>3</sub>D, CD<sub>3</sub>H, and CD<sub>4</sub> (Figure 31b, 31c, 31e, and 31f).

### 3. Results



### 3. Results



**Figure 31:** Photocatalytic formation rates of the  $\text{CH}_4$ ,  $\text{CD}_4$ ,  $\text{CH}_3\text{D}$  and  $\text{CD}_3\text{H}$  for: (a) reaction system-ii, (b) reaction system-iii, (c) reaction system-v and (d) reaction system-vi, employing 1 wt % Pt  $\text{TiO}_2$ , photocatalyst concentration =  $0.5 \text{ g L}^{-1}$ , acetic acid concentration =  $0.5 \text{ M}$ ,  $\text{pH} \approx \text{pD} = 2$ , reactor volume =  $50 \text{ m L}$ , irradiation time =  $15 \text{ h}$ , irradiation intensity :  $I_{250\text{-}I_{450}} = 30 \text{ mW cm}^{-2}$ .

**Figure 32:** Photocatalytically formed amounts of the  $\text{CH}_4$ ,  $\text{CD}_4$ ,  $\text{CH}_3\text{D}$  and  $\text{CD}_3\text{H}$  for: (a) reaction system-ii, (b) reaction system-iii, (c) reaction system-v and (d) reaction system-vi, employing 1 wt % Pt  $\text{TiO}_2$ , photocatalyst concentration =  $0.5 \text{ g L}^{-1}$ , acetic acid concentration =  $0.5 \text{ M}$ ,  $\text{pH} \approx \text{pD} = 2$ , reactor volume =  $50 \text{ m L}$ , irradiation time =  $15 \text{ h}$ , irradiation intensity :  $I_{250\text{-}I_{450}} = 30 \text{ mW cm}^{-2}$ .

A comparison between the evolved amounts of methane being different in isotopic composition is presented in Figure 33. The results obtained for methanes (*i.e.*,  $\text{CH}_4$ ,  $\text{CH}_3\text{D}$ ,  $\text{CD}_3\text{H}$ ,  $\text{CD}_4$ ) are different from the published literature [36, 37, 84, 111]. According to the reported literature,  $\text{CD}_3\text{H}$  and  $\text{CH}_4$  are the expected species from reaction systems (ii and iii) having  $\text{H}_2\text{O}$  as a solvent with  $\text{CD}_3\text{COOD}$  and  $\text{CH}_3\text{COOD}$ , respectively. Here, data presented in Figure 33 shows

### 3. Results

that the reaction systems (ii and iii) result in the formation of  $\text{CD}_3\text{H}$  and  $\text{CH}_4$ , respectively, as major reaction products besides  $\text{CH}_3\text{D}$  as the minor product. Moreover, the expected reaction product from reaction systems (v and vi) containing  $\text{D}_2\text{O}$  as a solvent with  $\text{CH}_3\text{COOH}$  and  $\text{CH}_3\text{COOD}$  is  $\text{CH}_3\text{D}$ . Unlike the published reports [84, 111], a proton exchange at methyl group ( $\text{CH}_3$ ) of acetic acid has been observed for these reaction systems (v and vi). Unexpectedly,  $\text{CD}_4$  was found to be the major reaction product in higher amounts from reaction systems having  $\text{D}_2\text{O}$  as a solvent with  $\text{CH}_3\text{COOH}$  and  $\text{CH}_3\text{COOD}$ .

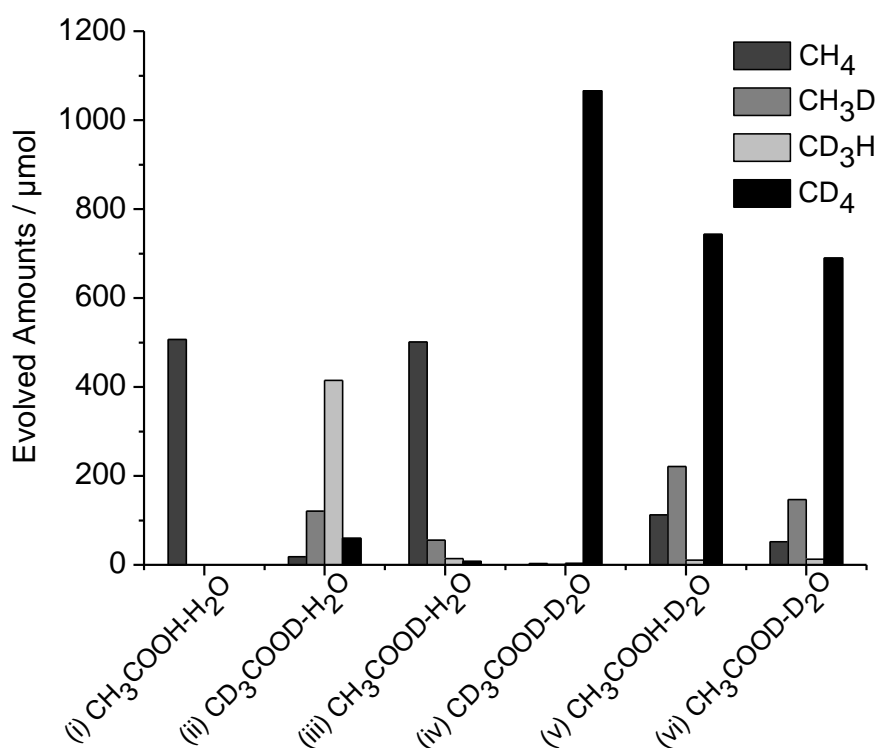


**Figure 33:** Amounts of the  $\text{CH}_4$ ,  $\text{CH}_3\text{D}$ ,  $\text{CD}_3\text{H}$ , and  $\text{CD}_4$ , photocatalytically formed from aqueous suspensions containing 1 wt %  $\text{Pt/TiO}_2$  as the photocatalyst after an irradiation time of 15 h. *Experimental conditions:* as in Figure 31 – 32.

### 3. Results

#### 3.2.5.4 Nuclear magnetic resonance study

Nuclear magnetic resonance (NMR) spectroscopy with H<sub>2</sub>O suppression has been performed in order to confirm the proton exchange reaction (PER) determined by quadrupole mass spectrometer (QMS) mainly at the methyl group (CH<sub>3</sub>) of acetic acid during photocatalytic experiments for the reaction systems (ii) Pt/TiO<sub>2</sub>-CD<sub>3</sub>COOD-H<sub>2</sub>O and (v) Pt/TiO<sub>2</sub>-CH<sub>3</sub>COOH-D<sub>2</sub>O. The NMR studies were carried out for reaction systems (ii) and (v) only, in the solid liquid phase before and after the illumination. For a typical experiment, suspension from reaction system (ii) Pt/TiO<sub>2</sub>-CD<sub>3</sub>COOD-H<sub>2</sub>O was deaerated and transferred to the NMR tube before illumination. The NMR tube was then transferred to the sample holder and the NMR spectrum was measured. The spectrum taken before illumination for reaction system (ii) is presented in the Figure 34. It can be seen in Figure 34 that only a resonance peak corresponding to the H<sub>2</sub>O signal is obvious while no other signal was detected. The same procedure was repeated for the suspension from reaction systems (v) Pt/TiO<sub>2</sub>-CH<sub>3</sub>COOH-D<sub>2</sub>O. Figure 35 shows the NMR spectrum obtained from reaction system (v) prior to the illumination. Here, the resonance signals corresponding to the H<sub>2</sub>O and methyl (CH<sub>3</sub>) group of acetic acid were observed only (Figure 35).

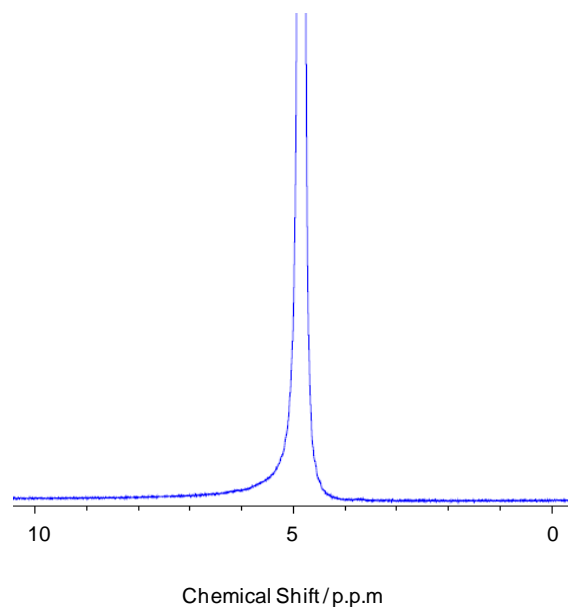


**Figure 34:** <sup>1</sup>H NMR spectra for reaction system (ii) Pt/TiO<sub>2</sub>-CD<sub>3</sub>COOD-H<sub>2</sub>O, employing 1 wt % Pt/TiO<sub>2</sub>, photocatalyst concentration = 0.5 g L<sup>-1</sup>, acetic acid concentration = 0.5 M, before illumination.

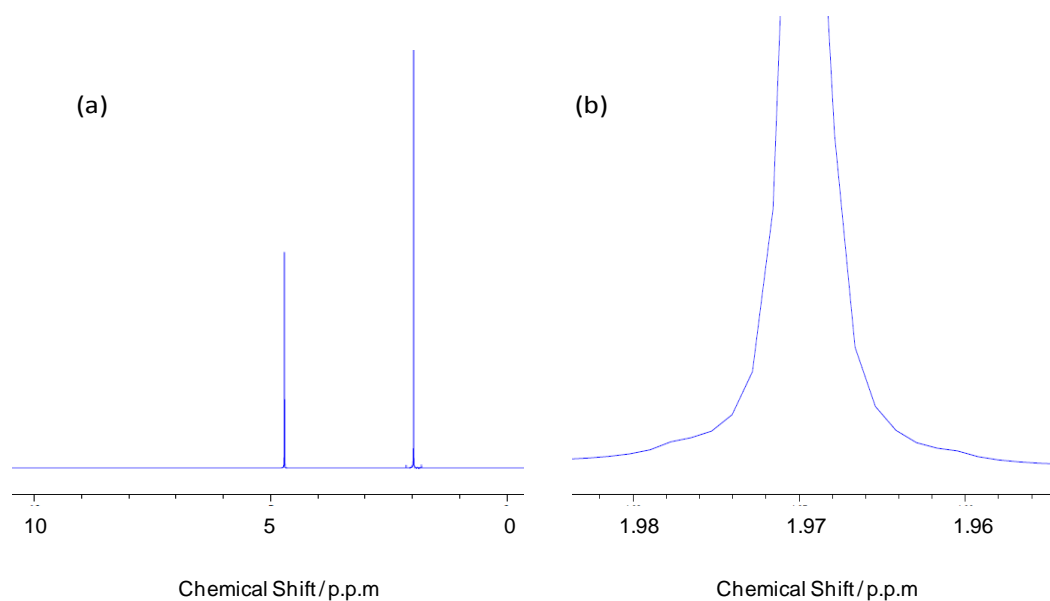


**Figure 35:** <sup>1</sup>H NMR spectra for reaction system (v) Pt/TiO<sub>2</sub>-CH<sub>3</sub>COOH-D<sub>2</sub>O, employing 1 wt % Pt/TiO<sub>2</sub>, photocatalyst concentration = 0.5 g L<sup>-1</sup>, acetic acid concentration = 0.5 M, before illumination (a) Full spectrum, (b) Zoom image representing methyl (CH<sub>3</sub>) group of acetic acid.

### 3. Results

Afterwards, a photocatalytic reaction was performed in a photoreactor attached to the quadrupole mass spectrometer (QMS) employing suspension from reaction system (ii) Pt/TiO<sub>2</sub>-CD<sub>3</sub>COOD-H<sub>2</sub>O. Immediately after 15 h of illumination, the obtained suspension was transferred to the Argon (Ar) purged NMR tube *via* a syringe. This NMR tube was then placed in the NMR sample holder and measured immediately. The spectrum obtained after the illumination of suspension is shown in Figure 36a. A quintet signal with intensity (1:2:3:2:1,  $J = 2.2$  Hz) as expected for CHD<sub>2</sub> moiety was observed for illuminated suspension from reaction system (ii) Pt/TiO<sub>2</sub>-CD<sub>3</sub>COOD-H<sub>2</sub>O. The multiplicity was calculated according to the following relation:

$$M = 2 \times n \times I + 1 \quad \text{Equation 21}$$

Here,  $n$  and  $I$  are the number and spin of the interacting atoms, respectively. The obtained quintet signal from NMR employing reaction systems (ii) Pt/TiO<sub>2</sub>-CD<sub>3</sub>COOD-H<sub>2</sub>O was assigned to the formation of CHD<sub>2</sub>COOD(H) species. This is the confirmation of our hypothesis about the occurrence of proton exchange reaction at the methyl group of acetic acid during a photocatalytic reaction.

The spectrum obtained from NMR spectroscopy for the reaction system (v) Pt/TiO<sub>2</sub>-CH<sub>3</sub>COOH-D<sub>2</sub>O is presented in Figure 36b (after illumination). The same procedure for sample preparation was repeated for this system (v) as defined for the reaction system (ii). Prior to the illumination, the suspension from reaction system (v) exhibits a typical resonance peak, which corresponds to the methyl group (CH<sub>3</sub>) of acetic acid (Figure 35). After the suspension was illuminated, NMR determines a triplet signal (1:1:1,  $J = 2.2$  Hz) having identical intensities besides the CH<sub>3</sub> signal of acetic acid (Figure 36b). By using the relation described in Equation 21, the obtained NMR signal from reaction system (v) Pt/TiO<sub>2</sub>-CH<sub>3</sub>COOH-D<sub>2</sub>O was assigned to CH<sub>2</sub>DCOOH(D) species.

However, in both reaction systems (ii) Pt/TiO<sub>2</sub>-CD<sub>3</sub>COOD-H<sub>2</sub>O and (v) Pt/TiO<sub>2</sub>-CH<sub>3</sub>COOH-D<sub>2</sub>O, the proton exchange reaction at the carboxylic group (COOH) of acetic acid occurred quickly. It should also be kept in mind that due to the employment of reaction systems having (ii) H<sub>2</sub>O and (v) D<sub>2</sub>O as a solvent, the NMR spectra demonstrated a slight shift ( $\approx 0.972$ ) in the H<sub>2</sub>O signal (Figure 34, and 35b). This shift in H<sub>2</sub>O signal leads to a small shift in the quintet and triplet signals within the limits of  $\approx 1.1$  (Figure 35b and 36). However, the quintet and triplet signals still observed in close approximation with the peak depicting CH<sub>3</sub> from CH<sub>3</sub>COOH.



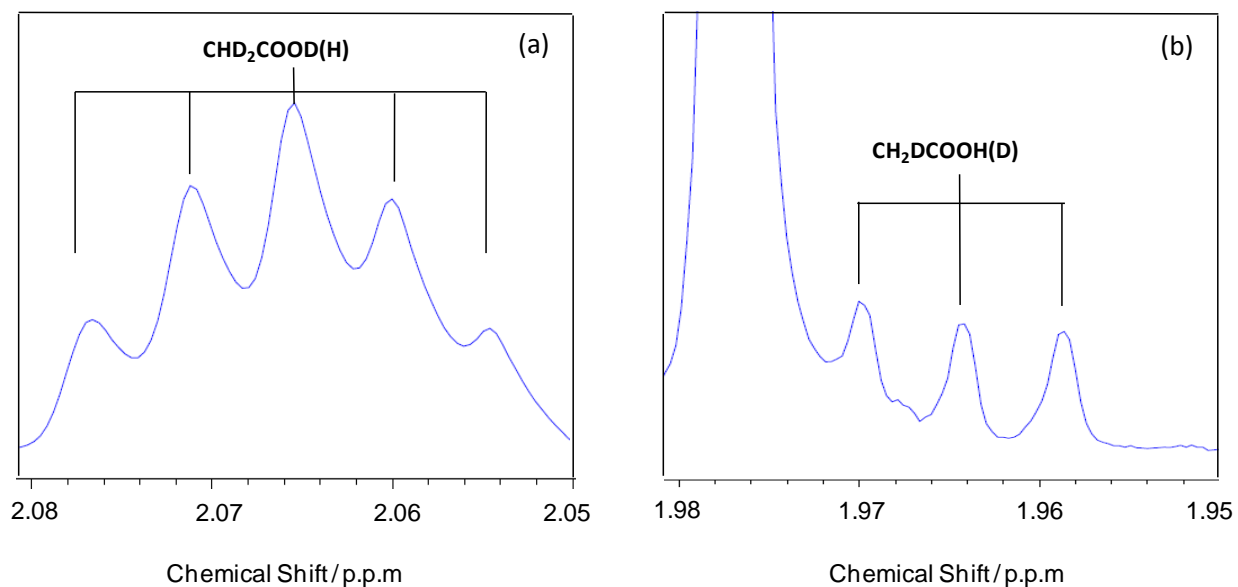


**Figure 36:**  $^1\text{H}$  NMR spectra for (a) reaction system (ii)  $\text{Pt/TiO}_2\text{-CD}_3\text{COOD-H}_2\text{O}$  and (b) reaction system (v)  $\text{Pt/TiO}_2\text{-CH}_3\text{COOH-D}_2\text{O}$ , employing 1 wt %  $\text{Pt/TiO}_2$ , photocatalyst concentration =  $0.5 \text{ g L}^{-1}$ , acetic acid concentration = 0.5 M, reactor volume = 50 m L, irradiation time = 15 h, irradiation intensity :  $I_{250}\text{-}I_{450} = 30 \text{ mWcm}^{-2}$ .

## 4. Discussion

### 4. Discussion

This chapter will analyze the results obtained from the experimental work presented in chapter 3. The discussion will start by interpreting the influence of different experimental parameters affecting the product distribution resulting from the photocatalytic conversion of aqueous acetic acid in the presence of co-catalyst loaded TiO<sub>2</sub>. Starting from the effect of various co-catalyst loadings on the surface of TiO<sub>2</sub> particles, the effect of different initial acetic acid concentrations ( $c_0$ ) on the photocatalytic reaction rates and corresponding reaction product distribution will be explained. Depending on the various pH values, different reaction paths for the photo-induced degradation of aqueous acetic acid will be specified. Finally, details about the fundamental process for the photocatalytic decomposition of aqueous acetic acid on the basis of isotopic labelling studies will be elucidated.

#### 4.1 General Remarks

In the present work, the photocatalytic transformation of aqueous acetic acid into main reaction products *e.g.*, carbon dioxide (CO<sub>2</sub>), hydrogen (H<sub>2</sub>), methane (CH<sub>4</sub>) and ethane (C<sub>2</sub>H<sub>6</sub>) over co-catalyst loaded TiO<sub>2</sub> has been investigated. The quantitative analyses were made only for the gaseous products being generated inside the aqueous suspensions and exiting the photoreactor. Due to the employment of a batch reactor with respect to the suspensions, the possibility of taking the liquid samples during the photocatalytic reaction was limited. However, the employed photoreactor facilitates a continuous flow of the evolved gases to the quadrupole mass spectrometer (QMS). Thus, the data shown in this work refers to the quantitative amounts of gaseous products only. The amounts of the gaseous reaction products exiting the photoreactor are mainly dependent on the equilibrium between liquid – vapour phase [112].

During 15 h of illumination, the formation rates in all experimental runs (Figure 14, 15, 18, 21, 25, 28, and 31) for almost all reaction products did not remain constant. The results presented in literature also show a same behaviour when CH<sub>3</sub>COOH or other organic molecules were employed as electron donors [104, 113]. A possible explanation for the observed decreasing trend in the formation rates of the formed reaction products could be that the photoreactor employed in

this study does not allow a continuous flow of suspensions. Therefore, a decrease in the concentration of the reactants results in the decrease of formation rates of all gaseous reaction products. However, it can be seen in Table 3, 4, and 5 that the fractional conversions  $X_C = \frac{n(\text{CO}_2) + n(\text{CH}_4) + 2n(\text{C}_2\text{H}_6)}{2n_0}$  as well as  $X_H = \frac{n(\text{H}_2) + 2n(\text{CH}_4) + 3n(\text{C}_2\text{H}_6)}{2n_0}$  (where,  $n(\text{CO}_2)$ ,  $n(\text{CH}_4)$ ,  $n(\text{H}_2)$ ,  $n(\text{C}_2\text{H}_6)$ , and  $n_0$  are the evolved amounts of  $\text{CO}_2$ ,  $\text{CH}_4$ ,  $\text{H}_2$ ,  $\text{C}_2\text{H}_6$ , and the initial amount of  $\text{CH}_3\text{COOH}$  present in the suspension, respectively) calculated after 15 h of illumination for initial acetic acid concentration  $\geq 0.5$  M exhibit less than 4 % conversion of acetic acid into the detected reaction products (Table (3 – 5), (columns 8, 9)). Therefore, the change of concentration seems not to be the reason for the observed decrease in reaction rate. This means that during a photocatalytic reaction for the conversion of acetic acid, the surface of photocatalyst is changed. The reason behind these surface changes of the photocatalyst material might be the type of reaction mechanism occurred during photocatalytic degradation of aqueous organic compound. Moreover, a comparison between the expected atomic ratios of  $\text{CH}_3\text{COOH}$  molecule ( $\frac{n(\text{C})}{n(\text{O})} = 1$ ,  $\frac{n(\text{H})}{n(\text{O})} = 2$ , and  $\frac{n(\text{H})}{n(\text{C})} = 2$ ) and the experimentally obtained ratios between the atoms composing  $\text{CH}_3\text{COOH}$  ( $0.6 < \frac{n(\text{C})}{n(\text{O})} < 0.9$ ,  $1.0 < \frac{n(\text{H})}{n(\text{O})} < 2.0$ , and  $1.4 < \frac{n(\text{H})}{n(\text{C})} < 2.1$ ) exhibits the existence of other reaction products besides the main products ( $\text{CO}_2$ ,  $\text{CH}_4$ ,  $\text{H}_2$ , and  $\text{C}_2\text{H}_6$ ). The qualitative gas phase analysis in the QMS also provides evidence for the production of other organic compounds (*e.g.*,  $\text{HCHO}$ ,  $\text{CH}_3\text{OH}$ ,  $\text{C}_2\text{H}_5\text{OH}$ , and  $\text{HCOOH}$ ), but the formed concentrations of these compounds were observed to be rather low in the gas phase exiting the photoreactor (Figure 23). The difference in the obtained amounts from all reaction products in all experimental runs exhibits an experimental error of  $\pm 10$  %.

In general, the excitation of a semiconductor material by the photons having energy higher than the energy of its band-gap ( $E_g$ ) leads to the transfer of electrons from valence band (VB) to the conduction band (CB) of the semiconducting material while creating positively charge holes ( $h_{\text{VB}}^+$ ) at the valence band edge ( $E_{\text{VB}}$ ) of semiconductor. Considering the  $\text{TiO}_2$  as a semiconducting photocatalyst, under anaerobic reaction conditions, a fast recombination between photo-generated valence band holes ( $h_{\text{VB}}^+$ ) and conduction band electrons ( $e_{\text{CB}}^-$ ) is expected. In the absence of  $\text{O}_2$ , the light-induced semiconductor  $e_{\text{CB}}^-$  move freely in  $\text{TiO}_2$ . Due to the lattice vibration, the photo-excited  $e_{\text{CB}}^-$  immediately release their energy and recombine with the photo-

## 4. Discussion

generated  $h_{VB}^+$  even in the presence of a  $h_{VB}^+$  scavenger/electron donor. It can be seen in Figure 37, that the driving force for an interfacial electron transfer of the P25  $TiO_2$   $e_{CB}^-$  to protons ( $H^+$ ) being present at the  $TiO_2$  CB is very small. On the other hand, the valence band position of  $TiO_2$  seems (Figure 37) to be suitable for the oxidation reaction of  $H_2O$  as well as  $CH_3COOH$ . Consequently, a reaction system, containing bare  $TiO_2$  as a photocatalyst and aqueous acetic acid as an electron donor, does not give the significant amounts of the reaction products (Figure 14) during photo-induced transformation of aqueous acetic acid due to the rapid  $e_{CB}^-$  and  $h_{VB}^+$  recombination. In order to suppress the fast recombination between photo-generated charge carriers ( $e_{CB}^-$  and  $h_{VB}^+$ ), the surface of  $TiO_2$  is modified with various co-catalysts such as noble metals or metal oxides. The co-catalysts loaded onto the surface of  $TiO_2$  act as electron sinks thus hindering the rapid  $e_{CB}^-$  and  $h_{VB}^+$  recombination. A detailed discussion about co-catalyst loaded photocatalyst has been given in the following chapter (4.2.1).

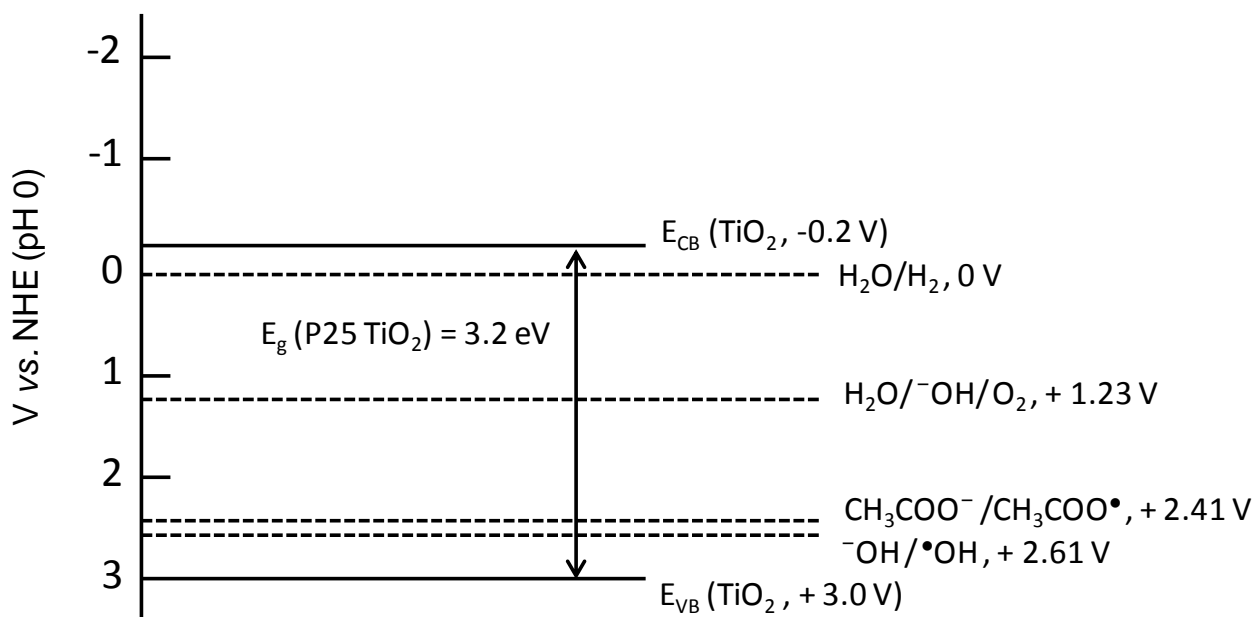


**Figure 37:** Schematic illustration of energy band diagram for  $TiO_2$  P25 along with the reduction and oxidation potential of  $H_2O$  [114], one electron oxidation potential of acetate ( $CH_3COO^-$ ) [115], and oxidation potential of  $\cdot OH$  [114], respectively.

## 4.2 Factors influencing the reaction rates and product distribution

### 4.2.1 Effect of co-catalyst

During a photocatalytic reaction, semiconductor (SC) materials play a key role in defining the oxidation and reduction reactions. However, the photocatalytic reactions mainly for the production of  $H_2$  in significant amounts require the assistance of a co-catalyst material. In these reactions, the deposition of co-catalysts such as noble metals or metal oxides on the surface of photocatalyst *i.e.*,  $TiO_2$  acts as an efficient conduction band electrons ( $e_{CB}^-$ ) trap and facilitates the reduction of protons ( $H^+$ ) adsorbed on the surface of co-catalysts into hydrogen atoms ( $\bullet H$ ) (Figure 38). These adsorbed  $\bullet H$  further dimerize to form  $H_2$ . In parallel to this reaction, the  $TiO_2$  photo-generated valence band holes ( $h_{VB}^+$ ) react with the surface adsorbed  $RCOOH$  or  $H_2O$  yielding  $RCOO\bullet$  and  $\bullet OH$ . The formed  $\bullet OH$  further oxidize organic molecules adsorbed on the surface of photocatalyst material (Figure 37, and 38). The deposition of co-catalyst material also improves the reduction of  $H^+$  by shifting the position of Fermi level towards more negative potential value (Figure 38). Hence, the interfacial charge transport becomes more efficient.

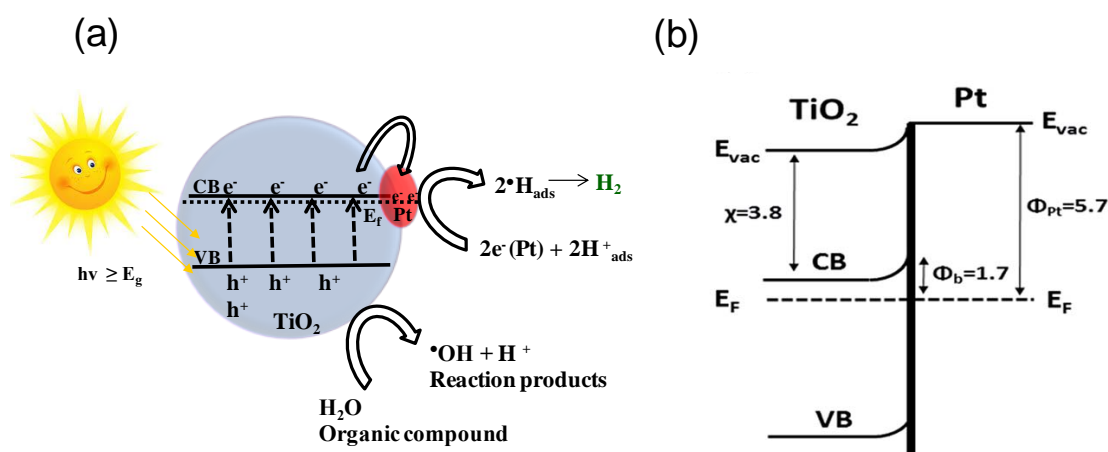


**Figure 38:** (a) Schematic illustration of photocatalytic  $H_2$  evolution reaction, and (b) energy band diagram for  $Pt/TiO_2$  junction. ( $E_{vac}$ ,  $E_F$ ,  $\Phi_{Pt}$ ,  $\chi$ ,  $\Phi_b$  represents vacuum level, fermi level, work function of Pt, electron affinity of  $TiO_2$  conduction band and Schottky barrier height, respectively (all values in eV)) [116].

## 4. Discussion

The use of a co-catalyst is not limited to the  $H^+$  reduction reaction only, but it can also assist the transfer of an electron to the excited semiconductor [66, 117-120]. In order to obtain significant yields of the required product, the choice of a suitable co-catalyst is pre-requisite. This work is an appraisal for the photocatalytic decomposition of aqueous acetic acid into useful solar fuels employing various noble metals such as Pt, Rh, Au, and Ag as well as metal-oxides *e.g.*,  $IrO_2$  and  $RuO_2$  loaded  $TiO_2$  particles under anaerobic conditions. The choice of particularly  $IrO_2$  and  $RuO_2$  metal-oxides as co-catalyst mainly for the reduction reaction has been made due to their metallic properties [121, 122]. Numerous published reports demonstrate the significance of  $IrO_2$  and  $RuO_2$  acting as both  $H_2$  evolution and  $O_2$  evolution co-catalysts [123-131]. It is obvious from the Figure 17 that the photocatalytic activity increases significantly when  $TiO_2$  is loaded with the above mentioned co-catalysts as compared to the bare  $TiO_2$  (Figure 14). According to the evolved amounts of  $CO_2$ , the photocatalytic activity is found to increase in the following order:  $Ag/TiO_2 < Au/TiO_2 < Rh/TiO_2 < RuO_2/TiO_2 < IrO_2/TiO_2 < Pt/TiO_2$ . Figure 15 and 16 clearly indicates that during photocatalytic decomposition of aqueous acetic acid, the loading of various co-catalysts onto the surface of  $TiO_2$  strongly affects the reaction rates and the evolved amounts of gaseous products over 15 h of irradiation.

The initial (after 2 h illumination) as well as overall (after 15 h illumination) photonic efficiencies for the main reaction products ( $CO_2$ ,  $CH_4$ , and  $H_2$ ) have also been calculated and are presented in Figure 39. The details regarding the calculations of photonic efficiency have been given in chapter 2.6. The initial and overall photonic efficiencies measured for  $CO_2$  and  $CH_4$  evolution by utilizing the variety of noble metals as well as metal-oxides exhibits Pt and  $IrO_2$  loaded  $TiO_2$  as the efficient photocatalyst (Figure 39a, and 39c). In comparison to this, only  $Pt/TiO_2$  and  $Rh/TiO_2$  show significant photocatalytic activities for  $H_2$  evolution reaction (Figure 39b). Additionally, It can be seen in Table 3 (column 18) that the ratio between the sum of formed amount of hydrocarbons ( $CH_4$ , and  $C_2H_6$ ) and the formed amount of  $H_2$  was calculated to be varying in the range of 1.5 – 10.5.

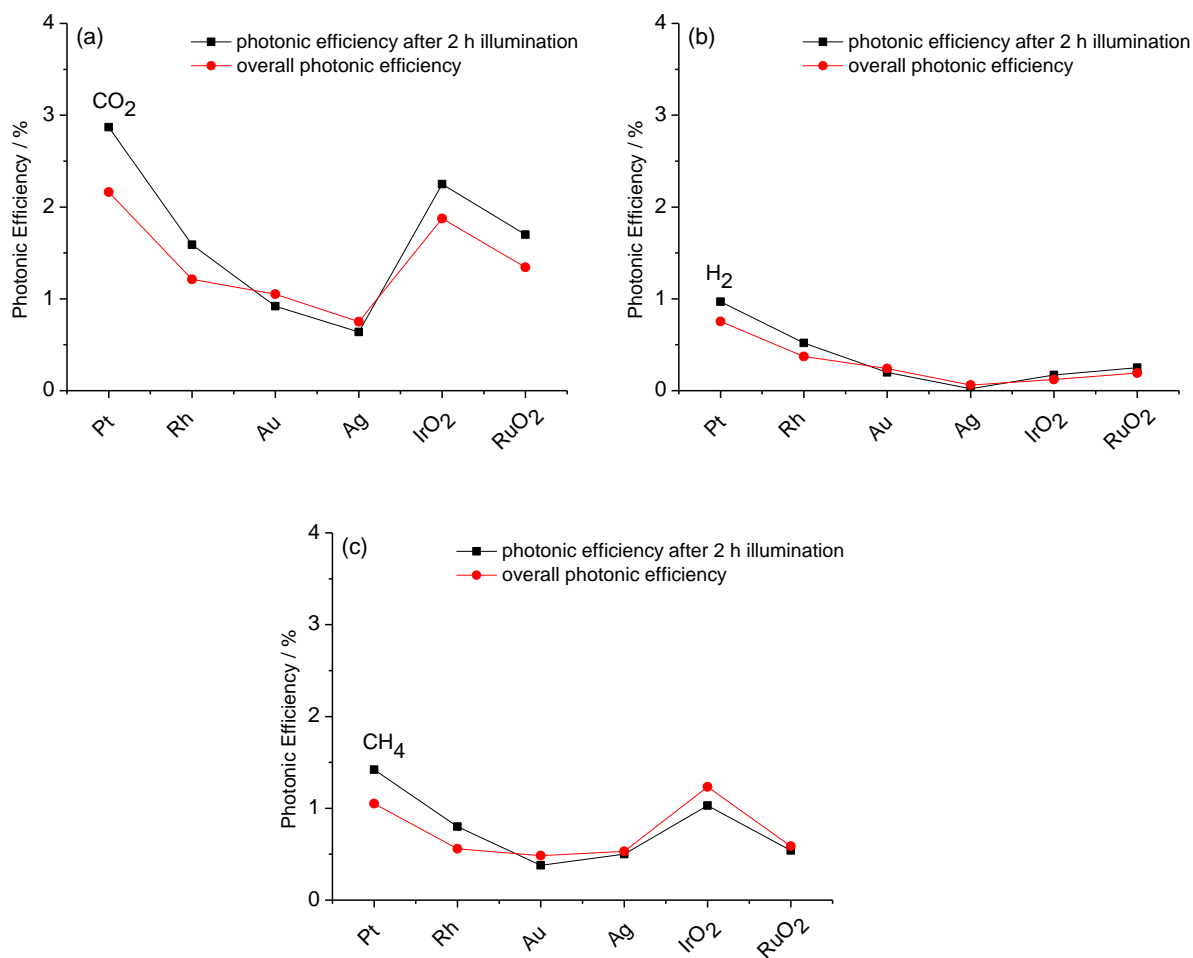


**Figure 39:** Photonic efficiency for the main reaction products, *i.e.*, (a) CO<sub>2</sub>, (b) H<sub>2</sub>, and (c) CH<sub>4</sub>, calculated for the initial (after 2 h illumination) and overall (after 15 h illumination) formation rates. *Experimental conditions:* as in Figure 15 – 16.

## 4. Discussion

**Table 3:** Effect of the different co-catalyst on the amounts of the main reaction products photocatalytically formed during 15 h of irradiation.

1	2	3	4	5	6	7	8	9	10	11	12	13
M/TiO <sub>2</sub>	$c_0$	$n_0$	$n(\text{CO}_2)$	$n(\text{H}_2)$	$n(\text{CH}_4)$	$n(\text{C}_2\text{H}_6)$	$X_C$	$X_H$	$\frac{n(\text{H}_2)}{n(\text{CO}_2)}$	$\frac{n(\text{CH}_4)}{n(\text{CO}_2)}$	$\frac{n(\text{C}_2\text{H}_6)}{n(\text{CO}_2)}$	$\frac{n(\text{C}_2\text{H}_6)}{n(\text{CH}_4)}$
	M	$\mu\text{mol}$	$\mu\text{mol}$	$\mu\text{mol}$	$\mu\text{mol}$	$\mu\text{mol}$	–	–	–	–	–	–
Pt/TiO <sub>2</sub>	0.5	25000	1027	358	511	24	0.032	0.029	0.35	0.50	0.02	0.05
Rh/TiO <sub>2</sub>	0.5	25000	580	177	266	13	0.017	0.015	0.31	0.46	0.02	0.05
Au/TiO <sub>2</sub>	0.5	25000	499	115	230	20	0.015	0.013	0.23	0.46	0.04	0.09
Ag/TiO <sub>2</sub>	0.5	25000	357	29	252	6	0.012	0.011	0.08	0.71	0.02	0.02
IrO <sub>2</sub> /TiO <sub>2</sub>	0.5	25000	890	58	586	24	0.030	0.026	0.07	0.66	0.03	0.04
RuO <sub>2</sub> /TiO <sub>2</sub>	0.5	25000	638	92	279	7	0.019	0.013	0.14	0.44	0.01	0.03

*Experimental conditions:* photocatalyst concentration = 0.5 g L<sup>-1</sup>, initial acetic acid concentration ( $c_0$ ) = 0.5 M, pH 2, suspension volume = 50 mL, irradiation time = 15 h, irradiation intensity  $I_{250-450}$  = 30 mW cm<sup>-2</sup>.



**Table 3 (continued):** Effect of the different co-catalyst on the amounts of the main reaction products photocatalytically formed during 15 h of irradiation.

14	15	16	17	18	19			
$\frac{2n(\text{C}_2\text{H}_6)}{n(\text{CH}_4)+2n(\text{C}_2\text{H}_6)}$	$\frac{n(\cdot\text{CH}_3)}{n(\text{H}\cdot)}$	$\frac{n(\text{CH}_4)+2n(\text{C}_2\text{H}_6)}{n(\text{CH}_4)+2n(\text{H}_2)}$	$\frac{n(\cdot\text{CH}_3)}{n(\text{CO}_2)}$	$\frac{n(\text{CH}_4) + 2n(\text{C}_2\text{H}_6)}{n(\text{CO}_2)}$	$\frac{n(\text{H}\cdot)}{n(\text{CO}_2)}$	$\frac{n(\text{CH}_4) + 2n(\text{H}_2)}{n(\text{CO}_2)}$	$\frac{n(\text{CH}_4)+n(\text{C}_2\text{H}_6)}{n(\text{H}_2)}$	M/TiO <sub>2</sub>
–	–	–	–	–	–	–	–	
0.09		0.46		0.54		1.19	1.49	Pt/TiO <sub>2</sub>
0.09		0.47		0.50		1.07	1.58	Rh/TiO <sub>2</sub>
0.15		0.59		0.54		0.92	2.17	Au/TiO <sub>2</sub>
0.05		0.85		0.74		0.87	8.90	Ag/TiO <sub>2</sub>
0.08		0.90		0.71		0.79	10.52	IrO <sub>2</sub> /TiO <sub>2</sub>
0.05		0.63		0.46		0.73	3.11	RuO <sub>2</sub> /TiO <sub>2</sub>

*Experimental conditions:* photocatalyst concentration = 0.5 g L<sup>-1</sup>, initial acetic acid concentration ( $c_0$ ) = 0.5 M, pH 2, suspension volume = 50 mL, irradiation time = 15 h, irradiation intensity  $I_{250-450}$  = 30 mW cm<sup>-2</sup>.

## 4. Discussion

Figure 40 presents the plots of evolved amounts of  $n(\text{CH}_4)$ ,  $n(\text{H}_2)$ ,  $n(\text{C}_2\text{H}_6)$ ,  $n(\text{H}^\bullet)$ , and  $n(\bullet\text{CH}_3)$  (where,  $n(\text{H}^\bullet) = 2n(\text{H}_2) + n(\text{CH}_4)$ , and  $n(\bullet\text{CH}_3) = n(\text{CH}_4) + 2n(\text{C}_2\text{H}_6)$ ) against the formed amounts of  $\text{CO}_2$  during 15 h of illumination. The higher amounts of  $\text{CH}_4$  seem to be associated with the rapid reaction rate of photo-decarboxylation (*i.e.*, the evolution of  $\text{CO}_2$  in higher amounts) in all experimental runs (Figure 40a). However, the formation of  $\text{H}_2$  in significant amount does not have any relation with the photo-decarboxylation reaction rate. An increment in the evolved amount of  $\text{CO}_2$  was observed to give an augmentation in the formed amounts of both  $\bullet\text{CH}_3$  and  $\bullet\text{H}$  (Figure 40b). On the contrary, the trend shown by metal-oxide loaded  $\text{TiO}_2$  particles was found to be different.

Considering the effect of only noble metal co-catalyst loaded  $\text{TiO}_2$ , it can be seen (Figure 17) that the amounts of  $\text{CO}_2$ ,  $\text{H}_2$ ,  $\text{CH}_4$ , and  $\text{C}_2\text{H}_6$  formation increase in the following sequence:  $\text{Ag}/\text{TiO}_2 < \text{Au}/\text{TiO}_2 < \text{Rh}/\text{TiO}_2 < \text{Pt}/\text{TiO}_2$ . Fu *et al.* [132] studied the hydrogen evolution reaction (HER) from aqueous glucose suspensions employing 1 wt % metal-loaded  $\text{TiO}_2$  particles. They observed an increase in the photocatalytic activity for  $\text{H}_2$  production employing various metal-loaded  $\text{TiO}_2$  in the following order:  $\text{Ag}/\text{TiO}_2 \approx \text{Ru}/\text{TiO}_2 < \text{Au}/\text{TiO}_2 \approx \text{Rh}/\text{TiO}_2 < \text{Pt}/\text{TiO}_2 < \text{Pd}/\text{TiO}_2$ . The authors ascribed this order to the work function ( $\Phi$ ) values of the noble metals.

In comparison to the  $\text{TiO}_2$ , the large  $\Phi$  of noble metals creates a Schottky barrier at the metal/ $\text{TiO}_2$  contact thus reducing the rapid recombination of photo-generated charge carriers ( $e_{\text{CB}}^-$  and  $h_{\text{VB}}^+$ ). Consequently the photocatalytic activity is increased. The higher value of  $\Phi$  however results in the formation of Schottky barrier with larger barrier height. Hence, the photocatalytic activity becomes more significant [132]. The photocatalytic activity with respect to the  $\Phi$  value employing metal loaded  $\text{TiO}_2$  particles along with 2-propanol and ethanol has also been reported in literature [37, 133, 134]. The  $\Phi$  of a material does not correspond to its bulk, but it is actually defined with respect to the surface of a material based on its stoichiometry, exposed crystal facets and nearby species [135, 136]. For instance, it has been reported in literature that the deposition of  $\text{RuO}_2$  films at ambient temperature onto  $\text{BaTiO}_3$ ,  $\text{SrTiO}_3$  and  $\text{TiO}_2$  depicts 6.1 and 6.2 eV as  $\Phi$  values of  $\text{RuO}_2$  [137, 138].

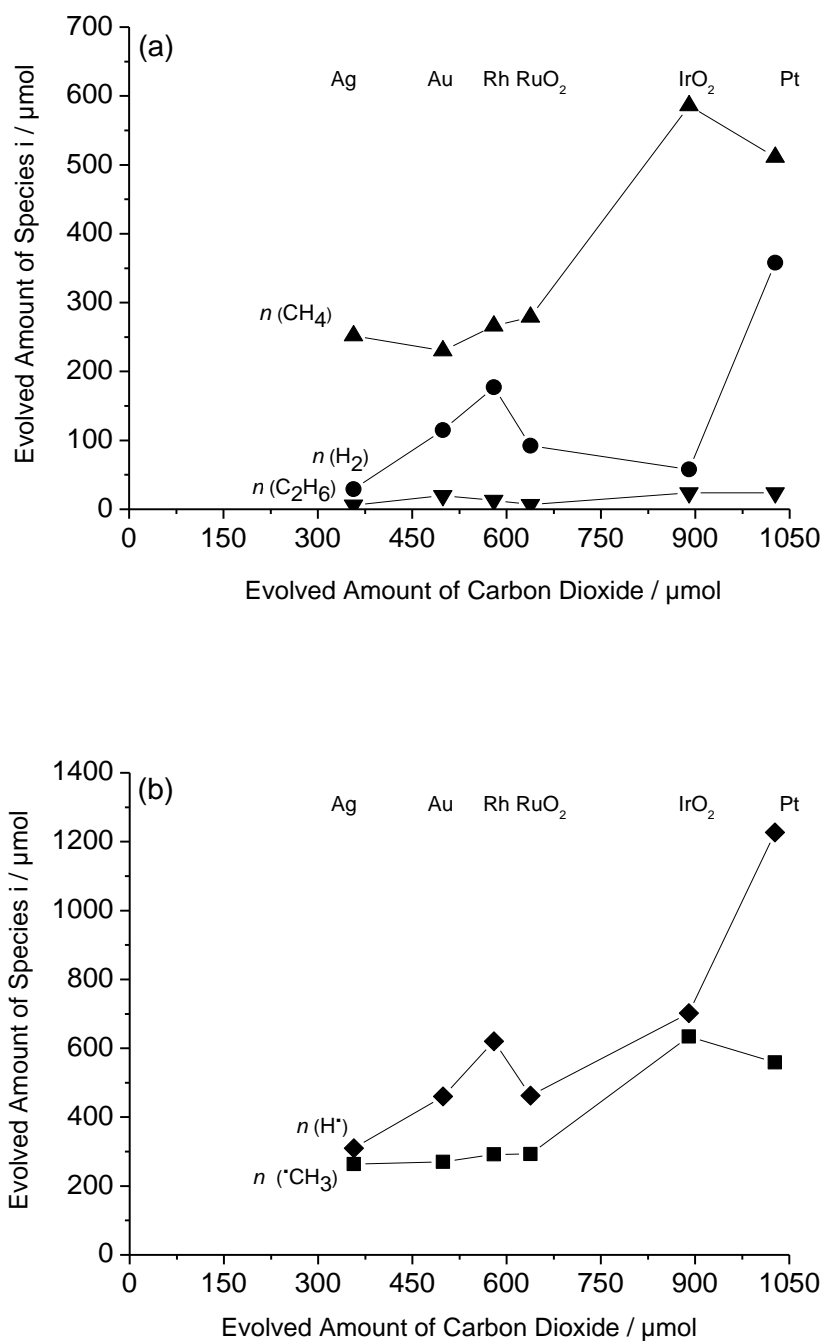


**Figure 40:** Amounts of (a)  $\text{CH}_4$ ,  $\text{H}_2$ , and  $\text{C}_2\text{H}_6$ , and (b)  $\text{H}^\bullet$ , and  $\text{CH}_3^\bullet$  evolved during 15 h of irradiation of aqueous acetic acid in the presence of co-catalyst-loaded  $\text{TiO}_2$  vs. amount of  $\text{CO}_2$ . *Experimental conditions:* as in Figure 15 – 16.

## 4. Discussion

In another study [139], the  $\Phi$  of RuO<sub>2</sub> films deposited onto the SiO<sub>2</sub>-Si was reported as 5.2 eV before any calcination treatment. However, the calcination of the employed RuO<sub>2</sub> films at 300 °C as well as 500 °C resulted in comparatively lower work function values such as 5.17 eV and 5.03 eV, respectively. The authors attributed this decrease in the  $\Phi$  values to the improved crystallinity of the films at higher temperature values.

This means that the various synthesis methods used to prepare the metal or metal-oxide loaded photocatalyst result in shifting the  $\Phi$  of the respective co-catalyst. Therefore, the results obtained by loading of the metals or metal oxides onto the surface of photocatalyst employing different synthesis conditions cannot be compared. Sakata *et al.* [37] observed that using various metal loaded TiO<sub>2</sub> powders in the aqueous suspensions of ethanol, the formation rates for H<sub>2</sub> increased as follow: Ag/TiO<sub>2</sub> < Cu/TiO<sub>2</sub> < Au/TiO<sub>2</sub> < Rh/TiO<sub>2</sub> < Pd/TiO<sub>2</sub> < Pt/TiO<sub>2</sub>. Sakata and co-workers [37] also examined the role of various metal-loaded TiO<sub>2</sub> for CH<sub>4</sub> formation from aqueous carboxylic acid (acetic acid, and propionic acid) suspensions. They observed the order for the formation rate of CH<sub>4</sub> as: Ag/TiO<sub>2</sub> < Rh/TiO<sub>2</sub> < Au/TiO<sub>2</sub> < Cu/TiO<sub>2</sub> < Pd/TiO<sub>2</sub> < Pt/TiO<sub>2</sub>. Even though, the  $\Phi$  seemed to affect the photocatalytic activity for both H<sub>2</sub> and CH<sub>4</sub> formation to a great extent, the other physio-chemical factors associated with the metal-semiconductor cannot be neglected. For example, (1) the bond dissociation energy for the metal-hydrogen (metal-H) or metal-carbon (metal-C) bonds, (2) the enthalpy of the adsorbed reactants and formed products, etc. However, in the present work, these factors will not be discussed.

Here, Figure 41 depicts the plots of formed amounts of  $n(\text{CO}_2)$ ,  $n(\text{CH}_4)$ ,  $n(\text{H}_2)$ ,  $n(\text{H}^\bullet)$ , and  $n(\bullet\text{CH}_3)$  against reported work function ( $\Phi$ ) values of the metal or metal oxide co-catalyst. It is clear from Figure 41 that the formed amounts of all reaction products such as: ( $n(\text{CO}_2)$ ), ( $n(\text{CH}_4)$ ), ( $n(\text{H}_2)$ ) and reaction intermediates *i.e.*, ( $n(\text{H}^\bullet)$ , and ( $n(\bullet\text{CH}_3)$ ) are directly proportional to the increasing  $\Phi$  values of the respective noble metal co-catalysts. On the contrary, the pattern shown by the metal-oxide (IrO<sub>2</sub> and RuO<sub>2</sub>) co-catalysts for the formed amounts of reaction products as well as reaction intermediates *vs.*  $\Phi$  is different (Figure 41). During the photocatalytic transformation of aqueous acetic acid, IrO<sub>2</sub> and RuO<sub>2</sub> do not seem to be very active for H<sub>2</sub> evolution reaction, but higher amounts of CO<sub>2</sub> and CH<sub>4</sub> were obtained. The formed amounts of CO<sub>2</sub> and CH<sub>4</sub> using IrO<sub>2</sub> as a co-catalyst are comparable with those obtained by utilizing Pt as a co-catalyst (Figure 41).

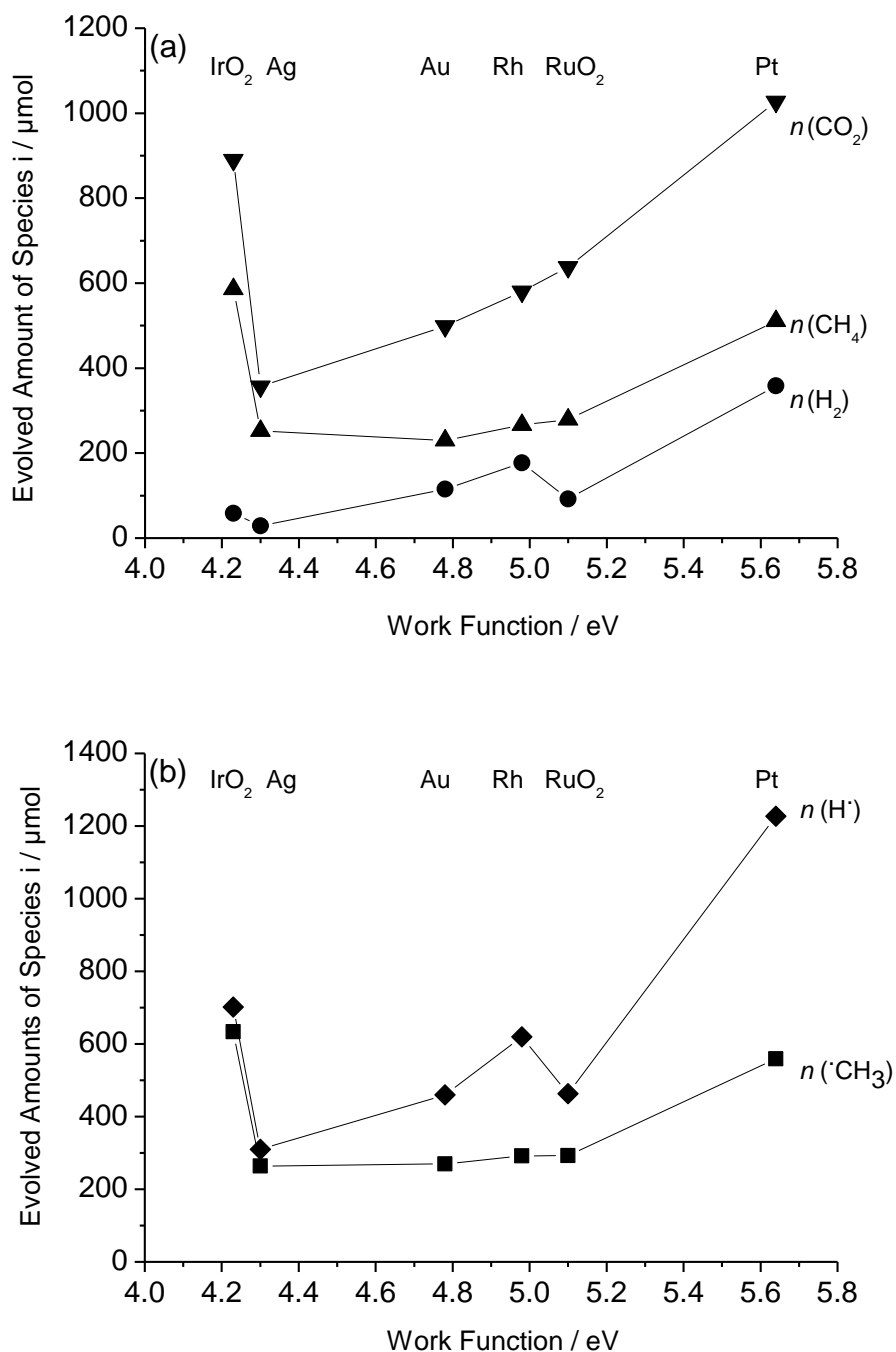


**Figure 41:** Amounts of (a)  $\text{CO}_2$ ,  $\text{CH}_4$ ,  $\text{H}_2$ , and  $\text{C}_2\text{H}_6$ , and (b)  $\text{H}^\bullet$ , and  $\text{CH}_3^\bullet$ , evolved during 15 h of irradiation of aqueous acetic acid in the presence of co-catalyst-loaded  $\text{TiO}_2$  vs. work function of the respective co-catalyst. The values of the work function have been taken from Ref. [140], [141], and [142]. *Experimental conditions:* as in Figure 15 – 16.

## 4. Discussion

Due to the differences in the obtained photocatalytic activity using metals or metal oxides loaded  $\text{TiO}_2$  particles, it is therefore important to discuss the surface reactions occurring at the surface of metal- $\text{TiO}_2$  and metal-oxide- $\text{TiO}_2$  separately. Generally, the higher photocatalytic activity employing noble metal- $\text{TiO}_2$  is attributed to the efficient separation of photo-generated charge carrier caused by the interface formed at metal- $\text{TiO}_2$  contact. An electric field is actually produced at the metal- $\text{TiO}_2$  interface thus the fast recombination between photo-generated  $e_{\text{CB}}^-$  and  $h_{\text{VB}}^+$  is hindered. For metals having large  $\Phi$  values in comparison to the  $\Phi$  of  $\text{TiO}_2$ , the interfacial electron transfer from conduction band of  $\text{TiO}_2$  into the metals becomes more efficient. A slight band bending at the metal/ $\text{TiO}_2$  interface is also an important factor which facilitates the electron transfer between metal and  $\text{TiO}_2$  [137].

Usually, in photocatalytic reaction systems consisting of metal/ $\text{TiO}_2$  and aqueous organic suspensions, the  $\text{H}^+$  are reduced on the metal surface resulting in the formation of adsorbed  $\bullet\text{H}$  (Equation 7). Also, the organic compound *i.e.*,  $\text{CH}_3\text{COOH}$  in the present study, is oxidized at the  $\text{TiO}_2$  surface yielding  $\text{CH}_3\text{COO}\bullet$ , followed by the decomposition of  $\text{CH}_3\text{COO}\bullet$  into  $\bullet\text{CH}_3$  and  $\text{CO}_2$  (Equation 6). The oxidation of the  $\text{CH}_3\text{COOH}$  molecule at the surface of  $\text{TiO}_2$  occurs due to the transfer of an electron to the VB of  $\text{TiO}_2$ . Subsequently, the generated reaction intermediates ( $\bullet\text{CH}_3$ ) are scattered all over the surface of metal loaded  $\text{TiO}_2$ . The reaction between the scattered  $\bullet\text{CH}_3$  and the  $\bullet\text{H}$  adsorbed at the metal surface results in the formation of  $\text{CH}_4$  as the final reaction product (Equation 9). Moreover, the dimerization of  $\bullet\text{H}$  and  $\bullet\text{CH}_3$  gives  $\text{H}_2$  and  $\text{C}_2\text{H}_6$  as the final reaction products (Equation 8, and 10) resulting from the photo-induced degradation of aqueous acetic acid. However, the reactions 8 and 9 seemed to compete depending on the employed reaction conditions (Figure 17).

The photocatalytic degradation of aqueous acetic acid was supposed to follow a slightly different reaction pathway employing metal-oxide loaded  $\text{TiO}_2$  as photocatalyst. Depending on the synthesis conditions, the metal-oxide co-catalyst can serve as either (1) electrons sink, or (2) holes trap. It has been reported by Sakata *et al.* [143] that the photocatalytic activity for hydrogen evolution reaction (HER) from aqueous ethanol suspensions increases in the following order:  $\text{TiO}_2 \ll \text{RuO}_2/\text{TiO}_2 < \text{Pd}/\text{TiO}_2 < \text{Pt}/\text{TiO}_2$ . The authors ascribed the significant amounts of  $\text{H}_2$  formation employing  $\text{RuO}_2$  to the fact that this acts as a reduction co-catalyst and exhibits the properties like Pt. They claimed that employing metal as well as metal loaded  $\text{TiO}_2$  particles, the

photo-generated  $h\nu_{VB}^+$  react with the ethanol molecules and continue the oxidation process at the surface of  $TiO_2$  while  $e_{CB}^-$  gathered in the particles of  $TiO_2$  causing a cathodic shift in its Fermi level. Hence, the  $H^+$  reduction reaction becomes more favourable. Generally, in the presence of an oxidizing agent such as methanol or ethanol,  $TiO_2$  can store a large number of photo-generated electrons but the driving force of  $TiO_2$  conduction band electron ( $e_{CB}^-$ ) for an interfacial electron transfer to protons ( $H^+$ ) being present at the  $TiO_2$  conduction band is very small [144-146]. Thus, the cathodic shift in the Fermi level caused by the loading of co-catalyst enhances the interfacial charge transfer reaction [45, 46, 147-149]. In another study, Uddin *et al.* [137] examined the dye degradation reaction employing  $RuO_2/TiO_2$  as a photocatalyst under aerobic conditions. They credited the efficient photocatalytic activity obtained for this reaction to the existence of a Schottky barrier at the  $RuO_2/TiO_2$  contact. The electrons at the surface of  $TiO_2$  captured by the  $O_2$  (acting as electron acceptor) while the transfer of electrons from  $RuO_2$  to the  $TiO_2$  VB suggests that the  $RuO_2$  acts as an oxidizing co-catalyst. It can be seen from Figure (17 and 40) that the formed amounts of  $n(CO_2)$ ,  $n(CH_4)$  and  $n(\bullet CH_3)$  employing  $RuO_2/TiO_2$  as a photocatalyst could be considered in the sequence given by  $\Phi$  values. However, the formed amounts of  $n(H_2)$  and  $n(H\bullet)$  were observed to be rather smaller with respect to the order of  $\Phi$  values.

The use of  $IrO_2/TiO_2$  photocatalyst for the degradation of aqueous acetic acid was found to be very efficient for the  $CH_4$  production (Figure 40, and 41). The calculated ratio (Table 3 (column 15)) between the formed amounts of methyl radical ( $\bullet CH_3$ ) and hydrogen atom ( $H\bullet$ ) ( $\frac{n(\bullet CH_3)}{n(H\bullet)} = 0.9$ ) depicts the capability of  $IrO_2$  as a reduction co-catalyst *i.e.*, facilitating the formation of  $H\bullet$ . However, the reaction of  $H\bullet$  with  $\bullet CH_3$  seemed to be a favourable reaction ( $\frac{n(CH_4)+n(C_2H_6)}{n(H_2)} = 10.5$ ) as can be seen in Table 3 (column 18). It should also be noted that  $Pt/TiO_2$  and  $IrO_2/TiO_2$  exhibit comparable photocatalytic activities for  $CO_2$  and  $CH_4$  formation (Figure 42). This suggests that the  $\Phi$  value for both  $Pt$  (5.65 eV) and  $IrO_2$  (4.23 eV) is not the key parameter here. Meekins *et al.* [144] reported that the  $IrO_2$  loaded on the surface of  $TiO_2$  acts as a hole acceptor unless a hole equilibrium is achieved by both oxides. They also stated that the transfer of trapped holes from  $TiO_2$  to  $IrO_2$  is also possible. Liu *et al.* demonstrated the efficient photocatalytic activity for  $O_2$  evolution reaction employing  $IrO_2/TiO_2$  as holes acceptor [150]. Hence, it is assumed that, when metal-oxides are used as co-catalyst, they act as holes acceptor

## 4. Discussion

while facilitating the oxidative step on their surface, whereas the reduction of  $H^+$  occurs at the  $TiO_2$  surface.

It can be concluded from the above discussion that, during a photocatalytic reaction, the chemical nature of metal-oxide co-catalyst does not change. On the other hand, it has been reported in literature that structural changes arise in both  $RuO_2$  and  $IrO_2$  co-catalysts during the electrochemical  $H_2$  production reaction [151-154]. Thus, the structural changes of the employed metal-oxides in the present study for the photocatalytic decomposition of the aqueous acetic acid cannot be neglected. The formation rates of the reaction products as well as reaction intermediates resulting in different product distribution could be attributed to these changes.

However,  $Pt/TiO_2$  was found to be the photocatalyst exhibiting the highest photonic efficiency under the experimental conditions of this study for both oxidation and reduction reaction during light-induced transformation of aqueous acetic acid into valuable solar fuels. Therefore, this photocatalyst has been used to investigate other parameters that affect the photocatalytic reaction.

### 4.2.2 Effect of concentration

Generally, the concentration of a compound is known to affect its reaction rate. With a specific time interval, the changes in the formed amounts of reaction products are related to the concentration of reactants. However, the variations in the ratios of these reaction products are not essential. It can be seen in Figure 18, 19, 20 as well as in Table 4 that both the formation rates and the corresponding product distribution vary with the change in the initial acetic acid concentration. It is also obvious from Figure 20 that an increase in the initial concentration ( $c_0$ ) of acetic acid up to 0.05 M ( $n_0 = 2500 \mu\text{mol}$ ,  $n_0$  represents the amount of initial acetic acid molecules present in the suspension) results in an increment of the formed amounts of all reaction products. The concentration over the range  $0.05 \text{ M} \leq c_0 \leq 1 \text{ M}$  (corresponding to  $2500 \mu\text{mol} \leq n_0 \leq 50000 \mu\text{mol}$ ) gives approximately constant product distribution. For the acetic acid  $c_0 > 1 \text{ M}$  ( $n_0 = 50000 \mu\text{mol}$ ), a decrease in the formation rate of all reaction intermediates as well as reaction products is obvious (Figure 18, Table 4). The photonic efficiencies were also calculated for the main reaction products ( $CO_2$ ,  $CH_4$  and  $H_2$ ) evolved during the light induced decomposition of aqueous acetic acid at varying initial concentrations and are shown in Figure 42. Usually, at a specific initial concentration of the reactant and particular irradiance intensity,



## 4. Discussion

the number of photons absorbed by the photocatalyst as well as the number of active sites on the surface of the photocatalyst remains constant. An increase in the concentration of the reactant leading to an increase in the formation rates of the reaction products during photocatalytic H<sub>2</sub> evolution reaction (HER) has been published in literature [155]. On the other hand, it has also been shown that an increase in the concentration of reactant up to a specific value results in lowering the HER [104, 156, 157]. However, the results obtained in this study depict the change in formation rate as well as product distribution with respect to the initial concentration of acetic acid.

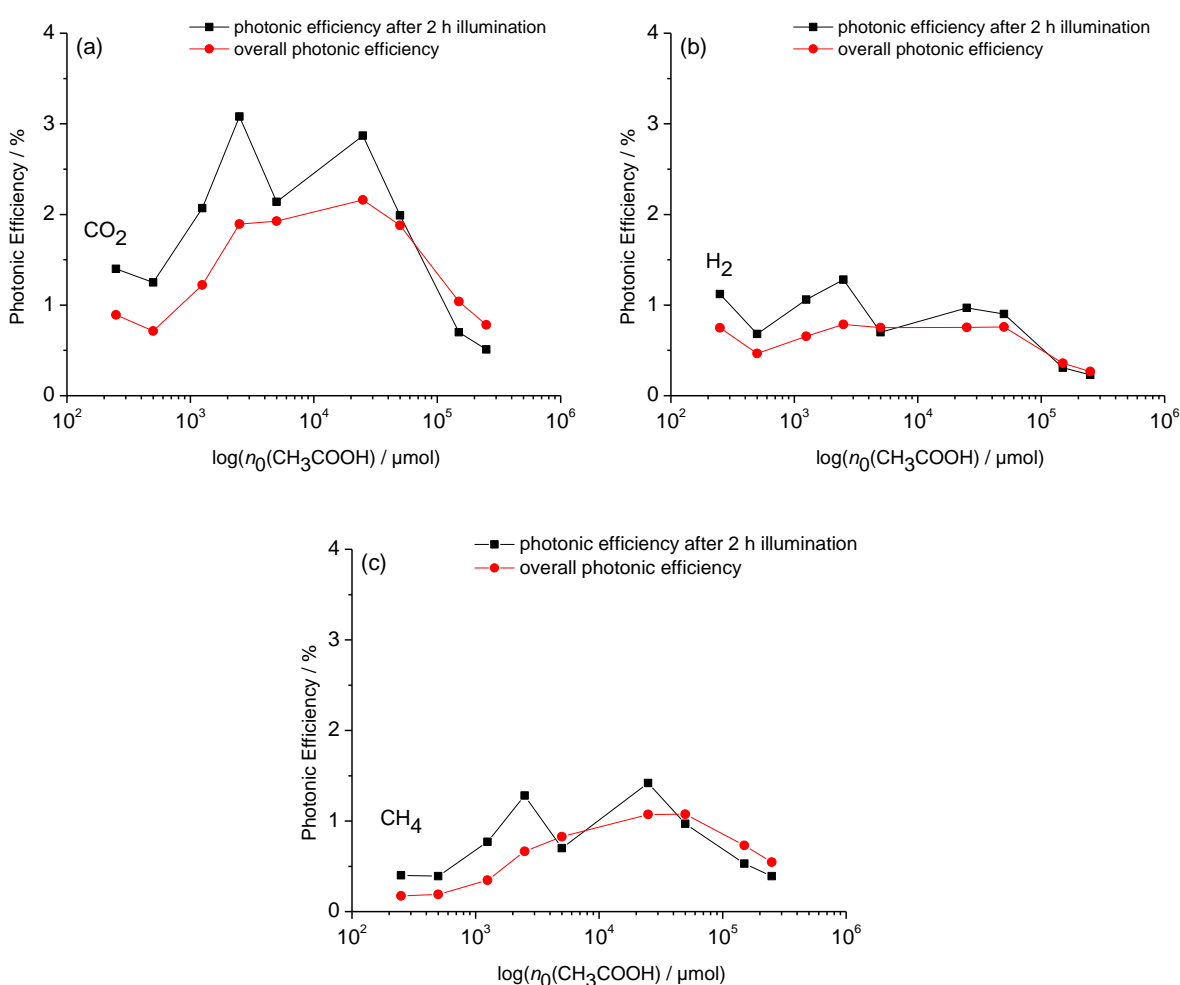


**Figure 42:** Photonic efficiency for the main reaction products, *i.e.*, (a) CO<sub>2</sub>, (b) H<sub>2</sub>, and (c) CH<sub>4</sub>, calculated for the initial (after 2 h illumination) and overall (after 15 h illumination) formation rates. *Experimental conditions:* as in Figure 18 – 19.

## 4. Discussion

Yoneyama and co-workers [90] studied the effect of various acetic acid concentrations on the formation rates of the main reaction products employing Pt/TiO<sub>2</sub> under anaerobic conditions. The initial concentration values chosen in their work were in the following range:  $1 \text{ M} \leq c_0 \leq 8.2 \text{ M}$ , at the constant pH value (3.1). They observed CO<sub>2</sub>, CH<sub>4</sub>, H<sub>2</sub>, and C<sub>2</sub>H<sub>6</sub> as main reaction products. They found an increase in the formation rates of all reaction products while increasing the concentration of acetic acid up to 5 M. A further increase in the concentration values results in a decreased formation rate for all reaction products. Zheng *et al.* [100] also investigated the effect of initial acetic acid concentration on the formation rates of the main reaction products using Pt/TiO<sub>2</sub> under anaerobic conditions. They reported an increase in the formation rates for all reaction products (CO<sub>2</sub>, CH<sub>4</sub>, H<sub>2</sub>, and C<sub>2</sub>H<sub>6</sub>) up to  $0.11 \text{ M} \leq c_0$ . Though, a further increase of up to  $0.26 \text{ M} \leq c_0$  results in lowering the formation rates of all reaction products. In another study, Mozia *et al.* [35] demonstrated the optimal concentration of acetic acid to be 1 M with Fe<sub>2</sub>O<sub>3</sub>-TiO<sub>2</sub> photocatalyst. The differences in the optimal concentration values might correspond to the different experimental conditions or different photocatalysts. The decrease in the photocatalytic activity after a specific initial concentration of the reactant could be attributed to the blockage of the active sites on the surface of photocatalyst [157].

The experimental results obtained from this study employing Pt/TiO<sub>2</sub> as a photocatalyst at pH 2 show that an increase in initial concentration of acetic acid results in a decrease of  $\frac{n(\text{H}_2)}{n(\text{CO}_2)}$  ratio and increase in  $\frac{n(\text{CH}_4)}{n(\text{CO}_2)}$  ratio as presented in Figure 43 and Table 4 (column 10, and 11). On the other hand, the change in the initial concentration of aqueous acetic acid does not seem to affect the ratio between C<sub>2</sub>H<sub>6</sub> and CH<sub>4</sub> formation to a great extent (Figure 43, Table 4 (column 13)).

According to the data presented in Figure 43, it can be estimated that almost 13% of the formed  $\bullet\text{CH}_3$  undergo a dimerization while resulting in C<sub>2</sub>H<sub>6</sub> formation as the final product. Yoneyama *et al.* [90] observed that a raise in the initial concentration of acetic acid up to 6 M while keeping other parameters constant results in an increase in the ratio of formed amounts of CH<sub>4</sub> and C<sub>2</sub>H<sub>6</sub>. They stated that the formation rate of C<sub>2</sub>H<sub>6</sub> is directly proportional to the increasing concentration of acetic acid. The authors also suggested that the formation rate of  $\bullet\text{CH}_3$  and the ratio  $\frac{n(\text{CH}_4)}{n(\text{C}_2\text{H}_6)}$

should be inversely proportional to each other *i.e.*,  $\left(\frac{1}{n(\bullet\text{CH}_3)} \sim \frac{n(\text{CH}_4)}{n(\text{C}_2\text{H}_6)}\right)$ . The formation rate ( $r$ ) of methyl radical ( $\bullet\text{CH}_3$ ) is given by :  $\left(r(\bullet\text{CH}_3) = \frac{n(\text{CH}_4) + 2n(\text{C}_2\text{H}_6)}{\Delta t}\right)$ . According to the experimental

## 4. Discussion

conditions of the present work, the relationship between the formed amounts of  $C_2H_6$  and  $CH_4$  should be:  $\frac{n(C_2H_6)}{n(CH_4)} \sim (n(CH_4) + 2n(C_2H_6))$ . However, it can be clearly seen in Table 4 that the expected linear relationship between formed amounts of  $C_2H_6$  and  $CH_4$  could not be proven.

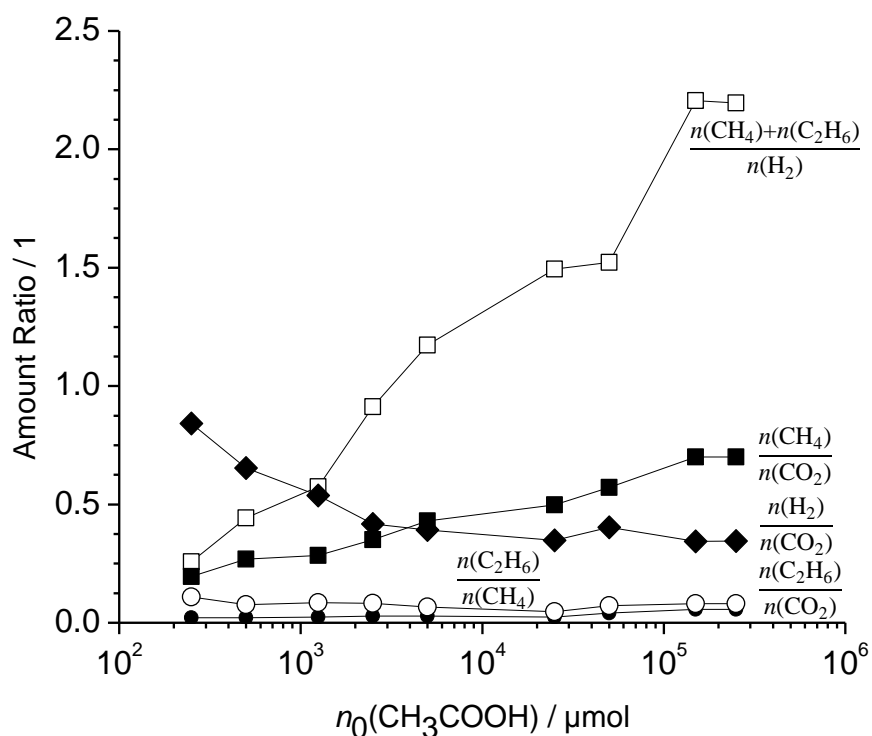


**Figure 43:** Ratios between the detected amounts of methane  $n(CH_4)$ , ethane  $n(C_2H_6)$ , molecular hydrogen  $n(H_2)$ , and carbon dioxide  $n(CO_2)$  vs. the initial amount  $n_0$  of acetic acid. *Experimental conditions:* as in Figure 18 – 19.

## 4. Discussion

**Table 4:** Effect of the acetic acid concentration on the amounts of the main reaction products photocatalytically formed during 15 h of irradiation.

1	2	3	4	5	6	7	8	9	10	11	12	13
M/TiO <sub>2</sub>	$c_0$	$n_0$	$n(\text{CO}_2)$	$n(\text{H}_2)$	$n(\text{CH}_4)$	$n(\text{C}_2\text{H}_6)$	$X_C$	$X_H$	$\frac{n(\text{H}_2)}{n(\text{CO}_2)}$	$\frac{n(\text{CH}_4)}{n(\text{CO}_2)}$	$\frac{n(\text{C}_2\text{H}_6)}{n(\text{CO}_2)}$	$\frac{n(\text{C}_2\text{H}_6)}{n(\text{CH}_4)}$
	M	μmol	μmol	μmol	μmol	μmol	–	–	–	–	–	–
Pt/TiO <sub>2</sub>	0.005	250	424	357	83	9	1.050	1.100	0.84	0.20	0.02	0.11
Pt/TiO <sub>2</sub>	0.01	500	338	221	91	7	0.443	0.424	0.65	0.27	0.02	0.08
Pt/TiO <sub>2</sub>	0.025	1250	581	312	165	14	0.310	0.274	0.54	0.28	0.02	0.08
Pt/TiO <sub>2</sub>	0.05	2500	900	375	316	26	0.254	0.217	0.42	0.35	0.03	0.08
Pt/TiO <sub>2</sub>	0.1	5000	915	358	394	26	0.136	0.122	0.39	0.43	0.03	0.07
Pt/TiO <sub>2</sub>	0.5	25000	1027	358	511	24	0.032	0.029	0.35	0.50	0.02	0.05
Pt/TiO <sub>2</sub>	1	50000	893	360	511	37	0.015	0.015	0.40	0.57	0.04	0.07
Pt/TiO <sub>2</sub>	3	150000	495	170	347	28	0.003	0.003	0.34	0.70	0.06	0.08
Pt/TiO <sub>2</sub>	5	250000	371	128	260	21	0.001	0.001	0.35	0.70	0.06	0.08

*Experimental conditions:* photocatalyst concentration = 0.5 g L<sup>-1</sup>, 0.005 M ≤ initial acetic acid concentration ( $c_0$ ) ≤ 5 M, pH 2, suspension volume = 50 mL, irradiation time = 15 h, irradiation intensity  $I_{250-450} = 30 \text{ mW cm}^{-2}$ .

**Table 4 (continued):** Effect of the acetic acid concentration on the amounts of the main reaction products photocatalytically formed during 15 h of irradiation.

14	15	16	17	18	19			
$\frac{2n(\text{C}_2\text{H}_6)}{n(\text{CH}_4)+2n(\text{C}_2\text{H}_6)}$	$\frac{n(\cdot\text{CH}_3)}{n(\text{H}\cdot)}$	$\frac{n(\text{CH}_4)+2n(\text{C}_2\text{H}_6)}{n(\text{CH}_4)+2n(\text{H}_2)}$	$\frac{n(\cdot\text{CH}_3)}{n(\text{CO}_2)}$	$\frac{n(\text{CH}_4) + 2n(\text{C}_2\text{H}_6)}{n(\text{CO}_2)}$	$\frac{n(\text{H}\cdot)}{n(\text{CO}_2)}$	$\frac{n(\text{CH}_4) + 2n(\text{H}_2)}{n(\text{CO}_2)}$	$\frac{n(\text{CH}_4)+n(\text{C}_2\text{H}_6)}{n(\text{H}_2)}$	M/TiO <sub>2</sub>
–	–	–	–	–	–	–	–	–
0.18		0.13		0.24		1.88	0.26	Pt/TiO <sub>2</sub>
0.13		0.20		0.31		1.58	0.44	Pt/TiO <sub>2</sub>
0.15		0.24		0.33		1.36	0.57	Pt/TiO <sub>2</sub>
0.14		0.35		0.41		1.18	0.91	Pt/TiO <sub>2</sub>
0.12		0.40		0.49		1.21	1.17	Pt/TiO <sub>2</sub>
0.09		0.46		0.54		1.19	1.49	Pt/TiO <sub>2</sub>
0.13		0.48		0.66		1.38	1.52	Pt/TiO <sub>2</sub>
0.14		0.59		0.81		1.39	2.21	Pt/TiO <sub>2</sub>
0.14		0.59		0.81		1.39	2.20	Pt/TiO <sub>2</sub>

*Experimental conditions:* photocatalyst concentration = 0.5 g L<sup>-1</sup>, 0.005 M ≤ initial acetic acid concentration (c<sub>0</sub>) ≤ 5 M, pH 2, suspension volume = 50 mL, irradiation time = 15 h, irradiation intensity I<sub>250-450</sub> = 30 mW cm<sup>-2</sup>.

## 4. Discussion

Figure 42, 43 and Table 4 clearly demonstrate that the change in initial concentration of acetic acid up to 0.05 M ( $n_0 = 2500 \mu\text{mol}$ ) results in the formation of reaction products enriched with  $\text{H}_2$  (*i.e.*,  $\frac{n(\text{CH}_4)+n(\text{C}_2\text{H}_6)}{n(\text{H}_2)} < 1$ ) suggesting the decomposition of  $\text{CH}_3\text{COOH}$  besides other organic compounds formed during the photo-induced transformation of acetic acid. Conversely, an increase in the initial acetic acid concentration ( $c_0 > 1 \text{ M}$  ( $n_0 = 50000 \mu\text{mol}$ )) gives the reaction products enriched in hydrocarbons (*i.e.*,  $\frac{n(\text{CH}_4)+n(\text{C}_2\text{H}_6)}{n(\text{H}_2)} > 1$ ). Overall, 0.5 M was found to be the optimum initial concentration of aqueous acetic acid in order to obtain both  $\text{CH}_4$  and  $\text{H}_2$  in significant amounts using Pt/TiO<sub>2</sub> as a photocatalyst.

### 4.2.3 Effect of pH

The formation rates and corresponding product distribution is known to be strongly dependent on the pH values of the suspension. During photocatalytic degradation of aqueous acetic acid, the experimental results of the present study show  $\text{CO}_2$ ,  $\text{H}_2$ ,  $\text{CH}_4$ , and  $\text{C}_2\text{H}_6$  as the main reaction products from a suspension containing Pt/TiO<sub>2</sub> as a photocatalyst and 0.5 M acetic acid at pH 2. However, change in the pH value over the range  $2 \leq \text{pH} \leq 11$ , results in completely different formation rates and products distribution as presented in Figure 21, 22, 23, and 24. It can be seen in Figure 24, that the amounts of  $\text{CO}_2$ ,  $\text{H}_2$ ,  $\text{CH}_4$ , and  $\text{C}_2\text{H}_6$  evolved after 15 h of irradiation are decreasing with increasing pH values. The photonic efficiencies calculated for the main reaction products at different pH regimes are presented in Figure 44. Figure 44 clearly indicates that the initial and overall photonic efficiencies significantly vary for  $\text{CO}_2$  at pH 2, whereas for  $\text{H}_2$  and  $\text{CH}_4$ , it did not seem to change greatly. Moreover, at pH 5, no change was observed in the initial and final photonic efficiencies for all reaction products. This means that the reaction rates for all reaction products remains stable over the entire time of illumination at pH 5. This observation could be attributed to the formation of a buffer system (at pH 5) which acts as to resist the changes occurring during the photocatalytic reaction. Also, the overall photonic efficiencies for  $\text{H}_2$  evolution reaction were measured to be almost constant over a range of  $2 \leq \text{pH} \leq 9$  (Figure 44). However, a sudden decrease in the photonic efficiencies was measured for  $\text{CO}_2$  and  $\text{CH}_4$  at  $\text{pH} > 5$ .

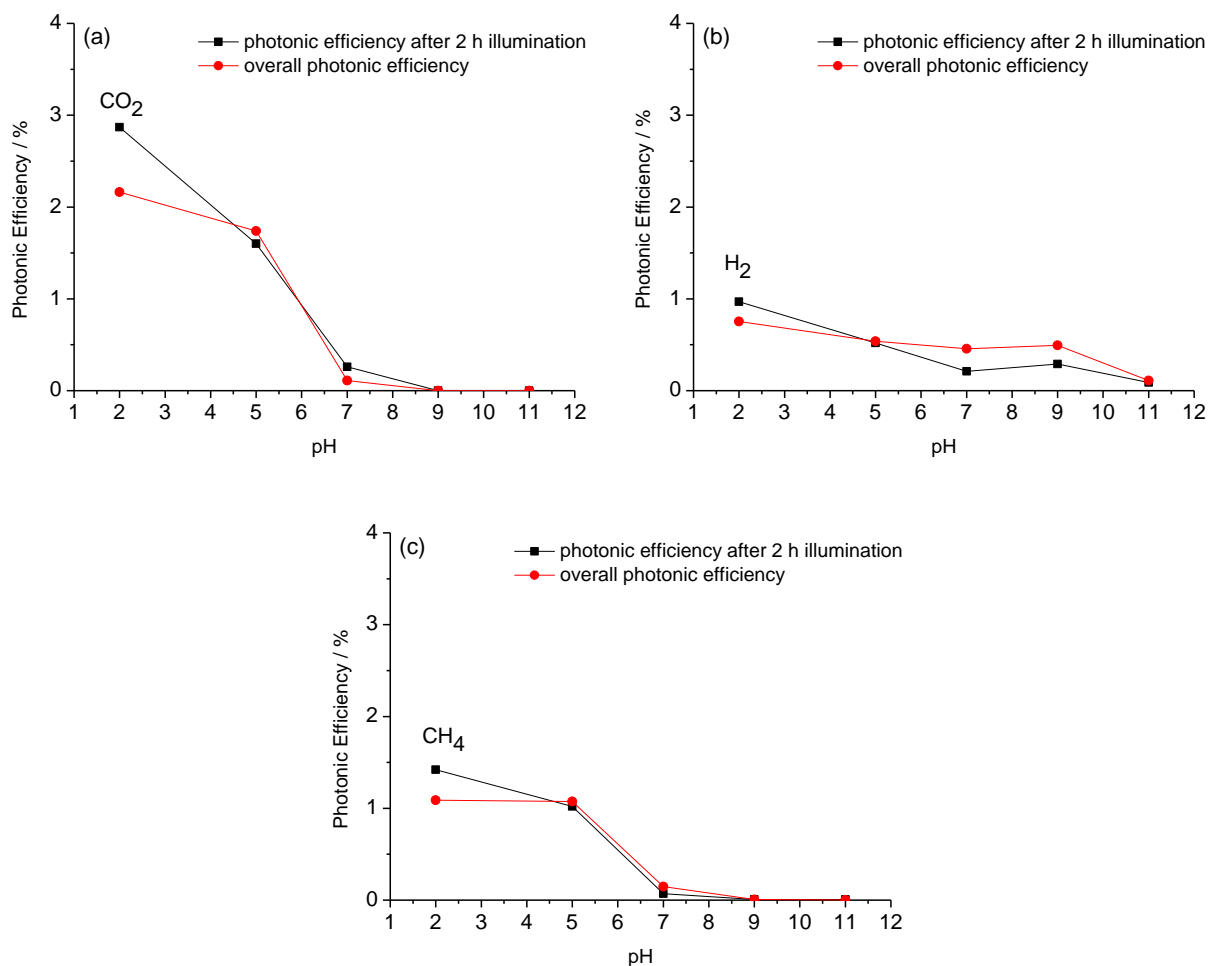


**Figure 44:** Photonic efficiency for the main reaction products, *i.e.*, (a)  $\text{CO}_2$ , (b)  $\text{H}_2$ , and (c)  $\text{CH}_4$ , calculated for the initial (after 2 h illumination) and overall (after 15 h illumination) formation rates. *Experimental conditions:* as in Figure 21 – 22.

According to the published values of the dissociation constant for acetic acid ( $\text{pK}_a = 4.75$ ) [158] and the zero point charge of  $\text{TiO}_2$  ( $\text{pH}_{\text{zpc}} \approx 6.25$ ) [159], three different situations can be assumed in order to explain the different product distribution as shown in Figure 45.

(1) For  $\text{pH} < \text{pK}_a$ , the surface of the  $\text{TiO}_2$  is saturated with the positive charges whereas acetic acid exists mainly in its protonated form ( $\text{CH}_3\text{COOH}$ ).

#### 4. Discussion

(2) For  $\text{pK}_a < \text{pH} < \text{pH}_{\text{zpc}}$ ,  $\text{TiO}_2$  is still positively charged but most of the acetic acid exists in its deprotonated form ( $\text{CH}_3\text{COO}^-$ ) thus a strong attraction between the acetate ions and  $\text{TiO}_2$  surface is assumed.

(3) For  $\text{pH} > \text{pH}_{\text{zpc}}$ , both the surface of  $\text{TiO}_2$  and acetate ions are negatively charged, so a repulsion between them is expected. But the adsorption of acetate ion by its methyl group is considered to be more likely in this situation.

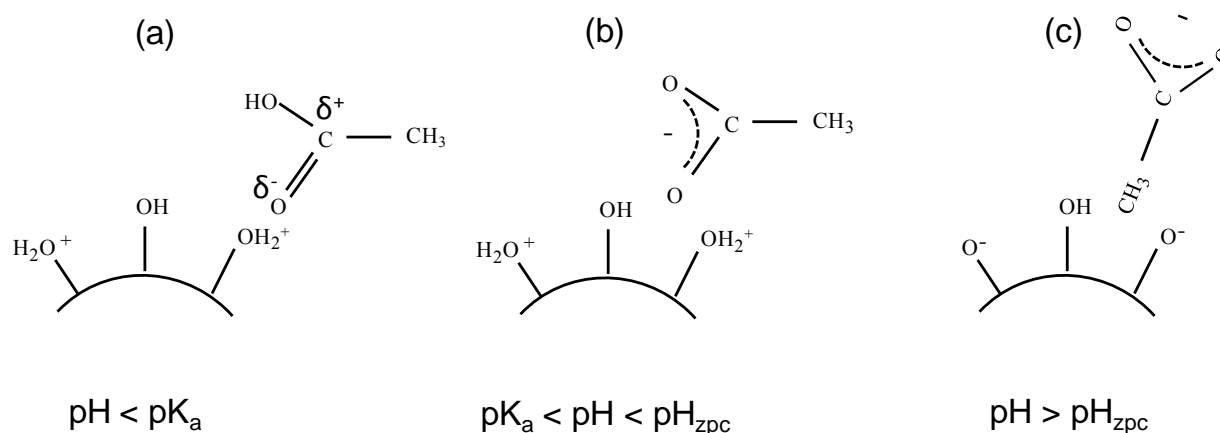


**Figure 45:** Schematic illustration of the interaction between acetic acid / acetate and the  $\text{TiO}_2$  surface in different pH regimes.

During the photocatalytic oxidation of an organic molecule by  $h\nu_{\text{VB}}^+$  of the semiconductor, its adsorption onto the surface of semiconductor is a key factor. It can be seen from Figure 45 that the adsorption between acetic acid/acetate ion and the surface of  $\text{TiO}_2$  through the carboxylic group of acetic acid/acetate ( $\text{CH}_3\text{COOH}/\text{CH}_3\text{COO}^-$ ) is possible only in acidic pH medium. Hence, the formation of reaction products resulting from  $\bullet\text{CH}_3$  as the intermediate is more favourable at  $\text{pH} < 7$  (Equation 6, Figure 46, and Table 5).

It is also obvious from Figure 46 that the significant amounts of  $n(\bullet\text{CH}_3)$  detected by quadrupole mass spectrometer (QMS) only for  $\text{pH} < 7$  while an increase in  $\text{pH} (> 7)$  results in lowering the detection of  $n(\bullet\text{CH}_3)$  intermediate by QMS. Nosaka *et al.* [160] calculated the ratios between amounts of  $n(\bullet\text{CH}_3)$  and  $n(\bullet\text{CH}_2\text{COOH})$  formed during photocatalytic transformation of  $0.1 \text{ mol L}^{-1}$  acetic acid employing  $\text{Pt}/\text{TiO}_2$  as a photocatalyst. They found that in acidic pH media, almost



## 4. Discussion

75 % of acetic acid molecules are oxidized by a  $h\nu_{VB}^+$  resulting in the formation of  $\bullet\text{CH}_3$  as reaction intermediates (Equation 6). Yoneyama *et al.* [90] also calculated the formed amounts of  $\bullet\text{CH}_3$  for  $3.9 < \text{pH} < 7.5$  with Pt/TiO<sub>2</sub> as a photocatalyst. They observed a decrease in the formation of  $\bullet\text{CH}_3$  by 90 % when pH was changed from 3.9 – 7.5. Same results for total number of  $\bullet\text{CH}_3$  formation over  $2 < \text{pH} < 11$  were given by QMS in this study and can be seen in Figure 46. Therefore, the situation where  $\text{pH} > \text{pH}_{zpc}$ , the dominant reaction for the photocatalytic decomposition of aqueous acetic acid is assumed to be the indirect reaction between acetate ion ( $\text{CH}_3\text{COO}^-$ ) on the side of its methyl group ( $\text{CH}_3$ ) and the  $\bullet\text{OH}$  (generated according to Equation 2) while resulting in the formation of  $\bullet\text{CH}_2\text{COO}^-$  intermediate (Equation 4). This argument is based on the results obtained by Wolff and co-workers [80] as discussed in chapter 1.2.4.1.

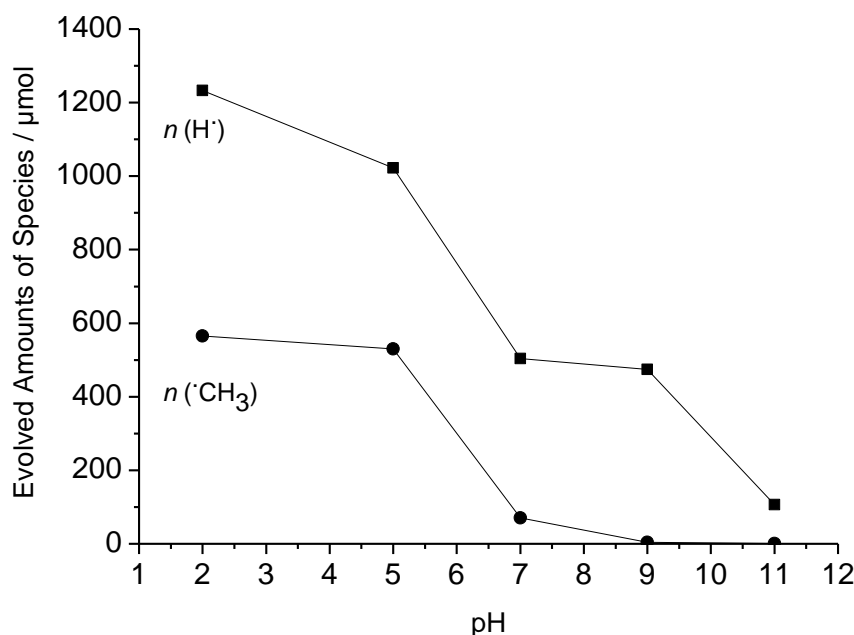


**Figure 46:** Amounts of  $\text{H}^\bullet$ , and  $\bullet\text{CH}_3$ , evolved during 15 h of irradiation of aqueous acetic acid in the presence of co-catalyst-loaded TiO<sub>2</sub> vs. pH values of the employed suspension. *Experimental conditions:* as in Figure 21 – 22.

## 4. Discussion

**Table 5:** Effect of the initial pH value on the amounts of the main reaction products photocatalytically formed during 15 h of irradiation.

1	2	3	4	5	6	7	8	9	10	11	12	13
M/TiO <sub>2</sub>	pH	$n_0$	$n(\text{CO}_2)$	$n(\text{H}_2)$	$n(\text{CH}_4)$	$n(\text{C}_2\text{H}_6)$	$X_C$	$X_H$	$\frac{n(\text{H}_2)}{n(\text{CO}_2)}$	$\frac{n(\text{H}_2)}{n(\text{CH}_4)}$	$\frac{n(\text{H}_2)}{n(\text{C}_2\text{H}_6)}$	$\frac{n(\text{C}_2\text{H}_6)}{n(\text{CH}_4)}$
	–	μmol	μmol	μmol	μmol	μmol	–	–	–	–	–	–
Pt/TiO <sub>2</sub>	2	25000	1027	357	517	24	0.032	0.029	0.34	0.69	15	0.04
Pt/TiO <sub>2</sub>	5	25000	826	256	510	10	0.027	0.026	0.30	0.50	25	0.01
Pt/TiO <sub>2</sub>	7	25000	53	217	70	0.26	0.002	0.007	4.09	3.10	834	0.003
Pt/TiO <sub>2</sub>	9	25000	–	235	4.0	0.18	–	0.004	–	58	1305	0.04
Pt/TiO <sub>2</sub>	11	25000	–	57	0.61	0.01	–	0.001	–	86	5300	0.01

*Experimental conditions:* photocatalyst concentration = 0.5 g L<sup>-1</sup>, initial acetic acid concentration ( $c_0$ ) = 0.5 M,  $2 \leq \text{initial pH} \leq 9$ ,  $n_0$  = number of initial acetic acid molecules, suspension volume = 50 mL, irradiation time = 15 h, irradiation intensity  $I_{250-450} = 30 \text{ mW cm}^{-2}$ .

**Table 5 (continued):** Effect of the initial pH value on the amounts of the main reaction products photocatalytically formed during 15 h of irradiation.

14	15		16		17		18	19
$\frac{2n(\text{C}_2\text{H}_6)}{n(\text{CH}_4)+2n(\text{C}_2\text{H}_6)}$	$\frac{n(\cdot\text{CH}_3)}{n(\text{H}\cdot)}$	$= \frac{n(\text{CH}_4)+2n(\text{C}_2\text{H}_6)}{n(\text{CH}_4)+2n(\text{H}_2)}$	$\frac{n(\cdot\text{CH}_3)}{n(\text{CO}_2)}$	$= \frac{n(\text{CH}_4) + 2n(\text{C}_2\text{H}_6)}{n(\text{CO}_2)}$	$\frac{n(\text{H}\cdot)}{n(\text{CO}_2)}$	$= \frac{n(\text{CH}_4) + 2n(\text{H}_2)}{n(\text{CO}_2)}$	$\frac{n(\text{CH}_4)+n(\text{C}_2\text{H}_6)}{n(\text{H}_2)}$	pH
–	–	–	–	–	–	–	–	–
0.09		0.46		0.54		1.19	1.49	2
0.04		0.51		0.64		1.23	2.03	5
0.007		0.13		1.33		9.50	0.32	7
0.08		0.009		–		–	0.01	9
0.03		0.005		–		–	0.01	11

*Experimental conditions:* photocatalyst concentration = 0.5 g L<sup>-1</sup>, initial acetic acid concentration ( $c_0$ ) = 0.5 M,  $2 \leq$  initial pH  $2 \leq 9$ ,  $n_0$  = number of initial acetic acid molecules, suspension volume = 50 mL, irradiation time = 15 h, irradiation intensity  $I_{250-450} = 30 \text{ mW cm}^{-2}$ .

## 4. Discussion

At pH values 2 and 5, the formed amounts of CH<sub>4</sub> were found to be higher in comparison to the formed amounts of H<sub>2</sub> (Table 5). Other than the formed amounts, the reaction rates also seemed to be quite different when pH of the suspension changes from 2 to 5. Figure 21 illustrates almost constant formation rates during 15 h of illumination for all main reaction products at pH ≥ 5. In comparison to this, the formation rates of the main reaction products at pH 2 decreases with the irradiation time. Moreover, the formed amounts of H<sub>2</sub> evolution were found to be in close approximation over a range of 5 ≤ pH ≤ 9. Zheng *et al.* [100] reported that the significant amounts for H<sub>2</sub> and CH<sub>4</sub> evolution from photocatalytic decomposition of aqueous acetic acid employing Pt/TiO<sub>2</sub> can only be obtained at acidic pH values. In contrast to the results published by Zheng *et al.* [100] and the results obtained in this work, Sakata and co-workers [37] observed higher amounts of H<sub>2</sub> evolution in alkaline pH medium. Therefore, the reaction pathway for the photocatalytic decomposition of aqueous acetic acid cannot be generalized. Depending on the experimental conditions, it is possible to obtain different product distribution.

It can be seen in Figure 24 that the formation of CO<sub>2</sub> stops at pH > 5. The reason behind this observation is the conversion of CO<sub>2</sub> into carbonate (CO<sub>3</sub><sup>2-</sup>) and bicarbonate (HCO<sub>3</sub><sup>-</sup>) at pH ≥ 7 [109], thus the detection of CO<sub>2</sub> in the gas phase is not possible. However, CO<sub>2</sub> in the form of CO<sub>3</sub><sup>2-</sup> and HCO<sub>3</sub><sup>-</sup> remain in the suspension. Moreover, the suppression of hydrocarbons formation at pH ≥ 7 can be explained with respect to the shift in the position of valence band (VB) and conduction band (CB) of TiO<sub>2</sub> at various pH values. In our study, the value of the flat band potential for TiO<sub>2</sub> P25 has been determined to be: U<sub>fb</sub> = - 0.58 V with respect to the normal hydrogen electrode (NHE) at pH 7. Generally, the change in the pH value of the suspension cause a shift in the flat band potential of TiO<sub>2</sub> (Figure 47) according to the following Equation 22:

$$U_{fb}(pH) = U_{fb}(pH 0) - 59 \times 10^{-3} \times pH \quad V \text{ vs. NHE} \quad \text{Equation 22}$$

It is well known that the band gap (E<sub>g</sub>) of TiO<sub>2</sub> P25 is 3.2 eV. According to the relation E<sub>VB</sub> = E<sub>CB</sub> - E<sub>g</sub> ≈ U<sub>fb</sub> - E<sub>g</sub>, the VB position of TiO<sub>2</sub> is therefore affected by the change in pH value. Increasing the pH towards more basic regime shifts the VB of TiO<sub>2</sub> towards a more negative value (Figure 47). As a result, the oxidation power of h<sub>VB</sub><sup>+</sup> becomes less in order to carry out the oxidation of acetic acid molecule (Figure 37, and 47). It is also reported that the critical potential

## 4. Discussion

value (pH independent) after which the direct  $h\nu_{VB}^+$  oxidation of acetic acid is not possible is  $\approx +2.41$  V vs. NHE [37, 88, 161, 162]. Thus, the shift in VB position of  $TiO_2$  at  $pH > 7$ , which is close to the critical potential values of acetic acid, can explain the suppression of  $CH_4$  formation.

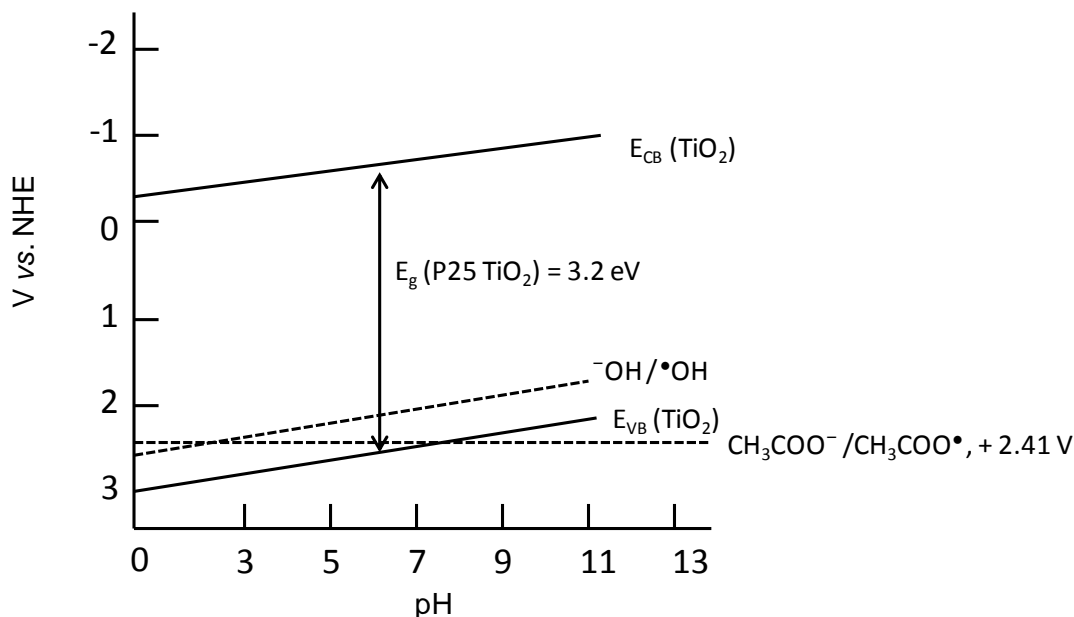


**Figure 47:** Schematic illustration of energy band diagram for  $TiO_2$  P25 at  $0 \leq pH \leq 11$  along with the one electron oxidation potential of acetate ( $CH_3COO^-$ ) [115].

However, the decrease in the formed amounts of all reaction products at  $pH > 9$  also corresponds to the surface agglomeration. In general, at  $pH > 9$ , the  $TiO_2$  particles gathered while forming the large aggregates thus affecting the photocatalytic activity [163]. The decrease in the formed amounts of  $H_2$  evolution at  $pH > 9$  can be explained according to surface agglomeration which results in decreasing the surface area of the  $TiO_2$  particles.

### 4.2.4 Isotopic labelling studies

In a photocatalytic reaction system where  $H_2$  is formed with simultaneous degradation of an organic molecule, controversies exist in the published literature. For instance, according to some researchers during a photocatalytic reaction for simultaneous  $H_2$  production and organic pollutant

## 4. Discussion

degradation, H<sub>2</sub> is formed by a photocatalytic H<sub>2</sub>O splitting reaction [103, 164]. In contrast to this, other researchers reported that in the presence of an organic pollutant, H<sub>2</sub> is being formed by the reforming of organic molecules [56, 165]. In order to solve these controversies isotopic labelling experiments have been performed to confirm the origin of H<sub>2</sub> evolution reaction (HER). Most of the published reports explained the HER by means of isotopic labelling experiments for molecules such as CH<sub>3</sub>OH [43] or HCHO [166] resulting in only H<sub>2</sub> and CO<sub>2</sub> formation as the final reaction products. Detailed analysis for the isotopic studies of photocatalytic degradation of aqueous acetic acid resulting in H<sub>2</sub> and CH<sub>4</sub> besides CO<sub>2</sub> as main reaction products does not exist in literature. Only few reports are published depicting the HER from photocatalytic transformation of aqueous acetic acid during isotopic labelling experiments [36, 37, 84]. In the present work, we have investigated the effect of various acetic acid (CH<sub>3</sub>COOH, CD<sub>3</sub>COOD, and CH<sub>3</sub>COOD), as well as solvent isotopes (*i.e.*, H<sub>2</sub>O/D<sub>2</sub>O) on the formation rates and product distribution resulting from photocatalytic conversion of aqueous acetic acid. Additionally, for the first time, proton exchange reaction at both carboxylic and methyl group of aqueous acetic acid in the presence of co-catalyst loaded TiO<sub>2</sub> has been investigated in detail. As already explained in chapter 3.2.5, the employed isotopic reaction systems for the photocatalytic degradation of aqueous acetic acid are as follow: (i) Pt/TiO<sub>2</sub>-CH<sub>3</sub>COOH-H<sub>2</sub>O, (ii) Pt/TiO<sub>2</sub>-CD<sub>3</sub>COOD-H<sub>2</sub>O, (iii) Pt/TiO<sub>2</sub>-CH<sub>3</sub>COOD-H<sub>2</sub>O, (iv) Pt/TiO<sub>2</sub>-CD<sub>3</sub>COOD-D<sub>2</sub>O, (v) Pt/TiO<sub>2</sub>-CH<sub>3</sub>COOH-D<sub>2</sub>O, and (vi) Pt/TiO<sub>2</sub>-CH<sub>3</sub>COOD-D<sub>2</sub>O.

It has been observed in all experimental runs that the photocatalytic transformation of aqueous acetic acid results in the formation of CO<sub>2</sub> as the main reaction product. Using acetic acid and water being different in isotopic composition (i – vi), the formation rates as well as the amounts of the evolved CO<sub>2</sub> during the photocatalytic reaction are presented in Figure 25, 26, 27, and Table 6 respectively. The initial and overall photonic efficiencies calculated for the evolved amounts of CO<sub>2</sub> in all reaction systems (i – vi) are also presented in Figure 48. It can be seen in Figure 48, that the difference between the calculated initial and overall photonic efficiencies is smaller for the reaction systems (iv, v, and vi) having D<sub>2</sub>O as a solvent in comparison to the reaction systems (i, ii, and iii) containing H<sub>2</sub>O as a solvent. The formation rates and the corresponding formed amounts of CO<sub>2</sub> seemed to be dependent on the employed isotopes (Figure 25, Table 6). For example, the formation rates of CO<sub>2</sub> obtained from reaction systems (iii, iv, and v) containing D<sub>2</sub>O as a solvent were observed to be higher as well as more stabilized than the

formation rates of CO<sub>2</sub> acquired from reaction systems (i, ii, and iii) having H<sub>2</sub>O as a solvent (Figure 25, Table 6).

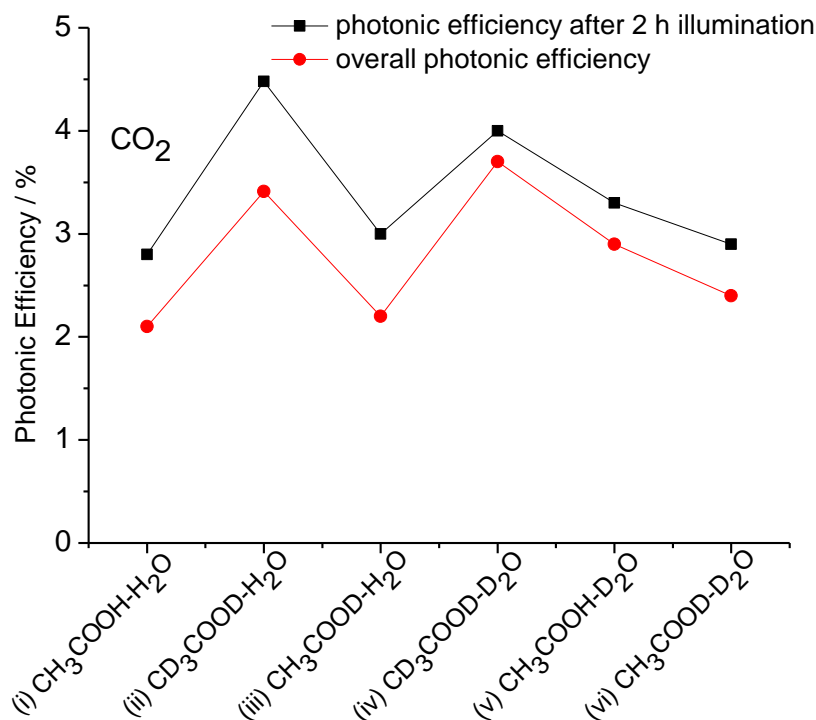


**Figure 48:** Photonic efficiency of the evolved amounts of CO<sub>2</sub>, calculated for the initial (after 2 h illumination) and overall (after 15 h illumination) formation rates for reaction systems (i – vi). *Experimental conditions:* as in Figure 25 – 26.

Additionally, the formation rates and amounts of molecular hydrogen (H<sub>2</sub>), molecular deuterium (D<sub>2</sub>), and HD from all six reaction systems (i – vi) are presented in Figure 28, 29, 30 and Table 6. Different isotopes *i.e.*, H<sub>2</sub>, D<sub>2</sub>, and HD were detected from all reaction systems (i – vi) depending on the employed reaction conditions. The photonic efficiencies calculated for H<sub>2</sub> and D<sub>2</sub> evolved from reaction systems (i – vi) are shown in Figure 49. It can be seen in Figure 49, that the reaction systems (i, ii, and iii) having H<sub>2</sub>O as a solvent results in a different initial and overall photonic efficiencies. On the other hand, the reaction systems (iv, v and vi) saturated with D<sub>2</sub>O exhibits approximately the same initial and overall photonic efficiencies.

## 4. Discussion

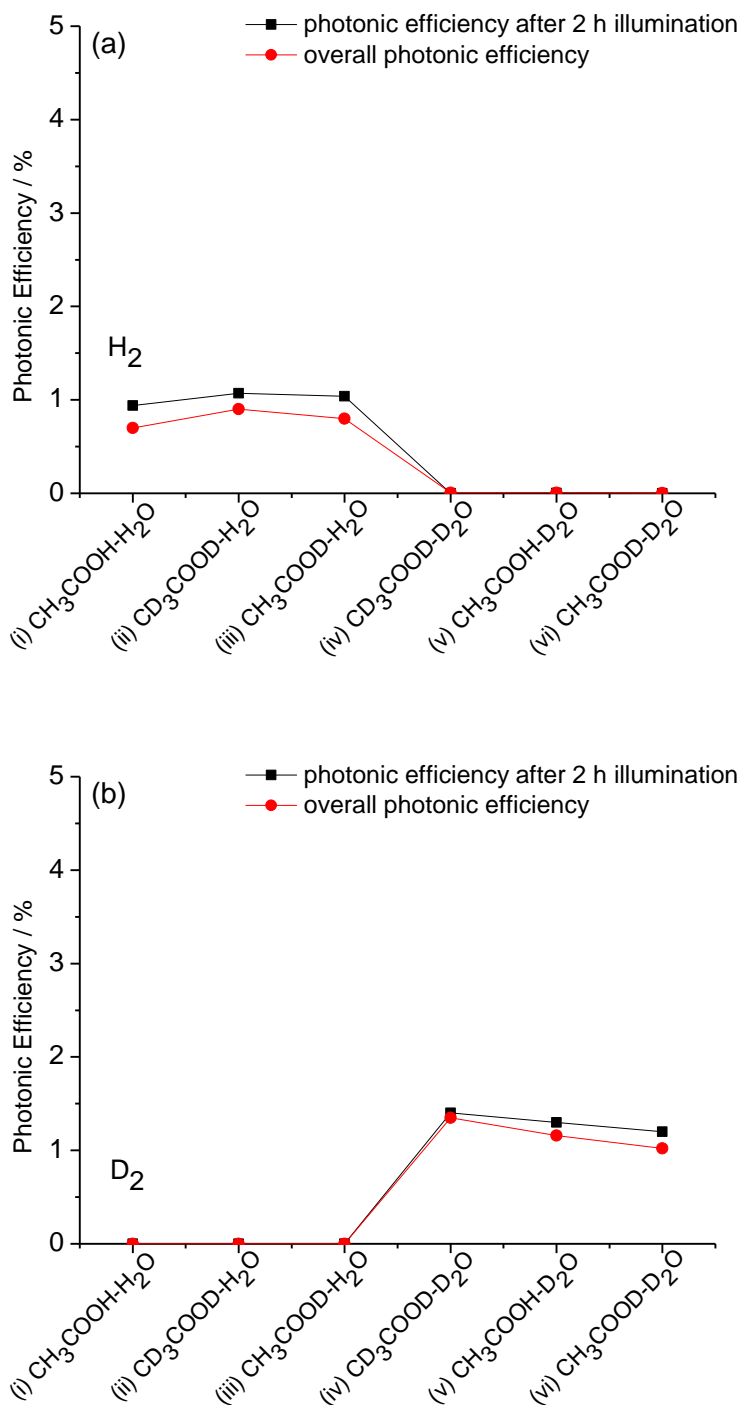


**Figure 49:** Photonic efficiency of the evolved amounts of (a) H<sub>2</sub>, and (b) D<sub>2</sub>, calculated for the initial (after 2 h illumination) and overall (after 15 h illumination) formation rates for reaction systems (i – iv). *Experimental conditions:* as in Figure 28 – 29.



**Table 6:** Amounts and ratios calculated between the formed amounts resulting from aqueous acetic acid (0.5 M) in the presence of 1wt % Pt/TiO<sub>2</sub> at pH ≈ pD = 2.

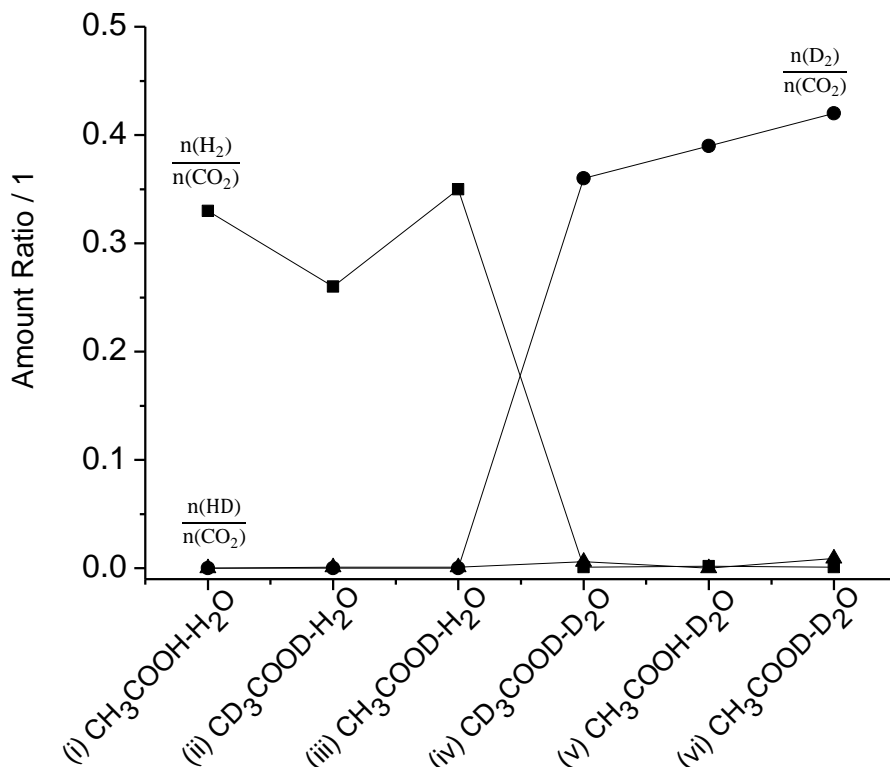
Sr. No.	Reaction System	$n(\text{H}_2)$ μmol	$n(\text{D}_2)$ μmol	$n(\text{HD})$ μmol	$n(\text{CO}_2)$ μmol	$\frac{n(\text{H}_2)}{n(\text{CO}_2)}$ --	$\frac{n(\text{D}_2)}{n(\text{CO}_2)}$ --	$\frac{n(\text{HD})}{n(\text{CO}_2)}$ --
(i)	Pt/TiO <sub>2</sub> -CH <sub>3</sub> COOH-H <sub>2</sub> O	357	--	--	1057	0.33	--	--
(ii)	Pt/TiO <sub>2</sub> -CD <sub>3</sub> COOD-H <sub>2</sub> O	421	0.46	1.9	1622	0.26	0.0002	0.001
(iii)	Pt/TiO <sub>2</sub> -CH <sub>3</sub> COOD-H <sub>2</sub> O	377	0.23	1.5	1067	0.35	0.0002	0.001
(iv)	Pt/TiO <sub>2</sub> -CD <sub>3</sub> COOD-D <sub>2</sub> O	3.19	642	11.8	1769	0.001	0.36	0.006
(v)	Pt/TiO <sub>2</sub> -CH <sub>3</sub> COOH-D <sub>2</sub> O	3.77	555	0.35	1404	0.002	0.39	0.0002
(vi)	Pt/TiO <sub>2</sub> -CH <sub>3</sub> COOD-D <sub>2</sub> O	1.09	488	11	1153	0.0009	0.42	0.009

Table 6 clearly indicates that the reaction systems (i, ii, and iii) containing H<sub>2</sub>O as the solvent depict H<sub>2</sub> as the major reaction product while negligible amounts of D<sub>2</sub> and HD were also detected which might come from an impurity. In contrast to this, for reaction systems (iv, v, and vi) D<sub>2</sub> was found to be the dominant reaction product with minor amounts of H<sub>2</sub> and HD, when D<sub>2</sub>O was used as the solvent (Table 6).

Overall, the reaction systems having D<sub>2</sub>O as solvent or CD<sub>3</sub>COOD as sacrificial reagent seem to result in higher reaction rates and higher amounts of the corresponding evolved reaction products (Figure 28, Table 6). For example, the formation rates for D<sub>2</sub> evolution from systems (iv, v, and vi) were observed to be more stable and higher over the entire irradiation time (15 h) in comparison to the H<sub>2</sub> formation rates from systems (i, ii, and iii) (Figure 28).

Moreover, Table 6 and Figure 50 summarize the ratios calculated between the formed amounts of H<sub>2</sub>, D<sub>2</sub> and CO<sub>2</sub>.

## 4. Discussion



**Figure 50:** Ratios between the evolved amounts of methane  $n(\text{CH}_4)$ , ethane  $n(\text{C}_2\text{H}_6)$ , molecular hydrogen  $n(\text{H}_2)$ , and carbon dioxide  $n(\text{CO}_2)$  vs. isotopic reaction systems (i – vi). *Experimental conditions:* as in Figure 25 – 30.

It can be seen in Table 6 and Figure 50 that the ratios between the formed amounts of  $\frac{n(\text{H}_2)}{n(\text{CO}_2)}$  and  $\frac{n(\text{D}_2)}{n(\text{CO}_2)}$  for reaction systems containing either (i)  $\text{H}_2\text{O}$  or (iv)  $\text{D}_2\text{O}$  as the solvent, remains almost constant. However, a slight difference ( $\approx 0.1$ ) between the ratios is observed for H/D mixture reaction systems *i.e.*, ii, iii, v, and vi. Also, negligible amounts of HD do not illustrates any considerable difference for the  $\frac{n(\text{HD})}{n(\text{CO}_2)}$  ratio.

Moreover, it can be seen in Figure 31, 32, 33, and Table 7 that during the photocatalytic decomposition of aqueous acetic acid employing reaction systems (i – vi), four types of methane being different in isotopic composition *i.e.*,  $\text{CH}_4$ ,  $\text{CH}_3\text{D}$ ,  $\text{CD}_3\text{H}$ , and  $\text{CD}_4$  were detected by quadrupole mass spectrometer (QMS).

**Table 7:** Formed amounts of CH<sub>4</sub>, CH<sub>3</sub>D, CD<sub>3</sub>H and CD<sub>4</sub> during photocatalytic decomposition of aqueous acetic acid in all reaction systems (i – vi).

Sr. No.	Reaction System	$n(\text{CH}_4)$ μmol	$n(\text{CH}_3\text{D})$ μmol	$n(\text{CD}_3\text{H})$ μmol	$n(\text{CD}_4)$ μmol
(i)	Pt/TiO <sub>2</sub> -CH <sub>3</sub> COOH-H <sub>2</sub> O	507	--	--	--
(ii)	Pt/TiO <sub>2</sub> -CD <sub>3</sub> COOD-H <sub>2</sub> O	17.9	121	415	59.3
(iii)	Pt/TiO <sub>2</sub> -CH <sub>3</sub> COOD-H <sub>2</sub> O	501	55.6	14.3	8.04
(iv)	Pt/TiO <sub>2</sub> -CD <sub>3</sub> COOD-D <sub>2</sub> O	2.81	1.05	3.79	1066
(v)	Pt/TiO <sub>2</sub> -CH <sub>3</sub> COOH-D <sub>2</sub> O	112	221	10.4	743
(vi)	Pt/TiO <sub>2</sub> -CH <sub>3</sub> COOD-D <sub>2</sub> O	51.9	147	12.5	690

For the formation of methane employing reaction systems (i) Pt/TiO<sub>2</sub>-CH<sub>3</sub>COOH-H<sub>2</sub>O, two reaction pathways are reported in literature. For instance, a reaction between  $\bullet\text{CH}_3$  and  $\bullet\text{H}$ , where  $\bullet\text{H}$  is the product of the reduction of a proton (H<sup>+</sup>) formed (1) by deprotonation of CH<sub>3</sub>COOH (Equation 6) or (2) by dissociation of solvent (H<sub>2</sub>O) (Equation 2) [37]. Clusius *et al.* [111] investigated a reaction system Pt/TiO<sub>2</sub>-CH<sub>3</sub>COOH-D<sub>2</sub>O, mainly to see the origin for methane formation. They observed CH<sub>3</sub>D as the main reaction product when Pt was finely deposited on the surface of photocatalyst. On the other hand, CH<sub>4</sub> was obtained as major reaction product when the Pt particles were present on the surface of TiO<sub>2</sub> in the form of large patches. For the current study, TEM micrographs (Figure 9, and 10) obtained for Pt/TiO<sub>2</sub> particles shows a uniform distribution of Pt particles onto the surface of TiO<sub>2</sub> with a particle size for both Pt and TiO<sub>2</sub> in the range between 15 – 20 nm. Considering the results published by Clusius and co-workers, the major reaction product from reaction systems (v) of this work is expected to be CH<sub>3</sub>D. Unexpectedly, the obtained results here from all reaction systems (i – vi) are entirely different in comparison to those already published in literature [37, 84, 111]. Table 6 and Table 7 clearly indicate that a proton exchange reaction at both methyl group and carboxylic group of acetic acid exists in the reaction systems containing H/D mixtures (ii, iii, v, and vi).

Singleton and co-workers [167] investigated the isotopic labelling studies for carboxylic acids. They claimed that the photo-induced conversion of carboxylic acids (RCOOH, R is any atom

#### 4. Discussion

attached to carboxylic group) containing H-atoms only results in the formation of large number of by-products. In contrast to this, the photocatalytic transformation of carboxylic acids (RCOOD) where H is replaced by D results in the formation of reaction products more rapidly. Hence, the amounts of formed by-products become lower. This argument seemed to be true in order to explain the results obtained in the present study. If the amounts of formed by-products will be less, there will be more reaction sites available thus facilitating the higher adsorption of acetic acid molecules on to the surface of TiO<sub>2</sub>.

The adsorption of acetic acid molecule is pre-requisite in order to obtain significant photocatalytic activity for all reaction products (chapter 4.2.3). On the other hand, if the generation of by-products during the photocatalytic reaction will be higher, the active reaction sites on the surface of semiconductor might be poisoned thus leading to a lower photocatalytic activity for all reaction products. A comparison among the reaction products evolved from reaction systems (i, ii, iii) having H<sub>2</sub>O as a solvent to the reaction systems (iv, v, vi) containing D<sub>2</sub>O as a solvent (Figure 25 – 30, and Table 6, and 7) demonstrates that isotopically different solvents affect the formation rates of almost all reaction products. Moreover, a comparison between the reaction rates as well as reaction products evolved from reaction system (ii) Pt/TiO<sub>2</sub>-CD<sub>3</sub>COOD-H<sub>2</sub>O, (iii) Pt/TiO<sub>2</sub>-CH<sub>3</sub>COOD-H<sub>2</sub>O, (v) Pt/TiO<sub>2</sub>-CH<sub>3</sub>COOH-D<sub>2</sub>O, and (vi) Pt/TiO<sub>2</sub>-CH<sub>3</sub>COOD-D<sub>2</sub>O determines that the photo-decarboxylation is faster for the CD<sub>3</sub>COOD species than for CH<sub>3</sub>COOH or CH<sub>3</sub>COOD species.

It has been reported in literature that the dissociation constant (pK<sub>a</sub>) values for carboxylic acids RCOOH having H-atoms is higher in D<sub>2</sub>O suspension than in H<sub>2</sub>O suspensions [168]. Robinson *et al.* [169] measured the pK<sub>a</sub> for the following reaction systems: (1) CH<sub>3</sub>COOH in H<sub>2</sub>O, pK<sub>a</sub> = 4.756, (2) CH<sub>3</sub>COOH in D<sub>2</sub>O, pK<sub>a</sub> = 5.313, (3) CD<sub>3</sub>COOD in H<sub>2</sub>O, pK<sub>a</sub> = 4.771, (4) CD<sub>3</sub>COOD in D<sub>2</sub>O, pK<sub>a</sub> = 5.325. However, at the experimental conditions of the present study (pH ≈ pD = 2), different pK<sub>a</sub> for CH<sub>3</sub>COOH, CD<sub>3</sub>COOD, and CH<sub>3</sub>COOD do not seem to affect the reaction rates. As explained in chapter 4.2.3, at pH ≈ pD = 2, the interaction between positively charged TiO<sub>2</sub> surface and the neutral organic probe molecule will be higher. This means that organic probe molecules will be oxidized by TiO<sub>2</sub> valence band holes (h<sub>VB</sub><sup>+</sup>) in all cases (reaction systems (i – vi)) according to the Equation 6. However, it is assumed here that the oxidation of CD<sub>3</sub>COOD is faster than CH<sub>3</sub>COOH or CH<sub>3</sub>COOD by h<sub>VB</sub><sup>+</sup> of TiO<sub>2</sub>.

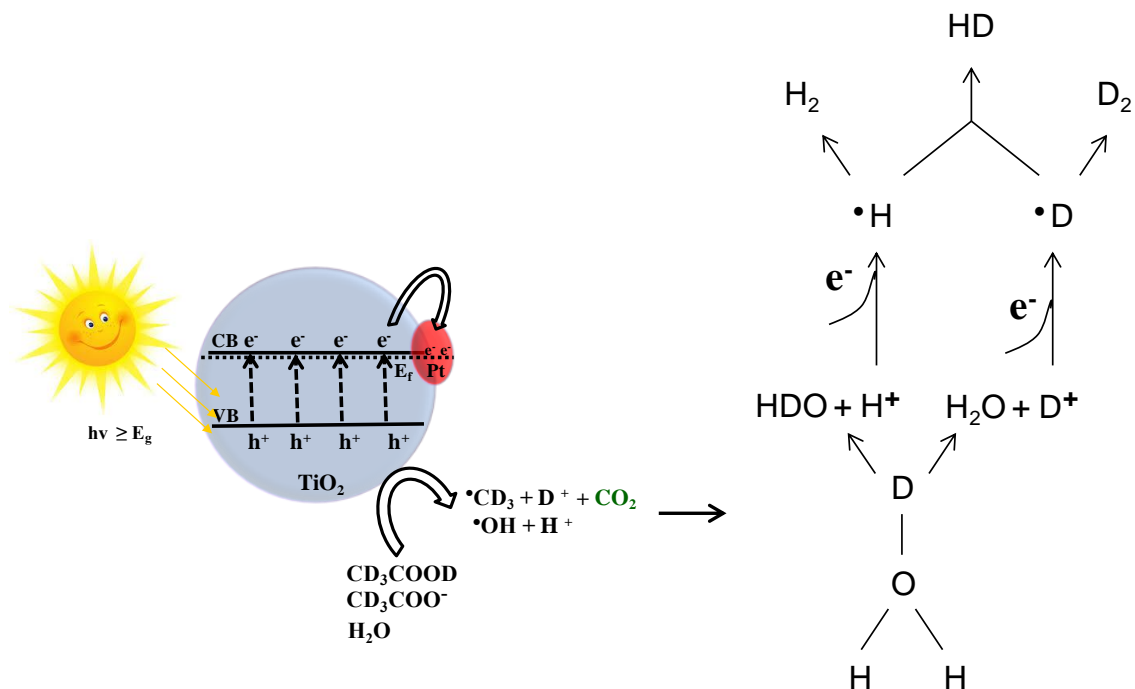
## 4. Discussion

Figure 25 and 28 clearly indicate that the reaction rates are higher in the D<sub>2</sub>O suspensions (iv, v, and vi) than in H<sub>2</sub>O suspensions (i, ii, and iii). It has been reported by Robertson *et al.* [170] that the employment of isotopically different solvent (H<sub>2</sub>O, D<sub>2</sub>O) in a photocatalytic reaction system results in different formation rates of the reaction products. The authors claimed that the reaction proceeding by  $\bullet\text{OH}$  is faster than  $\bullet\text{OD}$  because  $\bullet\text{OD}$  has less oxidation energy than  $\bullet\text{OH}$  by a factor of 20 kJ mol<sup>-1</sup>. However, the results obtained here exhibit higher formation rates (Figure 25 and 28) and corresponding formed amounts (Figure 27, 30 and Table 6) from D<sub>2</sub>O suspensions than from H<sub>2</sub>O suspensions. Considering the argument about higher oxidation power of  $\bullet\text{OH}$  than  $\bullet\text{OD}$  and the obtained results of this work, it can be concluded that at the employed experimental conditions (pH  $\approx$  pD = 2, Pt/TiO<sub>2</sub>), the photocatalytic degradation of aqueous acetic acid proceeds mainly by the direct reaction of TiO<sub>2</sub> h<sub>VB</sub><sup>+</sup> with the organic probe molecule (Equation 6) yielding  $\bullet\text{CH}_3/\bullet\text{CD}_3$ , H<sup>+</sup>/D<sup>+</sup> and CO<sub>2</sub>. Therefore, the obtained formation rates and formed amounts of reaction products are independent of the respective solvent. It should also be noted that in the same reaction system, the reaction pathway where  $\bullet\text{OH}/\bullet\text{OD}$  reacts with acetic acid molecule yielding  $\bullet\text{CH}_2\text{COOH}/\bullet\text{CD}_2\text{COOH}/\bullet\text{CH}_2\text{COOD}$  (Equation 4) also exists as minor reaction pathway. These results are confirmation of proposed reaction mechanism for the photo-induced degradation of aqueous acetic acid in acidic pH media (chapter 4.2.3).

The formed H<sup>+</sup>/D<sup>+</sup> according to Equation 6 reduced on the surface of co-catalyst yielding  $\bullet\text{H}/\bullet\text{D}$ , which subsequently dimerize at the surface of co-catalyst while forming H<sub>2</sub>/D<sub>2</sub>. The formation of H<sub>2</sub> or D<sub>2</sub> as a major reaction product was observed to be mainly dependent on the solvent being employed.

Table 6 depicts that besides the formation of H<sub>2</sub> and D<sub>2</sub>, HD as another type reaction product was produced in lower amounts. Taking into account the H/D mixture reaction system (ii) Pt/TiO<sub>2</sub>-CD<sub>3</sub>COOD-H<sub>2</sub>O, the step wise formation of H<sub>2</sub>, D<sub>2</sub>, and HD as a reaction product can be explain according to the Figure 51.

## 4. Discussion



**Figure 51:** Reaction scheme representing the proton exchange reaction during photocatalytic decomposition of reaction systems (ii) Pt/TiO<sub>2</sub>-CD<sub>3</sub>COOD-H<sub>2</sub>O.

It should also be noted that even if the proton exchange reaction is considered between the systems (ii, iii, v, and vi) where hydrogen and deuterium exist together, the significant amounts of molecular hydrogen and molecular deuterium likely originate from the solvent (Figure 30). It is therefore concluded that due to the proton exchange reaction, the formation of molecular hydrogen is a result of protons from both acetic acid as well as water. However, the ratio between the total number of molecules from acetic acid and solvent is higher. Therefore, it is obvious to get more protons participating in molecular hydrogen from water. However, it has been clarified that the photocatalytic H<sub>2</sub>O splitting reaction into H<sub>2</sub> and O<sub>2</sub> does not exist here. The formation of molecular hydrogen coming from water molecules is a result of water dissociation reaction into H<sup>+</sup> and •OH (Equation 2).

## 4. Discussion

To confirm the proton exchange reaction determined by quadrupole mass spectrometer (QMS), reaction systems (ii) Pt/TiO<sub>2</sub>-CD<sub>3</sub>COOD-H<sub>2</sub>O and (v) Pt/TiO<sub>2</sub>-CH<sub>3</sub>COOH-D<sub>2</sub>O were also tested by nuclear magnetic resonance (NMR) spectroscopy. The NMR spectroscopy was performed for the samples (1) before illumination (Figure 34, 35) and (2) after illumination (Figure 36). It can be seen in Figure 34, 35, and 36 that new peaks appeared in the NMR spectra only for irradiated suspensions. For the reaction system (ii) Pt/TiO<sub>2</sub>-CD<sub>3</sub>COOD-H<sub>2</sub>O, the formation of quintet signal exhibited by NMR spectrometer which corresponds to CD<sub>2</sub>HCOOD(H) species evidently confirms the occurrence of a proton exchange at the methyl group of acetic acid during a photocatalytic reaction. The same results were also obtained for reaction system (v) Pt/TiO<sub>2</sub>-CH<sub>3</sub>COOH-D<sub>2</sub>O, where the NMR spectrum depicts the formation of a triplet signal corresponding to CH<sub>2</sub>DCOOH(D) species. It should also be noted that the suspensions do not show any resonance signals corresponding to new species before illumination (Figure 34, and 35). This means that the proton exchange reaction is typically a photo-induced reaction occurring at the surface of co-catalyst (Figure 52) instead of a thermal reaction. The proton exchange caused by thermal process cannot be completely excluded here because of the presence of Pt nanoparticles. However, with respect to the illumination time of the suspension, the occurrence of proton exchange by thermal process at the methyl group of acetic acid is insignificant.

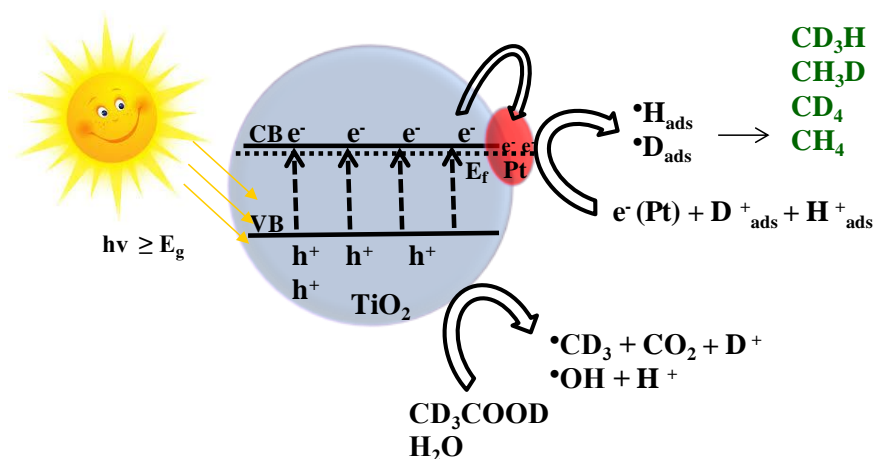


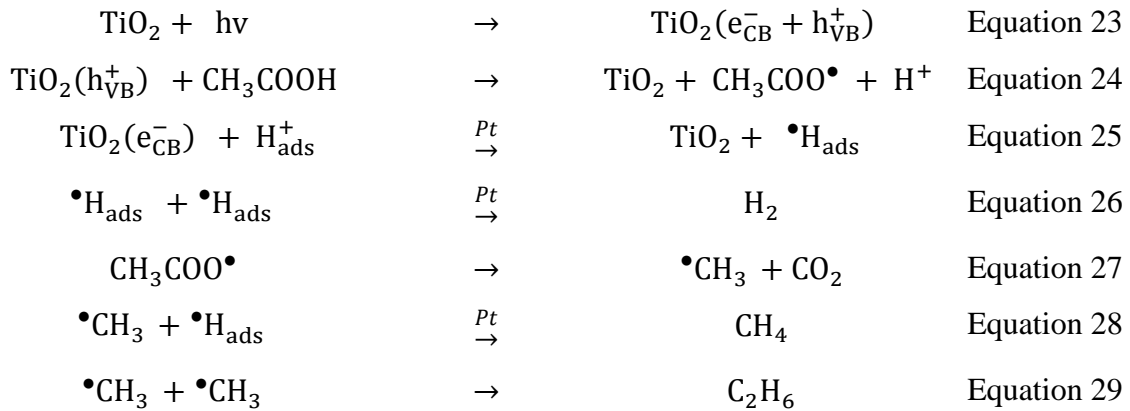
**Figure 52:** Reaction scheme representing the proton exchange reaction during photocatalytic decomposition of reaction systems (ii) Pt/TiO<sub>2</sub>-CD<sub>3</sub>COOD-H<sub>2</sub>O.

## 4. Discussion

### 4.3 Mechanistic considerations

#### 4.3.1 Basic processes for the photocatalytic degradation of aqueous acetic acid

According to the above mentioned results and discussion, the fundamental process for the photo-induced transformation of aqueous acetic acid in acidic pH media over co-catalyst loaded TiO<sub>2</sub> can be proposed as: (1) generation of charge carriers ( $h_{VB}^+$  and  $e_{CB}^-$ ) upon light illumination (Equation 23), (2) the reactions of the photo-generated charge carriers with the species adsorbed on the surface of photocatalyst as well as co-catalyst (*i.e.*, Pt) (Equation 24 – 25) and (3) subsequent reactions between the formed transient radical intermediates (Equation 26 – 29).



Generally, the direct transfer of  $h_{VB}^+$  is supposed to occur among the semiconductor surface-bound species *e.g.*, H<sub>2</sub>O molecule while forming H<sup>+</sup> as well as  $\bullet\text{OH}$ . Moreover, a reaction between the light-induced  $h_{VB}^+$  and semiconductor surface adsorbed CH<sub>3</sub>COOH molecule also occurs resulting in the formation of CH<sub>3</sub>COO $\bullet$  followed by the decomposition of CH<sub>3</sub>COO $\bullet$  into the methyl radical ( $\bullet\text{CH}_3$ ) and CO<sub>2</sub> as shown in Equation 24 and 27. During the photocatalytic decomposition of aqueous acetic acid employing either bare TiO<sub>2</sub> or metal loaded TiO<sub>2</sub>, the generation of  $\bullet\text{CH}_3$  as a reaction intermediate has been confirmed *via* EPR studies [84, 160, 171-173]. Various published reports also demonstrated the occurrence of surface methylation due to a rapid reaction of  $\bullet\text{CH}_3$  with different metals such as Pt, Au, and Ag as well as metal-oxides *e.g.*, TiO<sub>2</sub>, and CuO nanoparticles [174-179]. As a result of surface methylation, (1) the positively charged surface of photocatalyst at acidic pH might form the agglomerates of nanoparticles due



to the reduction in the surface charge or (2) active sites required to carry out the photocatalytic reaction might be blocked. Consequently, the photocatalytic activity for the degradation of organic compound will be suppressed [180]. In addition to this, the band positions are known to be shifted due to the generation of metal-hydrogen (metal-H) as well as metal-carbon (metal-C) bonds at the surface of respective metals. Hence, an interfacial electron transfer between metal nanoparticles and the redox species is affected to a great extent [135, 136]. This might be a reason of decrease in reaction rates with increasing illumination time in all experimental runs of the present study (Figure 14, 15, 18, and 21).

During the light-induced transformation of aqueous acetic acid using metal or metal-oxide loaded TiO<sub>2</sub>, production of the important gases that can be used as solar fuels *i.e.*, H<sub>2</sub> and CH<sub>4</sub>, is defined by the reactions presented in Equation 26 and 28, respectively. Here, the  $e_{CB}^-$  act as to reduce the Pt-surface adsorbed protons (H<sub>ads</sub><sup>+</sup>) while resulting adsorbed H-atoms ( $\bullet$ H<sub>ads</sub>) (Equation 25). Subsequently, a radical-radical reaction at the surface of Pt occurs while giving rise to the formation of H<sub>2</sub> (Equation 26) or CH<sub>4</sub> (Equation 28). Moreover, the formation of C<sub>2</sub>H<sub>6</sub> arises by the dimerization of two  $\bullet$ CH<sub>3</sub> as given in Equation 29. It can be seen in Table 3 – 5 (Column 14) that from total number of  $\bullet$ CH<sub>3</sub> formed under experimental conditions of this study, almost 5 – 18 % dimerize evolving C<sub>2</sub>H<sub>6</sub> as the final product. The estimated percentage has been calculated by doing a rough calculation of formed amounts of  $\bullet$ CH<sub>3</sub> converted into C<sub>2</sub>H<sub>6</sub> ( $= 2n(\text{C}_2\text{H}_6)$ ) and the total formed amounts of  $\bullet$ CH<sub>3</sub> ( $= n(\text{CH}_4) + 2n(\text{C}_2\text{H}_6)$ ).

The reaction pathway for the photocatalytic decomposition of aqueous acetic acid at acidic pH media (Equation 23 – 29) depicts that the ratio of the formed  $\bullet$ CH<sub>3</sub> ( $n(\bullet\text{CH}_3) = n(\text{CH}_4) + 2n(\text{C}_2\text{H}_6)$ ) amounts and  $\bullet$ H ( $n(\bullet\text{H}) = n(\text{CH}_4) + 2n(\text{H}_2)$ ) amounts should be equal to 1. However, Table 3 – 5 (column 15) and Figure 53 demonstrate the calculated ratio from the quantified experimental data as  $< 1$ .

## 4. Discussion

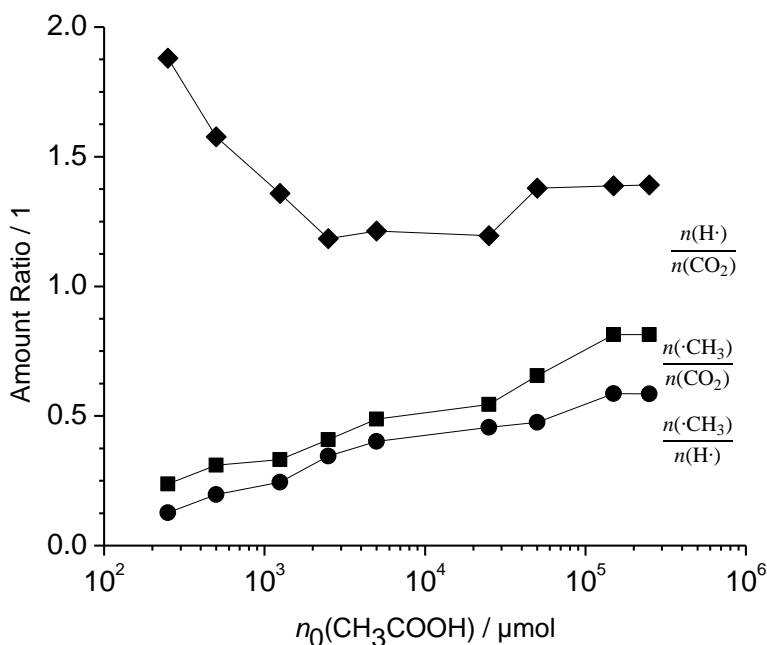


**Figure 53:** Ratios between the detected amounts of hydrogen atoms  $n(\cdot\text{H})$ , methyl radicals  $n(\cdot\text{CH}_3)$ , and carbon dioxide  $n(\text{CO}_2)$  vs. the initial amount  $n_0$  of acetic acid. *Experimental conditions:* as in Figure 18 – 19.

This means that during the photocatalytic reaction, either (1) the oxidation of  $\cdot\text{CH}_3$  and evolved hydrocarbons took place, or (2)  $\text{CH}_3\text{COOH}$  transforms into other organic compounds (not quantified in the present study). This argument is based on the following explanation:

(1) According to the reaction Equation 27, the photo-decarboxylation of  $\text{CH}_3\text{COO}\cdot$  should give a ratio between formed amounts of  $\cdot\text{CH}_3$  and  $\text{CO}_2$  as:  $\frac{n(\cdot\text{CH}_3)}{n(\text{CO}_2)} = 1$ . It can be seen in Table 3 and 4 (column 16) and Figure 53 that under the experimental conditions of the current study, the maximum value calculated for  $\frac{n(\cdot\text{CH}_3)}{n(\text{CO}_2)}$  ratio is equal to 0.81. (2) Based upon the stoichiometric calculations (Equation 23 – 29) during the photo-induced decomposition of aqueous acetic acid, the expected amounts for  $\text{H}_2$  and  $\text{C}_2\text{H}_6$  formation should be equal ( $n(\text{H}_2) = n(\text{C}_2\text{H}_6)$ ), while the ratio between  $\frac{n(\cdot\text{H})}{n(\text{CO}_2)}$  should be unity. In contrast to this, the analysis of the obtained data depicts

## 4. Discussion

the formation of H<sub>2</sub> with comparatively higher amounts than C<sub>2</sub>H<sub>6</sub> ( $n(\text{H}_2) > n(\text{C}_2\text{H}_6)$ ) in all experimental runs as can be seen in Table 3 – 5 (column 5, and 7). The, calculated ratio between the formed amounts of •H and CO<sub>2</sub> is found to vary in the range of 1.88 – 0.73 as given in Table 3, and 4 (column 17) and Figure 39.

These calculations clearly indicate the formation of higher amounts of H<sub>2</sub> and CO<sub>2</sub> than expected from the stoichiometry of the reaction, thus, confirming the formation of other organic molecules than CH<sub>4</sub> and C<sub>2</sub>H<sub>6</sub>. These formed organic compounds are then assumed to further decompose evolving H<sub>2</sub> and CO<sub>2</sub> as the reaction products. The formation of organic molecules other than CH<sub>4</sub> and C<sub>2</sub>H<sub>6</sub> during the photocatalytic conversion of aqueous acetic acid can be explained according to reaction Equations 30 – 39:



In general, other than the employed organic molecule (CH<sub>3</sub>COOH in this study), the  $\text{h}_{\text{VB}}^+$  also react with the H<sub>2</sub>O molecules adsorbed on the surface of the TiO<sub>2</sub> as well as  $\text{}^-\text{OH}$  present at the surface of TiO<sub>2</sub> yielding •OH as a reaction intermediate (Equation 30 – 31) [14]. The abstraction of H• from CH<sub>3</sub>COOH molecule by reaction with the •OH yields •CH<sub>2</sub>COOH (Equation 32). During the photo-induced decomposition of aqueous acetic acid, the existence of •CH<sub>2</sub>COOH has been confirmed *via* EPR spectroscopy [160, 171-173]. Hydrogen (H•) abstraction from CH<sub>3</sub>COOH by •OH is known to occur only at the α-position of acetic acid as given in Equation 40. Depending on the pH values of the employed suspension, the rate constant for this reaction is

#### 4. Discussion

reported to be  $\geq 1 \times 10^9 \text{ L mol}^{-1} \text{ s}^{-1}$  [181]. Therefore, the abstraction of  $\text{H}^\bullet$  from  $\text{CH}_3\text{COOH}$  molecule yielding  $\text{CH}_3\text{COO}^\bullet$  according to the reaction Equation 40 is unlikely to take place.



The abstraction of  $\text{H}^\bullet$  from  $\text{CH}_3\text{COOH}$  molecule by its reaction with a  $\bullet\text{CH}_3$  yielding  $\bullet\text{CH}_2\text{COOH}$  as reaction intermediate and  $\text{CH}_4$  as the final reaction product (Equation 41) has been reported in literature [37, 90, 171]. Rate constants for this reaction are reported as:  $2 \times 10^2$  and  $6 \times 10^2 \text{ L mol}^{-1} \text{ s}^{-1}$  [182, 183]. This reaction is therefore assumed to be a minor reaction.



On the contrary, the removal of  $\text{H}^\bullet$  from organic probe molecules by their reaction with a  $\text{H}^\bullet$  (Equation 42 – 44) are known to have higher rate constants ( $< 1 \times 10^5$ ,  $2.3 \times 10^6$  and  $9.8 \times 10^4 \text{ L mol}^{-1} \text{ s}^{-1}$ ) [184].



It is assumed that the formation of  $\bullet\text{CH}_2\text{COOH}$  predominantly occurs *via* reaction 32. The reaction given by Equation 41 and 44 are only minor reaction pathways.

According to the qualitative analysis *via* QMS, traces for propane ( $\text{C}_3\text{H}_8$ ) formation have been observed in this work. The formation of  $\text{C}_3\text{H}_8$  can be defined according to the radical-radical reaction between  $\bullet\text{CH}_2\text{COOH}$  and  $\bullet\text{CH}_3$  forming propanoic acid ( $\text{C}_2\text{H}_5\text{COOH}$ ) (Equation 33) followed by its oxidation by  $\text{h}_{\text{VB}}^+$  and resulting in the formation of  $\bullet\text{C}_2\text{H}_5$  and  $\text{CO}_2$  (Equation 34 – 35). The formed  $\bullet\text{C}_2\text{H}_5$  further reacts with a  $\bullet\text{CH}_3$  and yields  $\text{C}_3\text{H}_8$  as the final reaction product (Equation 37).

Many reports are published in literature discussing the photocatalytic transformation of aqueous acetic acid into hydrocarbons (*e.g.*,  $\text{CH}_4$ ,  $\text{C}_2\text{H}_6$ ) and other organic compounds under anaerobic

## 4. Discussion

suspension [35, 37, 83, 94, 112, 185]. The formation of comparatively minor amounts of propane ( $C_3H_8$ ) as another hydrocarbon besides the evolution of  $CH_4$  and  $C_2H_6$  has also been reported [35, 112, 185, 186]. Moreover,  $\bullet C_2H_5$  can also react with  $\bullet H_{ads}$  resulting in the formation of  $C_2H_6$  as the final reaction product (Equation 36).

It is clear from Figure 23 that the formation of organic molecules ( $C_xH_{2x+2}$  with  $x \leq 3$ ) as by-products occurred during the photocatalytic conversion of aqueous acetic acid. Sakata *et al.* [37] studied the photocatalytic decomposition of aqueous acetic acid employing Pt/TiO<sub>2</sub> as a photocatalyst at pH 2.1. They performed vapour phase analysis of the irradiated suspensions and observed the formation of  $CH_3OH$ ,  $C_2H_5OH$ ,  $(CH_3)_2CO$ , and  $C_2H_5COOH$  as reaction products in the liquid phase. In comparison to the carbon bound reaction products present in the gas phase, the carbon-contents in the liquid phase calculated from the given data were approximately 1.4% only. Mozia *et al.* [35] also carried out the liquid phase analysis of the suspension obtained after the photocatalytic degradation reaction of aqueous acetic acid employing Fe-modified TiO<sub>2</sub> as a photocatalyst. The authors reported the formation of  $CH_3OH$ ,  $C_2H_5OH$ ,  $(CH_3)_2CO$ ,  $CH_3CHO$ , and  $CH_3COOCH_3$  as the reaction products, but the amounts of these products were detected to be  $\leq 10\mu M$ . Hamid and co-workers discussed the details about the possible reaction pathways for the formation of reaction products in the liquid phase [83]. As the formed amounts of liquid phase reaction products were reported to be very low, it is supposed that the oxidation of the carbon contents present in these organic probe molecules result in the formation of  $CO_2$  and  $H_2$  as the final reaction products.

The possible reaction paths for the formation of alcohols are given in Equations (38 – 39). It should also be kept in mind that a reaction between alkyl radicals and the surface of TiO<sub>2</sub> might result in the alkylation of the TiO<sub>2</sub> surface thus leading to the formation of methanol and other organic compounds by hydrolysis of the chemical bond as shown in Equation 45 – 46.



Kandiel and co-workers [34, 187] explained the transformation of aqueous  $CH_3OH$  into  $HCHO$  and  $HCOOH$  formation, which are then subsequently oxidized to form  $H_2$  and  $CO_2$  as the final

#### 4. Discussion

reaction products. Figure 23 exhibits the traces of HCHO and HCOOH detected by QMS in the gas phase exiting the photoreactor, hence, confirming the formation of alcohols as a side product during photocatalytic decomposition of aqueous acetic acid. The reaction pathways for the oxidation of C<sub>2</sub>H<sub>5</sub>OH into H<sub>2</sub> and CO<sub>2</sub> are also reported in literature [188-190].

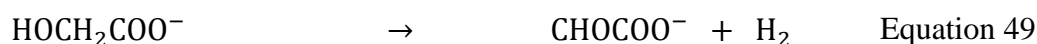
The photocatalytic reaction rates were found to be dependent on the pH value of the suspensions containing semiconductor materials and organic molecules (Figure 21). For instance, Kormann and co-workers [159] reported the effect of pH values on the photocatalytic reaction rates with respect to both electrostatic attractive and repulsive interactions among TiO<sub>2</sub> surface charge and organic probe molecules. The organic compound used in their studies was trichloroacetic acid and bis (2-chloroethyl) amine. In the present study, a decreasing trend in the formation of hydrocarbons was observed when the pH values increased towards more basic region (Figure 24, Table 5). It is also clear from reaction Equations 28 and 29 that the formation of hydrocarbons requires the presence of an alkyl radical as a reaction intermediate. It should also be noted that significant amounts of •CH<sub>3</sub> can only be generated when the adsorption of CH<sub>3</sub>COOH from the side of carboxylic group (COOH) on TiO<sub>2</sub> surface is preferred (Figure 45). In results of such adsorption, the decomposition of acetic acid proceeds by a direct reaction between h<sub>VB</sub><sup>+</sup> and acetic acid molecule (Equation 24). Nevertheless, this situation is favourable only in acidic suspensions. Hamid *et al.* [83] investigated the effect of various pH values by photoelectrochemical studies employing Pt/TiO<sub>2</sub> electrodes and acetic acid. They obtained higher photocurrents during photocatalytic oxidation of acetic acid at pH 2 in comparison to the photocurrents obtained at pH 9. Thus, the authors claimed a higher adsorption of acetic acid molecule onto the surface of TiO<sub>2</sub> in acidic pH media than in alkaline pH medium. This means, at basic pH medium acetate molecules adsorb on the surface of TiO<sub>2</sub> by the side of its methyl group thus leading to the formation of •CH<sub>2</sub>COO<sup>-</sup> (Equation 32) intermediate in higher amounts. Consequently, the reaction will follow a different pathway leading to the other reaction products (Equation 33). Even though, the number of formed •CH<sub>3</sub> becomes less at pH ≥ 7, the formation of •CH<sub>3</sub> as a reaction intermediate cannot be completely ruled out. However, the subsequent reaction products from •CH<sub>3</sub> at pH ≥ 7 are different from those formed at pH ≤ 7. The results obtained here, clearly indicate the formation of H<sub>2</sub> as the only product formed in significant amounts at pH ≥ 7 (Figure 23, Table 5). The formation of H<sub>2</sub> in alkaline media can be attributed to the

decomposition of alcohols or organic acids into  $\text{H}_2$  and  $\text{CO}_3^{2-}$  or  $\text{HCO}_3^-$  which was formed during the photocatalytic transformation of aqueous acetic acid [83]. It has been shown in literature that during photocatalytic transformation of alcohols, a change in pH does not affect the formation rate of  $\text{H}_2$  evolution significantly [34].

Moreover, the formation of organic acids yielding  $\text{H}_2$  as the reaction product can be explained according to the following reactions (Equation 47 – 49):



There is also a possibility that  $\bullet\text{CH}_2\text{COO}^-$  reacts with the surface of  $\text{TiO}_2$  (Equation 47):



The formation of hydrocarbons ( $\text{CH}_4$ ,  $\text{C}_2\text{H}_6$ ) in smaller amounts at  $\text{pH} \geq 7$  (Table 5) indicates that the direct hole oxidation reaction between  $\text{TiO}_2$   $h_{\text{VB}}^+$  and acetate molecules exists as a minor reaction (Equation 24). Therefore, the formation of alcohols or organic acids at  $\text{pH} > 7$  must be a rapid reaction.

#### 4.3.2 Kolbe vs. Hofer-Moest reaction mechanism

According to the above mentioned results and discussion, it is concluded that the photocatalytic transformation of aqueous acetic acid at acidic pH values results in the formation of reaction products rich in hydrocarbons. For example,  $\text{CH}_4$  was detected in larger amounts along with  $\text{C}_2\text{H}_6$  and  $\text{C}_3\text{H}_8$  as minor reaction products. This confirms that in acidic suspensions ( $\text{pH} < 7$ , 0.5 M acetic acid, and Pt/ $\text{TiO}_2$ ), the photo-induced transformation of aqueous acetic acid mainly follows a photo-Kolbe reaction mechanism. According to the Kolbe mechanism, hydrocarbons as well as  $\text{CO}_2$  are formed as main reaction products. It should also be noted that under acidic conditions the formation of alcohols as minor reaction products have also been detected in this study. This suggests that besides the photo-Kolbe mechanism, there exists another reaction pathway for the

## 4. Discussion

photocatalytic decomposition of aqueous acetic acid which is known as Hofer-Moest reaction. According to the Hofer-Moest reaction, alcohols and aldehydes are formed as the reaction products. On the other hand, in alkaline suspensions ( $\text{pH} > 7$ , 0.5 M acetic acid, Pt/TiO<sub>2</sub>), the formation of H<sub>2</sub> is monitored as the main reaction product while hydrocarbons are produced in negligible amounts. Hence, the dominant reaction pathway for acetic acid decomposition at  $\text{pH} > 7$  is assumed to be the Hofer-Moest reaction. However, the existence of photo-Kolbe mechanism as minor reaction pathway at  $\text{pH} > 7$  cannot be excluded [191-193].

### 4.3.3 Proton exchange reaction

It has been observed here, that the formation of the fuels such as H<sub>2</sub> and CH<sub>4</sub> requires the presence of hydrogen atom (Equation 26, and 28). Therefore, the investigations regarding the origin of hydrogen atoms participating in H<sub>2</sub> and CH<sub>4</sub> generation are very important. For this purpose, isotopic labelling experiments with different isotopes of acetic acid and water have been performed here. A detailed discussion about isotopic labelling studies has been given in chapter 4.2.4. Briefly, for a reaction system containing Pt/TiO<sub>2</sub> as a photocatalyst in acidic ( $\text{pH} \approx \text{pD} = 2$ ) media with CD<sub>3</sub>COOD and H<sub>2</sub>O, a rapid proton exchange reaction exists which can be explain as follow (Equation 50):



For the photocatalytic reaction systems (ii) Pt/TiO<sub>2</sub>-CD<sub>3</sub>COOD-H<sub>2</sub>O, upon light illumination, the formation of H<sub>2</sub>, D<sub>2</sub> or HD can be explained according to the following reactions (Equation 51 – 57).

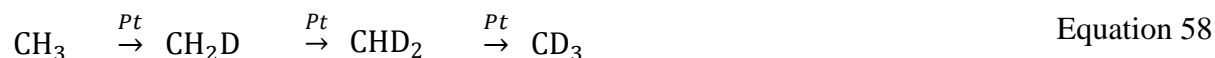




## 4. Discussion



However, the chemistry of  $\bullet\text{CH}_3/\bullet\text{CD}_3$ , resulting from the light induced decomposition of carboxylic acids (Equation 27, and 52) has been discussed by many researchers using QMS and NMR spectroscopic techniques [84, 194-197]. Usually, the proton exchange reaction occurring at methyl group ( $\text{CH}_3/\text{CD}_3$ ) of carboxylic acids in H/D mixture reaction systems is categorized in two types: (1) single exchange reaction, and (2) multiple exchange reaction. The responsible factors, according to which the protons exchange reaction proceeds by single exchange or multiple exchanges, are as follow: (1) particle size of co-catalyst deposited on the surface of semiconductor material, (2) temperature of the reaction system, and (3) pressure [198, 199]. Depending on the reaction conditions, if a single exchange reaction repeated multiple times (Equation 58), the same reaction products are obtained which might be formed during a multiple exchange reaction.



Kemball *et al.* [200] reported that the single exchange reaction does not require elevated temperature value for their occurrence and can be proceed at ambient temperature. In contrast to this, for a multiple exchange reaction, temperature value  $> 300$  °C are required. The experiments of the present study have been performed at ambient temperature. Therefore, it is assumed that in this study, for the suspensions containing H/D mixtures, a single exchange reaction occurs multiple times hence resulting in the formation of methane being different in isotopic composition (Table 7). Moreover, the importance of Pt nanoparticles cannot be neglected when a proton exchange reaction is considered. It has been reported by Khodakov *et al.* [201] that the irradiation of suspensions containing isotopically different carboxylic acids results in the adsorption of  $\bullet\text{H}/\bullet\text{D}$  as well as  $\bullet\text{CH}_3/\bullet\text{CD}_3$  on to the surface of Pt acting as a co-catalyst. Due to the adsorptions of  $\bullet\text{H}/\bullet\text{D}$  and  $\bullet\text{CH}_3/\bullet\text{CD}_3$ , there appear surface methyl groups thus undergoing proton exchange according to Equation 58. It has also been reported by Khodakov and co-

## 4. Discussion

workers that the size of Pt nanoparticles plays a very important role in defining the rate of proton exchange reaction. The authors claimed that the large Pt particle size results in lower proton exchange reaction rate while small particle size of Pt leads to the higher reaction rates for proton exchange reaction [201]. The particle size of the Pt nanoparticles used in the present study was found in the range of 15 – 25 nm (Figure 9 – 10). Hence, a single proton exchange reaction at the surface of Pt nanoparticles is assumed to occur in this study.

Here, blank experiments in the absence of Pt co-catalyst and TiO<sub>2</sub> photocatalyst employing following reaction systems have also been performed and tested by NMR: (1) TiO<sub>2</sub>-CH<sub>3</sub>COOH-D<sub>2</sub>O, (2) TiO<sub>2</sub>-CD<sub>3</sub>COOD-H<sub>2</sub>O, (3) CH<sub>3</sub>COOH-D<sub>2</sub>O, and (4) CD<sub>3</sub>COOD-H<sub>2</sub>O. Data obtained from both QMS and NMR spectroscopic techniques (data not shown here) do not show any proton exchange for these systems. These results lead to the conclusion that the proton exchange is a photocatalytic reaction which occurs either at the surface of Pt or TiO<sub>2</sub> following the pathways of single exchange reaction occurring multiple times. Moreover, due to a rapid exchange between H and D of methyl group, carboxylic group as well as solvent molecules under illumination, the protons participating in the formation of methane are assumed to come from both solvent and organic acid. However due to a big difference between the concentration of solvent and organic molecules, the main source of <sup>•</sup>H, required for the formation of molecular hydrogen and methane is solvent.

### 5. Summary and conclusions

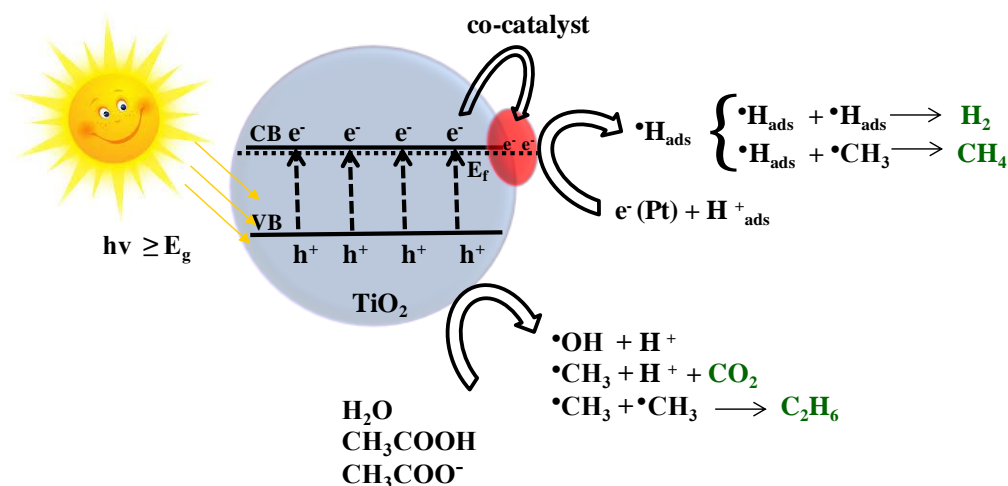
The pioneering work of Bard and co-workers published in 1980's demonstrated the photocatalytic decomposition of aqueous acetic acid into carbon dioxide ( $\text{CO}_2$ ), molecular hydrogen ( $\text{H}_2$ ) and hydrocarbons (*i.e.*,  $\text{CH}_4$ ,  $\text{C}_2\text{H}_6$ ) under anaerobic conditions employing both co-catalyst loaded  $\text{TiO}_2$  particles and  $\text{TiO}_2$  electrodes. However, controversies still exist in literature while discussing the reaction mechanism for the photocatalytic decomposition of aqueous acetic acid. A slight change in the reaction parameters leads to an entirely different product distribution, reaction rates and reaction pathways for the photo-induced degradation of aqueous acetic acid. The scientific question of the present thesis was to investigate the factors influencing the stoichiometry and reaction mechanism for the photocatalytic degradation of aqueous acetic acid in detail.

The photocatalytic experiments were performed in a photoreactor attached to a quadrupole mass spectrometer (QMS) which allows continuous detection of the evolved gaseous products. In general, it has been observed from most of the experimental runs performed in this work that the photo-induced transformation of aqueous acetic acid results in the formation of  $\text{CO}_2$ ,  $\text{H}_2$ , and  $\text{CH}_4$  as major reaction products, while traces of  $\text{C}_2\text{H}_6$  as minor reaction product were also detected. However, the formation rates and distribution of these major and minor reaction products were found to be greatly affected by the employed reaction conditions. Along with the major and minor reaction products (*i.e.*,  $\text{CO}_2$ ,  $\text{H}_2$ ,  $\text{CH}_4$ , and  $\text{C}_2\text{H}_6$ ), QMS also depicts the formation of many side-products (*e.g.*, alcohols, organic acids, and aldehydes) in the gas phase exiting the photoreactor. However, evolved amounts of these by-products was close to the detection limit of QMS, therefore, quantitative analysis for only major reaction products were carried out.

In order to check the influence of  $\text{TiO}_2$  surface modifications on the reaction rates and product distribution resulting from the photocatalytic conversion of aqueous acetic acid, experiments were performed with bare as well as various metals and metal oxides loaded  $\text{TiO}_2$  particles. Bare  $\text{TiO}_2$  exhibits an insignificant photocatalytic activity for all major and minor reaction products (*i.e.*,  $\text{CO}_2$ ,  $\text{H}_2$ ,  $\text{CH}_4$ , and  $\text{C}_2\text{H}_6$ ) formed during photocatalytic decomposition of aqueous acetic acid. On the other hand, the loading of noble metals such as Pt, Rh, Au, Ag, and metal-oxides such as  $\text{IrO}_2$  and  $\text{RuO}_2$  on the surface of  $\text{TiO}_2$  act as an efficient electron traps and significantly improves the photocatalytic activity for the light-induced decomposition of aqueous acetic acid

## 5. Summary and conclusions

into CO<sub>2</sub>, H<sub>2</sub>, CH<sub>4</sub>, and C<sub>2</sub>H<sub>6</sub> (Scheme 1). The choice of these particular metals or metal-oxides was made on the basis of their work function values. In order to obtain higher photocatalytic activity, it is necessary to use co-catalysts having work function values larger than the work function value of the photocatalyst. The comparison of the obtained results shows that TiO<sub>2</sub> loaded by different metals and metal oxides results in the formation of same reaction products (*i.e.*, CO<sub>2</sub>, H<sub>2</sub>, CH<sub>4</sub>, and C<sub>2</sub>H<sub>6</sub>) but entirely different formation rates and products distribution. The noble metal co-catalysts having higher work function values such as Pt, Rh, and Au observed to favour the reduction reaction (*i.e.*, formation of H<sub>2</sub>) more significantly as compared to Ag having a lower value of work function. The amounts of the evolved H<sub>2</sub> employing various metals loaded TiO<sub>2</sub> increase in the following order: Ag/TiO<sub>2</sub> < Au/TiO<sub>2</sub> < Rh/TiO<sub>2</sub> < Pt/TiO<sub>2</sub>. At the same time, the noble metal co-catalysts also act as to improve the separation of photogenerated charge carriers (e<sub>CB</sub><sup>-</sup> and h<sub>VB</sub><sup>+</sup>) thus enhancing the oxidation reaction (*i.e.*, formation of CO<sub>2</sub>, and CH<sub>4</sub>) in the same order. On the contrary, independent of the work function values, metal oxide co-catalysts such as IrO<sub>2</sub> and RuO<sub>2</sub> did not seem to be good candidates for H<sub>2</sub> evolution reaction but produced higher amounts of CO<sub>2</sub> and CH<sub>4</sub>. The formed amounts of CO<sub>2</sub> and CH<sub>4</sub> employing IrO<sub>2</sub>/TiO<sub>2</sub> were observed to be comparable with the amounts obtained by using Pt/TiO<sub>2</sub> as a photocatalyst.



**Scheme 1:** Schematic illustration for the photocatalytic decomposition of aqueous acetic acid over co-catalyst loaded TiO<sub>2</sub> particles.

## 5. Summary and conclusions

These observations suggest that the choice of a suitable co-catalyst which can carry out both oxidation and reduction reaction at the same time is very important. The idea behind this work was to choose an appropriate photocatalytic reaction system, which can be used to obtain significant amounts of future renewable energy fuels (i.e., H<sub>2</sub> and CH<sub>4</sub>). Here, the data analysis shows Pt/TiO<sub>2</sub> photocatalyst as the aspirant resulting in the formation of both oxidation and reduction products simultaneously with significant amounts. Thus, Pt/TiO<sub>2</sub> was employed as the photocatalyst to answer the further scientific questions of the present study.

Generally, in a photocatalytic reaction, the concentration of an organic electron donor is known to affect the reaction rates to a great extent. To study the effect of probe compound on the reaction rates and product distribution, experiments were performed employing various initial concentrations ( $c_0$ ) of acetic acid using Pt/TiO<sub>2</sub> as a photocatalyst at pH 2. Once again, the obtained results from all experiments resulted in the formation of CO<sub>2</sub>, H<sub>2</sub>, CH<sub>4</sub>, and C<sub>2</sub>H<sub>6</sub> as main reaction products. However, the product distribution was observed to vary greatly. An increase in the initial concentration from 0.005 M to 0.05 M was found to favour the formation of the H<sub>2</sub> as the principal reaction product while the formation of CH<sub>4</sub> was comparatively suppressed at these concentration values. Comparatively, a further increase in the initial concentration values between 0.05 M <  $c_0$  ≤ 5 M gives the reaction products rich in hydrocarbons (i.e., CH<sub>4</sub>). Moreover, an increase in the initial concentration of acetic acid from 0.005 M to 5 M (0.005 M ≤  $c_0$  ≤ 5 M) was found to show a decrease in the ratio  $\frac{n(\text{H}_2)}{n(\text{CO}_2)}$  and an increase in the ratio  $\frac{n(\text{CH}_4)}{n(\text{CO}_2)}$  while the ratio  $\frac{n(\text{C}_2\text{H}_6)}{n(\text{CH}_4)}$  was observed to be constant for all employed concentration values. An overall analysis of the obtained results determines that at 0.5 M concentration of acetic acid, both important energy fuels (i.e., H<sub>2</sub> and CH<sub>4</sub>) can be obtained in significant amounts. Therefore, the concentration of acetic acid was chosen to be 0.5 M for further analysis in this research.

The experiments for the photocatalytic decomposition of 0.5 M aqueous acetic acid employing Pt/TiO<sub>2</sub> as a photocatalyst were performed for 2 ≤ pH ≤ 11. The obtained results at pH < 7 exhibit that the initial step for the light-induced decomposition of aqueous acetic acid predominantly follows the photo-Kolbe reaction mechanism. According to the photo-Kolbe mechanism, under light illumination, a direct reaction between TiO<sub>2</sub> photo-generated h<sub>VB</sub><sup>+</sup> and CH<sub>3</sub>COOH adsorbed on the surface of TiO<sub>2</sub> results in the formation of •CH<sub>3</sub> as a reaction intermediate and CO<sub>2</sub> as reaction product. The formed •CH<sub>3</sub> then gives alkanes (Scheme 2) as the

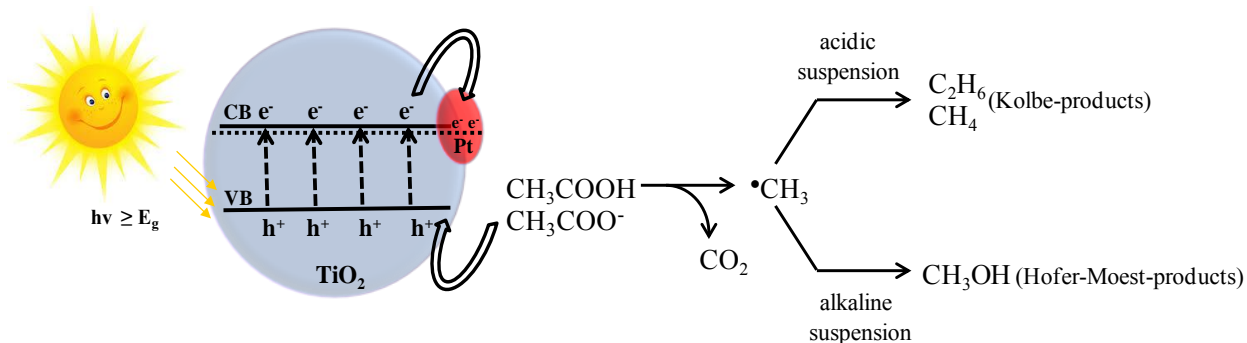
## 5. Summary and conclusions

reaction product. According to the stoichiometric calculations of  $\text{CH}_3\text{COOH}$ , it is expected that the photo-induced transformation of aqueous acetic acid should result in the following atomic ratios:  $\left(\frac{n(\text{C})}{n(\text{O})}=1, \frac{n(\text{H})}{n(\text{O})}=2, \text{ and } \frac{n(\text{H})}{n(\text{C})}=2\right)$ . However, the obtained atomic ratios of the reaction products at pH 2 are:  $\left(0.6 < \frac{n(\text{C})}{n(\text{O})} < 0.9, 1.0 < \frac{n(\text{H})}{n(\text{O})} < 2.0, \text{ and } 1.4 < \frac{n(\text{H})}{n(\text{C})} < 2.1\right)$ . These calculations clearly demonstrate that there exist other products instead of the main reaction products ( $\text{CO}_2$ ,  $\text{H}_2$ ,  $\text{CH}_4$ , and  $\text{C}_2\text{H}_6$ ). The qualitative analysis from QMS also confirms the formation of other organic probe molecules ( $\text{C}_x\text{H}_{2x+2}$ ,  $x \leq 3$ ) formed during the photocatalytic transformation of aqueous acetic acid. This means that besides the photo-Kolbe reaction mechanism, the photocatalytic decomposition of aqueous acetic acid simultaneously follows another reaction pathway which is called as Hofer-Moest reaction. According to the Hofer-Moest reaction pathway, the formation of alcohols, organic acids, and aldehydes is expected as the reaction products. The initial step for Hofer-Moest reaction also includes the direct oxidation of  $\text{CH}_3\text{COOH}$  into  $\bullet\text{CH}_3$  and  $\text{CO}_2$  by  $\text{TiO}_2 h_{\text{VB}}^+$ . Afterwards, the formed  $\bullet\text{CH}_3$  results in the formation of alcohols (Scheme 2).

The formation rates and the product distribution were observed to be strongly affected by change in initial pH values of the employed suspensions. For example, an increase in the pH value from 2 to 5 exhibits a slight decrease in the formed amounts of  $\text{H}_2$ , while  $\text{CH}_4$  and  $\text{CO}_2$  remained almost constant. A further increase in pH value between  $5 < \text{pH} \leq 9$ , depicts almost constant and significant amounts of  $\text{H}_2$  evolution while a rapid decrease in the formed amounts of  $\text{CO}_2$ ,  $\text{CH}_4$ , and  $\text{C}_2\text{H}_6$  was observed. At  $\text{pH} > 7$ ,  $\text{CO}_2$  cannot be detected in the gas phase due to its conversion into carbonate/bicarbonate ( $\text{CO}_3^{2-}$  and  $\text{HCO}_3^-$ ) which stays in the liquid phase in the suspension. However, the suppression of hydrocarbons at  $\text{pH} > 7$  clearly indicates that the photo-Kolbe reaction mechanism exists here as a minor reaction pathway. Also,  $\text{H}_2$  formation at  $\text{pH} > 7$  as the only reaction product evolved in significant amounts demonstrates that the reaction proceeds mainly by a Hofer-Moest mechanism. The formed Hofer-Moest reaction products such as alcohols and organic acids are further oxidized resulting in the formation of  $\text{H}_2$  and  $\text{CO}_2$  as the final reaction products. For  $\text{pH} > 7$ , insignificant amounts of evolved hydrocarbons depict that, under alkaline pH regime, Kolbe mechanism also exists as a minor reaction pathway. Further analysis shows that  $\text{pH} > 9$  results in a decreasing trend for  $\text{H}_2$  evolution. Studies confirmed that at  $\text{pH} \geq 10$ ,  $\text{TiO}_2$  particles exhibit surface agglomeration, hence, affecting the photocatalytic activity. This argument matches well with the obtained results of the present investigation. Thus,

## 5. Summary and conclusions

the pH 2 was found to be optimized value where both H<sub>2</sub> and CH<sub>4</sub> can be obtained with maximum observed formation rates.



**Scheme 2:** Schematic illustration for the Photo-Kolbe vs. Hofer-Moest reaction mechanisms.

Isotopic labelling experiments were performed by using isotopically different (1) solvents ( $\text{H}_2\text{O}/\text{D}_2\text{O}$ ) and (2) organic molecule ( $\text{CH}_3\text{COOH}$ ,  $\text{CD}_3\text{COOD}$ ,  $\text{CH}_3\text{COOD}$ ) employing Pt/ $\text{TiO}_2$  as a photocatalyst at  $\text{pH} = \text{pD} \approx 2$ . The detail of reaction systems is as follow: (i) Pt/ $\text{TiO}_2$ - $\text{CH}_3\text{COOH}$ - $\text{H}_2\text{O}$ , (ii) Pt/ $\text{TiO}_2$ - $\text{CD}_3\text{COOD}$ - $\text{H}_2\text{O}$ , (iii) Pt/ $\text{TiO}_2$ - $\text{CH}_3\text{COOD}$ - $\text{H}_2\text{O}$ , (iv) Pt/ $\text{TiO}_2$ - $\text{CD}_3\text{COOD}$ - $\text{D}_2\text{O}$ , (v) Pt/ $\text{TiO}_2$ - $\text{CH}_3\text{COOH}$ - $\text{D}_2\text{O}$ , and (vi) Pt/ $\text{TiO}_2$ - $\text{CH}_3\text{COOD}$ - $\text{D}_2\text{O}$ .

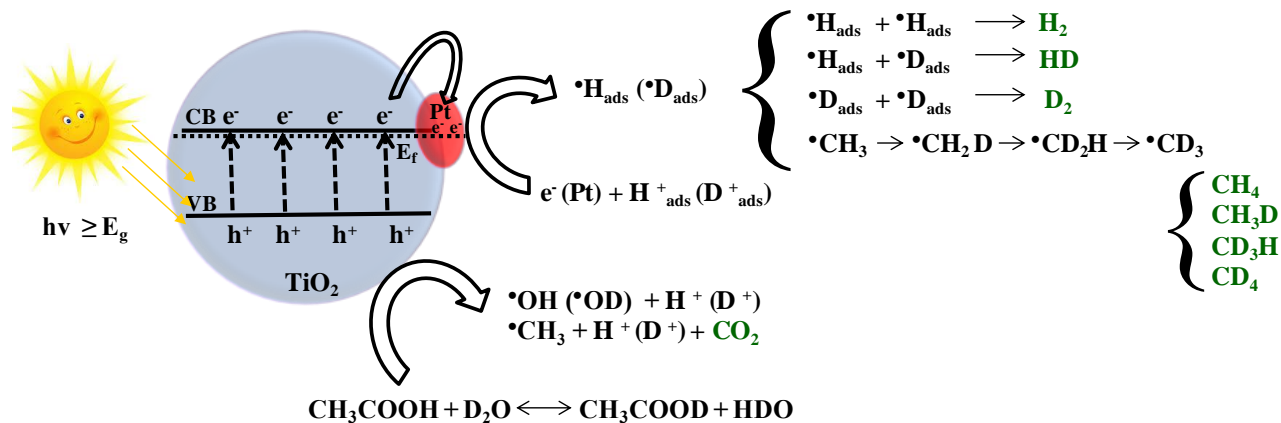
From all six reaction systems (i – vi), an obvious difference in the formed amounts of  $\text{CO}_2$  was observed. The reaction systems containing  $\text{D}_2\text{O}$  as a solvent (iv, v, and vi) exhibited higher reaction rates for  $\text{CO}_2$  formation in comparison to the reaction systems (i, ii, and iii) having  $\text{H}_2\text{O}$  as a solvent. However, independent from the employed solvent, the photo-decarboxylation rate of  $\text{CD}_3\text{COOD}$  was found to be faster than  $\text{CH}_3\text{COOH}$  and  $\text{CH}_3\text{COOD}$ . These results suggested that in acidic suspensions, the photocatalytic decomposition of aqueous acetic acid mainly proceed by a direct reaction between the  $\text{TiO}_2$  valence band hole ( $h_{\text{VB}}^+$ ) and acetic acid molecule yielding Kolbe-products. However, the occurrence of Hofer-Moest reaction as a minor pathway cannot be excluded.

The analyses of data for hydrogen evolution reaction from all reaction systems (i – vi) determines that the main source for molecular hydrogen evolution is the solvent. For example, the reaction systems (i, ii, and iii) containing  $\text{H}_2\text{O}$  as a solvent yield  $\text{H}_2$  as a major reaction product. On the other hand, the reaction systems (iv, v, and vi) having  $\text{D}_2\text{O}$  as a solvent yield  $\text{D}_2$  as the main reaction product. Considering a proton exchange reaction between the reaction systems being

## 5. Summary and conclusions

different in isotopic composition (ii, iii, v, and vi)), it was concluded that the protons participating in the formation of molecular hydrogen originates from both organic molecule and the solvent. However, due to a large excess of solvent molecules in comparison to organic molecule, the main source for molecular hydrogen formation was the solvent. Nevertheless, the participation of proton coming from organic acid in the formation of molecular hydrogen cannot be neglected.

The results obtained by quadrupole mass spectrometer (QMS) depict the formation of four types of methane being different in isotopic composition (*i.e.*, CH<sub>4</sub>, CH<sub>3</sub>D, CD<sub>3</sub>H, and CD<sub>4</sub>). A proton exchange was found at both the methyl group and the carboxylic group of acetic acid. The observed proton exchange mainly at the methyl group of acetic acid was further confirmed *via* nuclear magnetic resonance (NMR) spectroscopy. It was revealed by <sup>1</sup>H NMR that during a photocatalytic reaction for systems (ii) Pt/TiO<sub>2</sub>-CD<sub>3</sub>COOD-H<sub>2</sub>O and (v) Pt/TiO<sub>2</sub>-CH<sub>3</sub>COOH-D<sub>2</sub>O, the transformations exist as follow: CD<sub>3</sub>COOD → CHD<sub>2</sub>HCOOH(D) and CH<sub>3</sub>COOH → CDH<sub>2</sub>HCOOH(D), respectively. A schematic illustration for proton exchange reaction is given in Scheme 3.



**Scheme 3:** Schematic illustration for the proton exchange reaction during photocatalytic decomposition of aqueous acetic acid over Pt/TiO<sub>2</sub> particles.



## 5. Summary and conclusions

Blank experiments such as: (1) before illumination (ii) Pt/TiO<sub>2</sub>-CD<sub>3</sub>COOD-H<sub>2</sub>O, and (v) Pt/TiO<sub>2</sub>-CH<sub>3</sub>COOH-D<sub>2</sub>O, and (2) after illumination (vii) TiO<sub>2</sub>-CD<sub>3</sub>COOD-H<sub>2</sub>O, and (viii) TiO<sub>2</sub>-CH<sub>3</sub>COOH-D<sub>2</sub>O, were also performed and tested by NMR spectroscopy. Blank experiments confirmed that the proton exchange between the solvent and reactant is a photo-induced reaction which occurs mainly at the surface of Pt co-catalyst. Due to the proton exchange reaction at both methyl and carboxylic group of acetic acid, once again it is concluded that the protons participating in the formation of methane originates from both reactant acid and the solvent.

Hence, the obtained experimental results within this thesis suggest that, with a suitable combination of co-catalyst loaded photocatalyst, the photocatalytic degradation of industrial waste can be efficiently obtained either in the favour of a mixture of gasses rich in hydrocarbons and poor in molecular hydrogen or vice versa. This terminology would be greatly helpful to fulfil the requirements of natural gases.

## 6. References

### 6. References

- [1] S. N. Habisreutinger, L. S. Mende, J. K. Stolarczyk, Photocatalytic reduction of CO<sub>2</sub> on TiO<sub>2</sub> and other semiconductors, *Angewandte Chemie, International Edition*, 52 (2013) 7372-7408.
- [2] J. P. Dorian, H. T. Franssen, D. R. Simbeck, Global challenges in energy, *Energy Policy*, 34 (2006) 1984-1991.
- [3] F. Ahmed, M. Naeem, M. Iqbal, ICT and renewable energy: a way forward to the next generation telecom base stations, *Telecommunication Systems*, 64 (2017) 43-56.
- [4] A. Eibner, Über Lichtwirkungen auf Malerfarbstoffe, in, *Verlag der Chemiker-Zeitung*, 1911.
- [5] M. Landau, Le phénomène de la photocatalyse, *Compt. Rend.*, 156 (1913) 1894-1896.
- [6] E. Keidel, The fading of aniline dyes in the presence of titanium white, *Farben-Zeitung*, 34 (1929) 1242-1243.
- [7] A. Terenin, The desorption of adsorbed gases from metals and semiconductors, and their adsorption under the influence of light, *Problems in Kinetics and Katalysis*, 8 (1955) 17-33.
- [8] A. Fujishima, K. Honda, Photolysis-decomposition of water at the surface of an irradiated semiconductor, *Nature*, 238 (1972) 37-38.
- [9] C. Thomas, Fuel cell and battery electric vehicles compared, *International Journal of Hydrogen Energy*, 34 (2009) 6005-6020.
- [10] M. Balat, Potential importance of hydrogen as a future solution to environmental and transportation problems, *International Journal of Hydrogen Energy*, 33 (2008) 4013-4029.
- [11] J. Barber, P.D. Tran, From natural to artificial photosynthesis, *Journal of Royal Society Interface*, 10 (2013) 20120984.
- [12] M. Matsuoka, M. Kitano, M. Takeuchi, K. Tsujimaru, M. Anpo, J. M. Thomas, Photocatalysis for new energy production: recent advances in photocatalytic water splitting reactions for hydrogen production, *Catalysis Today*, 122 (2007) 51-61.
- [13] X. Chen, S. Shen, L. Guo, S. S. Mao, Semiconductor-based photocatalytic hydrogen generation, *Chemical Reviews*, 110 (2010) 6503-6570.
- [14] J. Schneider, M. Matsuoka, M. Takeuchi, J. Zhang, Y. Horiuchi, M. Anpo, D. W. Bahnemann, Understanding TiO<sub>2</sub> photocatalysis: mechanisms and materials, *Chemical Reviews*, 114 (2014) 9919-9986.
- [15] A. J. Bard, Photoelectrochemistry and heterogeneous photo-catalysis at semiconductors, *Journal of Photochemistry*, 10 (1979) 59-75.
- [16] A. J. Bard, Photoelectrochemistry, *Science*, 207 (1980) 139-144.
- [17] A. J. Bard, Design of semiconductor photoelectrochemical systems for solar energy conversion, *Journal of Physical Chemistry*, 86 (1982) 172-177.
- [18] A. Mills, G. Porter, Photosensitized dissociation of water using dispersed suspensions of n-type semiconductors, *Journal of Chemical Society Faraday Transactions. 1: Physical Chemistry in Condensed Phases*, 78 (1982) 3659-3669.
- [19] A. J. Bard, M. A. Fox, Artificial photosynthesis: solar splitting of water to hydrogen and oxygen, *Accounts of Chemical Research*, 28 (1995) 141-145.
- [20] J. Lehn, J. Sauvage, R. Ziessel, Photochemical water splitting continuous generation of hydrogen and oxygen by irradiation of aqueous suspensions of metal loaded strontium-titanate, in, *Nouveau Journal de Chimie*, 4 (1980) 623-627.
- [21] M. R. Hoffmann, S. T. Martin, W. Choi, D. W. Bahnemann, Environmental applications of semiconductor photocatalysis, *Chemical Reviews*, 95 (1995) 69-96.
- [22] A. Fujishima, X. Zhang, D. A. Tryk, TiO<sub>2</sub> photocatalysis and related surface phenomena, *Surface Science Reports*, 63 (2008) 515-582.

## 6. References

- [23] O. Alfano, D. Bahnemann, A. Cassano, R. Dillert, R. Goslich, Photocatalysis in water environments using artificial and solar light, *Catalysis Today*, 58 (2000) 199-230.
- [24] R. J. Braham, A. T. Harris, Review of major design and scale-up considerations for solar photocatalytic reactors, *Industrial & Engineering Chemistry Research*, 48 (2009) 8890-8905.
- [25] A. G. Mata, S. V. Martínez, A. Á. Gallegos, M. Ahmadi, J. A. H. Pérez, F. Ghanbari, S. S. Martínez, Recent Overview of Solar Photocatalysis and Solar Photo-Fenton Processes for Wastewater Treatment, *International Journal of Photoenergy*, 2017 (2017).
- [26] R. Navarro, M. S. Sanchez, M. A. Galvan, F. D. Valle, J. Fierro, Hydrogen production from renewable sources: biomass and photocatalytic opportunities, *Energy & Environmental Science*, 2 (2009) 35-54.
- [27] G. Colón, Towards the hydrogen production by photocatalysis, *Applied Catalysis A: General*, 518 (2016) 48-59.
- [28] M. Yasuda, T. Matsumoto, T. Yamashita, Sacrificial hydrogen production over TiO<sub>2</sub>-based photocatalysts: Polyols, carboxylic acids, and saccharides, *Renewable and Sustainable Energy Reviews*, (2017).
- [29] S. Naskar, F. Lübke, S. Hamid, A. Freytag, A. Wolf, J. Koch, I. Ivanova, H. Pfnür, D. Dorfs, D. W. Bahnemann, Synthesis of Ternary and Quaternary Au and Pt Decorated CdSe/CdS Heteronanoplatelets with Controllable Morphology, *Advanced Functional Materials*, 27 (2017).
- [30] A. Nada, M. Barakat, H. Hamed, N. Mohamed, T. Veziroglu, Studies on the photocatalytic hydrogen production using suspended modified TiO<sub>2</sub> photocatalysts, *International Journal of Hydrogen Energy*, 30 (2005) 687-691.
- [31] R. M. Navarro, M. Pena, J. Fierro, Hydrogen production reactions from carbon feedstocks: fossil fuels and biomass, *Chemical Reviews*, 107 (2007) 3952-3991.
- [32] H. Kisch, Semiconductor Photocatalysis Mechanistic and Synthetic Aspects, *Angewandte Chemie-International Edition*, 52 (2013) 812-847.
- [33] T. A. Kandiel, R. Dillert, A. Feldhoff, D. W. Bahnemann, Direct synthesis of photocatalytically active rutile TiO<sub>2</sub> nanorods partly decorated with anatase nanoparticles, *The Journal of Physical Chemistry C*, 114 (2010) 4909-4915.
- [34] T. A. Kandiel, R. Dillert, L. Robben, D. W. Bahnemann, Photonic efficiency and mechanism of photocatalytic molecular hydrogen production over platinumized titanium dioxide from aqueous methanol solutions, *Catalysis Today*, 161 (2011) 196-201.
- [35] S. Mozia, A. Heciak, A. W. Morawski, Photocatalytic acetic acid decomposition leading to the production of hydrocarbons and hydrogen on Fe-modified TiO<sub>2</sub>, *Catalysis today*, 161 (2011) 189-195.
- [36] B. Kraeutler, A. J. Bard, Heterogeneous photocatalytic synthesis of methane from acetic acid-new Kolbe reaction pathway, *Journal of the American Chemical Society*, 100 (1978) 2239-2240.
- [37] T. Sakata, T. Kawai, K. Hashimoto, Heterogeneous photocatalytic reactions of organic acids and water. New reaction paths besides the photo-Kolbe reaction, *The Journal of Physical Chemistry*, 88 (1984) 2344-2350.
- [38] G. L. Chiarello, E. Selli, Photocatalytic hydrogen production, *Recent Patents on Engineering*, 4 (2010) 155-169.
- [39] A. Kudo, Y. Miseki, Heterogeneous photocatalyst materials for water splitting, *Chemical Society Reviews*, 38 (2009) 253-278.
- [40] A. L. Linsebigler, G. Lu, J. T. Yates Jr, Photocatalysis on TiO<sub>2</sub> surfaces: principles, mechanisms, and selected results, *Chemical Reviews*, 95 (1995) 735-758.

## 6. References

- [41] K. Hashimoto, H. Irie, A. Fujishima, TiO<sub>2</sub> photocatalysis: a historical overview and future prospects, *Japanese Journal of Applied Physics*, 44 (2005) 8269.
- [42] A. Fujishima, X. Zhang, Titanium dioxide photocatalysis: present situation and future approaches, *Comptes Rendus Chimie*, 9 (2006) 750-760.
- [43] T. A. Kandel, I. Ivanova, D. W. Bahnemann, Long-term investigation of the photocatalytic hydrogen production on platinized TiO<sub>2</sub>: an isotopic study, *Energy & Environmental Science*, 7 (2014) 1420-1425.
- [44] R. Asahi, T. Morikawa, T. Ohwaki, K. Aoki, Y. Taga, Visible-light photocatalysis in nitrogen-doped titanium oxides, *science*, 293 (2001) 269-271.
- [45] V. Subramanian, E. E. Wolf, P. V. Kamat, Catalysis with TiO<sub>2</sub>/gold nanocomposites. Effect of metal particle size on the Fermi level equilibration, *Journal of the American Chemical Society*, 126 (2004) 4943-4950.
- [46] A. Takai, P. V. Kamat, Capture, store, and discharge. Shuttling photogenerated electrons across TiO<sub>2</sub> silver interface, *Acs Nano*, 5 (2011) 7369-7376.
- [47] M. d. O. Melo, L. A. Silva, Photocatalytic production of hydrogen: an innovative use for biomass derivatives, *Journal of the Brazilian Chemical Society*, 22 (2011) 1399-1406.
- [48] J. Ran, J. Zhang, J. Yu, M. Jaroniec, S. Z. Qiao, Earth-abundant cocatalysts for semiconductor-based photocatalytic water splitting, *Chemical Society Reviews*, 43 (2014) 7787-7812.
- [49] M. Woodhouse, B. Parkinson, Combinatorial approaches for the identification and optimization of oxide semiconductors for efficient solar photoelectrolysis, *Chemical Society Reviews*, 38 (2009) 197-210.
- [50] S. Hwang, M. C. Lee, W. Choi, Highly enhanced photocatalytic oxidation of CO on titania deposited with Pt nanoparticles: kinetics and mechanism, *Applied Catalysis B: Environmental*, 46 (2003) 49-63.
- [51] D. Hufschmidt, D. Bahnemann, J. J. Testa, C. A. Emilio, M. I. Litter, Enhancement of the photocatalytic activity of various TiO<sub>2</sub> materials by platinisation, *Journal of Photochemistry and Photobiology A: Chemistry*, 148 (2002) 223-231.
- [52] R. Tung, Schottky-barrier formation at single-crystal metal-semiconductor interfaces, *Physical Review letters*, 52 (1984) 461.
- [53] K. Maeda, K. Domen, Surface Nanostructures in Photocatalysts for Visible-Light-Driven Water Splitting, in: C. A. Bignozzi (Ed.) *Photocatalysis*, 2011, pp. 95-119.
- [54] S. Liu, C. Han, Z. R. Tang, Y. J. Xu, Heterostructured semiconductor nanowire arrays for artificial photosynthesis, *Materials Horizons*, 3 (2016) 270-282.
- [55] M.I. Litter, Heterogeneous photocatalysis: Transition metal ions in photocatalytic systems, *Applied Catalysis B: Environmental*, 23 (1999) 89-114.
- [56] G. L. Chiarello, M. H. Aguirre, E. Selli, Hydrogen production by photocatalytic steam reforming of methanol on noble metal-modified TiO<sub>2</sub>, *Journal of Catalysis*, 273 (2010) 182-190.
- [57] D. Eastman, Photoelectric work functions of transition, rare-earth, and noble metals, *Physical Review B*, 2 (1970) 1.
- [58] M. Anpo, M. Takeuchi, The design and development of highly reactive titanium oxide photocatalysts operating under visible light irradiation, *Journal of Catalysis*, 216 (2003) 505-516.
- [59] M. Hara, J. Nunoshige, T. Takata, J. N. Kondo, K. Domen, Unusual enhancement of H<sub>2</sub> evolution by Ru on TaON photocatalyst under visible light irradiation, *Chemical Communications*, 0 (2003) 3000-3001.

## 6. References

- [60] J. Kennedy, W. Jones, D. J. Morgan, M. Bowker, L. Lu, C. J. Kiely, P. P. Wells, N. Dimitratos, Photocatalytic hydrogen production by reforming of methanol using Au/TiO<sub>2</sub>, Ag/TiO<sub>2</sub> and Au-Ag/TiO<sub>2</sub> catalysts, *Catalysis, Structure & Reactivity*, 1 (2015) 35-43.
- [61] W. T. Chen, A. Chan, D. S. Waterhouse, T. Moriga, H. Idriss, G. I. Waterhouse, Ni/TiO<sub>2</sub>: a promising low-cost photocatalytic system for solar H<sub>2</sub> production from ethanol–water mixtures, *Journal of Catalysis*, 326 (2015) 43-53.
- [62] A. V. Korzhak, N. I. Ermokhina, A. L. Stroyuk, V. K. Bukhtiyarov, A. E. Raevskaya, V. I. Litvin, S. Y. Kuchmiy, V. G. Ilyin, P. A. Manorik, Photocatalytic hydrogen evolution over mesoporous TiO<sub>2</sub>/metal nanocomposites, *Journal of Photochemistry and Photobiology A: Chemistry*, 198 (2008) 126-134.
- [63] K. Yamaguti, S. Sato, Photolysis of water over metallized powdered titanium dioxide, *Journal of the Chemical Society, Faraday Transactions 1: Physical Chemistry in Condensed Phases*, 81 (1985) 1237-1246.
- [64] K. C. Christoforidis, P. Fornasiero, Photocatalytic hydrogen production: A rift into the future energy supply, *ChemCatChem*, 9 (2017) 1523-1544.
- [65] D.Y. Leung, X. Fu, C. Wang, M. Ni, M. K. Leung, X. Wang, X. Fu, Hydrogen Production over Titania-Based Photocatalysts, *ChemSusChem*, 3 (2010) 681-694.
- [66] S. G. Kumar, L. G. Devi, Review on modified TiO<sub>2</sub> photocatalysis under UV/visible light: selected results and related mechanisms on interfacial charge carrier transfer dynamics, *The Journal of Physical Chemistry A*, 115 (2011) 13211-13241.
- [67] J. Yang, D. Wang, H. Han, C. Li, Roles of cocatalysts in photocatalysis and photoelectrocatalysis, *Accounts of Chemical Research*, 46 (2013) 1900-1909.
- [68] W. J. Foo, C. Zhang, G. W. Ho, Non-noble metal Cu-loaded TiO<sub>2</sub> for enhanced photocatalytic H<sub>2</sub> production, *Nanoscale*, 5 (2013) 759-764.
- [69] G. D. Moon, J. B. Joo, I. Lee, Y. Yin, Decoration of size-tunable CuO nanodots on TiO<sub>2</sub> nanocrystals for noble metal-free photocatalytic H<sub>2</sub> production, *Nanoscale*, 6 (2014) 12002-12008.
- [70] S. D. Gupta, P. K. Jha, Vibrational and elastic properties as a pointer to stishovite to CaCl<sub>2</sub> ferroelastic phase transition in RuO<sub>2</sub>, *Earth and Planetary Science Letters*, 401 (2014) 31-39.
- [71] M. T. Uddin, O. Babot, L. Thomas, C. I. Olivier, M. Redaelli, M. D. Arienzo, F. Morazzoni, W. Jaegermann, N. Rockstroh, H. Junge, New insights into the photocatalytic properties of RuO<sub>2</sub>/TiO<sub>2</sub> mesoporous heterostructures for hydrogen production and organic pollutant photodecomposition, *The Journal of Physical Chemistry C*, 119 (2015) 7006-7015.
- [72] A. Kudo, H. Kato, Effect of lanthanide-doping into NaTaO<sub>3</sub> photocatalysts for efficient water splitting, *Chemical Physics Letters*, 331 (2000) 373-377.
- [73] A. Iwase, H. Kato, A. Kudo, A novel photodeposition method in the presence of nitrate ions for loading of an iridium oxide cocatalyst for water splitting, *Chemistry Letters*, 34 (2005) 946-947.
- [74] K. Maeda, T. Takata, M. Hara, N. Saito, Y. Inoue, H. Kobayashi, K. Domen, GaN : ZnO solid solution as a photocatalyst for visible-light-driven overall water splitting, *Journal of the American Chemical Society*, 127 (2005) 8286-8287.
- [75] K. Maeda, K. Teramura, D. L. Lu, N. Saito, Y. Inoue, K. Domen, Noble-metal/Cr<sub>2</sub>O<sub>3</sub> core/shell nanoparticles as a cocatalyst for photocatalytic overall water splitting, *Angewandte Chemie-International Edition*, 45 (2006) 7806-7809.
- [76] M. Khan, M. A. Oufi, A. Tossef, Y. A. Salik, H. Idriss, On the role of CoO in CoO<sub>x</sub>/TiO<sub>2</sub> for the photocatalytic hydrogen production from water in the presence of glycerol, *Catalysis, Structure & Reactivity*, 1 (2015) 192-200.

## 6. References

- [77] A. V. Puga, Photocatalytic production of hydrogen from biomass-derived feedstocks, *Coordination Chemistry Reviews*, 315 (2016) 1-66.
- [78] J. Koskikallio, Alcoholysis, acidolysis and redistribution of esters, *Carboxylic Acids and Esters* (1969), (1969) 103-136.
- [79] D. Bahnemann, Mechanisms of organic transformations on semiconductor particles, in: *Photochemical conversion and storage of solar energy*, Springer, 1991, pp. 251-276.
- [80] K. Wolff, Mechanistische Untersuchungen zum Oxidationsprozess an der belichteten Titandioxid/Wasser-Grenzfläche, in, 1993.
- [81] H. Belhadj, S. Melchers, P. K. Robertson, D. W. Bahnemann, Pathways of the photocatalytic reaction of acetate in H<sub>2</sub>O and D<sub>2</sub>O: A combined EPR and ATR-FTIR study, *Journal of Catalysis*, 344 (2016) 831-840.
- [82] B. Kraeutler, A. J. Bard, Heterogeneous photocatalytic preparation of supported catalysts. Photodeposition of platinum on titanium dioxide powder and other substrates, *Journal of the American Chemical Society*, 100 (1978) 4317-4318.
- [83] S. Hamid, I. Ivanova, T. H. Jeon, R. Dillert, W. Choi, D. W. Bahnemann, Photocatalytic conversion of acetate into molecular hydrogen and hydrocarbons over Pt/TiO<sub>2</sub>: pH dependent formation of Kolbe and Hofer-Moest products, *Journal of Catalysis*, 349 (2017) 128-135.
- [84] B. Kraeutler, C. D. Jaeger, A. J. Bard, Direct observation of radical intermediates in the photo-Kolbe reaction-heterogeneous photocatalytic radical formation by electron spin resonance, *Journal of the American Chemical Society*, 100 (1978) 4903-4905.
- [85] H. Kolbe, Untersuchungen über die Elektrolyse organischer Verbindungen, *European Journal of Organic Chemistry*, 69 (1849) 257-294.
- [86] B. Giese, Radicals in organic synthesis: formation of carbon-carbon bonds, Pergamon Pr, 1986.
- [87] B. Kraeutler, A. J. Bard, Photoelectrosynthesis of ethane from acetate ion at an n-type titanium dioxide electrode. The photo-Kolbe reaction, *Journal of the American Chemical Society*, 99 (1977) 7729-7731.
- [88] B. Kraeutler, A. J. Bard, The Photoassisted Decarboxylation of Acetate on n-Type Rutile Electrodes. The Photo-Kolbe Reaction, *Nouveau Journal de Chimie*, 3 (1979) 31.
- [89] S. Sato, Photo-Kolbe reaction at gas-solid interfaces, *The Journal of Physical Chemistry*, 87 (1983) 3531-3537.
- [90] H. Yoneyama, Y. Takao, H. Tamura, A. J. Bard, Factors influencing product distribution in photocatalytic decomposition of aqueous acetic acid on platinized titania, *The Journal of Physical Chemistry*, 87 (1983) 1417-1422.
- [91] S. Mozia, Generation of Useful Hydrocarbons and Hydrogen during Photocatalytic Decomposition of Acetic Acid on CuO/Rutile Photocatalysts, *International Journal of Photoenergy*, 2009 (2009) 8.
- [92] S. Mozia, A. Heciak, A. W. Morawski, The influence of physico-chemical properties of TiO<sub>2</sub> on photocatalytic generation of C<sub>1</sub>-C<sub>3</sub> hydrocarbons and hydrogen from aqueous solution of acetic acid, *Applied Catalysis B: Environmental*, 104 (2011) 21-29.
- [93] S. Mozia, A. Heciak, D. Darowna, A.W. Morawski, A novel suspended/supported photoreactor design for photocatalytic decomposition of acetic acid with simultaneous production of useful hydrocarbons, *Journal of Photochemistry and Photobiology A: Chemistry*, 236 (2012) 48-53.
- [94] S. Mozia, A. Kułagowska, A. W. Morawski, Formation of Combustible Hydrocarbons and H<sub>2</sub> during Photocatalytic Decomposition of Various Organic Compounds under Aerated and Deaerated Conditions, *Molecules*, 19 (2014) 19633-19647.

## 6. References

- [95] H. Bahruji, M. Bowker, P. R. Davies, F. Pedrono, New insights into the mechanism of photocatalytic reforming on Pd/TiO<sub>2</sub>, *Applied Catalysis B: Environmental*, 107 (2011) 205-209.
- [96] G. Atherton, M. Fleischmann, F. Goodridge, Kinetic study of the Hofer-Moest reaction, *Transactions of the Faraday Society*, 63 (1967) 1468-1477.
- [97] H. Hofer, M. Moest, Ueber die Bildung von Alkoholen bei der Elektrolyse fettsaurer Salze, *European Journal of Organic Chemistry*, 323 (1902) 284-323.
- [98] L.A. Huck, P. Wan, Photochemical deuterium exchange of the m-methyl group of 3-methylbenzophenone and 3-methylacetophenone in acidic D<sub>2</sub>O, *Organic letters*, 6 (2004) 1797-1799.
- [99] A. Mirich, T. H. Miller, E. Klotz, B. Mattson, Heterogeneous catalysis: deuterium exchange reactions of hydrogen and methane, *Journal of Chemical Education*, 92 (2015) 2087-2093.
- [100] X. J. Zheng, L. F. Wei, Z. H. Zhang, Q. J. Jiang, Y. J. Wei, B. Xie, M. B. Wei, Research on photocatalytic H<sub>2</sub> production from acetic acid solution by Pt/TiO<sub>2</sub> nanoparticles under UV irradiation, *International Journal of Hydrogen Energy*, 34 (2009) 9033-9041.
- [101] J. Arana, O. G. Diaz, J. D. Rodriguez, J. H. Melián, C. G. i Cabo, J. P. Peña, M. C. Hidalgo, J. A. N. Santos, Role of Fe<sup>3+</sup>/Fe<sup>2+</sup> as TiO<sub>2</sub> dopant ions in photocatalytic degradation of carboxylic acids, *Journal of Molecular Catalysis A: Chemical*, 197 (2003) 157-171.
- [102] K. Maeda, K. Domen, New non-oxide photocatalysts designed for overall water splitting under visible light, *The Journal of Physical Chemistry C*, 111 (2007) 7851-7861.
- [103] K. Maeda, K. Domen, Photocatalytic Water Splitting: Recent Progress and Future Challenges, *Journal of Physical Chemistry Letters*, 1 (2010) 2655-2661.
- [104] I. Ivanova, T. A. Kandiel, Y. J. Cho, W. Choi, D. Bahnemann, Mechanisms of Photocatalytic Molecular Hydrogen and Molecular Oxygen Evolution over La-Doped NaTaO<sub>3</sub> Particles: Effect of Different Cocatalysts and Their Specific Activity, *ACS Catalysis*, (2018) 2313-2325.
- [105] H. Kato, K. Asakura, A. Kudo, Highly efficient water splitting into H<sub>2</sub> and O<sub>2</sub> over lanthanum-doped NaTaO<sub>3</sub> photocatalysts with high crystallinity and surface nanostructure, *Journal of the American Chemical Society*, 125 (2003) 3082-3089.
- [106] S. Brunauer, P. H. Emmett, E. Teller, Adsorption of gases in multimolecular layers, *Journal of the American chemical society*, 60 (1938) 309-319.
- [107] G. Kortüm, W. Braun, G. Herzog, Prinzip und Meßmethodik der diffusen Reflexionsspektroskopie, *Angewandte Chemie*, 75 (1963) 653-661.
- [108] G. C. Netto, T. Sauer, H. J. Jose, R. D. F. P. M. Moreira, E. Humeres, Evaluation of relative photonic efficiency in heterogeneous photocatalytic reactors, *Journal of the Air & Waste Management Association*, 54 (2004) 77-82.
- [109] J. Zosel, W. Oelßner, M. Decker, G. Gerlach, U. Guth, The measurement of dissolved and gaseous carbon dioxide concentration, *Measurement Science and Technology*, 22 (2011) 072001.
- [110] E. L. Purlee, On the solvent isotope effect of deuterium in aqueous acid solutions, *Journal of the American Chemical Society*, 81 (1959) 263-272.
- [111] K. Clusius, W. Schanzer, Zur Elektrolyse deuteriumhaltiger Fettsäuren. V. Der Mechanismus der Methanbildung bei der Elektrolyse der Essigsäure, *Zeitschrift für Physikalische Chemie*, 192 (1942) 273-291.
- [112] S. Mozia, A. Heciak, A. W. Morawski, The influence of physico-chemical properties of TiO<sub>2</sub> on photocatalytic generation of C 1–C 3 hydrocarbons and hydrogen from aqueous solution of acetic acid, *Applied Catalysis B: Environmental*, 104 (2011) 21-29.
- [113] A. Patsoura, D. I. Kondarides, X. E. Verykios, Photocatalytic degradation of organic pollutants with simultaneous production of hydrogen, *Catalysis Today*, 124 (2007) 94-102.

## 6. References

- [114] H. L. Tan, R. Amal, Y. H. Ng, Alternative strategies in improving the photocatalytic and photoelectrochemical activities of visible light-driven BiVO<sub>4</sub>: a review, *Journal of Materials Chemistry A*, 5 (2017) 16498-16521.
- [115] L. Ebersson, Studies on the Kolbe Electrolytic Synthesis, *Acta Chemica Scandinavica*, 17 (1963) 2004-2018.
- [116] M. Kim, A. Razzaq, Y. K. Kim, S. Kim, S. I. In, Synthesis and characterization of platinum modified TiO<sub>2</sub>-embedded carbon nanofibers for solar hydrogen generation, *RSC Advances*, 4 (2014) 51286-51293.
- [117] J. Yang, D. Wang, H. Han, C. Li, Roles of cocatalysts in photocatalysis and photoelectrocatalysis, *Accounts of chemical research*, 46 (2013) 1900-1909.
- [118] M. A. Henderson, A surface science perspective on TiO<sub>2</sub> photocatalysis, *Surface Science Reports*, 66 (2011) 185-297.
- [119] Z. Zhang, J. T. Yates Jr, Band bending in semiconductors: chemical and physical consequences at surfaces and interfaces, *Chemical Reviews*, 112 (2012) 5520-5551.
- [120] T. D. N. Phan, A. E. Baber, J. A. Rodriguez, S. D. Senanayake, Au and Pt nanoparticle supported catalysts tailored for H<sub>2</sub> production: From models to powder catalysts, *Applied Catalysis A: General*, 518 (2016) 18-47.
- [121] J. Riga, C. T. Noel, J. Pireaux, R. Caudano, J. Verbist, Y. Gobillon, Electronic structure of rutile oxides TiO<sub>2</sub>, RuO<sub>2</sub> and IrO<sub>2</sub> studied by X-ray photoelectron spectroscopy, *Physica Scripta*, 16 (1977) 351.
- [122] T. Ishikawa, Y. Abe, M. Kawamura, K. Sasaki, Formation process and electrical property of IrO<sub>2</sub> thin films prepared by reactive sputtering, *Japanese journal of applied physics*, 42 (2003) 213.
- [123] D. Galizzioli, F. Tantardini, S. Trasatti, Ruthenium dioxide: a new electrode material. II. Non-stoichiometry and energetics of electrode reactions in acid solutions, *Journal of Applied Electrochemistry*, 5 (1975) 203-214.
- [124] E. Kötz, S. Stucki, Ruthenium dioxide as a hydrogen evolving cathode, *Journal of applied electrochemistry*, 17 (1987) 1190-1197.
- [125] L. Chen, D. Guay, A. Lasia, Kinetics of the Hydrogen Evolution Reaction on RuO<sub>2</sub> and IrO<sub>2</sub> Oxide Electrodes in H<sub>2</sub>SO<sub>4</sub> Solution: An AC Impedance Study, *Journal of The Electrochemical Society*, 143 (1996) 3576-3584.
- [126] L. D. Burke, N. S. Naser, B. M. Ahern, Use of iridium oxide films as hydrogen gas evolution cathodes in aqueous media, *Journal of Solid State Electrochemistry*, 11 (2007) 655-666.
- [127] M. Yuan, Y. Zhu, L. Deng, R. Ming, A. Zhang, W. Li, B. Chai, Z. Ren, IrO<sub>2</sub>-TiO<sub>2</sub> electrocatalysts for the hydrogen evolution reaction in acidic water electrolysis without activation, *New Journal of Chemistry*, 41 (2017) 6152-6159.
- [128] R. Kötz, S. Stucki, Stabilization of RuO<sub>2</sub> by IrO<sub>2</sub> for anodic oxygen evolution in acid media, *Electrochimica acta*, 31 (1986) 1311-1316.
- [129] P. Amama, K. Itoh, M. Murabayashi, Effect of RuO<sub>2</sub> deposition on the activity of TiO<sub>2</sub>: Photocatalytic oxidation of trichloroethylene in aqueous phase, *Journal of materials science*, 39 (2004) 4349-4351.
- [130] A. A. Ismail, L. Robben, D. W. Bahnemann, Study of the Efficiency of UV and Visible-Light Photocatalytic Oxidation of Methanol on Mesoporous RuO<sub>2</sub>-TiO<sub>2</sub> Nanocomposites, *ChemPhysChem*, 12 (2011) 982-991.



## 6. References

- [131] Q. Jiang, L. Li, J. Bi, S. Liang, M. Liu, Design and synthesis of TiO<sub>2</sub> hollow spheres with spatially separated dual cocatalysts for efficient photocatalytic hydrogen production, *Nanomaterials*, 7 (2017) 24.
- [132] X. Fu, J. Long, X. Wang, D. Y. Leung, Z. Ding, L. Wu, Z. Zhang, Z. Li, X. Fu, Photocatalytic reforming of biomass: a systematic study of hydrogen evolution from glucose solution, *International Journal of Hydrogen Energy*, 33 (2008) 6484-6491.
- [133] Y. Nosaka, K. Norimatsu, H. Miyama, The function of metals in metal compounded semiconductor photocatalysts, *Chemical Physics Letters*, 106 (1984) 128-131.
- [134] S. Teratani, J. Nakamichi, K. Taya, K. Tanaka, Photocatalytic dehydrogenation of 2-propanol over TiO<sub>2</sub> and metal/TiO<sub>2</sub> powders, *Bulletin of the Chemical Society of Japan*, 55 (1982) 1688-1690.
- [135] Y. Ping, R. Sundararaman, W. A. Goddard III, Solvation effects on the band edge positions of photocatalysts from first principles, *Physical Chemistry Chemical Physics*, 17 (2015) 30499-30509.
- [136] P. Deák, J. Kullgren, B. Aradi, T. Frauenheim, L. Kavan, Water splitting and the band edge positions of TiO<sub>2</sub>, *Electrochimica Acta*, 199 (2016) 27-34.
- [137] M. T. Uddin, Y. Nicolas, C. I. Olivier, T. Toupance, M. M. Müller, H. J. Kleebe, K. Rachut, J. r. Ziegler, A. Klein, W. Jaegermann, Preparation of RuO<sub>2</sub>/TiO<sub>2</sub> mesoporous heterostructures and rationalization of their enhanced photocatalytic properties by band alignment investigations, *The Journal of Physical Chemistry C*, 117 (2013) 22098-22110.
- [138] R. Schafranek, J. Schaffner, A. Klein, In situ photoelectron study of the (Ba, Sr) TiO<sub>3</sub>/RuO<sub>2</sub> contact formation, *Journal of the European Ceramic Society*, 30 (2010) 187-192.
- [139] D. J. Yun, H. m. Ra, S. B. Jo, W. Maeng, S. h. Lee, S. Park, J. W. Jang, K. Cho, S. W. Rhee, Effects of postannealing process on the properties of RuO<sub>2</sub> films and their performance as electrodes in organic thin film transistors or solar cells, *ACS applied materials & interfaces*, 4 (2012) 4588-4594.
- [140] J. R. Rumble, *CRC handbook of chemistry and physics*, CRC Press, Taylor & Francis Group, Boca Raton; London; New York, 2017.
- [141] B. R. Chalamala, Y. Wei, R. H. Reuss, S. Aggarwal, B. E. Gnade, R. Ramesh, J. M. Bernhard, E. D. Sosa, D. E. Golden, Effect of growth conditions on surface morphology and photoelectric work function characteristics of iridium oxide thin films, *Applied physics letters*, 74 (1999) 1394-1396.
- [142] E. V. Jelenkovic, K. Tong, Thermally grown ruthenium oxide thin films, *Journal of Vacuum Science & Technology B: Microelectronics and Nanometer Structures Processing, Measurement, and Phenomena*, 22 (2004) 2319-2325.
- [143] T. Sakata, K. Hashimoto, T. Kawai, Catalytic properties of ruthenium oxide on n-type semiconductors under illumination, *The Journal of Physical Chemistry*, 88 (1984) 5214-5221.
- [144] B. H. Meekins, P. V. Kamat, Role of water oxidation catalyst IrO<sub>2</sub> in shuttling photogenerated holes across TiO<sub>2</sub> interface, *The Journal of Physical Chemistry Letters*, 2 (2011) 2304-2310.
- [145] D. Bahnemann, A. Henglein, J. Lilie, L. Spanhel, Flash photolysis observation of the absorption spectra of trapped positive holes and electrons in colloidal titanium dioxide, *The Journal of Physical Chemistry*, 88 (1984) 709-711.
- [146] H. H. Mohamed, R. Dillert, D. W. Bahnemann, TiO<sub>2</sub> nanoparticles as electron pools: Single- and multi-step electron transfer processes, *Journal of Photochemistry and Photobiology A: Chemistry*, 245 (2012) 9-17.

## 6. References

- [147] M. Jakob, H. Levanon, P. V. Kamat, Charge distribution between UV-irradiated TiO<sub>2</sub> and gold nanoparticles: determination of shift in the Fermi level, *Nano letters*, 3 (2003) 353-358.
- [148] P. D. Cozzoli, M.L. Curri, A. Agostiano, Efficient charge storage in photoexcited TiO<sub>2</sub> nanorod-noble metal nanoparticle composite systems, *Chemical communications*, (2005) 3186-3188.
- [149] P.V. Kamat, Manipulation of charge transfer across semiconductor interface. A criterion that cannot be ignored in photocatalyst design, *The Journal of Physical Chemistry Letters*, 3 (2012) 663-672.
- [150] L. Liu, Z. Ji, W. Zou, X. Gu, Y. Deng, F. Gao, C. Tang, L. Dong, In situ loading transition metal oxide clusters on TiO<sub>2</sub> nanosheets as co-catalysts for exceptional high photoactivity, *ACS Catalysis*, 3 (2013) 2052-2061.
- [151] C. Chabanier, E. Irissou, D. Guay, J. Pelletier, M. Sutton, L. Lurio, Hydrogen absorption in thermally prepared RuO<sub>2</sub> electrode, *Electrochemical and solid-state letters*, 5 (2002) E40-E42.
- [152] C. Chabanier, D. Guay, Activation and hydrogen absorption in thermally prepared RuO<sub>2</sub> and IrO<sub>2</sub>, *Journal of Electroanalytical Chemistry*, 570 (2004) 13-27.
- [153] L. Å. Näslund, A. R. S. Ingason, S. Holmin, J. Rosen, Formation of RuO(OH)<sub>2</sub> on RuO<sub>2</sub>-based electrodes for hydrogen production, *The Journal of Physical Chemistry C*, 118 (2014) 15315-15323.
- [154] R. K. Karlsson, A. Cornell, L. G. Pettersson, Structural changes in RuO<sub>2</sub> during electrochemical hydrogen evolution, *The Journal of Physical Chemistry C*, 120 (2016) 7094-7102.
- [155] A. F. Alkaim, T. A. Kandiel, R. Dillert, D. W. Bahnemann, Photocatalytic hydrogen production from biomass-derived compounds: a case study of citric acid, *Environmental technology*, 37 (2016) 2687-2693.
- [156] E. P. Melián, C. R. López, D. E. Santiago, R. Q. Cabrera, J. O. Méndez, J. D. Rodríguez, O. G. Díaz, Study of the photocatalytic activity of Pt-modified commercial TiO<sub>2</sub> for hydrogen production in the presence of common organic sacrificial agents, *Applied Catalysis A: General*, 518 (2016) 189-197.
- [157] A. F. Alkaim, T. A. Kandiel, F. H. Hussein, R. Dillert, D. W. Bahnemann, Solvent-free hydrothermal synthesis of anatase TiO<sub>2</sub> nanoparticles with enhanced photocatalytic hydrogen production activity, *Applied Catalysis A: General*, 466 (2013) 32-37.
- [158] A. M. Toth, M. D. Liptak, D. L. Phillips, G. C. Shields, Accurate relative pK<sub>a</sub> calculations for carboxylic acids using complete basis set and Gaussian-n models combined with continuum solvation methods, *The Journal of Chemical Physics*, 114 (2001) 4595-4606.
- [159] C. Kormann, D. Bahnemann, M. R. Hoffmann, Photolysis of chloroform and other organic molecules in aqueous titanium dioxide suspensions, *Environmental science & technology*, 25 (1991) 494-500.
- [160] Y. Nosaka, M. Kishimoto, J. Nishino, Factors governing the initial process of TiO<sub>2</sub> photocatalysis studied by means of in-situ electron spin resonance measurements, *The Journal of Physical Chemistry B*, 102 (1998) 10279-10283.
- [161] S. N. Shukla, O. J. Walker, Anode phenomena in the electrolysis of potassium acetate solutions. Part II. Discharge potential of the acetate ion, *Transactions of the Faraday Society*, 27 (1931) 722-730.
- [162] T. Dickinson, W. W. Jones, Mechanism of Kolbe's electrosynthesis. Part 1.—Anode potential phenomena, *Transactions of the Faraday Society*, 58 (1962) 382-387.

- [163] S. Malato, P. F. Ibáñez, M. Maldonado, J. Blanco, W. Gernjak, Decontamination and disinfection of water by solar photocatalysis: recent overview and trends, *Catalysis Today*, 147 (2009) 1-59.
- [164] K. Maeda, K. Domen, New non-oxide photocatalysts designed for overall water splitting under visible light, *Journal of Physical Chemistry C*, 111 (2007) 7851-7861.
- [165] J. G. Highfield, M. H. Chen, P. T. Nguyen, Z. Chen, Mechanistic investigations of photo-driven processes over TiO<sub>2</sub> by in-situ DRIFTS-MS: Part 1. Platinization and methanol reforming, *Energy & Environmental Science*, 2 (2009) 991-1002.
- [166] H. Belhadj, S. Hamid, P. K. Robertson, D. W. Bahnemann, Mechanisms of Simultaneous Hydrogen Production and Formaldehyde Oxidation in H<sub>2</sub>O and D<sub>2</sub>O over Platinized TiO<sub>2</sub>, *ACS Catalysis*, 7 (2017) 4753-4758.
- [167] D. L. Singleton, G. Paraskevopoulos, R. S. Irwin, Rates and mechanism of the reactions of hydroxyl radicals with acetic, deuterated acetic, and propionic acids in the gas phase, *Journal of the American Chemical Society*, 111 (1989) 5248-5251.
- [168] G. N. Lewis, P. W. Schutz, The ionization of some weak electrolytes in heavy water, *Journal of the American Chemical Society*, 56 (1934) 1913-1915.
- [169] R. Robinson, M. Paabo, R. G. Bates, Deuterium isotope effect on the dissociation of weak acids in water and deuterium oxide, National Bureau of Standards, (1969).
- [170] P. K. Robertson, D. W. Bahnemann, L. A. Lawton, E. Bellu, A study of the kinetic solvent isotope effect on the destruction of microcystin-LR and geosmin using TiO<sub>2</sub> photocatalysis, *Applied Catalysis B: Environmental*, 108 (2011) 1-5.
- [171] M. Kaise, H. Nagai, K. Tokuhashi, S. Kondo, S. Nimura, O. Kikuchi, Electron spin resonance studies of photocatalytic interface reactions of suspended M/TiO<sub>2</sub> (M= Pt, Pd, Ir, Rh, Os, or Ru) with alcohol and acetic acid in aqueous media, *Langmuir*, 10 (1994) 1345-1347.
- [172] Y. Nosaka, K. Koenuma, K. Ushida, A. Kira, Reaction mechanism of the decomposition of acetic acid on illuminated TiO<sub>2</sub> powder studied by means of in situ electron spin resonance measurements, *Langmuir*, 12 (1996) 736-738.
- [173] M. Kaise, H. Kondoh, C. Nishihara, H. Nozoye, H. Shindo, S. Nimura, O. Kikuchi, Photocatalytic reactions of acetic acid on platinum-loaded TiO<sub>2</sub>: ESR evidence of radical intermediates in the photo-Kolbe reaction, *Journal of the Chemical Society, Chemical Communications*, (1993) 395-396.
- [174] I. Rusonik, H. Polat, H. Cohen, D. Meyerstein, Reaction of methyl radicals with metal powders immersed in aqueous solutions, *European Journal of Inorganic Chemistry*, 2003 (2003) 4227-4233.
- [175] O. G. Oster, R. B. Ziv, G. Yardeni, I. Zilbermann, D. Meyerstein, On the reactions of methyl radicals with TiO<sub>2</sub> nanoparticles and granular powders immersed in aqueous solutions, *Chemistry-A European Journal*, 17 (2011) 9226-9231.
- [176] R. B. Ziv, I. Zilbermann, O. O. Golberg, T. Zidki, G. Yardeni, H. Cohen, D. Meyerstein, On the Lifetime of the Transients (NP) (CH<sub>3</sub>)<sub>n</sub> (NP= Ag<sup>0</sup>, Au<sup>0</sup>, TiO<sub>2</sub> Nanoparticles) Formed in the Reactions Between Methyl Radicals and Nanoparticles Suspended in Aqueous Solutions, *Chemistry-A European Journal*, 18 (2012) 4699-4705.
- [177] R. B. Ziv, I. Zilbermann, T. Zidki, G. Yardeni, V. Shevchenko, D. Meyerstein, Coating Pt<sup>0</sup> Nanoparticles with Methyl Groups: The Reaction Between Methyl Radicals and Pt<sup>0</sup> NPs Suspended in Aqueous Solutions, *Chemistry-A European Journal*, 18 (2012) 6733-6736.
- [178] T. Zidki, R. B. Ziv, U. Green, H. Cohen, D. Meisel, D. Meyerstein, The effect of the nano-silica support on the catalytic reduction of water by gold, silver and platinum nanoparticles–nanocomposite reactivity, *Physical Chemistry Chemical Physics*, 16 (2014) 15422-15429.

## 6. References

- [179] R. B. Ziv, T. Zidki, I. Zilbermann, G. Yardeni, D. Meyerstein, Effect of Hydrogen Pretreatment of Platinum Nanoparticles on their Catalytic Properties: Reactions with Alkyl Radicals—A Mechanistic Study, *ChemCatChem*, 8 (2016) 2761-2764.
- [180] N. Lakshminarasimhan, A. D. Bokare, W. Choi, Effect of agglomerated state in mesoporous TiO<sub>2</sub> on the morphology of photodeposited Pt and photocatalytic activity, *The Journal of Physical Chemistry C*, 116 (2012) 17531-17539.
- [181] P. Neta, M. Simic, E. Hayon, Pulse radiolysis of aliphatic acids in aqueous solutions. I. Simple monocarboxylic acids, *The Journal of Physical Chemistry*, 73 (1969) 4207-4213.
- [182] B. C. Gilbert, R. O. Norman, G. Placucci, R. C. Sealy, Electron spin resonance studies. Part XLV. Reactions of the methyl radical with some aliphatic compounds in aqueous solution, *Journal of the Chemical Society, Perkin Transactions 2*, (1975) 885-891.
- [183] M. J. Davies, B. C. Gilbert, C. B. Thomas, J. Young, Electron spin resonance studies. Part 69. Oxidation of some aliphatic carboxylic acids, carboxylate anions, and related compounds by the sulphate radical anion (SO<sub>4</sub><sup>-</sup>), *Journal of the Chemical Society, Perkin Transactions 2*, (1985) 1199-1204.
- [184] G. V. Buxton, C. L. Greenstock, W. P. Helman, A. B. Ross, W. Tsang, Critical review of rate constants for reactions of hydrated electrons: chemical kinetic data base for combustion chemistry. Part 3: Propane, *J. Phys. Chemical Reference Data*, 17 (1988) 513-886.
- [185] S. Mozia, A. Heciak, A. W. Morawski, Preparation of Fe-modified photocatalysts and their application for generation of useful hydrocarbons during photocatalytic decomposition of acetic acid, *Journal of Photochemistry and Photobiology A: Chemistry*, 216 (2010) 275-282.
- [186] A. Heciak, A. W. Morawski, B. Grzmil, S. Mozia, Cu-modified TiO<sub>2</sub> photocatalysts for decomposition of acetic acid with simultaneous formation of C1–C3 hydrocarbons and hydrogen, *Applied Catalysis B: Environmental*, 140 (2013) 108-114.
- [187] T. A. Kandiel, R. Dillert, D. W. Bahnemann, Enhanced photocatalytic production of molecular hydrogen on TiO<sub>2</sub> modified with Pt–polypyrrole nanocomposites, *Photochemical & Photobiological Sciences*, 8 (2009) 683-690.
- [188] G. R. Bamwenda, S. Tsubota, T. Nakamura, M. Haruta, Photoassisted hydrogen production from a water-ethanol solution: a comparison of activities of Au/TiO<sub>2</sub> and Pt/TiO<sub>2</sub>, *Journal of Photochemistry and Photobiology A: Chemistry*, 89 (1995) 177-189.
- [189] M. Antoniadou, V. Vaiano, D. Sannino, P. Lianos, Photocatalytic oxidation of ethanol using undoped and Ru-doped titania: acetaldehyde, hydrogen or electricity generation, *Chemical Engineering Journal*, 224 (2013) 144-148.
- [190] A. V. Puga, A. Forneli, H. García, A. Corma, Production of H<sub>2</sub> by ethanol photoreforming on Au/TiO<sub>2</sub>, *Advanced Functional Materials*, 24 (2014) 241-248.
- [191] G. Atherton, M. Fleischmann, F. Goodridge, Kinetic study of the Hofer-Moest reaction, *Transactions of the Faraday Society*, 63 (1967) 1468-1477.
- [192] S. Glasstone, A. Hickling, The Mechanism of the Kolbe Electrosynthesis and Allied Reactions, *Transactions of The Electrochemical Society*, 75 (1939) 333-352.
- [193] A. J. Fry, *Synthetic organic electrochemistry*, John Wiley & Sons, 1989.
- [194] H. E. Zimmerman, D. I. Schuster, A new approach to mechanistic organic photochemistry. IV. Photochemical rearrangements of 4, 4-diphenylcyclohexadienone, *Journal of the American Chemical Society*, 84 (1962) 4527-4540.
- [195] H. E. Zimmerman, V. R. Sandel, Mechanistic organic photochemistry. II. 1, 2 Solvolytic photochemical reactions, *Journal of the American Chemical Society*, 85 (1963) 915-922.
- [196] H. E. Zimmerman, The meta effect in organic photochemistry: Mechanistic and exploratory organic photochemistry, *Journal of the American Chemical Society*, 117 (1995) 8988-8991.

## 6. References

- [197] M. Laferrière, C. N. Sanramé, J. Scaiano, A remarkably long-lived benzyl carbanion, *Organic Letters*, 6 (2004) 873-875.
- [198] A. Frennet, Chemisorption and exchange with deuterium of methane on metals, *Catalysis Reviews Science and Engineering*, 10 (1974) 37-68.
- [199] A. Frennet, C. Hubert, Transient kinetics in heterogeneous catalysis by metals, *Journal of Molecular Catalysis A: Chemical*, 163 (2000) 163-188.
- [200] C. Kemball, The catalytic exchange of hydrocarbons with deuterium, in: *Advances in Catalysis*, Elsevier, 1959, pp. 223-262.
- [201] A. Khodakov, N. Barbouth, Y. Berthier, J. Oudar, P. Schulz, Effect of Pt particle size on H/D exchange of methane over alumina- and zeolite-supported catalysts, *Journal of the Chemical Society, Faraday Transactions*, 91 (1995) 569-573.

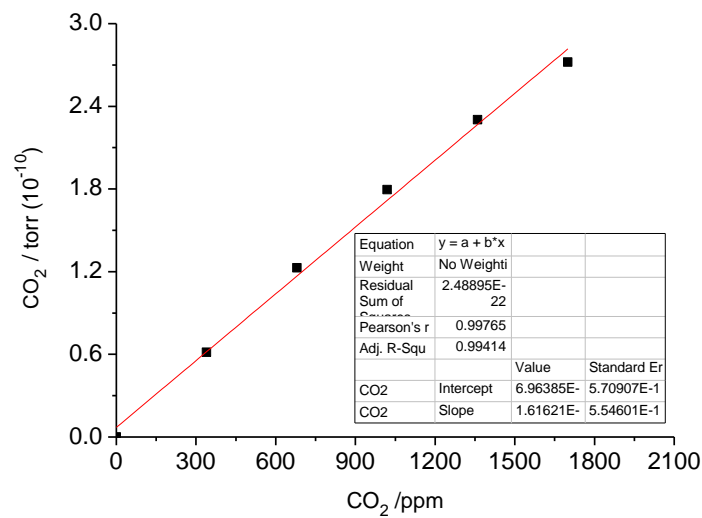
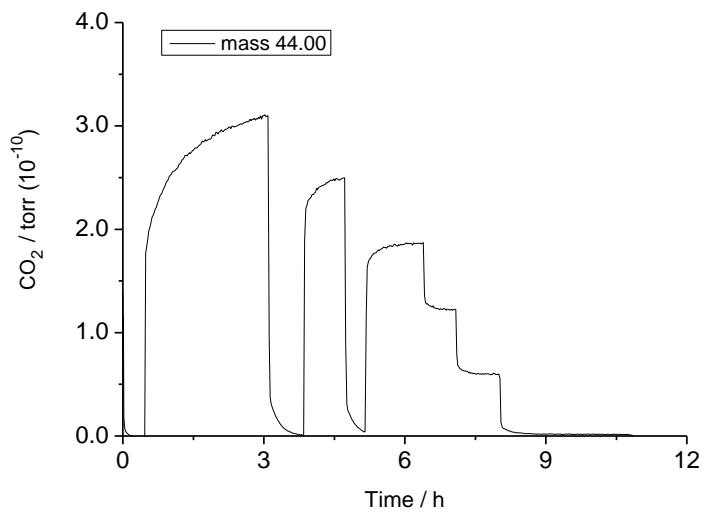
## 7. Appendix

## 7. Appendix

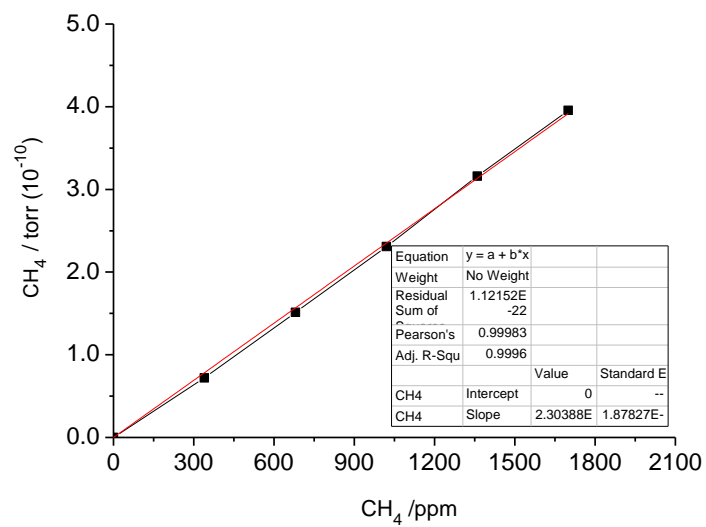
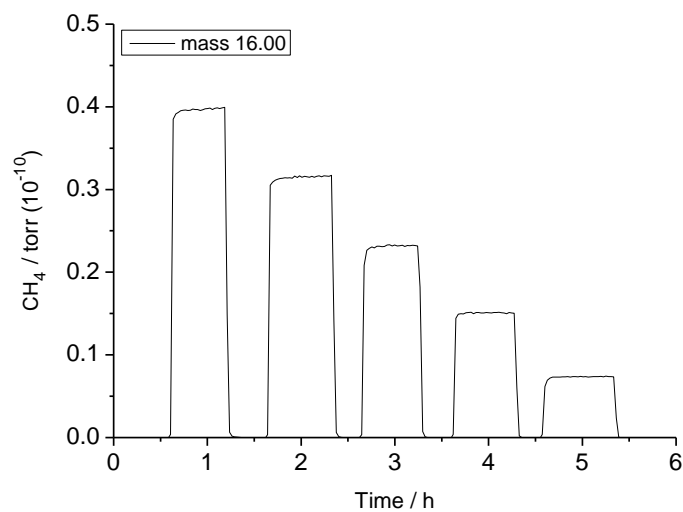
### 7.1 Additional information

Calibration curves for the main reaction products obtained by QMS.

- CO<sub>2</sub> = mass 44.00

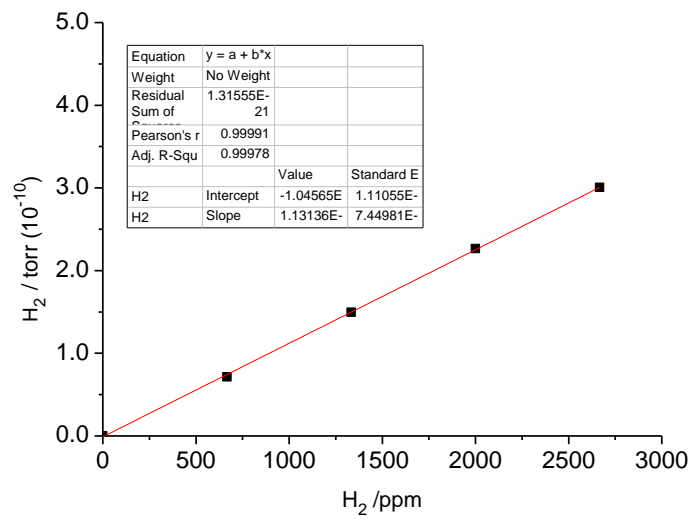
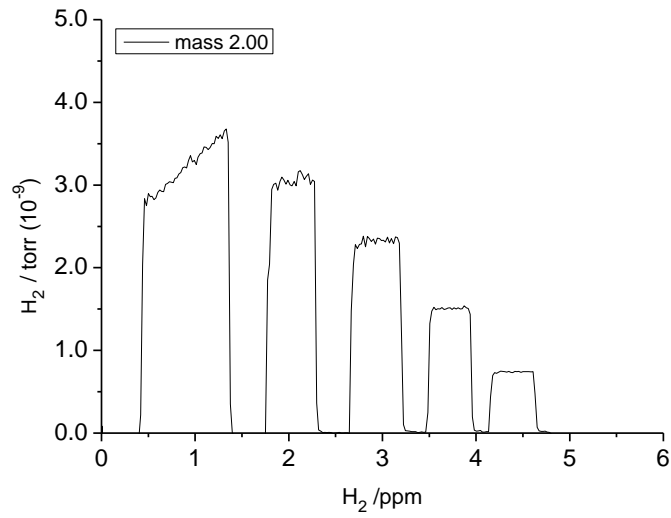


- CH<sub>4</sub> = mass 16.00



## 7. Appendix

- $H_2 = \text{mass } 2.00$





## 7.2 Publications

### Published papers

1. **S. Hamid**, R. Dillert, D.W. Bahnemann, Photocatalytic reforming of aqueous acetic acid into molecular hydrogen and hydrocarbons over cocatalyst-loaded TiO<sub>2</sub>: shifting the product distribution, *Journal of Physical Chemistry C* (2018), *In press*.
2. **S. Hamid**, I. Ivanova, T.H. Jeon, R. Dillert, W. Choi, D.W. Bahnemann, Photocatalytic conversion of acetate into molecular hydrogen and hydrocarbons over Pt/TiO<sub>2</sub>: pH dependent formation of Kolbe and Hofer-Moest products, *Journal of Catalysis*, 349 (2017) 128 – 135.
3. H. Belhadj, **S. Hamid**, P.K. Robertson, D.W. Bahnemann, Mechanisms of Simultaneous Hydrogen Production and Formaldehyde Oxidation in H<sub>2</sub>O and D<sub>2</sub>O over Platinized TiO<sub>2</sub>, *ACS Catalysis*, 7 (2017) 4753 – 4758.
4. I. Ivanova, **S. Hamid**, J. Schneider, D. W. Bahnemann, New insights into the photocatalytic hydrogen production: mechanistic aspects and material design, *Current Topics in Catalysis*, 12 (2016) 81 – 99.
5. J. Nie, A.O. Patrocínio, **S. Hamid**, F. Sieland, J. Sann, S. Xia, D. W. Bahnemann, J. Schneider, New Insights into the Plasmonic Enhancement for Photocatalytic H<sub>2</sub> Production by Cu-TiO<sub>2</sub> upon Visible Light Illumination, *Physical Chemistry Chemical Physics*, (2018) 5264 – 5273.
6. S. Naskar, F. Lübke, **S. Hamid**, A. Freytag, A. Wolf, J. Koch, I. Ivanova, H. Pfnür, D. Dorfs, D.W. Bahnemann, Synthesis of Ternary and Quaternary Au and Pt Decorated CdSe/CdS Heteronanoplatelets with Controllable Morphology, *Advanced Functional Materials*, 27 (2017) 1 – 11.

## 7. Appendix

7. G. Yang, D. Chen, H. Ding, J. Feng, J.Z. Zhang, Y. Zhu, **S. Hamid**, D.W. Bahnemann, Well-designed 3D ZnIn<sub>2</sub>S<sub>4</sub> nanosheets/TiO<sub>2</sub> nanobelts as direct Z-scheme photocatalysts for CO<sub>2</sub> photoreduction into renewable hydrocarbon fuel with high efficiency, *Applied Catalysis B: Environmental*, 219 (2017) 611 – 618.

### Submitted papers

1. **S. Hamid**, J. Schneider, R. Dillert, D.W. Bahnemann, Spectroscopic analysis of proton exchange during the photocatalytic decomposition of aqueous acetic acid: an Isotopic study on product distribution and reaction rate, Revision submitted to *ACS Catalysis* (2018).

2. N. Karamat, M. F. Ehsan, M. N. Ashiq, S. Ijaz, M. N. Haq, **S. Hamid**, D. W. Bahnemann, LaNdZr<sub>2</sub>O<sub>7</sub> supported SnSe nanocomposites for the photocatalytic CO<sub>2</sub> reduction and Foron blue dye degradation, Major revision submitted to *Applied Surface Science* (2018).

### 7.3 Conferences and presentations

#### 7.3.1 Oral presentations

**S. Hamid**, I. Ivanova, T.H. Jeon, R. Dillert, W. Choi, D.W. Bahnemann, ‘Photocatalytic conversion of acetate into molecular hydrogen and hydrocarbons over surface modified TiO<sub>2</sub>: pH dependent formation of Kolbe and Hofer-Moest products’ at 28th International Conference on Photochemistry (ICP), Strasbourg, France, July 16 – 21, 2017.

**S. Hamid**, J. Schneider, R. Dillert, D.W. Bahnemann, ‘Spectroscopic analysis of proton exchange for the photocatalytic transformation of aqueous acetic acid: an isotopic study’, AdvPhotoCat-E 2017, Heraklion, Greece, July 14 – 16, 2017.

**S. Hamid**, I. Ivanova, R. Dillert, D.W. Bahnemann ‘Factors influencing the photocatalytic decomposition of aqueous acetic acid over TiO<sub>2</sub>: a mechanistic study’, The 21st International Conference on Semiconductor Photocatalysis & Solar Energy Conversion (SPASEC-21), Atlanta, Georgia, United States of America, November 13 – 17, 2016.

**S. Hamid**, I. Ivanova, R. Dillert, D.W. Bahnemann, ‘The pH dependent photocatalytic decomposition of aqueous acetic acid into hydrogen and hydrocarbons over platinized-TiO<sub>2</sub>’, New Photocatalytic Materials for Environment, Energy and Sustainability (NPM-1), Gottingen, Germany, June 6 – 10, 2016.

**S. Hamid**, I. Ivanova, D.W. Bahnemann, ‘Effect of various sacrificial reagents on the TiO<sub>2</sub> photocatalyzed hydrogen production’, 3rd German Russian summer school, Saint Petersburg, Peterhof, Russia, June 15 – 18, 2015.

## 7. Appendix

### 7.3.2 Poster presentations

**S. Hamid**, I. Ivanova, D.W. Bahnemann, ‘The pH dependent photocatalytic decomposition of aqueous acetic acid into hydrogen and hydrocarbons over platinized-TiO<sub>2</sub>’, Nanoday 2016, Laboratorium für Nano- und Quantenengineering, Hannover, Germany, September 29, 2016.

**S. Hamid**, I. Ivanova, D.W. Bahnemann, ‘Methanol and sodium acetate as electron donors for the photocatalyzed hydrogen production on surface-modified-TiO<sub>2</sub>’, Nanoday 2015, Laboratorium für Nano- und Quantenengineering, Hannover, Germany, October 1st, 2015.

**S. Hamid**, I. Ivanova, D.W. Bahnemann, ‘Methanol and sodium acetate as electron donors for the photocatalyzed hydrogen production on surface-modified-TiO<sub>2</sub>’, Photocatalytic and Advanced Oxidation Technologies for the Treatment of Water, Air, Soil and Surfaces (PAOT-3), Gdansk, Poland, September 1 – 4 ,2015.

### 8. Curriculum vitae

#### Personal information:

Last Name, First Name	Hamid, Saher
Date of Birth	18.01.1989
Gender	Female
Nationality	Pakistani
Marital Status	Married

#### Education and training:

**From 03/2015 to 06/2018:** PhD Student/ Research Assistant at Institut für Technische Chemie (Photocatalysis and Nanotechnology), Leibniz Universität Hannover under the supervision of Prof. Dr. Detlef W. Bahnemann.

**From 09/2013 to 11/2014:** Research Assistant at National Centre for Nanoscience and Technology, University of Chinese Academy of Sciences, Beijing, China.

**From 12/2010 to 10/2012:** Masters of Science (M.S.) in Nanotechnology, Centre of Excellence in Solid State Physics, University of the Punjab, Lahore, Pakistan.

**From 10/2006 to 08/2010:** Bachelors of Science (B.sc (Hons.)) in Computational Physics, Centre for High Energy Physics, University of the Punjab, Lahore, Pakistan.